NON-NEWTONIAN PRESSURE LOSS AND DISCHARGE COEFFICIENTS FOR SHORT SQUARE-EDGED ORIFICE PLATES

by

BUTTEUR MULUMBA NTAMBA NTAMBA

B.Eng: Electromechanical Engineering (University of Lubumbashi)

Thesis submitted in fulfilment of requirements for the degree
Master Technology: Mechanical Engineering

in the FACULTY OF ENGINEERING

at the CAPE PENINSULA UNIVERSITY OF TECHNOLOGY

Supervisor: Dr V.G. Fester

Cape Town

November 2011

ABSTRACT

Despite the extensive research work carried out on flow through short square-edged orifice plates over the last century (e.g. Johansen, 1930; Benedict, 1977; Alvi et al., 1978; Swamee, 2005; ESDU, 2007), gaps in the engineering data still exist for certain ranges of flow conditions and geometries. The majority of data available in the literature are for Newtonian fluids in the turbulent flow regime (ESDU, 2007). Insufficient data have been observed for the orifice with pipe diameter ratio, β = 0.2, in the laminar flow regime. There are no experimental data for β = 0.3 and 0.57. The objective of this thesis was to conduct wide-ranging experimental studies of the flow in orifice plates, which included those geometrical configurations, by measuring pressure loss coefficients and discharge coefficients across the orifice plates using both Newtonian fluids and non-Newtonian fluids in both laminar and turbulent flow regimes.

The test work was conducted on the valve test rig at the Cape Peninsula University of Technology. Four classical circular short square-edged orifice plates having, β = 0.2, 0.3, 0.57 and 0.7, were tested. In addition, two generation 0 Von Koch orifice plates (Von Koch, 1904), with equivalent cross sectional area were also tested for β = 0.57. Water was used as Newtonian fluid to obtain turbulent regime data and also for calibration purposes to ensure measurement accuracy and carboxymethyl cellulose, bentonite and kaolin slurries were used at different concentrations to obtain laminar and transitional loss coefficient data. The hydraulic grade line method was used to evaluate pressure loss coefficients (Edwards et al., 1985), while the flange tap arrangement method was used to determine the discharge coefficients (ESDU, 2007). A tube viscometer with three different pipe diameters was used to obtain the rheological properties of the fluids.

The results for each test are presented in the form of pressure loss coefficient (k_{or}) and discharge coefficient (C_d) against pipe Reynolds number (Re). The results obtained in this investigation show that the pressure loss coefficient is constant in the turbulent flow regime and depends on the Reynolds number in laminar flow regime for all β ratios tested. In the laminar flow regime the pressure loss coefficient decreases with the increase of Reynolds number. Average values of pressure loss coefficient of k_{or} = 1213, 226.93, 13.32 and 3.57 were found for β = 0.2, 0.3, 0.57 and 0.7, respectively, in the turbulent flow regime. Discharge coefficient values increase with increasing Reynolds number in laminar flow while its remains at constant values of C_d = 0.72, 0.67, 0.63 and 0.68 for β = 0.2, 0.3, 0.57, and 0.7, respectively, for turbulent flow.

A correlation which can predict pressure loss coefficient from laminar to turbulent flow regime was also derived.

A direct comparison was made between circular orifice and triangular orifices plates tested. The differences in pressure loss and discharge coefficients between circular and triangular orifice plate with sharp apex were -6% and 2.1% respectively and -0.5% and 1.5% respectively for the triangular orifice plate with round apex.

This thesis adds new pressure loss coefficient and discharge coefficient data to the literature. It also adds a new correlation for pressure loss which is important for designing energy efficient piping systems.

DECLARATION

I, Butteur Mulumba Ntamba Ntamba, hereby declare that the content of this thesis represents my own unaided work, and that the thesis has not previously been submitted for academic examination towards any qualification. Furthermore, it represents my own opinions and not necessarily those of the Cape Peninsula University of Technology.

…… 10 / 11 / 2011

Butteur Mulumba Ntamba Ntamba

DEDICATION

This thesis is dedicated to:

The Almighty God: for breath that has been given to me.

My father: who recently left us. This thesis is the fruit of your encouragement.

My family, mother, brother and sister: thank you for being supportive.

My nieces and nephews: this might be an inspiration for your future.

"A saint is a sinner who keeps on trying" ***N.R. Mandela***

"There is an appointed time for everything. And there is a time for every event under heaven" ***Ecclesiastes 3: 1***

ACKNOWLEDGEMENTS

Dr Veruscha Fester ─ for her supervision and for giving me the opportunity to work on a challenging project over the past two years.

A.M. Kabwe ─ for always being there when needed.

Prof Liz van Aswegen ─ for linguistic revision.

Richard du Toit ─ for his splendid laboratory supervisor role.

M. R. Chowdhury ─ for being an excellent collaborator on this project.

The Material Science and Technology Group ─ the staff and students for their continuous support.

The Cape Peninsula University of Technology and the Research and Development department for the opportunity granted to further my studies at their institution.

The National Research Foundation (NRF) ─ for its sustained support of the research.

TERMS AND CONCEPTS

Discharge coefficient: The ratio between the actual and theoretical volumetric flow rate.

Entry length: The length required for the fluid to develop a steady distance-independent velocity profile inside a contraction or die or conduit.

Fractal shape: A fragmented geometric shape that can be split into parts, each of which is at least approximately a reduced-size copy of the whole.

Friction factor: The ratio between the wall shear stress and kinetic energy of the liquid in a control volume in a pipeline.

Laminar flow: Known also as streamline flow, it occurs when a fluid flows in parallel layers with no disruption between the layers.

Long orifice: An orifice in which the jet formed downstream of the orifice entry tends to re-attach to the orifice wall is defined as a long or thick orifice.

Loss coefficient: The non-dimensionalised difference in total pressure between the extreme ends of two long straight pipes when there is a zero loss component between the two pipes and when the real fitting is installed.

Newtonian fluid: Any fluid that has a directly proportional relationship between shear stress and shear rate. Water is an example of a Newtonian fluid.

Non-Newtonian fluid: Any fluid whose flow properties differ in any way from those of a Newtonian fluid.

Orifice plate: A thin plate with a hole in the middle. It is used to measure the flow rates of fluids or to restrict flow.

Reynolds number: The ratio between viscous and inertial forces is proportional to the Reynolds number. The number is expressed in terms of the density, velocity, characteristic length and the viscosity of the fluid. This number is also used to define whether the flow is laminar or turbulent.

Shear stress: Shear stress is a stress state where the shape of a material tends to change (usually by "sliding" forces – torque by transversely-acting forces) without particular volume change.

Short orifice: A category of orifice plate in which flow reattachment on the orifice wall does not occur.

Transducer: A device that converts one type of energy to another, or responds to a physical parameter. A transducer is, in its fundamental form, a passive component. If the component is electrical, it generally has two electrical terminals.

Transition: The region or process acting between the laminar and turbulent flow regimes.

Turbulent flow: Characterised by chaotic, disordered and unsteady motion of fluid in which fluid particles follow an irregular and erratic path with violent mixing of fluid particles, which is difficult to visualise, measure and predict.

Velocity profile: The velocity profile represents an instantaneous velocity distribution across the pipe diameter.

***Vena contracta*:** The point in a fluid stream where the cross sectional area is the least.

Viscosity: A measure of the resistance to flow of a fluid under an applied force.

β ratio: The ratio between the orifice bore and pipe diameter.

TABLE OF CONTENTS

LIST OF FIGURES

LIST OF TABLES

NOMENCLATURE

SYMBOL	DESCRIPTION	UNIT
A	Cross section area of the pipe	m^2
A_{vc}	Cross-sectional area at *vena contracta* plane	mm^2
C_c	Contraction coefficient	-
D	Pipe diameter	mm
d	Orifice plate bore diameter	mm
Eu	Euler number	-
Eu_l	Liquid Euler number	-
Eu_{tp}	Two-phases Euler number	-
g	Gravitational acceleration	m/s^2
G	Elasticity modulus	-
K	Fluid consistency coefficient	$Pa.s^n$
k	Pipe roughness	-
k_{gross}	Gross orifice pressure loss coefficient	-
k_{net}	Net orifice pressure loss coefficient	-
k_{or}	Orifice pressure loss coefficient	-
L_{fitt}	Fitting length	m
L_u	Upstream length	m
n	Flow behaviour index	-
P	Static pressure	Pa
Q	Volumetric flow rate	m^3/s
r	Plug radius	m
R	Pipe radius	m
Re	Reynolds number	-
Re_3	Slatter Reynolds number	-
Re_l	Liquid Reynolds number	-
Re_{M-R}	Metzner-Reed Reynolds number	-
t	Orifice plate bore thickness	mm
t^*	Orifice plate thickness	mm
u	Point velocity	m/s

V	Mean velocity	m/s
Vann	Annulus velocity	m/s
Z	Height of the pipe centre-line above datum	m
ΔP	Total pressure loss	Pa

GREEK SYMBOLS

SYMBOL	**DESCRIPTION**	**UNIT**
ρ	Density	kg/m^3
α	Porosity	-
β	Orifice diameter ratio	
μ	Dynamic viscosity of the fluid	Pa.s
$\dot{\gamma}$	Shear rate	s^{-1}
f	Friction factor	-
τ	Shear stress	Pa
τ_y	Yield stress	Pa

SUBSCRIPT

1	First point of measurement
2	Second point of measurement
3	Third point of measurement
B	Bingham
HB	Herschel-Bulkley
loss	losses
∞	infinite
or	orifice
M-R	Metzner-Reed
VC	*Vena contacta*
ann	annulus

CHAPTER 1

1.1 INTRODUCTION

A standard orifice plate is one of a variety of obstruction-type flow meters that is used extensively to measure the flow rate of fluid in a pipe; it consists of a thin plate with a hole in the middle (Samanta et al., 1999). Orifices are also used for various engineering applications such as cooling holes, fuel lines, hydraulic systems, air conditioning and water pipe systems (ESDU, 2007). Even though studies in orifice plates have been done, gaps in the data still exist. For example, using Newtonian fluids, pressure measurement (wall static pressure and pressure drop across the orifice plate) and pressure loss coefficient are scarce. The data are available mostly for mid-range diameter ratio values, i.e., $\beta = 0.4 – 0.6$. Normally in practice the discharge coefficient is used to relate flow rate to differential pressure across the orifice plate. Except for rare cases, most of the pressure loss coefficient and discharge coefficient data found in the literature is based on Newtonian fluids. However, studies in the field of non-Newtonian fluids have not been extensive, despite their importance in the field of polymer processing, flow of petroleum products, biomedical engineering, biochemical engineering, food processing, and mineral processing plants, where the liquid involved shows non-Newtonian character. In such applications, the flow remains laminar even at large flow rates (Bohra, 2004).

1.2 PROBLEM STATEMENT

There is insufficient non-Newtonian laminar and turbulent pressure loss and discharge coefficient data published in the literature for short square-edged orifices. Little research has been done using air as a working fluid through fractal-shaped orifice plates; the investigation has not yet been extended to liquids. None of correlations found in the literature can predict pressure loss coefficient from laminar to turbulent flow.

1.3 AIM AND OBJECTIVES

The aim of this work was to:

- Experimentally determine the pressure loss coefficient for short square-edged orifices at different diameter ratio β in the range of Reynolds number 1 to 100 000.
- Experimentally determine the discharge coefficient for short square-edged orifices at different diameter ratio from laminar flow to turbulent flow.

- Compare pressure loss coefficients and discharge coefficient between generation 0 Von Koch fractal-orifices and circular orifices with the same flow area.
- Derive a correlation for pressure loss coefficient that can predict data from laminar to turbulent flow.

1.4. METHODOLOGY

In order to complete this study, the following work was conducted:

The experimental tests were done on the fitting test rig in the slurry laboratory at the Cape Peninsula University of Technology, using a 46 mm (ID) straight pipe. The pressure loss coefficient for short square-edged orifice plates with diameter ratio $\beta = 0.2$; $\beta = 0.3$; $\beta = 0.57$ and $\beta = 0.7$ was determined using the hydraulic grade line (HGL) approach. Sufficient length was provided for the flow to be considered fully developed before any pressure measurements were taken. For determining the discharge coefficient, a D and D/2 and flange pressure tapping arrangement was used.

Tube viscometry was used to determine the properties of the fluid. Water was used to calibrate the test rig. Time-independent non-Newtonian fluids (kaolin and carboxymethyl cellulose) were used at different concentrations for investigations.

Results are presented in the form of loss coefficient against Reynolds number and discharge coefficient against Reynolds number in the range of laminar flow to turbulent flow.

1.5 DELINEATION OF THE STUDY

Newtonian and non-Newtonian fluids or slurries were tested in short concentric square-edged orifice plates with diameter ratio $\beta = 0.2$; $\beta = 0.3$; $\beta = 0.57$ and $\beta = 0.7$. The thicknesses of the orifice plates were 6 mm and the internal pipe diameter was 46 mm.
The following areas were not treated in this thesis:

- long orifice plates
- eccentric and segmental short orifices.

1.6 SIGNIFICANCE OF RESEARCH

The experimental results obtained in this work add pressure loss coefficient and discharge coefficient data to the literature where data lacunae are present or are inconsistent.

CHAPTER 2

2.1 INTRODUCTION

This chapter will review the theories and literature that are relevant to the understanding of losses that occur as a Newtonian or non-Newtonian fluid passes through an orifice plate. The definition and purpose of orifice plates are given. The methodology used to determine pressure loss coefficients and discharge coefficients across the orifice plates is presented. Since non-Newtonian fluids are among the fluids tested in this study, fundamentals of rheology are given and the methods and procedure for characterisation of non-Newtonian fluids are presented. The work done to date on orifices is summarised and the main findings are highlighted. The chapter is concluded with some identified research topics.

2.2 ORIFICE PLATES

2.2.1 Definition

An orifice plate is a constrictive device mounted between a pair of flanges in a straight run of smooth pipe and is used mostly for flow detection. Inserted in a straight pipe, an orifice plate causes change in energy in the form of a loss in static pressure and an increase in the velocity through the orifice. Orifices are also known as head loss flow meters. They are differential pressure producing devices and can be characterised by:

- orifice edge geometry
- β ratio which is the ratio of orifice bore diameter (d) to pipe diameter (D)
- orifice thickness (t) to bore diameter (d).

Figure 2.1 shows the schematic diagram of an orifice plate inserted in a straight pipe.

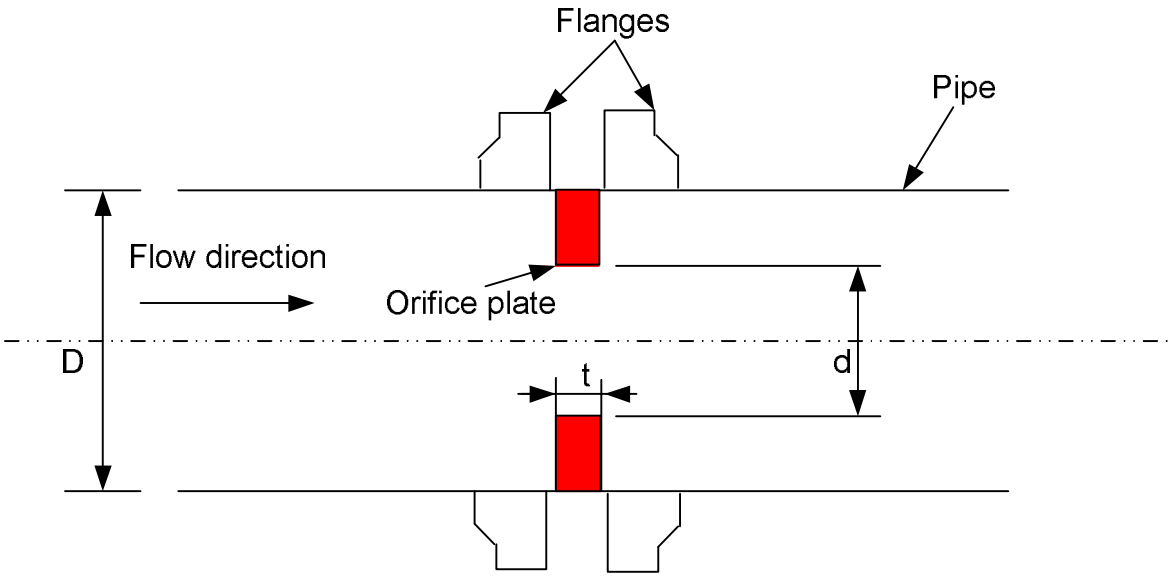

Figure 2.1 : Schematic diagram of a short square-edged orifice inserted in a smooth run pipe

2.2.2 Ideal flow condition for orifice installation

It is not easy to reach the ideal flow condition, also known as the reference flow condition, because of various pipe fittings upstream and downstream of the orifice. These fittings produce distortions of the flow velocity profiles which affect the flow characteristics through the orifice plate, the pressure gradient upstream and downstream of the orifice plate. A flow condition is recognised as ideal if the flow has the following features (ESDU, 2007):

- Axysymetric
- Fully developed
- Swirl free
- Steady uniform

Such conditions can be achieved depending on length of pipe upstream and downstream of the fitting inserted in the pipe, and also on the size of fittings or disturbances inserted in the pipe. In the case of orifice plates, the minimum length of pipe required for the flow to be fully developed depends on the diameter ratio, as the required length increases with the increase in diameter ratio (ANSI/API, 1995). Samanta et al. (1999) found that a 50D length was sufficient for the flow to be fully developed, but Prabu et al. (1995) suggests that even while no upstream disturbances were present, at least 22D length is required, for diameter ratio of 0.75. Figure 2.2 below portrays the minimum length required for the flow from the valve to the orifice and from

the orifice to the valve (ANSI/API, 1995). The majority of discharge coefficient and pressure loss coefficient data found in the literature are obtained by assuming an ideal flow condition (ESDU, 2007).

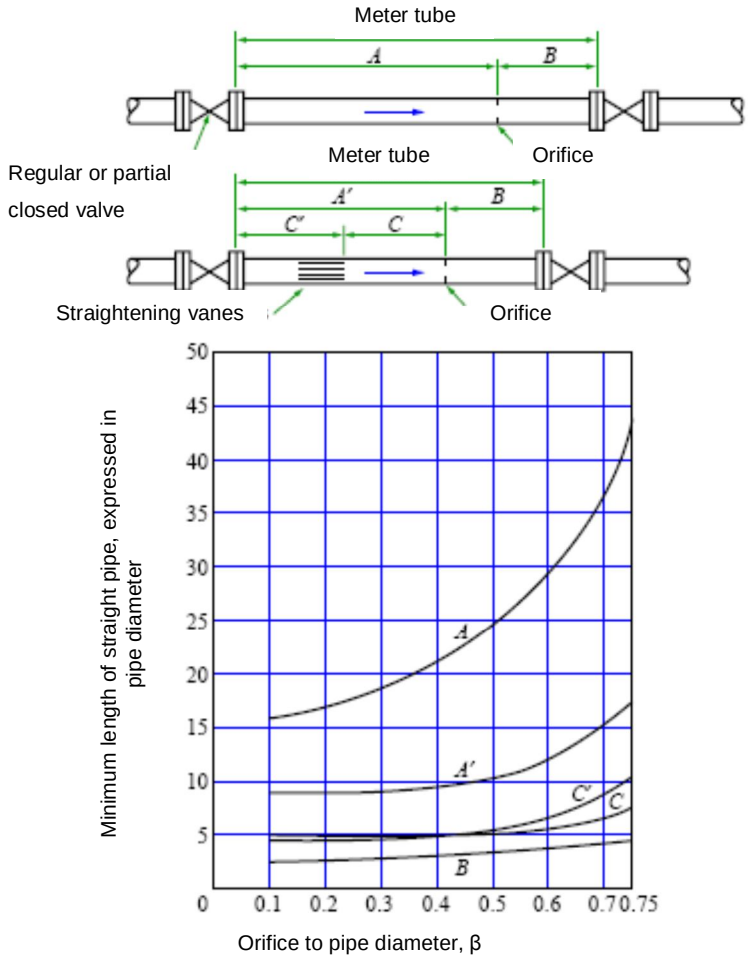

Figure 2.2 : Upstream and downstream pipe lengths for an upstream partly closed valve from ANSI/API, 1995

2.2.3 Flow through orifice plate

A fluid flowing inside of a pipe, where an orifice plate is inserted, possesses pressure and velocity. As the fluid passes through the orifice, the fluid converges and the velocity of the fluid increases to a maximum value in order to maintain steady flow of fluid throughout the flow section. At this point, the pressure is at a minimum value. The maximum flow velocity and the minimum static pressure do not occur at the bore of the orifice, but occur downstream of the orifice plate. This jet, where the fluid is at highest velocity and lowest static pressure, is known as the *vena contracta*. The cross sectional area and location of the *vena contracta* are

dependent on the geometry of the orifice plate and the properties of the fluid being measured. Normally, the *vena contacta* occurs at an axial distance of 0.5D from the orifice upstream face (ESDU, 2007). As the fluid diverges to fill the entire pipe area, the velocity decreases to the original value. The pressure is irrecoverable; therefore, the output pressure will always be less than the input pressure. The pressures on both sides of the orifice plate are measured, resulting in differential pressure which is proportional to the flow rate (Husain, 1995; ESDU, 2007).

The ratio between the *vena contracta* cross section area and the orifice plate bore cross section area is known as the contraction coefficient C_C. The contraction coefficient C_C is an important parameter for the determination of the flow characteristic regimes of fluids through orifice plates (ESDU, 2007). The parameter is obtained using the following equation:

$$C_c = \frac{A_{vc}}{A_2} \qquad \text{Equation 2.1}$$

where A_{vc} is the jet cross-sectional area at *vena contracta* plane and A_2 is the orifice cross-sectional area.

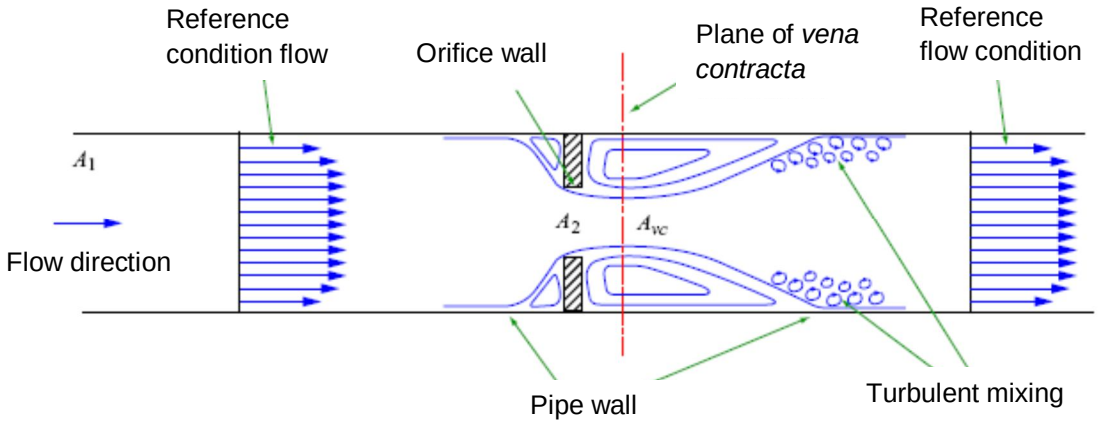

Figure 2.3: Schematic presentation of typical flow through orifice (ESDU, 2007)

The characteristic flow regimes for a square-edge orifice that occur in incompressible turbulent flow was illustrated by Ward-Smith (1979) and summarised by ESDU (2007) as given below.

- When the flow remains separated from the orifice wall, the flow regime is known as fully-separated. Typically, this flow occurs in the range $t < \frac{t}{d} < 0.75$, where the contraction coefficient is increasing monotonically from $C_C = 0.61$ at $\frac{t}{d} = 0$ to $C_C = 0.8$ at $\frac{t}{d} = 0.75$.

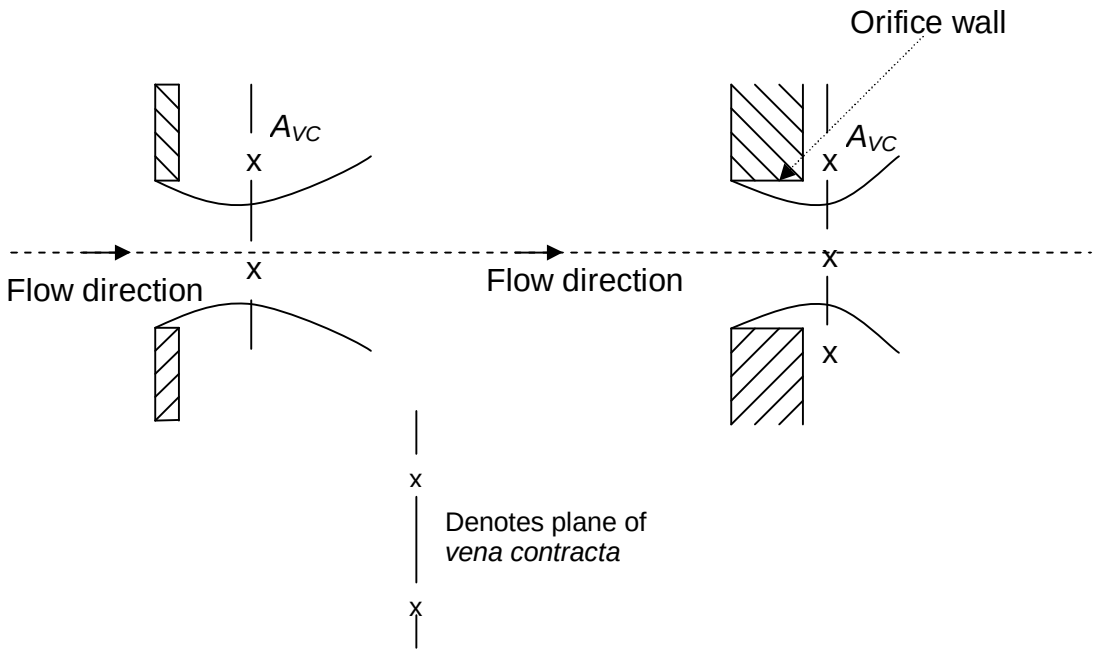

Figure 2.4 : Fully-separated regimes (ESDU, 2007)

- As the thickness of the orifice is increased, the jet tends to converge on the inner wall of the orifice. This regime is known as marginally-separated and typically occurs over a small but finite range around $\frac{t}{d}$ = 0.75.

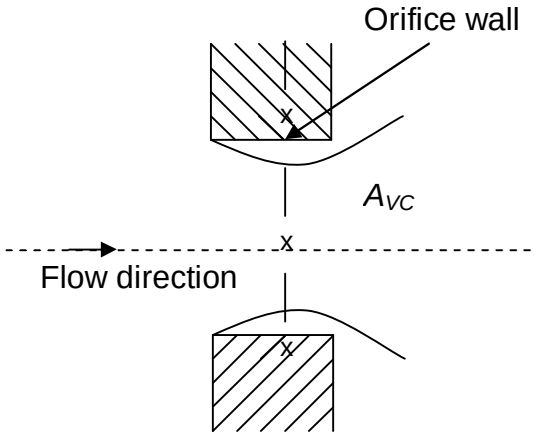

Figure 2.5 : Marginally-separated regimes (ESDU, 2007)

- With further increase in t, the jet just reattaches to the orifice and immediately separates again. This is known as the marginally-reattached flow regime.

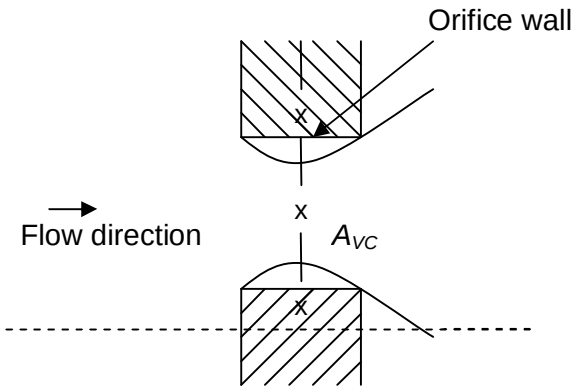

Figure 2.6 : Marginally-reattached flow regimes (ESDU, 2007)

- For larger t and higher Re, the flow reattaches in the form of a turbulent boundary layer to the orifice wall. This regime is known as a fully-reattached flow regime and occurs for $\frac{t}{d} > 0.75$, where C_C is constant at $C_C \approx 0.61$.

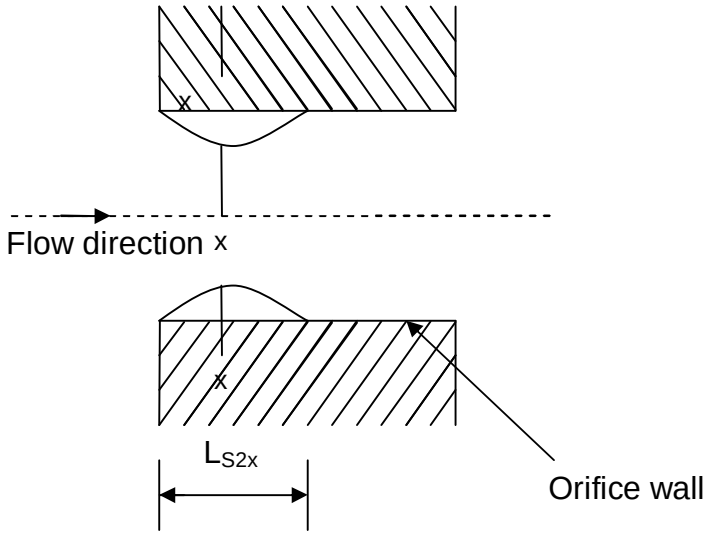

Figure 2.7 : Fully-reattached regimes (ESDU, 2007)

2.2.4 Parameters influencing the flow through orifice plate

In the reference flow condition, the characteristics of the flow through an orifice plate depend upon the orifice edge geometry, the pipe Reynolds number, and the orifice to pipe diameter, β (ESDU, 2007).

2.2.4.1 Orifice plates geometries

It was found experimentally that the flow through an orifice plate depends also on the orifice geometry. The geometry of orifice plate is defined using the following parameters as illustrated in Figure 2.8 (ESDU, 2007):

- Orifice plate bore diameter, d,
- Pipe diameter, D,
- Orifice plate bore thickness, t,
- Orifice plate thickness, t^*,
- Diameter ratio, $\beta = \frac{d}{D}$,
- Porosity, $\propto = \frac{d^2}{D^2}$,
- Plate bore thickness/diameter ratio, $\frac{t}{d}$,
- Entry edge profile, i.e square, knife, beveled, rounded with edge radius, r , quadrant, or chamfered edge with chamfer length l_e and chamfer angle ∅
- Exit edge profile, i.e square, square back-cut or back bevel with back bevel angle φ.

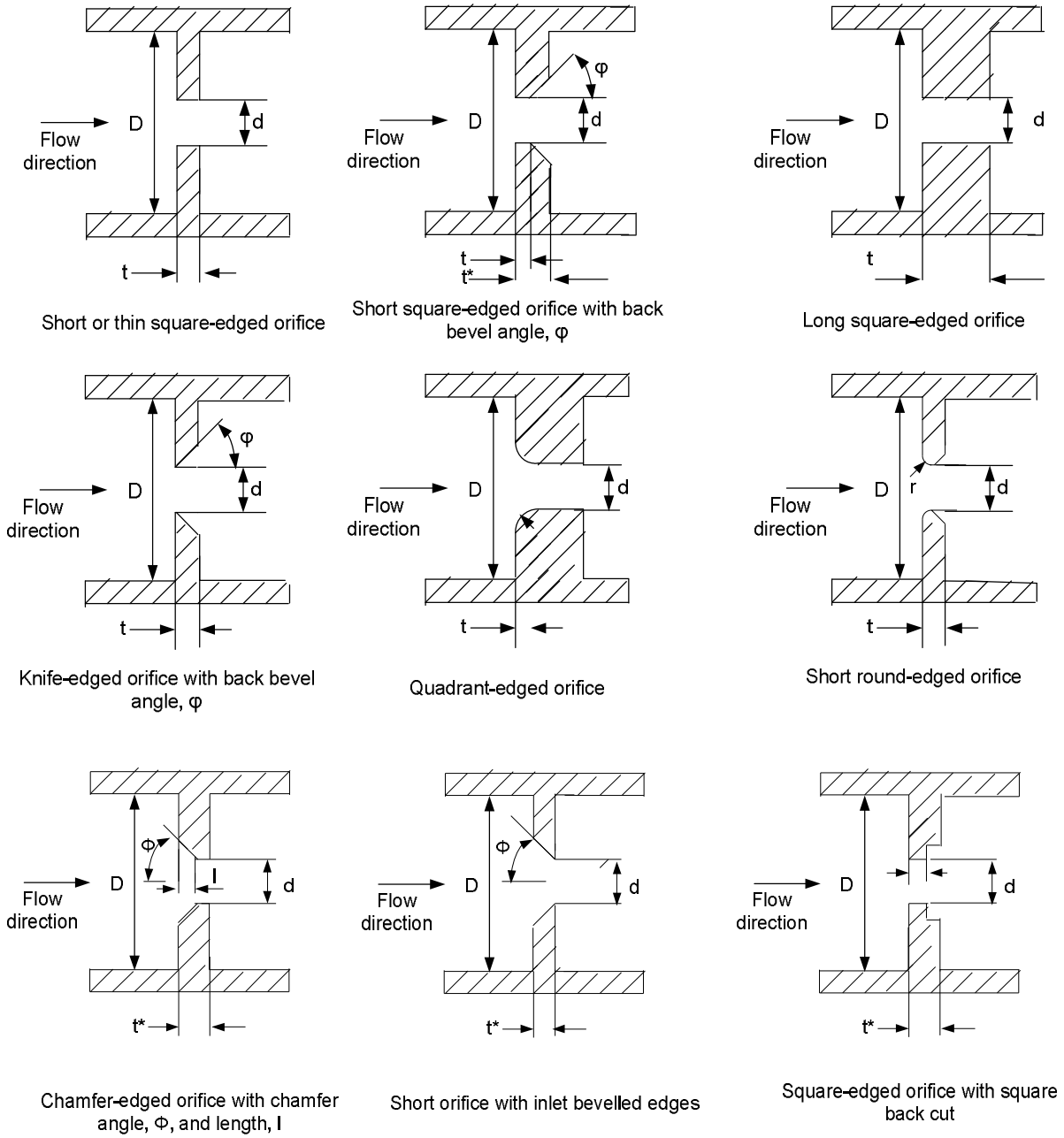

Figure 2.8 : Different orifice plate geometries (ESDU, 2007)

2.2.4.2 Effect of Reynolds number and β

The Reynolds number (Re) is a dimensionless group that gives a measure of the ratio of inertial forces to viscous forces, and consequently, it quantifies the relative importance of these two types of forces for given flow conditions. Osborne Reynolds (1842−1912) was the first who established this theory. He experimentally found that when the Reynolds number is less than 2 000, there is a laminar flow regime, and a turbulent flow regime occurs when the Reynolds number is more than 4 000. Between 2 000 and 4 000 in other words, between the laminar and turbulent flow regime there is an unstable region called the transitional flow regime (Serway, 1992).

$$Re_D = \frac{\rho V D}{\mu} \qquad \text{Equation 2.2}$$

Equation 2.2 expresses the pipe Reynolds number. The Reynolds number can also be expressed in terms of orifice bore diameter by the equation below:

$$Re_d = \frac{Re}{\beta} \qquad \text{Equation 2.3}$$

At pipe Reynolds numbers less than 10, the flow remains attached to the orifice plate wall. The flow separates at the entry of the orifice wall to form a jet downstream of the orifice as the pipe Reynolds number increases. The transition from laminar to turbulent flow takes place in the jet at $Re_D \approx 2000$, but re-laminarisation may occur downstream of the orifice plate depending on the diameter ratio. Transition to turbulent flow is well established at higher pipe Reynolds number and the nature and geometry of the flow is then largely insensitive to further increases in the Reynolds number. A value of $Re_D = 10^4$ can be taken as the lower limit for a single holed orifice for practical purposes (ESDU, 2007).

2.2.5 Classification of orifice plates

2.2.5.1 Short and long orifices

- For a short orifice, the ratio between plate bore thickness and the bore diameter is less than 0.75, ($\frac{t}{d} < 0.75$). Ward-Smith (1979) experienced that the flow characteristic regime is fully separated.
- However, when the ratio between plate thickness and the bore diameter is more than 1, ($\frac{t}{d} > 1$), it can then be called a long orifice; the characteristic flow regime is fully reattached at the orifice wall (Ward-Smith, 1979).

2.2.5.2 Circular orifice

Circular orifice plates can be concentric, segmental, or eccentric.

- The *concentric orifice plate* is the most common of the three types. The orifice is equidistant (concentric) to the inside diameter of the pipe. Segmental and eccentric orifices plates are functionally identical to the concentric orifice (McNally Institute, 2010).
- The circular section of the *segmental orifice* is concentric with the pipe. The segmental portion of the orifice eliminates damming of foreign materials on the upstream side of the orifice when mounted in a horizontal pipe. Depending on the type of fluid, the segmental section is placed on either the top or the bottom of the horizontal pipe to increase the accuracy of the measurement. The orifice hole is placed at the bottom for gas service and top for liquids. These kinds of orifice plates are used for measurements where solids are entrained in gas or liquid flow streams. Industries using these orifice plates include sewage treatment, steel, water conditioning, paper and petrochemical (McNally Institute, 2010).
- *Eccentric orifices plates* shift the edge of the orifice to the inside of the pipe wall. This design also prevents upstream damming. The eccentric orifice plate normally is inscribed in a circle that is 98% of the pipe diameter, so the solids or slurries may pass through. The orifice hole is placed at the bottom for gas service and top for liquids. Eccentric orifice plates are used in many industries, including heavy and light chemicals, steel, paper, atomic and petrochemicals (McNally Institute, 2010).

2.2.5.3. Fractal shaped orifice

In many cases where orifice plates are used as flow meters, the pressure drop element is simply a flat metal plate with an orifice; most of these orifices are of the circular type. Recently industry has seen some application of fractals where fractal-shaped objects were used to enhance the distribution of fluid in the molasses chromatography process for controlling exhaustion and regeneration in thin juice ion exchange and for providing uniform air circulation in a sugar silo (Abou El-Azem Aly et al., 2010). Because of the complexities in manufacturing fractal-shaped orifices and associated difficulties in the set up process and the control of the measured flow parameters, limited experimental studies are available. The construction of a fractal-shaped orifice is based on the curve of Von Koch (1904).

Created in 1904, the curve of Von Koch is still today one of the most popular fractal curves. The Von Koch curve can be constructed by starting with an equilateral triangle, then recursively altering each line segment as follows:

1. divide the line segment into three segments of equal length,
2. draw an equilateral triangle that has the middle segment from step 1 as its base and points outward,
3. remove the line segment that is the base of the triangle from step 2.

After one iteration of this process, the result is a shape similar to the Star of David.

Its three first generations are shown in Figure 2.9 below (Von Koch, 1904).

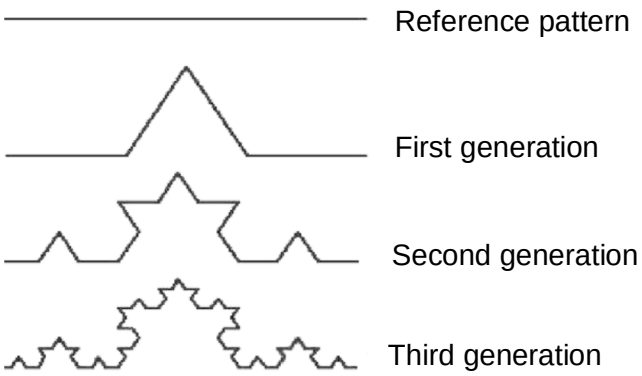

Figure 2.9: Construction of the Von Koch curve

Figure 2.10 shows different generations of fractal-shaped orifice plates, from first generation to third generation with its flow area and equivalent regular circular orifice.

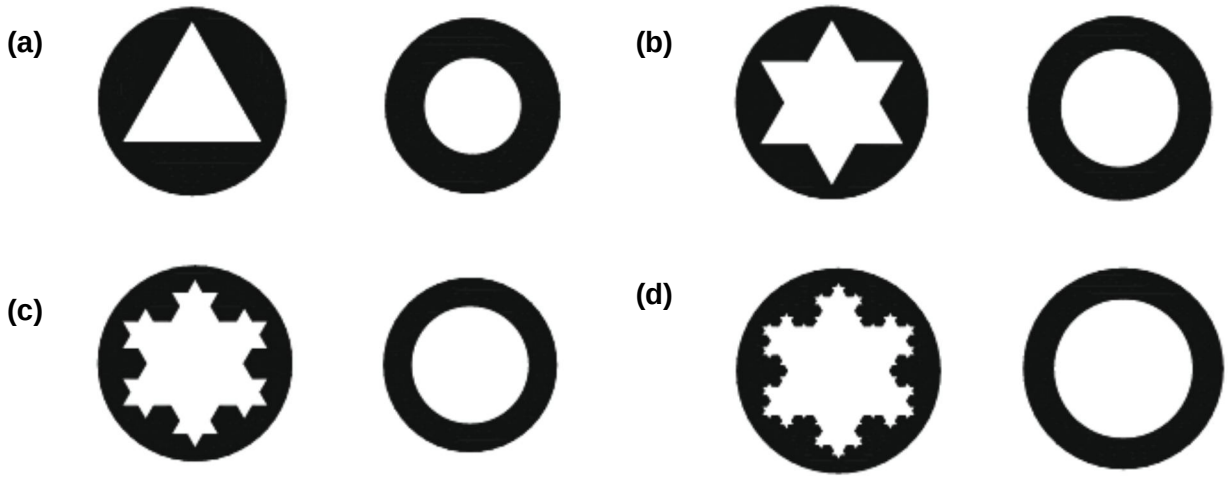

Figure 2.10 : Different generations of fractal-shaped orifices based on of flow area of the equivalent circular orifice (Abou El-Azem Aly et al., 2010)

2.2.6 Application of orifice plates

Although mainly used as a flow measurement device, there are several other reasons to install a restrictive device such as an orifice plate in a piping system. Some orifice applications are given below (McNally Institute, 2010):

- To create a false head for a centrifugal pump, allowing the pump to run at its BEP (Best Efficiency Point).
- To increase the line pressure.
- To decrease the flow through the line.
- To increase the fluid velocity in a line.

2.2.7 Advantages and disadvantages of orifice plates

The advantages and disadvantages of orifice plates are listed below.

2.2.7.1 Advantages

Orifice plates have been used for many years as accepted devices for bulk flow measurement in a variety of industries (Morrison et al., 1990). The major advantage of using these orifice flow meters, according to Abou El-Azem Aly et al. (2010), is that they have:

- simple geometry
- no moving part
- no lubrication or maintenance
- low cost of manufacturing which does not increase significantly with the pipe size
- easy installation or replacement
- the ability to select a proper calibration on the basis of the measurement of the geometry.

2.2.7.2 Disadvantages

Orifice plates have some disadvantages:

- They cause a high permanent pressure drop; the outlet pressure will be 60% to 80% of inlet pressure.
- They are subject to corrosion, which will eventually cause inaccuracies in the measured differential pressure.
- Orifice plate includes the long, straight pipe length requirement.

2.3 LOSSES THROUGH ORIFICE PLATES

2.3.1 Pressure loss coefficient

Normally the head losses through fittings such as orifice plates are considered minor losses and the losses from the friction in straight pipes, major losses. Minor losses may be ignored when there is a length of 1 000 diameters between each minor loss source on average (Streeter & Wylie, 1975). However, in short pipe systems, attention must be given as the so-called minor losses may outweigh the major losses (Miller, 1990).

Figure 2.11 shows the intensity of disturbance in the fluid introduced by reason of its passage through the fittings. At point M and Q, the velocity profile and the pressure gradients are fully developed. At point N this is not the case; the velocity profile and the pressure gradient are dependent on location.

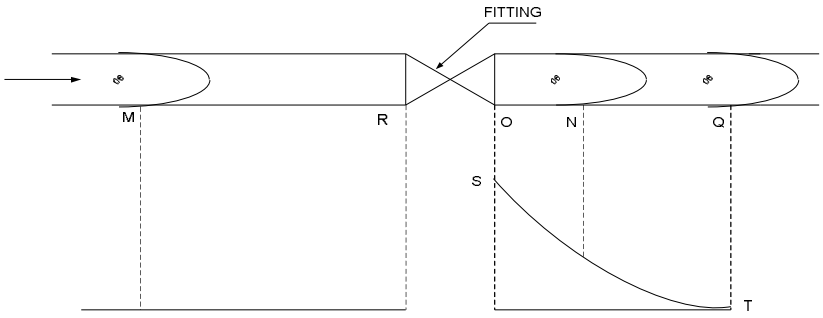

Figure 2.11 : Flow distribution due to passage through fittings (Beck, 1944)

In fact, to summarise, the loss produced by a fitting (Beck, 1944) consists of:

- Pressure drop within the fitting itself.
- Pressure drop in the upstream piping in excess of that which would normally occur if there were no fitting on line. This effect is small.
- Pressure drop in the downstream piping in excess of that normally occurring if there was no fitting in line. This effect may be comparatively large.

Miller (1990) defines the pressure loss coefficient as a non-dimensionless difference in overall pressure between the ends of two long straight pipes where there are no fittings, and when the real fitting is installed as shown in Figure 2.12.

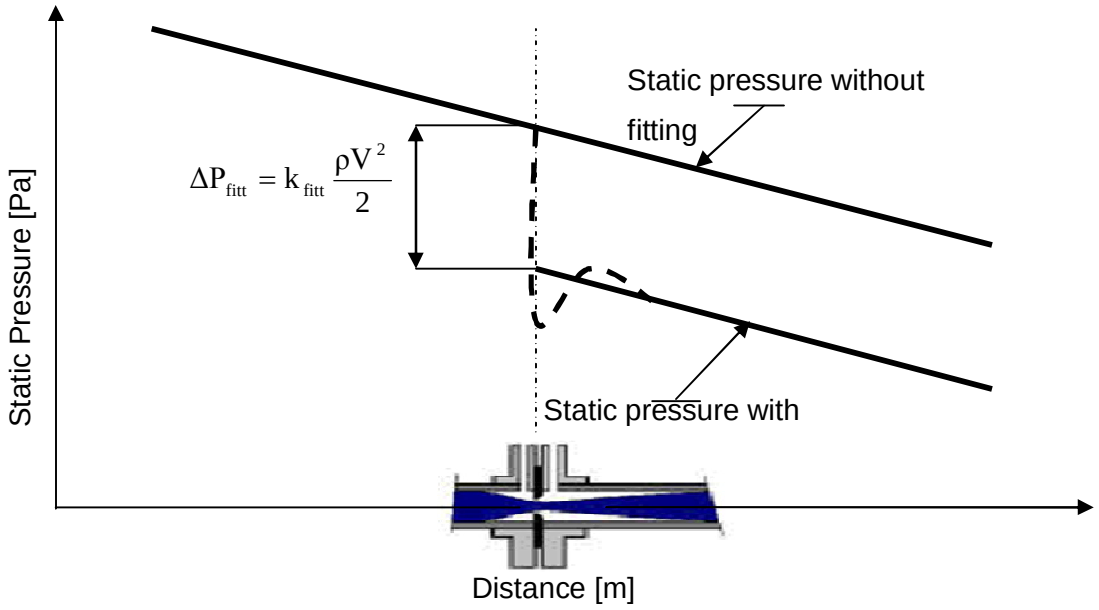

Figure 2.12 : Definition of the loss coefficient (Miller, 1990)

The fundamental equation governing the mechanics of fluids and deformable bodies is obtained from the principles of conservation.

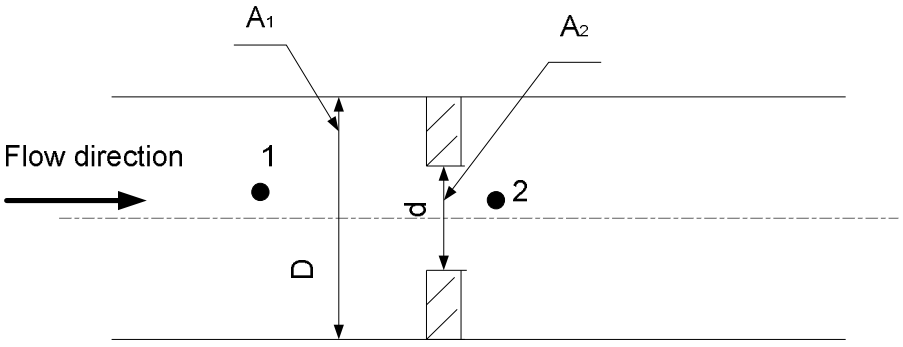

Figure 2.13 : Schematic of short orifice plate inserted in a straight pipe

The law of conservation of energy applied to a fluid under the condition of steady, uniform flow requires the total energy to remain constant. Therefore the sum of the potential energy, pressure energy, internal energy, and kinetic energy upstream of the orifice plate, must equal the sum of the potential energy, pressure energy, internal energy, and kinetic energy

downstream of the orifice plate, assuming that no heat has been added or lost (Murdock, 1976). In real fluids, the total energy of a streamline does not remain constant. As the fluid passes through an orifice plate between 1 and 2 as given in Figure 2.13, the velocity of the fluid must increase through the orifice. This increase in kinetic energy must be accompanied by a decrease in another form of energy. The loss of energy is indicated by the decrease of static pressure or differential pressure (Husain, 1995). The energy equation may be written as follows where the energy head lost through friction is denoted by $loss_{1\text{-}2}$ (Chadwick et al., 2004).

$$\frac{P_1}{\rho g} + \frac{V_1^2}{2g} + Z_1 = \frac{P_2}{\rho g} + \frac{V_2^2}{2g} + Z_2 + loss_{1-2} \qquad \text{Equation 2.4}$$

where $loss_{1-2}$ represents the sum of head losses upstream H_1, downstream H_2 and the head loss across H_{or} the orifice plate.

Many methods can lead to quantify head losses through fittings such as orifice plates, but it is important to mention that Equation 2.5 is extensively used.

$$H_{or} = k_{or}\frac{V_1^2}{2g} \qquad \text{Equation 2.5}$$

where k_{or} is called pressure loss coefficient or flow resistance coefficient.

$$k_{or} = H_{or}\frac{2g}{V_1^2} \qquad \text{Equation 2.6}$$

The orifice pressure loss coefficient can be obtained in terms of pressure drop by:

$$k_{or} = \frac{\Delta P_{or}}{\frac{1}{2}\rho V_1^2} \qquad \text{Equation 2.7}$$

Alternatively, the pressure loss coefficient can be expressed as a function of orifice plate bulk-mean velocity V_2, which is also referred to as the Euler number (ESDU, 2007).

$$Eu = \frac{\Delta P}{\frac{1}{2}\rho V_2^2} = \beta^4\frac{\Delta P}{\frac{1}{2}\rho V_1^2} = \beta^4 k_{or} \qquad \text{Equation 2.8}$$

Two methods can be used to calculate the loss coefficient: including or excluding the length of the fitting.

When the length of the fitting is included in the calculation of the loss coefficient, k_{fitt} is called k_{net}, and is obtained using the relation below (Turian et al., 1998):

$$k_{net} = \frac{1}{\frac{\rho V^2}{2}}\left[\Delta P - \frac{\rho V^2}{2}\frac{4f}{D}(L_u + L_{fitt} + L_d)\right] \quad \text{Equation 2.9}$$

where, L_u is the upstream length

L_{fitt} is the fitting length

L_d is the downstream length.

When the length of fitting is excluded in the calculation of the loss coefficient, k_{fitt} is called k_{gross} that can be obtained using Equation 2.9 (Turian et al., 1998):

$$k_{gross} = \frac{1}{\frac{\rho V^2}{2}}\left[\Delta P - \frac{\rho V^2}{2}\frac{4f}{D}(L_u + L_d)\right] \quad \text{Equation 2.10}$$

Most fittings have a physical length except for abrupt contractions and expansions. However, for a short orifice plate, the thickness of the orifice, which is its length, is negligible.

2.3.2 Determination of pressure loss coefficient

Two methods are generally used in the determination of fittings or orifice plate loss coefficients: the total pressure drop method and the hydraulic grade line (HGL). The two methods are based on the same principle for 1D flow.

The determination of the loss coefficient through fittings using the total pressure drop was used by Turian et al. (1998) and Pienaar (1998). Two pipes in series were joined by a fitting. This method consists of measuring the pressure drop between two points in the region of fully developed flow in a straight pipe across the fitting. Thus, by estimating the frictional losses in the straight pipe sections, the fitting loss can be determined from the measured pressure drops.

The hydraulic grade line approach (HGL) was used by Humpherys (1987) for the determination of pressure drop across the orifice plate in irrigation pipelines. Edwards et al. (1985) used the HGL approach to determine the pressure loss coefficient of different fitting such as: elbows, gate valves, globe valves, sudden expansions, sudden contractions and orifice plates. Baudouin (2003) used the HGL approach for the determination of loss coefficient in sudden contractions.

Banerjee et al. (1994), and Kabwe et al. (2010) used the hydraulic grade line approach for the determination of loss coefficients in valves.

The HGL approach consists of measuring and plotting the static pressure gradients upstream and downstream of the orifice plate in the region of the fully developed flow far from the orifice plane to avoid disturbances of the flow due to the presence of an orifice plate.

In this work, the hydraulic grade line approach will be used for the determination of loss coefficients. The method is briefly explained using the diagram shown in Figure 2.14.

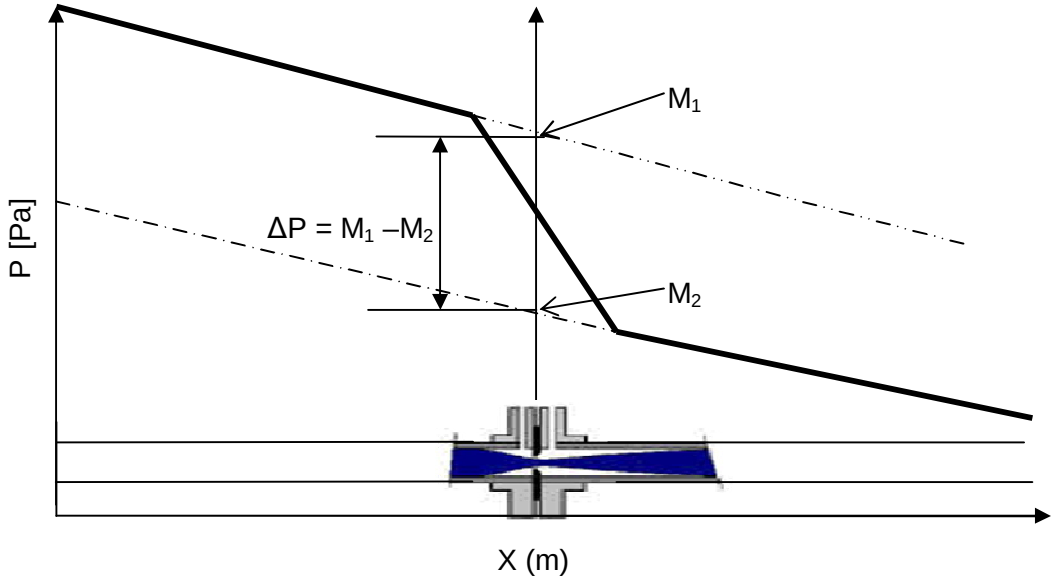

Figure 2.14 : Calculation of orifice loss coefficient

Static pressures (P) versus axial distance (X) points of coordinates (Pi, Xi) are plotted on a graph from the experimental data. The curves of static pressure drop follow a linear law and are straight lines up to a certain point near the orifice as shown in Figure 2.14, for the two pipes upstream and downstream of the orifice plate.

The coordinates of the points upstream of the orifice plate, which is the y-axis in this case, are used to calculate by linear regression the slope m_1 and intercept M_1 of the line upstream. The coordinates of the points downstream of the orifice plate are used to calculate, also by linear regression, the slope m_2 and intercept M_2 of the line downstream of the orifice plate. The pipes upstream and downstream of the orifice plate have the same diameters; the two hydraulic grade

lines upstream and downstream of the orifice plate have the same slopes; m_1 and m_2 are equal; and the pressure drop due to the orifice is given by:

$$\Delta P = M_1 - M_2 \qquad \text{Equation 2.11}$$

The pressure drop determined from Equation 2.11 can therefore be substituted in Equation 2.7 to calculate the pressure loss coefficient. The velocity of the fluid will be deduced from the flow rate of the fluid as the area of the duct is known.

2.3.3 Discharge coefficient

The knowledge of the discharge coefficient is an important aspect in the design of an orifice meter. This is possible only when the flow characteristics around the orifice plate are known (Sahin & Ceyhan, 1996). The discharge coefficient for an orifice plate is defined as the ratio of actual flow rate, Q_{actual}, to the maximum theoretical volume flow rate, $Q_{theoretical}$ (ESDU, 2007).

$$C_d = \frac{Q_{actual}}{Q_{theoretical}} \qquad \text{Equation 2.12}$$

The base flow may be described by using the laws of conservation of mass and momentum by assuming:

- One-dimensional axial flow.
- Constant static pressure at a certain section upstream of the orifice plate and at the plane of the *vena contracta*.

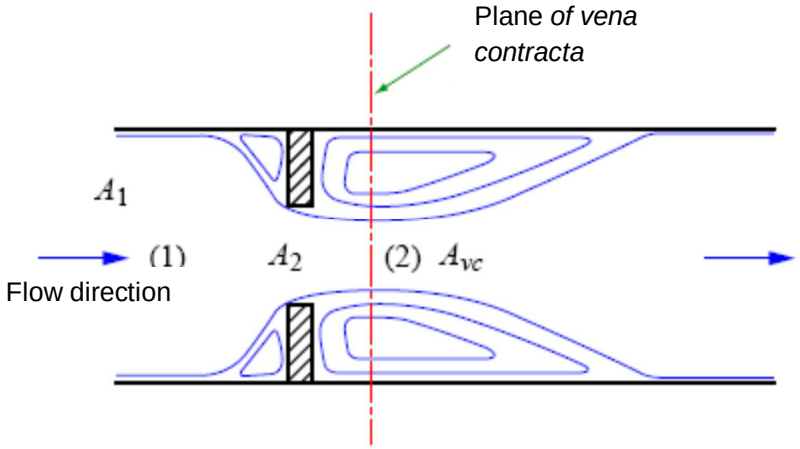

Figure 2.15 : Definition of discharge coefficient (ESDU, 2007)

From conservation of mass, it known that the mass flow through the pipe will be equal to the mass flow through the orifice plate.

The conservation of energy may be applied using a number of assumptions to the Bernoulli equation:

$$P_1 + \frac{1}{2}\rho V_1^2 = P_2 + \frac{1}{2}\rho V_2^2 \qquad \text{Equation 2.13}$$

For incompressible flow, the density of the fluid does not change significantly. In order to express the pressure drop across the orifice plate in terms of velocity and fluid density, the conservation of momentum equation is rearranged.

$$P_1 - P_2 = \frac{\rho}{2}(V_2^2 - V_1^2) = \frac{\rho V_2^2}{2}\left[1 - \left(\frac{V_1}{V_2}\right)^2\right] \qquad \text{Equation 2.14}$$

From conservation of mass, it is known that the ratio of the velocities is inversely proportional to the cross-sectional area ratio,

$$\frac{V_1}{V_2} = \frac{A_2}{A_1} \qquad \text{Equation 2.15}$$

Substitution of Equation 2.15 in Equation 2.14 gives:

$$V_2 = \sqrt{\frac{2(P_1 - P_2)}{\rho\left[1 - \left(\frac{A_2}{A_1}\right)^2\right]}} \qquad \text{Equation 2.16}$$

The pressure drop across the orifice plate, ΔP, is $P_1 - P_2$. It is known that $\left(\frac{A_2}{A_1}\right)^2 = \left(\frac{d}{D}\right)^4 = \beta^4$; therefore, $Q_{theoritical}$ is given:

$$Q_{\text{theoritical}} = \frac{\frac{\pi}{4}d^4}{\sqrt{1-\beta^4}}\sqrt{\frac{2\Delta P}{\rho}} \qquad \text{Equation 2.17}$$

Substitition of Equation 2.17 into Equation 2.12 gives:

$$C_d = \frac{Q_{\text{actual}}}{\frac{\pi}{4}d^2}\sqrt{1-\beta^4}\sqrt{\frac{\rho}{2\Delta P}} \qquad \text{Equation 2.18}$$

Therefore, the actual flow rate can be expressed as:

$$Q_{actual} = \frac{C_d \frac{\pi}{4} d^2}{\sqrt{1-\beta^4}} \sqrt{\frac{2\Delta P}{\rho}}$$ Equation 2.19

The parameter $\sqrt{1-\beta^4}$ is also known as the velocity of approach factor.

2.3.4 Methodology to determine discharge coefficient

The flow coefficient or the discharge coefficient, is always influenced by the location of the pressure taps. The value of the discharge coefficient must be consistent with the location of the pressure taps. Different types of pressure tap arrangements are used to measure pressure drop across the orifice plate in order to determine discharge coefficient. Among them, the following pressure tapping arrangements can be cited (ESDU, 2007):

- flange taps
- corner taps
- D and D/2 taps
- *vena contracta* taps
- pipe taps

With the exception of pipe taps, it is important to know that pressure tap arrangements for the determination of the discharge coefficient are not appropriate for the determination of the pressure loss coefficient. The reason is that it measures the largest pressure drop, but at the same time do not allow sufficient length downstream of the orifice plate for pressure recovery. Discharge coefficient data are mainly determined empirically and depend on a number of factors, such as (ESDU, 2007):

- geometry of the orifice plate
- the pipe Reynolds number
- tap location, pipe diameter
- diameter ratio

In this work only flange tapping and D and D/2 tapping arrangements will be used for the determination of the discharge coefficient.

2.3.4.1 Flange tapping arrangements

The spacing L1 shown in Figure 2.16 is the distance between the centreline of the upstream pressure tapping and the upstream face of the orifice. The spacing L2 of the downstream

pressure tapping is measured from the downstream face of the orifice plate. Flange tapping arrangements may produce errors in the pressure drop measurement. Measurements at low differential pressure, ΔP, produce inaccuracies due to fluctuations in the differential pressure caused by turbulent dynamic of properties of the flow. Flange pressure taps do not take into account variation of the orifice plate geometry, and the measurement may be taken at locations where the static pressure gradients are significant (ESDU, 2007).

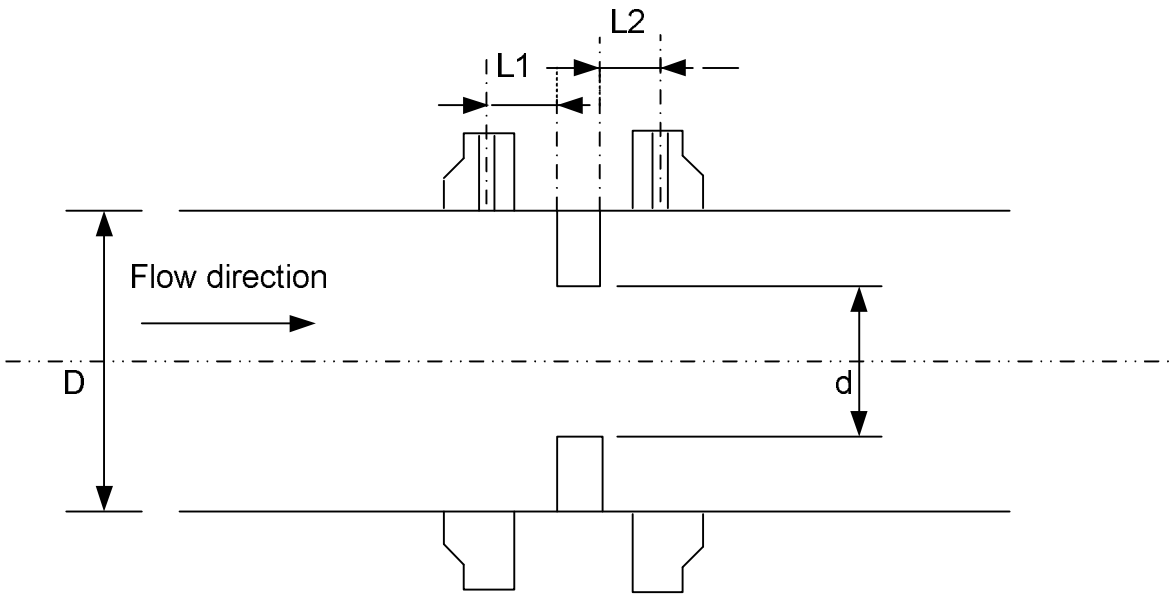

Figure 2.16 : Flange tapping arrangements

2.3.4.2 D and D/2 tapping arrangements

The spacing L1 shown in Figure 2.17 is the distance between the centreline of the upstream pressure tapping and the upstream face of the orifice plate, but the spacing L2 is the distance between the centreline of the downstream tapping and the upstream face of the orifice plate. The dimensions for the D and D/2 tapping arrangements do not depend on the geometry of the orifice plate. Therefore the D and D/2 tapping arrangement is considered the most reliable (ESDU, 2007).

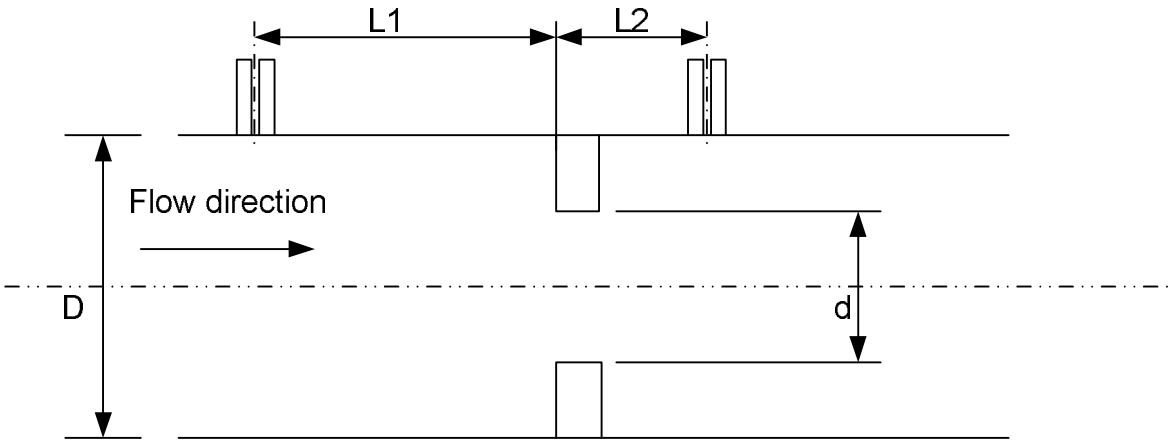

Figure 2.17 : D and D/2 tapping arrangements

The details of standard tap location from ISO (2002), ASME (2004) and ANSI/API (1995) are given in Table 2.1.

Table 2.1: Details of standard tap location

Tap arrangements	ASME MFC-3M	ISO 5167	ANSI/API 2530
Flange	L1 = 25.4 mm ± 0.5 mm $\beta > 0.6$ and D<150 mm L2 = 25.4mm ± 1 mm (β <0.6)	L1= 25.4 mm ± 0.5 mm $\beta > 0.6$ and D < 150 mm L2 = 25.4 mm ± 1 mm (β <0.6 β)	L1 = 25.4 mm ± 1.588 mm $\beta \leq 0.6$ and D ≤ 101.6 mm L2 = 25.4 mm ± (5.956-6.951β) for $0.4 < \beta \leq 0.75$
D and D/2	**L**1 = D ± 0.1 D L2 = 0.5 D ± 0.02 D for $\beta \leq 0.6$ L2 = 0.5 D ± 0.01 D for $\beta > 0.6$	L1 = D ± 0.1 D L2 = 0.5 D ± 0.02 D for $\beta \leq 0.6$ L2 = 0.5 D ± 0.01 D for $\beta > 0.6$	

2.3.5 Pipe length requirements

The fluid entering the orifice plate has to conform to certain requirements in order to ensure that flow measurements are within the accuracy required by the standards. The fluid must have an axisymetric, swirl-free and fully developed flow profile (ESDU, 2007). These conditions are achieved using adequate lengths of upstream and downstream pipes and flow conditioners.

2.4 CLASSIFICATION OF FLUIDS

There are two different ways to classify fluids: one according to their response to external applied pressure and the other to their effect under the action of shear stress (Chhabra & Richardson, 1999). Fluids can also be compressible or incompressible but in this thesis, only incompressible fluids will be treated. The flow characteristics of single-phase liquids, solutions and pseudo-homogenous mixtures (such as slurries) which may be treated as a continuum if they are stable in the absence of turbulent eddies are considered depending upon their response to externally imposed shearing action (Chhabra & Richardson, 1999). In general fluids belong to one of the two main categories - Newtonian fluids or non-Newtonian fluids.

2.4.1 Newtonian fluids

A Newtonian fluid is a fluid where a linear relationship between components of stress and rate of deformation tensors exists (Malkin, 1994). The complete definition of a Newtonian fluid is that it possesses not only a constant viscosity, but when the shear stress is plotted versus rate of strain; the curve is linear and passes through the origin of the co-ordinates (Chhabra & Richardson, 1999). The coefficient of viscosity, determined as a ratio of shear stress to shear rate of deformations, does not depend on conditions of flow. Note that the graphs plotting shear rate to shear stress are called rheograms (Liu, 2003). The general curve of a Newtonian fluid is shown in Figure 2.18:

A Newtonian fluid can be represented by the equation below,

$$\tau_0 = \mu_n \dot{\gamma} \qquad \text{Equation 2.20}$$

where is τ the shear stress, μ_n the viscosity and $\dot{\gamma}$ the shear rate.

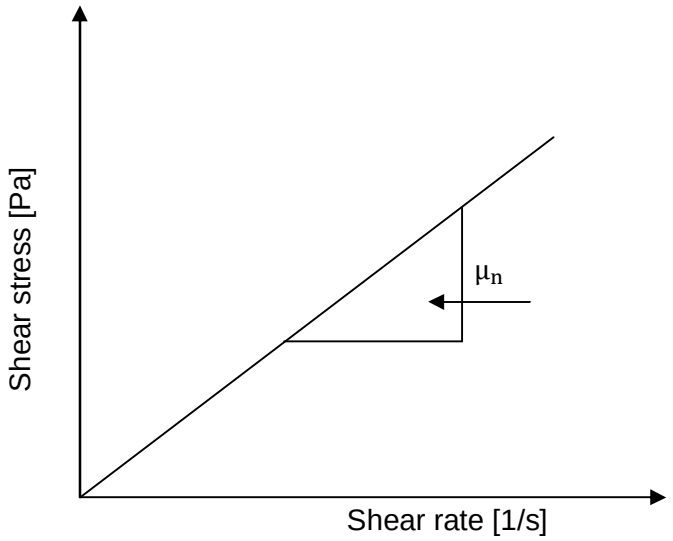

Figure 2.18 : Rheogram of Newtonian fluid

The viscosity represents the slope of the straight line in any rheogram of Newtonian fluid. The higher the viscosity of a fluid, the steeper the slope in the rheogram becomes (Liu, 2003) as shown in Figure 2.19.

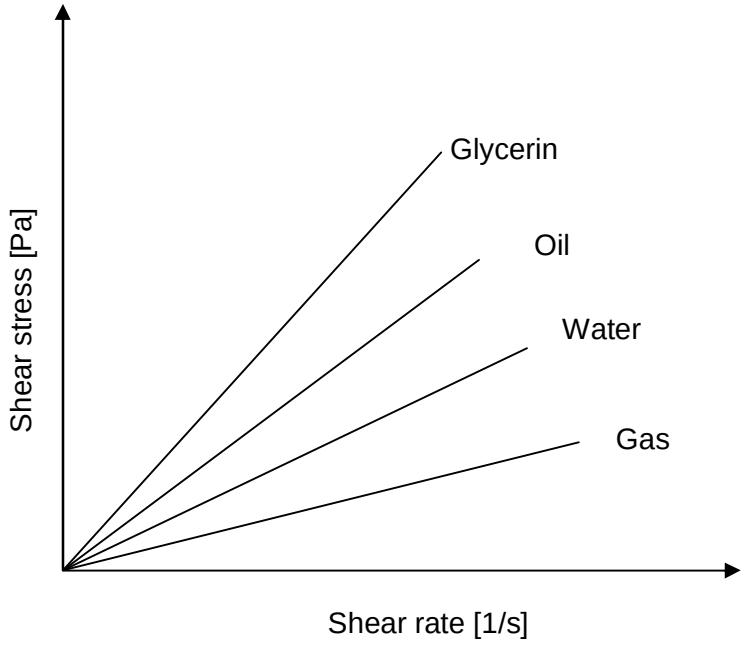

Figure 2.19 : Rheogram of various Newtonian fluids

2.4.2 Non-Newtonian fluids

A non-Newtonian fluid is characterised by the fact that the relationship between shear stress and shear rate is not a linear curve or does not pass through the origin (Chhabra & Richardson, 1999). This relationship is more complex and requires more than one parameter to be described. It means that the apparent viscosity, which expresses the ratio between shear stress and shear rate, is not constant at a given temperature and pressure but depends on flow conditions (Chhabra & Richardson, 1999).

Non-Newtonian fluids may be conveniently grouped into three general classes:

- Time-independent fluids
- Time-dependent fluids
- Visco-elastic fluids

Real non-Newtonian fluids often exhibit a combination of two or even three types of non-Newtonian fluid features indicated above. However, it is possible to identify the dominant non-Newtonian characteristics and to take these as the basis for the subsequent process calculation (Chhabra & Richardson, 1999).

2.4.2.1 Time-independent non-Newtonian fluids

Time-independent non-Newtonian fluids may be described by this form of relation (Chhabra & Richardson, 1999),

$$\dot{\gamma} = f(\tau_0) \qquad \text{Equation 2.21}$$

The inverse can be also considered, and is given by:

$$\tau_0 = f_1(\dot{\gamma}) \qquad \text{Equation 2.22}$$

According to the above equations, time-independent non-Newtonian fluids are fluids whose shear rate at any point is determined only by the value of shear stress at that point or vice versa. These fluids may be subdivided further into three types:

2.4.2.1.1 Pseudoplastic or shear-thinning fluids

A pseudoplastic fluid is a non-Newtonian fluid characterised by an apparent viscosity which decreases with the increasing shear rate. This common type of non-Newtonian fluid behaviour observed is shear-thinning (Chhabra & Richardson, 1999).

Among many mathematical expressions which can model a shear-thinning fluid, a power-law model can easily and simply express mathematically pseudoplastic behaviour. The relationship between shear rate and shear stress in the power model is given by the equation below (Chhabra & Richardson, 1999).

$$\tau_0 = K(\dot{\gamma})^n \qquad \text{Equation 2.23}$$

From Equation 2.23, the apparent viscosity of the fluids is thus given by:

$$\mu = \frac{\tau_0}{\dot{\gamma}} = K(\dot{\gamma})^{n-1} \qquad \text{Equation 2.24}$$

K and n are two empirical curve fitting parameters. K is known as the fluid consistency coefficient and n as the flow behaviour index.

If n < 1, the fluid exhibits shear-thinning properties

n = 1, the fluid shows Newtonian behaviour

n > 1, the fluid shows shear-thickening behaviour.

Sometimes there are significant deviations from the power-law model at very high and very low shear rates; in these cases it is necessary to use the model that takes account of limiting values of the viscosities μ_0 and μ_∞ (Chhabra & Richardson, 1999).

2.4.2.1.2 Viscoplastic fluids

The yield stress (τ_y) characterises this kind of fluid behaviour. Yield stress is a force that must be exceeded before the fluid will deform or flow. A viscoplastic fluid displays also an apparent viscosity which decreases with increasing shear rate (Chhabra & Richardson, 1999). The flow curve will therefore not pass through the origin but may be linear or non-linear. It is very important to note that a viscoplastic material also displays an apparent viscosity, which decreases with increasing shear rate for yield pseudo plastic fluids only, and is constant for Bingham plastic fluids (Chhabra & Richardson, 1999).

a) The Bingham plastic model (BP)

Bingham plastic is characterised by a constant plastic viscosity and yield stress. The plastic viscosity is the slope of the shear stress versus the shear rate curve. The Bingham plastic model is described by the equation 2.25 (Chhabra & Richardson, 1999).

$$\tau_0 = \tau_y + \mu_B(\dot{\gamma})$$ Equation 2.25

b) Yield pseudoplastic fluid model

This model of viscoplastic fluids possesses a yield stress and a non-linear flow curve on linear coordinates. The yield pseudoplastic fluids can be described by the Herschel-Bulkley model shown in equation 2.26 (Chhabra & Richardson, 1999).

$$\tau_0 = \tau_y + K(\dot{\gamma})^n$$ Equation 2.26

Figure 2.20 presents different time-independent fluids flow curves for easy comparison.

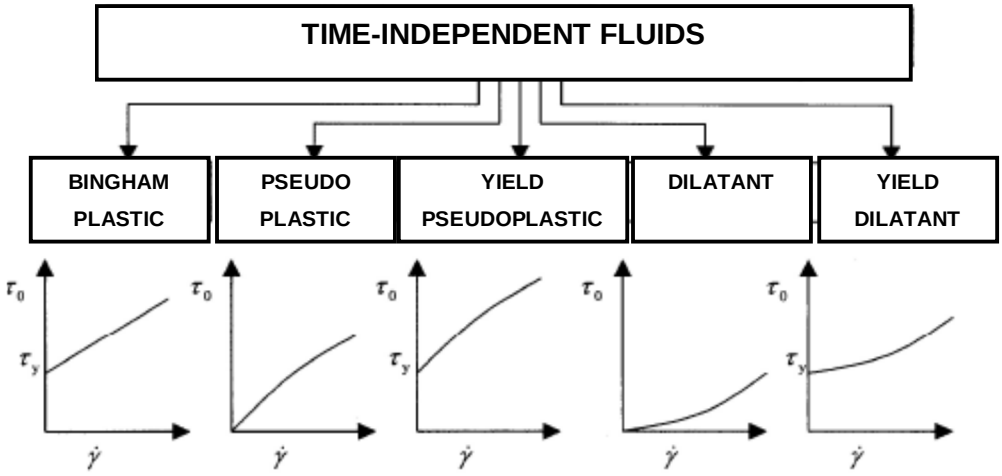

Figure 2.20 : Rheogram of time-independent fluids (Paterson & Cooke, 1999)

2.4.2.2. Time-dependent fluids

Apparent viscosities of non-Newtonian fluids may depend not only on the rate of shear but also on the time for which the fluid has been subjected to shearing (Chhabra & Richardson, 1999). There are some fluids that when sheared at a constant rate following a long period of rest, their apparent viscosities gradually become less as the internal structure of the material is progressively broken down. This category of non-Newtonian fluids can be subdivided into two groups:

2.4.2.2.1. Thixotropic fluid

When a material is sheared at a constant rate and the apparent viscosity decreases with the time of shearing, this material exhibits thixotropic behaviour (Chhabra & Richardson, 1999). If the flow curve is measured in a single experiment in which the shear rate is steadily increased at a constant rate from zero to some maximum value and then decreased at the same rate to

zero again, a hysteresis loop of the form is observed (Chhabra & Richardson, 1999). There is no hysteresis loop observed for time-independent fluids.

2.4.2.2.2. Rheopectic fluids

Rheopexy is also called negative thixotropy, because conversely to thixotropic fluids, the apparent viscosity or the corresponding shear stress of rheopectic fluids increases with time of shearing. In this case the hysteresis loop observed is inverted, as compared with a thixotropic material (Chhabra & Richardson, 1999).

Figure 2.21 presents different time-dependent fluids flow curves for easy comparison.

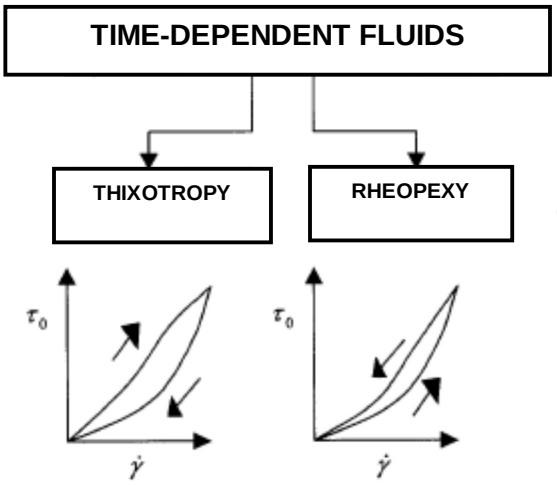

Figure 2.21 : Rheogram of time-dependent fluids (Paterson & Cooke, 1999)

2.4.2.3 Visco-elastic fluids

Many materials show both elastic and viscous effects under appropriate circumstances. The theory of elasticity states that the stress in a sheared body is directly proportional to strain. for tension, Hook's law applies and the coefficient of proportionality is known as Yung's modulus, G

$$\tau_0 = -G\frac{du}{dr} = G(\dot{\gamma}) \qquad \text{Equation 2.27}$$

where dx is the shear displacement of two elements separated by a distance dy.

When a perfect solid is deformed elastically, it regains its original form on removal of the stress. However, if the applied stress exceeds the characteristic yield stress of the material, complete recovery will not occur and creep will take place (Chhabra & Richardson, 1999).

2.4.3 Settling slurries

Settling slurries are pseudo-homogeneous mixtures where particles in suspension settle quickly relative to their residence time in the pipeline (Heywood & Brown, 1991). It can be said in other words, that a mixture in which solid and liquid phases are separated and the liquid properties are generally considered to be unaltered by the presence of solids. When transported in a pipeline, particles are supported by turbulent mixing and antiparticle collisions (Paterson & Cooke, 1999).

2.5 FLOWS THROUGH STRAIGHT PIPES

2.5.1 Introduction

The understanding of flow through straight pipes is very important in the determination of pressure loss coefficients in orifice plates and fittings. When considering a fluid flowing through a pipe, the flow may be laminar or turbulent, depending on the value of the Reynolds number. It has been experimentally proved that these two types of flow are fundamentally different in several aspects such as the velocity distribution and the flow resistance (Massey, 1975). This section will therefore discuss the relevant theories for determining frictional pressure loss in a straight pipe.

2.5.2 Shear stress distribution in pipe

It can be demonstrated from the force balance that in a pipe, the shear stress follows a linear law given by Equation 2.28, when the flow is fully developed and steady.

$$\tau_0 = \frac{r}{2}\frac{\Delta P}{L} \qquad \text{Equation 2.28}$$

where ΔP is the pressure gradient in the portion of a straight pipe of length L and the radial distance r (Chhabra & Richardson, 1999).

The shear stress distribution across the pipe cross-section is zero at the axis of the tube and maximum at the wall of the pipe as shown in Figure 2.22 below (Chhabra & Richardson, 1999).

$$\tau_0 = \frac{D\,\Delta P}{4L} \qquad \text{Equation 2.29}$$

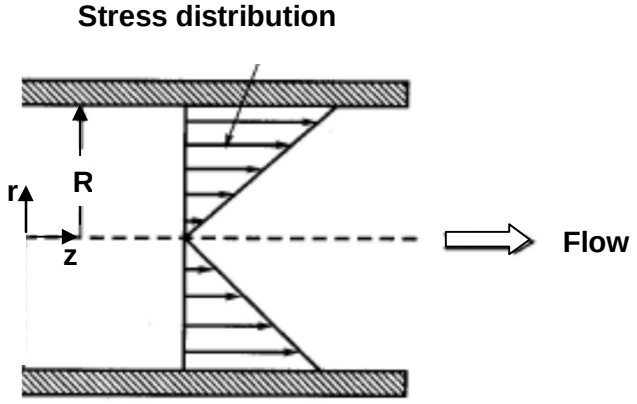

Figure 2.22 : Shear stress distribution (Chhabra & Richardson, 1999)

Note that Equation 2.29 is applicable to both laminar and turbulent flow of any fluid since it is based on a simple force balance (Chhabra & Richardson, 1999).

2.5.3 Laminar flow of Newtonian fluids in a straight pipe

2.5.3.1 Velocity distribution

In laminar flow, the velocity distribution of Newton fluids follows a parabolic law. The maximum velocity is attained at the pipe centre, decreasing gradually toward the pipe wall where it reaches zero (Massey, 1990), as shown in Figure 2.23. The velocity distribution is given by the equation below:

$$u = \frac{\tau_0}{2R\mu}(R^2 - r^2) \qquad \text{Equation 2.30}$$

where u is maximum at the centre of the pipe where r = 0 and is given by:

$$u_{max} = \frac{\tau_0 R}{2\mu} \qquad \text{Equation 2.31}$$

The mean velocity which is the average velocity is exactly half of the maximum velocity at the centre of the pipe and is:

$$V = \frac{u_{max}}{2} \qquad \text{Equation 2.32}$$

Replacing Equation 2.31 into Equation 2.32, the equation becomes:

$$V = \frac{\tau_0 R}{4\mu} \qquad \text{Equation 2.33}$$

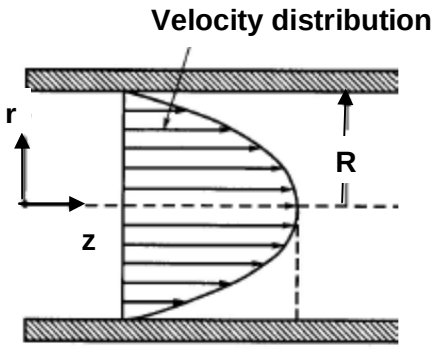

Figure 2.23 : Velocity distribution (Chhabra & Richardson, 1999)

2.5.3.2 Hagen-Poiseuille Formula

For an incompressible Newtonian fluid in laminar flow, the discharge through a pipe section of diameter D and length L, where a pressure difference ΔP exists, is given by Equation 2.34 (Massey, 1975).

$$Q = \frac{\pi D^4}{128\mu}\frac{\Delta P}{L} \qquad \text{Equation 2.34}$$

2.5.3.3 Friction factor

Normally the friction factor is dependent on both the Reynolds number and the pipe wall roughness. But in Newtonian laminar flow, the pipe wall roughness has no effect on the friction factor and the friction factor is given by Massey (1990):

$$f = \frac{16}{Re} \qquad \text{Equation 2.35}$$

2.5.4 Laminar flow of non-Newtonian fluids in a straight pipe

2.5.4.1 Shear stress and velocity distribution

Laminar flow for non-Newtonian fluids is characterised by the fact that the relationship of the shear stress arising from the friction between layers is not a linear curve starting at zero, as for Newtonian fluids (Chhabra & Richardson, 1999).

Considering the general equation which represents a general rheogram for pseudoplastic fluids:

$$-\frac{du}{dr} = f(\tau) \qquad \text{Equation 2.36}$$

The velocity distribution is obtained by integrating the above Equation 2.36 as follows:

$$du = -f(\tau)dr \qquad \text{Equation 2.37}$$

$$u = \int -f(\tau)dr + C \qquad \text{Equation 2.38}$$

Using the first boundary condition of no slip at pipe wall, the constant of integration can be evaluated.

Integrating the velocity profile over the cross section with respect to the usual boundary condition for pipe flow, we can obtain the flow rate as:

1. At r = R u = 0 (no slip at the pipe wall)
2. At r = 0, the slope of the velocity distribution is zero at the pipe centre line

$$Q = 2\pi \int_0^R urdr \qquad \text{Equation 2.39}$$

From the balance over a cylindrical control volume results:

$$\frac{r}{R} = \frac{\tau}{\tau_0} \qquad \text{Equation 2.40}$$

$$dr = \left(\frac{R}{\tau_0}\right)d\tau \qquad \text{Equation 2.41}$$

$$r^2 = \frac{\tau^2}{\tau_0^2}R^2 \qquad \text{Equation 2.42}$$

The flow rate will be given by the following equation:

$$Q = \frac{\pi R^3}{\tau_0^3}\int_0^{\tau_0} \tau^2 f(\tau)d\tau \qquad \text{Equation 2.43}$$

It is known that $R = \frac{D}{2}$ and $Q = VA$, thus:

$$\frac{32Q}{\pi D^3} = \frac{8V}{D} = \frac{4}{\tau_0^3}\int_0^{\tau_0} f(\tau)d\tau \qquad \text{Equation 2.44}$$

For a yield pseudoplastic fluid, in the laminar flow regime, the flow presents two zones, the core zone where the fluid is unsheared and moves as a solid plug and the annulus zone, where the fluid is sheared (Slatter, 1994).

The velocity distribution can be obtained by integrating the constitutive equation of the model of the fluid which is the Herschel-Bulkley model.

$$\tau = \tau_y + K\left(-\frac{du}{dr}\right)^n \qquad \text{Equation 2.26}$$

From equation 2.26 above, the following equation can be derived:

$$f(\tau) = -\frac{du}{dr} = \left(\frac{1}{K}\right)^{\frac{1}{n}}(\tau - \tau_y)^{\frac{1}{n}} \qquad \text{Equation 2.45}$$

Substituting Equation 2.45 into Equation 2.44, the nominal shear rate and the volumetric discharge are obtained from the following relation:

$$\frac{32Q}{\pi D^2} = \frac{8V}{D} = \frac{4n}{K^{\frac{1}{n}}\tau_0^2}(\tau_0 - \tau_y)^{\frac{1+n}{n}}\left[\frac{(\tau_0 - \tau_y)^2}{1+3n} + \frac{(\tau_0 - \tau_y)^2}{1+2n} + \frac{\tau_y^2}{1+n}\right] \qquad \text{Equation 2.46}$$

The following rheological relationship can be accommodated in the yield pseudoplastic model:

- Yield dilatant ($\tau_y > 0$ and $n > 1$)
- Yield pseudo plastic ($\tau_y > 0$ and $n < 1$)
- Bingham plastic ($\tau_y > 0$and $n = 1$)
- Dilatant ($\tau_y = 0$ and $n > 1$)
- Pseudoplastic ($\tau_y = 0$ and $n < 1$)
- Newtonian ($\tau_y = 0$ and $n = 1$)

A Newtonian fluid has the following characteristics: $\tau_y = 0, n = 1$ and $K = \mu$. Replacing those parameters in Equation 2.46, the equation yields:

$$\tau_0 = \mu\frac{8V}{D} \qquad \text{Equation 2.47}$$

It is shown in Equation 2.47 that the shear rate at the pipe wall of Newtonian fluids is 8V/D
The quantity 8V/D for non-Newtonian fluid is called the pseudo-shear rate.
The Rabinowitsch-Mooney relation can be related to true shear rate for non-Newtonian fluid.

2. 5.4.2 The Rabinowitsch-Mooney relation

The true shear rate can be obtained from the pseudo-shear rate of a non-Newtonian fluid by multiplying the pseudo-shear rate by the Rabinowitsch-Mooney relation (Rabinowitsch, 1929):

$$\left[-\frac{du}{dr}\right]_0 = \frac{8V}{D}\left[\frac{3n' + 1}{4n'}\right] \qquad \text{Equation 2.48}$$

where,

$$n' = \frac{d(Log\tau_0)}{d\left(Log\frac{8V}{D}\right)} \qquad \text{Equation 2.49}$$

This rheological characterisation allows converting a pseudo-shear diagram to a true rheogram. If the rheological parameters of the fluid are known, K' and n' can be obtained using the following relations which are used for pseudoplastic fluids and for yield pseudoplastic fluids.

$$K' = K\left(\frac{3n + 1}{4n}\right)^n \qquad \text{Equation 2.50}$$

$$n' = n \qquad \text{Equation 2.51}$$

2.5.4.3 Friction factor

The fanning friction factor for non-Newtonian fluids in laminar flow is given by the following relation (Chhabra & Richardson, 1999):

$$f = \frac{16}{Re_{MR}} \qquad \text{Equation 2.52}$$

Slatter (1999) developed a friction factor for non-Newtonian fluids with a yield stress:

$$f_{ann} = \frac{2\tau_0}{\rho V_{ann}^2} \qquad \text{Equation 2.53}$$

2.5.5 Turbulent flow for Newtonian fluid

Turbulent flow is a natural form of fluid motion and is characterised by large, random, swirling or eddy motions. In turbulent flow, the fluid particles move in irregular paths, causing an exchange of momentum from one portion of fluid to another (Streeter and Wylie, 1975). Turbulent flow is complex; an exact mathematical analysis has not been yet done. Predictions are obtained empirically from experiments.

The friction factor for turbulent flow can be calculated from the Colebrook-White equation (Massey, 1990):

$$\frac{1}{\sqrt{f}} = -4\log\left[\frac{k}{3.7D} + \frac{1.26}{Re\sqrt{f}}\right] \qquad \text{Equation 2.54}$$

Note that for smooth wall pipes and for Reynolds number values between 3 000 and 100 000, Blasius established a correlation for determination of the friction factor (Massey, 1990):

$$f = \frac{0.079}{\mathrm{Re}^{0.25}} \qquad \text{Equation 2.55}$$

The Moody diagram, as shown in Figure 2.24 is a useful graphical presentation of pipe Reynolds number against friction factor. If the pipe Reynolds number and the pipe roughness, k/D value is known, the friction factor can easily be read off the Moody diagram.

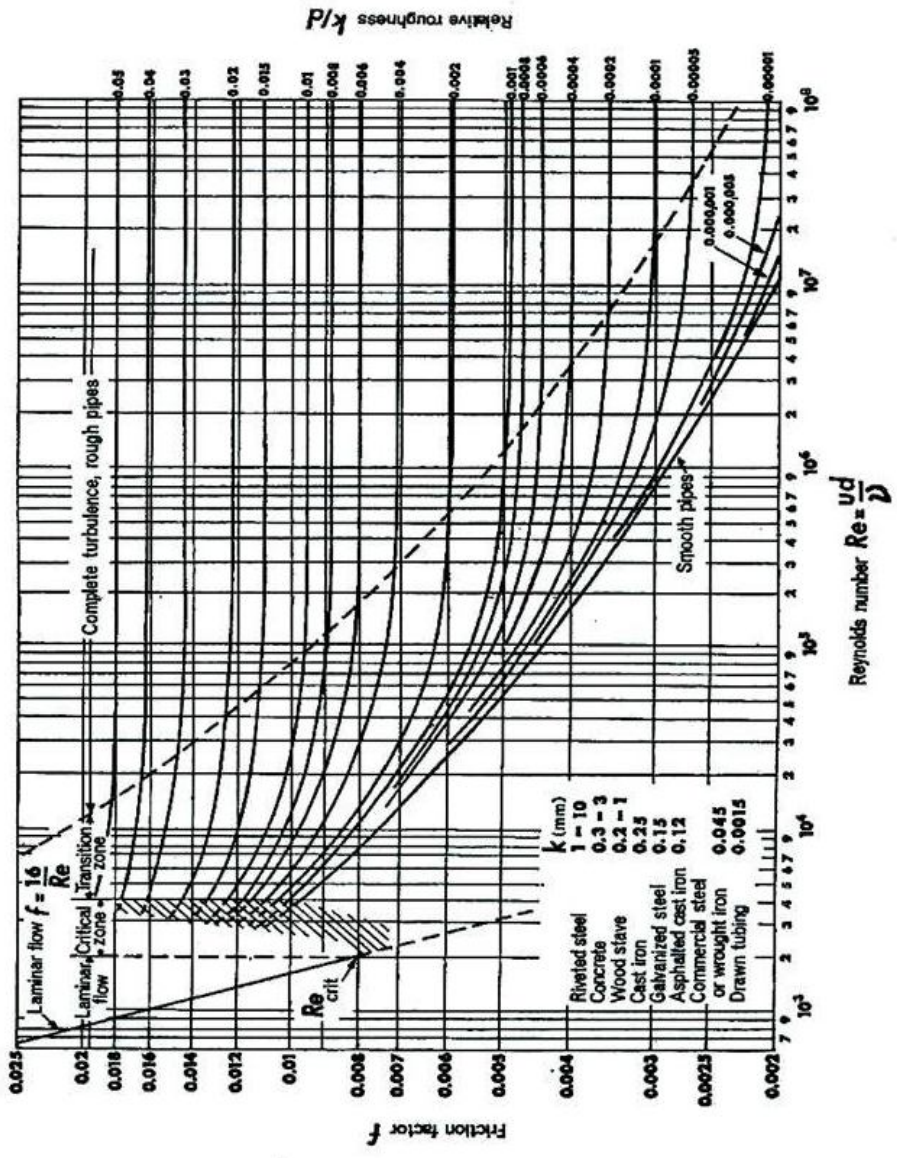

Figure 2.24 : Moody diagram (Massey, 1990)

2.6 HEAD LOSSES IN STRAIGHT PIPES

2.6.1 Energy loss in straight pipes

When a fluid flows through a pipe, there is a dissipation of energy. This energy is normally transformed to internal energy. When the flow occurs in a horizontal straight pipe of uniform diameter, the energy loss manifests itself as a head loss and is given by the head difference, ΔH, measured in meters of fluid. The head loss which occurs in fully developed flow in straight pipes can be calculated from the well-known Darcy-Weisbach equation (Massey, 1990):

$$\Delta H = \frac{4fL}{D}\frac{V^2}{2g} \qquad \text{Equation 2.56}$$

where f is the Fanning Factor Friction defined as follows:

$$f = \frac{2\tau_0}{\rho V^2} \qquad \text{Equation 2.57}$$

The velocity may be derived from the well-known equation of conservation of mass or equation of continuity.

$$V = \frac{Q}{A} \qquad \text{Equation 2.58}$$

2.7. RHEOLOGICAL CHARACTERISATION

2.7.1 Introduction

Rheology is the science of deformation and flow phenomena. The word *rheology* comes from the Greek “rheos” which means flow and “logos” meaning knowledge. Metzner and Reed define *rheology* as a branch of science dealing with relationships between the shear stress and the resulting shear rate of a fluid in the laminar flow region and any variable influencing such relationships (Metzner & Reed, 1955). In non-Newtonian laminar flow, it is important to rheologically characterise the fluids under study. Characterisation usually involves the measurement of the fluid flow properties over an appropriate shear rate (or shear stress) range (Chhabra & Richardson, 1999).

2.7.2 Rheological models and laws of non-Newtonian fluids

Various models exist to characterise non-Newtonian fluids. It is well known that viscosity is the only one rheological parameter for Newtonian fluid; however non-Newtonian fluid has two or three rheological parameters. Represented in Table 2.2 overleaf, are the models and laws of non-Newtonian fluids proposed in the literature, some of which will not be discussed in this work.

2.7.3 Rheometry

Chhabra and Richardson state that rheometry encompasses the collection of physical data from the tests on a representative sample of fluid under investigation, for the purpose of establishing the relationship between shear stress and shear rate, both qualitatively (identification of the applicable rheological model) and quantitatively (the actual values of the rheological constants in the model) (Chabbra & Richardson, 1999).

The instrument used to measure viscous properties is called a viscometer or rheometer. There are two principal types of rheometers: rotational viscometer and tube viscometer.

2.7.3.1 Rotational viscometer

The rotational viscometer can consist of a bob and cup, a cone-and-plate or a parallel plate geometry of which one is rotated to produce shear in the test fluid, found in the gap. The shear stress is determined by measuring the torque on one of the elements (Chabbra & Richardson, 1999).

Table 2.2: Rheological models

<table>
<tr><th colspan="4">RHEOLOGICAL CLASSIFICATION OF FLUIDS</th></tr>
<tr><th>NEWTONIAN FLUIDS
$\tau_0 = -\mu\frac{du}{dr}$</th><th colspan="3">NON-NEWTONIAN FLUIDS
$\tau_0 \neq -\mu\frac{du}{dr}$</th></tr>
<tr><td rowspan="2">Newtonian Fluids
$\tau_0 = -\mu\frac{du}{dr}$
Example: Water, glycerine, olive oil, corn syrup.</td><td colspan="2">Purely viscous fluids</td><td rowspan="2">Visco-elastic fluids</td></tr>
<tr><td>Time-independent fluids</td><td>Time-dependent</td></tr>
<tr><td></td><td>Pseudoplastic fluids
$\tau_0 = K\left(-\frac{du}{dr}\right)^n$,
$n < 1$
Example: Finite particle suspensions

Dilatant fluids
$\tau_0 = K\left(-\frac{du}{dr}\right)^n$,
$n > 1$
Example: Ultrafine irregular particle suspensions

The Carreau viscosity equation
$\frac{\mu - \mu_\infty}{\mu_0 - \mu_\infty} = \left\{1 + \left[\lambda\left(-\frac{du}{dr}\right)\right]^2\right\}^{\frac{n-1}{2}}$

Ideal plastic or Bingham fluids
$\tau_0 = \tau_y + K\left(-\frac{du}{dr}\right)$
Example:
Yield pseudoplastic fluids
$\tau_0 = \tau_y + K\left(-\frac{du}{dr}\right)^n$
Example: Water suspensions of clay and fly ash</td><td>Thixotropic fluids
$\tau_0 = K\left(-\frac{du}{dr}\right)^n + f(t)$,
f(t) decreasing
Example: Crude oils, bentonitic drilling fluid

Rheopectic or negative thixotropic fluids
$\tau_0 = K\left(-\frac{du}{dr}\right)^n + f(t)$,
f(t) increasing
Example: Rare liquid-solid suspensions</td><td>Visco-elastic fluids
$\tau_0 = -\mu\frac{du}{dr} + \alpha G$
where G is the modulus of elasticity

Example: Liquid solid combinations, pipe flow and polymerised fluid with drag reduction</td></tr>
</table>

2.7.3.2 Tube viscometer

A tube viscometer also known as a capillary viscometer, is the most commonly used instrument for the measurement of viscosity due, in part, to its relative simplicity, low cost and accuracy in the case of long capillaries (Chabbra & Richardson, 1999). A tube viscometer is a device which forces a sample of fluid to flow at a measured rate in laminar motion under a measured pressure gradient in a precision bore capillary tube of known diameter and length (Govier & Aziz, 1972). Because of their inherent similarity to many process flows, which typically involve pipes, capillary viscometers are widely used in process engineering applications (Chabbra & Richardson, 1999).

Data from tube viscometers are plotted as τ_0 versus 8V/D on a pseudo-shear diagram from which the rheological parameters can be obtained. The flow curve obtained is called a pseudo-shear diagram. The pseudo-shear diagram is usually converted to a true rheogram by using the Rabinowitsch-Mooney relation.

For a series of N data points in the laminar region, fixed values of τ_y, K and n can be used in Equation 2.46 to calculate pseudo shear rates $(8V/D)_{calc}$ for each τ_0 value. A realistic value of τ_y is then adjusted by minimising the error function. The error function E is the root square difference between observed data and calculated ones:

$$E = \sqrt{\frac{\sum_{i=1}^{N}\left[\left(\frac{8V}{D}\right)_{i\,abs} - \left(\frac{8V}{D}\right)_{i\,calc}\right]^2}{N-1}} \qquad \text{Equation 2.59}$$

K value for minimum error K_{min} is given by:

$$K_{min} = \frac{1}{\left[\frac{2\sum_{i=1}^{N}\left(\frac{8V}{D}\right)_i / 8}{\sum_{i=1}^{N}\left(\tau_0-\tau_y\right)^{\frac{1+n}{n}}\left[\frac{\left(\tau_0-\tau_y\right)^2}{1+3n} + \frac{2\tau_y\left(\tau_0-\tau_y\right)}{1+2n} + \frac{\tau_y^2}{1+n}\right]}\right]} \qquad \text{Equation 2.60}$$

- Only data from the flow laminar regime can be used. The viscous flow data in the laminar region should be coincident for different tubes diameters; if they are not, there is probably a wall slip effect that should first be corrected. The slip velocity must be calculated for each tube diameter and deducted from the measured main velocity (Heywood & Brown, 1991).

- Entrance and exit losses: It is important that the entrance and exit losses in the tubes that are used are minimised. This is possible by ensuring that the flow is fully developed before differential pressure readings are taken, usually at least 50 D is allowed.

2.8 NON-NEWTONIAN REYNOLDS NUMBER

There are a various expressions for the Reynolds numbers for non-Newtonian fluids. Some of them are presented in this work, especially the generalised Reynolds number and the Slatter Reynolds number.

2.8.1 Generalised Reynolds number or Metzner and Reed Reynolds number

Metzner and Reed (1955) developed a generalised approach applicable to the laminar pipe flow of any time-independent fluid

$$\tau_0 = \frac{D\,\Delta p}{4L} = K'\left(\frac{8V}{D}\right)^{n'} \qquad \text{Equation 2.61}$$

K' and n' are not constants, but vary with 8V/D. If the shear stress is plotted against 8V/D on a logarithmic scale Equation 2.61 is simply the equation of the tangent to the curve at a given value of 8V/D, n' being the slope of this tangent and K' is the intercept on the ordinate at 8V/D equal to unity (Skelland, 1967). Metzner & Reed (1955) proposed a generalized Reynolds number applicable to the pseudoplastic model from such considerations above as:

$$Re_{M-R} = \frac{8\rho V^2}{K'\left(\frac{8V}{D}\right)^{n'}} \qquad \text{Equation 2.62}$$

After transformation the relation above can be rewritten as:

$$Re_{M-R} = \frac{\rho V^{2-n'} D^{n'}}{8^{n'-1} K'} \qquad \text{Equation 2.63}$$

Applying the Rabinowitsch-Mooney relation by substituting Equations 2.50 and 2.51 into Equation 2.62 it results:

$$Re_{M-R} = \frac{8\rho V^2}{K\left(\frac{3n+1}{4n}\right)\left(\frac{8V}{D}\right)^{n}} \qquad \text{Equation 2.64}$$

After transformation the equation can be rewritten as:

$$Re_{M-R} = \frac{\rho V^{2-n} D^2}{8^{n-1} K \left(\frac{3n+1}{4n}\right)}$$ Equation 2.65

2.8.2 Slatter Reynolds number

The Metzner and Reed Reynolds number does not take into account the yield stress of non-Newtonian fluids. Slatter developed and has proposed a Reynolds number that places specific emphasis on the yield stress. The Slatter Reynolds number seeks to express the ratio of inertial forces to viscous shear forces in the sheared portion of the flow (Chabbra & Richardson, 1999). The final formulation of the Slatter Reynolds number is given by:

$$Re_3 = \frac{8\rho V_{ann}^2}{\tau_y + K\left(\frac{8V_{ann}}{D_{shear}}\right)^n}$$ Equation 2.66

For the fluid that exhibits a yield stress such as in kaolin slurries, there is a plug flow at the centre of the pipe, starting at distance r_{plug} where the shear stress becomes less than the yield stress.

$$r_{plug} = \frac{\tau_y}{\tau_0} R$$ Equation 2.67

D_{shear} is the sheared diameter which is calculated as

$$D_{shear} = D - D_{plug}$$ Equation 2.68

D_{plug} is the diameter of the plug and V_{ann} is the mean velocity in the annulus. The mean velocity is calculated as follows:

$$V_{ann} = \frac{Q_{ann}}{A_{ann}}$$ Equation 2.69

Q_{ann} being the flow rate in the annulus, and is given by:

$$Q_{ann} = Q - Q_{plug}$$ Equation 2.70

$$Q_{plug} = U_{plug} \cdot A_{plug}$$ Equation 2.71

$$U_{plug} = \frac{D}{2K^{\frac{1}{n}}\tau_0}\left(\frac{n}{n+1}\right)\left(\tau_0 - \tau_y\right)^{\frac{n+1}{n}} \quad \text{Equation 2.72}$$

And

$$A_{plug} = \pi r_{plug}^2 \quad \text{Equation 2.73}$$

The value of the transitional Slatter Reynolds number from laminar to turbulent flow in straight pipes is Re_3= 2100 (Lazarus & Slatter, 1988).

2.9 DIMENSIONAL ANALYSIS

In fluid mechanics and other related disciplines that rely on empirical data for solution, dimensional analysis is a method extensively used. The dimensional analysis method consists of determining the independent variables which have an influence on the dependent variable under study (Douglas et al., 2000). Mass (force), length and time are usually three fundamental dimensions. If the number of independent variable X, is greater than the three fundamental dimensions, then (X-3) dimensionless groups will appear in the expression. These groups assist in interpretation of models studied by ensuring that the conditions under which tests and observations take place at one scale are identical to those other scales (Massey, 1990). The Buckingham Π-theorem is probably the most systematic technique for establishing a dimensionless group.

The π groups must be independent of each other and no one group should be formed by multiplying together powers of other groups. This method offers the advantage of being simpler than the method of solving simultaneous equations for obtaining the values of the indices (the exponent values of the variables).

In this method of solving the equation, there are two conditions:

a. Each of the fundamental dimensions must appear in at least one of the m variables.

b. It must not be possible to form a dimensionless group from one of the variables within a recurring set. A recurring set is a group of variables forming a dimensionless group.

2.10 PREVIOUS WORK

There have been a large number of investigations in the field of pipe orifice flows. Several applications of orifice flow have been studied. The majority of investigations have been carried out using Newtonian fluids. Studies on orifice flow using non-Newtonian fluids have not received much attention, despite its importance in industries when liquids used exhibit non-Newtonian behaviour often at low temperatures.

Early in 1929, Johansen (1930) conducted a visualisation and experimental study of the flow characteristics of sharp-edged orifices. Johansen used as testing fluids: water, castor oil and mineral oil. Discharge coefficients for orifices with five different diameter ratios (β = 0.090, 0.209, 0.401, 0.595, and 0.794) were determined, in the range of Reynolds numbers from less than 1 to 25 000. Based on flow mechanisms observed in the dye injection test, he tried to interpret the resulting plot of the discharge coefficients. His findings were as follows:

- For Re < 10, the discharge coefficient C_d increases linearly and corresponds to the steady flow conditions seen in the dye test.
- A further increase in Reynolds number up to 250 results in a nonlinear increase in C_d up to its maximum, and corresponds to the formation of a divergent jet in the flow patterns.
- The discharge coefficient value, C_d, begins to decrease as vortices appear in the flow until it reaches a constant value approximately 0.615 as the flow becomes turbulent at Re > 2 000.
- He finally notes that as the diameter ratio increases, the Reynolds number at which these flow transitions occur is higher. Thus the flow remains laminar at higher Reynolds numbers for increased diameter ratio.

A test facility that could measure flow rate and pressure drop across brass orifices using water as test fluid was constructed by Medaugh and Johnson (1940). The authors found that the discharge coefficient C_d decreases with an increase of flow rate through the orifice. They observed also that as the orifice diameter increased, the discharge coefficient C_d decreased for the same pressure drop. It was concluded by the authors that by increasing the flow rate sufficiently, the discharge coefficient would eventually decrease to a steady value of 0.588, which was 6% lower than the data from Smith and Walker (1923) that were widely used at the time. The authors attributed this difference in values to potential problems in the Smith and Walker data due to the bowing of the thin plate from the pressure or from a depression that might have occurred around the orifice opening during the drilling process.

A comparison of loss characteristics of sharp-edged orifices, quadrant-edged orifices for varying edge radii, and nozzles was done by Alvi et al. (1878). Tests were conducted on flow geometries with diameter ratios of 0.2, 0.4, 0.6, and 0.8. Reynolds numbers were in the range of 1 to 10 000. The authors observed that sharp-edged orifices exhibit pressure drops similar to those of quadrant-edged orifices at low Reynolds numbers. They found that at high Reynolds numbers quadrant-edged orifices' pressure drops are closer to pressure drops in nozzles. According to the authors, flow characteristics of orifices can be divided into four regimes: Fully Laminar Region, Critical Reynolds Number Region, Re-laminarising Region, and Turbulent Flow Regime. An integrated picture of variation of parameters such as discharge coefficient, loss coefficient, settling length, pressure recovery length, and centre line velocity confirms this classification. They found that results may be reliably extrapolated to higher Reynolds number.

Edwards et al. (1985) investigated frictional head loss which is incurred when a range of Newtonian and non-Newtonian fluids flow through elbows, valves, expansions, contraction and orifices plates. The authors treated all the fittings in a similar manner for the estimation of head loss. Edwards and his co-authors demonstrated that head loss measurement for inelastic non-Newtonian fluids can be meaningfully correlated as plots of loss coefficient versus generalised Reynolds number.

An investigation on the effect of the rheological properties of non-Newtonian (power law) fluids on the discharge coefficient was conducted by Salas-Valerio and Steffe (1990). Corn starch solution at 5%, 7.5% and 10% were used as test fluids. It was found that the orifice discharge coefficient C_d was in the range of 0.6 – 0.7. The authors found also that the discharge coefficient C_d depended on the orifice diameter ratio, fluid velocity and rheological parameters of the fluid consistency index, K, and power lower index, n. The discharge coefficient C_d increases with the increasing of the velocity at lower velocities. The value of C_d tends to assume a constant value at high velocities. The authors found that the discharge coefficient decreases with the increase of the consistency coefficient. They used a generalised Reynolds number; they also proposed that C_d may be expressed as an exponential function of the generalised Reynolds number.

Experimental and numerical analysis was used by Sahin and Ceyhan (1996) to examine incompressible flow through orifices with diameter ratios of 0.5 and aspect ratios ranging from 0.0625 to 1. A gear pump was used in their experiments to circulate oil through an orifice with Reynolds numbers ranging from 1 to 150 at temperatures ranging from 30°C to 50°C. Two-

dimensional Navier-Stokes equations for axi-symmetric, viscous, incompressible flow through a square-edged orifice in a circular pipe were used for numerical analysis. The discharge coefficient equation was derived as:

$$C_d = \frac{1}{2\sqrt{2}}\left(\frac{1}{\beta}\right)^2 (1-\beta^4)^{\frac{1}{2}}\left(\frac{\rho V_{max}^2}{\Delta P}\right)^{\frac{1}{2}} \qquad \text{Equation 2.75}$$

where V_{max} is the velocity at the centrerline of the pipe.

The numerical results obtained were compared with their own experimental results and with those of Nigro et al. (1978), Alvi et al. (1978) and Johansen (1930), and were found to agree within 5%.

Excess pressure drop for very small orifices ranging from 10 μm to 1 mm orifice diameter and orifice thickness ranging from 10 μm to 109 μm were measured by Hasegawa et al. (1997). Distilled water, silicone oils and glycerin solutions were used as testing fluids. The relationship between pressure drop and flow rate was examined for Reynolds numbers ranging from 1 to 100. A numerical analysis of Newtonian fluid was also conducted afterwards. It was found that for large orifices the numerical analysis was almost the same, but the results were several times higher than the numerical analysis of Newtonian fluids for small orifices. If the orifice diameter or the fluid viscosity decreases, the under-prediction becomes worse. The authors explain this by giving some possible causes, which could be the material used in construction, burring that occurred in manufacturing, and boundary layer thickness that increases due to ionic effects of the liquid. None of these causes might produce the increases in pressure drop that was seen between experiments and numerical solution found the authors. However, the increases in the length-to-diameter ratio which increased as the orifice diameter decreased were examined as a possible cause of the discrepancy between numerical solution and experiments.

Effects of cavitations and plate thickness on the orifice discharge coefficient were investigated by Kim et al. (1998). The authors performed their investigation by conducting tests on three orifices with diameter ratios of 0.10, 0.15, and 0.33. The noise generated by cavitation was measured using a sound level meter and a hydrophone. Placed at 1.25D downstream from the orifice plate, the signal of the hydrophone was monitored and measured with a spectrum analyser. The sound level meter was placed at 0.9 m from the orifice plate in a sealed chamber (2.4 m x 1.2 m). The authors concluded that cavitation occurred for pipe Reynolds numbers ($Re_d = \beta Re$) above 14 000 for β = 0.10; 43 000 for β = 0.15, and 100 000 for β = 0.33. It was

finally established that for the all diameter ratios tested, cavitations had not affected the discharge coefficient for aspect ratios less than or equal to 0.55 over the entire range examined (4 000 < Re < 170 000).

Zhang and Cai (1999) examined the pressure drop characteristics of orifices with different profiles and contraction ratios where the orifice is used as an energy dissipator in flood conduits. An orifice installed as an energy dissipator in a flood conduit is required to dissipate a designed amount of energy at the design discharge. The primary concern of the authors was to identify a compromise orifice geometry (that is neither sharp-edged nor streamlined) that produces the lowest local pressure drop while achieving the desired energy loss, because at a given contraction ratio, a sharp-edged orifice, for example, causes too high a pressure drop, whereas a streamlined orifice plate may not meet the energy loss requirement. In flood conduits, in order to minimise the risk of cavitations and the resulting damage to concrete tunnels and orifices a small pressure drop is preferred. Therefore, a compromise can be made between the two parameters of the orifice geometry– the contraction ratio and the abruptness of transition. A model resembling a flood conduit used in dam construction was fabricated for the testing of four orifices with different diameter ratios ranging from 0.5 to 0.8. The test was conducted at the Reynolds numbers ranging from 1.04×10^5 to 2×10^5. The authors mentioned that for any orifice with a given β, the value of pressure loss coefficient, k, is larger than that of axisymmetric sudden enlargement, i.e.

$$k(\beta) \geq \frac{(1-\beta^4)^2}{\beta^4} \qquad \text{Equation 2.76}$$

and, C_{drop}, the pressure drop coefficient is smaller than the sudden enlargement.

In conclusion, the authors said that the orifice geometry (notably the abruptness of transition and the contraction ratio) strongly affects the wall-pressure distributions. Orifices in a discharge conduit are required to dissipate a desired amount of energy. Both sharp-edged and streamlined orifice plates can meet the energy dissipation requirements, but they cause too large pressure drops. A compromise between the contraction ratio and the abruptness of transition can be beneficial to minimise the pressure drop and lower the risk of cavitation. If the required energy loss increases, the optimal orifice dissipator should be more streamlined and has a smaller contraction ratio. The sloping-approach orifice (Figure 2.25) can be used when the energy-loss coefficient k is between 0.5 and 4.

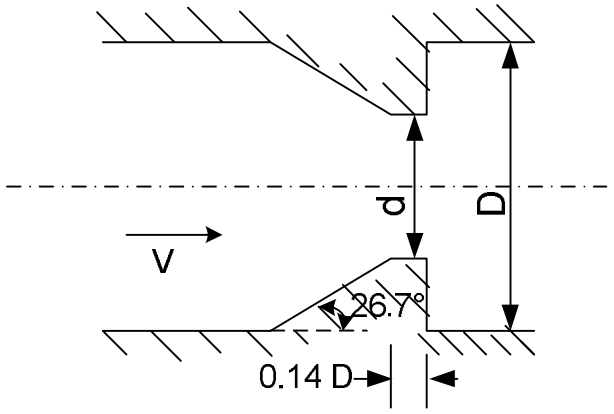

Figure 2.25: Slopping-approach orifice

An investigation on pressure drops resulting from the flow of a mixture of a gas and a non-Newtonian pseudoplastic liquid through orifices of varying diameter was conducted by Samanta et al. (1999). Three orifice plates were tested with diameters of 5.9 mm, 7.6 mm and 9.0 mm, and diameter ratios of 0.4646, 0.5984, and 0.7087 respectively. Pressure drop was measured using air as gas, and Salt carboxymethyl cellulose (SCMC) as the non-Newtonian liquid at temperatures of 31°C ± 1.5°C. Water and the SCMC were both used to collect single-phase data, with pressure drop ranging from 1 kPa to 26 kPa. Air-SCMC was used to collect two-phase data in the same pressure range with liquid Reynolds numbers ranging from 45 to 2200 and gas Reynolds number ranging from 230 to 2200. The authors presented a correlation predicting pressure drop in terms of Euler Number for both liquid and gas-liquid mixtures. The single phase Euler number was represented as function of Reynolds number and diameter ratio (Equation 2.77), while the two-phase Euler number was presented as function of the liquid Reynolds number, the gas Reynolds number, the diameter ratio, and the properties of the liquid (Equation 2.78).

$$Eu_l = 0.601 Re_l^{-0.048 \pm 0.044} \left(\frac{d}{D}\right)^{-4.380 \pm 0.248} \qquad \text{Equation 2.77}$$

$$Eu_{tp} = Eu_l \left[1 + 0.003 Re_l^{-0.536 \pm 0.630} Re_g^{0.797 \pm 0.60} \left(\frac{g\mu_{eff}^4}{\rho_l \sigma_l^3}\right)^{-0.125 \pm 0.166} \left(\frac{d}{D}\right)^{0.205 \pm 0.166}\right] \qquad \text{Equation 2.78}$$

In 2000, based on measurement of pressure drop across small-size orifice as function of flow rate, Della Valle and his co-authors show that it is possible to determine the extensional viscosity $\mu_e$of viscoelastic fluids and suspensions. A Boger fluid (Boger & Watters, 1993) and a Newtonian fluid with suspension of clay were used as working fluid. The authors constructed a nozzle flow meter that used orifices with 45º converging and diverging sections and diameters ranging from 0.6 to 3.0 mm. They showed that the extensional viscosity of viscoelastic fluid and suspensions can be determined from the following equation:

$$\mu_e = 3\mu R \qquad \text{Equation 2.79}$$

Where: 3μ = extensional viscosity of a Newtonian fluid

R = the vertical shift between the elastic fluid data and the Newtonian data on the Eu vs. Re plot.

The nozzle flow meter constructed by the authors was tested with water and oil at room temperature. The authors found that there was a dependence of Euler number on Reynolds number for both fluids. The results showed also that at low Reynolds numbers, the pressure drop increases proportionally with the viscosity and the flow is purely laminar while at high Reynolds numbers the flow is dominated by inertia. At high Reynolds numbers, the pressure drop becomes independent of viscosity.

In 2002 an experimental study on the determination of pressure drop characteristics of the viscous fluid through small diameter orifices was conducted by Mincks. He investigated a fluid which has temperature- and pressure-dependent properties. In his study, however, at the temperatures ($20 \leq T \leq 50^oC$) investigated, the properties did not change drastically with the temperature. Mincks noted that pressure drop across orifices can be presented as a function of aspect ratio, diameter ratio and Reynolds number. A correlation for non-dimensional pressure drop has been proposed by the author. He concluded that more studies at lower temperatures were needed to understand the effect of varying properties of the fluid on the pressure drop characteristics.

The relationship between Euler number and discharge coefficient was investigated by Morrison (2003). Discharge coefficient data were obtained for flows of nitrogen, air, water, gas-oil, and natural gas for β ratios ranging from 0.1 to 0.75, and flange tap as tapping measurement. After rearranging the generalised mass flow rate equation using the definition of the Euler number, the author states that the important non-dimensional parameter is not the Reynolds but the

Euler number. If the statement is true, then the viscosity of the fluid will no longer enter into the calculation of the flow rate, concludes the author. Therefore, the calculation of discharge coefficient C_d will also be simplified since one of the fluid properties is no longer needed and the accuracy in calculation of flow rate will increase by deleting the uncertainty in the viscosity term. Morrison plotted firstly discharge as a function of Reynolds number, and secondly discharge coefficient as a function of Euler number. From the second graph, the data show that there is a relationship between β ratio and Euler number which is expected, since smaller β ratios produce larger values of ΔP for a fixed value of mass flow rate and density. He noticed, however, that within a given β ratio, there is a large variation in discharge coefficient at a given Euler number. Morris plotted the ratio of discharge coefficient to Euler number as function of 1/ (Eu $\beta^{1.325}$); however, there is some spread in data for higher β ratio data. The author finally substituted the flow coefficient, $K = C_d/\sqrt{1-\beta^2}$, for the discharge coefficient and included an expansion factor, Y leading to a simple curve presented all the data.

In 2005, Swamee developed discharge equations for a Venturi meter and an orifice meter. He obtained the pipe discharge iteratively using experimental curves for discharge coefficients of a Venturi meter and an orifice meter. The orifice discharge equation is as follows:

$$C_d = \{[0.675 + 0.6\beta^2 - 0.02\ln Re]^{10} + [0.5 + 0.43\beta^2]^{10}\}^{0.1} \qquad \text{Equation 2.82}$$

Recently ESDU (2007) published a review of data for incompressible flow through orifice plates. The outcome of the review was to identify reliable data for the CFD validation studies carried out by ESDU for the update of correlations for pressure losses in orifice plates. A summary of different flow curves presenting discharge coefficients and pressure loss coefficients is shown respectively in Figures 2.25 and 2.26 for short orifice plates with different diameter ratios.

Abou El-Azm Aly et al. (2010) investigated the pressure drop through fractal-shaped orifices. The authors measured the pressure recovery at different stations downstream of the orifice. Pressure drop measured across fractal-shaped orifices was directly compared with the pressure drop obtained after regular circular orifices with the same flow area. They found that fractal-shaped orifices had a significant effect on the pressure drop, apart from the first generation or triangular shape, which was similar to the regular circular orifice. They concluded that the pressure drop across fractal-shaped orifices was lower than that from regular circular orifices of the same flow area due to the fact that the fractal orifices develop additional smaller velocity

scales when compared to the same-area circular orifice. According to the authors, it is feasible to use the fractal-shaped orifices as flow meters as they can sense the pressure across them accurately with lower losses than the regular circular-shaped orifices.

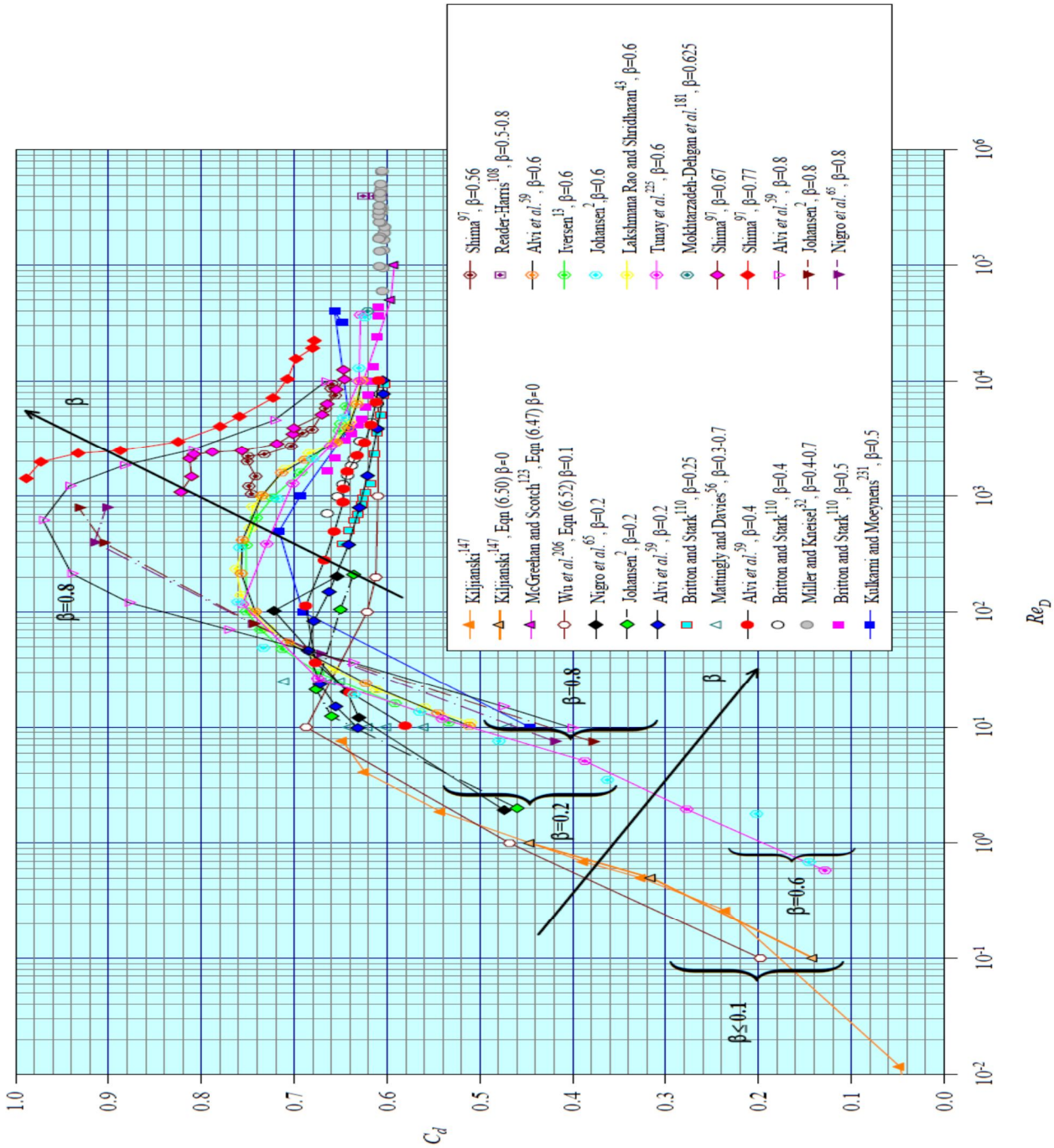

Figure 2.26 : Discharge coefficients for short orifice for D and D/2 tap arrangement (ESDU, 2007)

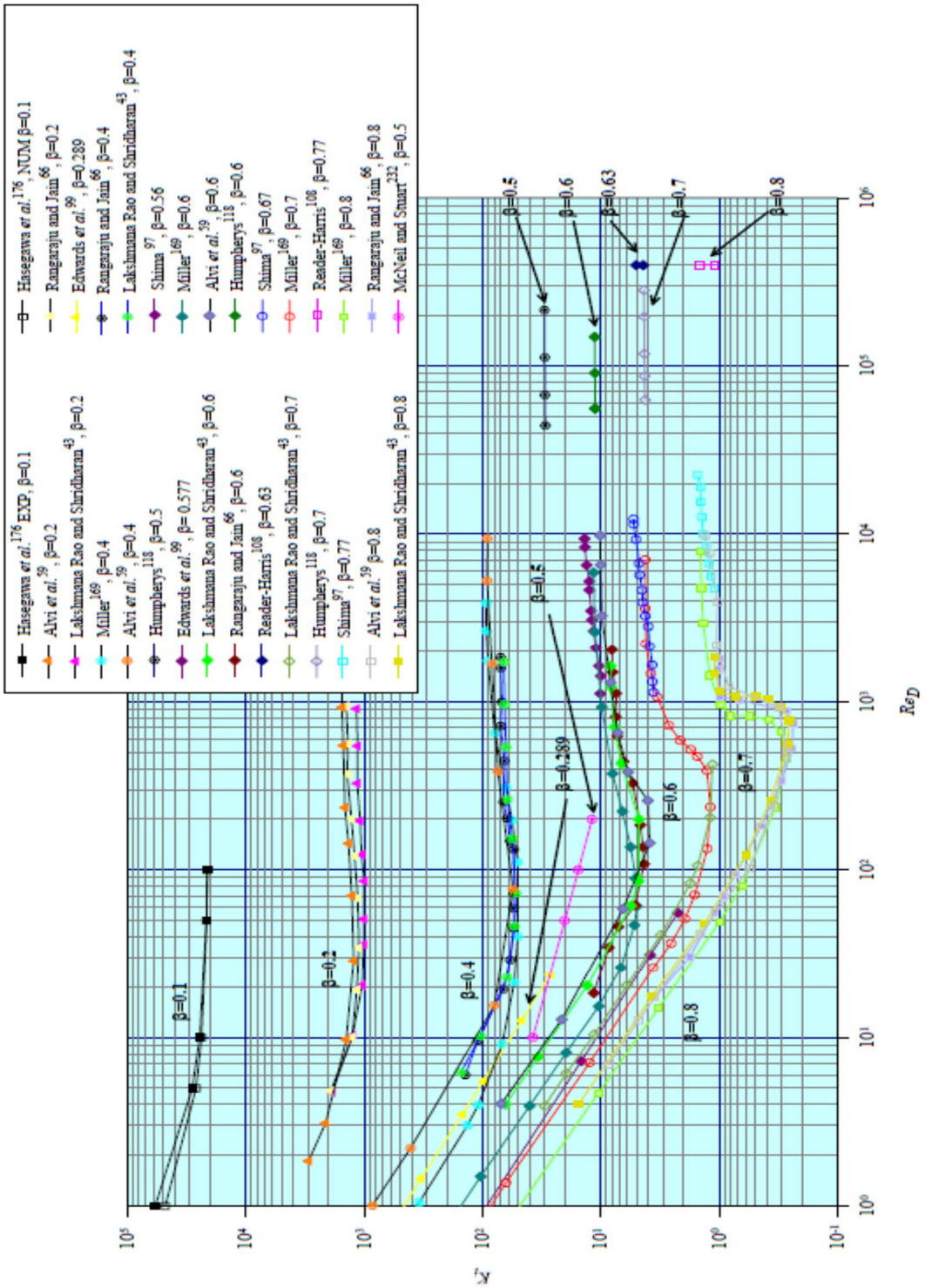

Figure 2.27 : Pressure loss coefficient data for short orifice plates in laminar to turbulent flow (ESDU, 2007)

2.10.1 Summary

The previous section gives chronologically the evolution of the study of flow through orifices since the 1930s to date. According to the investigation conducted, the first, attempt to study non-Newtonian fluid flowing through orifice plate appears in the 1980s. Table 2.3 below presents a summary of previous work.

Table 2.3: **Summary of work done (1930 – 2010)**

Author	Diameter ratio, β	Reynolds number	Findings and data presentation	Method
Newtonian fluids				
Johansen (1930)	0.090, 0.209, 0.401, 0.595, and 0.794	1 to 25 000	The author interpreted the plot of discharge coefficient based on the flow mechanisms observed in dye injection. Resultants were presented in plots of discharge coefficient versus square root of Re.	Experimental
Medaugh and Johnson (1940)		30 000 to 35 0000	The results were presented in plots of C_d versus ΔP, and C_d versus Re for high Reynolds numbers. Good agreement of data was observed compared with Smith (1886) and Strickland (1909) while they were 6% lower than Smith and Walker (1923).	Experimental
Alvi et al. (1978)	0.2, 0.4, 0.6, 0.8	1 to 10 000	The results agree well with data published by Zampaglione (1969) and Lakshmana Rao and Sridharan (1972). The resultants were presented in plots of Eu versus Re for different diameter ratio.	Experimental
ESDU 81039 (1981)	$0.001 > \propto < 1.00$	>10 000	The document provides data for the calculation of pressure losses in ducts containing orifice plates and perforated plates for incompressible flow. It also provides data for the determination of suitable geometrical parameters for a pressure reducing orifice in a duct.	Analytical
Sahin and Ceyhan (1996)	0.5	1 to 150	Data found in this investigation were compared with Nigro et al. (1978), Alvi et al. (1978) and Johansen (1930). Data agree well. The experimental and numerical data were plotted in a form of C_d versus square root of Re.	Experimental
Hasegawa et al. (1997)		1 to 1 000	Results were presented in plots of Eu versus Re for different orifice configurations. The authors compared their experimental results to a numerical solution. At small diameters the numerical solution under-predicts the pressure drop. This was even worse at very small diameters tested.	Experimental

Author	Diameter ratio, β	Reynolds number	Findings and data presentation	Method
Kim at al. (1998)	0.1, 0.15 and 0.33	4 000 to 100 000	They found that cavitation did occur in orifices but did not affect the C_d except for diameter ratio 0.1. Data were presented in plots of C_d versus Re and cavitation in dB versus Re.	Experimental
Zhang and Cai (1999)	0.5, 0.6, 0.69 and 0.8	104 000 to 200 000	The results were presented in plots of dimensionless pressure drop versus diameter ratio and dimensionless wall pressure versus position pipe.	Experimental
Mincks (2002)	0.023, 0.044 and 0.137	8 to 7 285	At smaller Re the Euler numbers increase with the aspect ratio while the influence of the aspect ratio is not significant at higher Reynolds numbers. The data were presented in plots of Eu versus Re.	Experimental
Morrison (2003)	0.1 to 0.75	10^3 to 10^8	The results were presented in plots of C_d versus Re firstly, then C_d versus Euler number secondly, and thirdly as ratio of discharge coefficient to Euler number versus Euler number. Data were finally presented in plots of ratio of flow coefficient and expansion factor to Euler number versus Euler number.	Experimental
Swamee (2005)			Discharge coefficient equation's has been developed for orifice meter and Venturi meter.	Analytical
Abou El-Azm Aly et al. (2010)			As the pressure recovery was measured at different stations downstream of the orifice, results were presented in plots of pressure drop versus downstream distance (x/D).	Experimental
Non-Newtonian fluids				
Edwards et al. (1985)	0.289 and 0.577	1 to 1000	Pressure loss coefficients were plotted versus Reynolds numbers.	Experimental
Salas-Valerio and Steffe (1990)		1 to 2 300	C_d decreases as consistency coefficient of the fluid increases for power law fluids. C_d was plotted versus generalised Re.	Experimental
Samanta et al. (1999)	0.4646, 0.5984, and 0.7087	45 to 2 200 for liquid and, 230 to 2 200 for gas	The authors developed Euler number's equations for liquid only and for two phases. The results were presented in plots of pressure drop versus volumetric flow rate and pressure versus position.	Experimental
Della Valle et al. (2000)		1 to 100 000	Plots of Euler number versus Re for all fluids tested. It is possible to determine extensional viscosity of viscoelastic fluids and suspensions.	Experimental

The equations to determine pressure loss coefficient and discharge coefficients available in the literature are presented in Table 2.4 and 2.5. Except McNeil's equation for pressure loss coefficient and Samanta's equation which are applicable for both Newtonian and non-Newtonian fluids, the rest of the equations are based on Newtonian fluids. All the equations found can only predict pressure loss coefficients either in laminar flow or in turbulent flow separately.

Table 2.4: Summary of discharge coefficient correlations for short orifices

Reference	Range of geometrical parameters	Range of flow parameters	Equation
McNeil et al. (1999)	$\beta = 0.471$	$20 \leq Re_d \leq 250$	$C_d = 6.9\,10^{-6}Re_D^2 - 2.82\,10^{-3}Re_D + 0.999$
Wu et al. (2002)	$\beta < 0.25$	Laminar to turbulent	$C_d = 0.61\left(1 + 1.07\exp^{-0.126\sqrt{Re_d}} - 2.07\exp^{-0.246\sqrt{Re_d}}\right)$
Benedict and Wyler (1973)	$0.15 < \beta < 0.75$	Turbulent flow	$C_d = \sqrt{\frac{1-\beta^4}{\frac{1}{C_c^2} - \beta^4 - 0.26 - 1.511(\beta - 0.35)^2 - 15Re_d^{-0.5} - 0.4505\beta^{3.8}Re_d^{-0.2}}}$ $C_c = 0.61375 + 0.1331\beta^2 - 0.26095\beta^4 + 0.51146\beta^6$
Swamee (2005)	$0.2 < \beta < 0.8$	Turbulent flow	$C_d = \{[0.675 + 0.6\beta^2 - 0.02\ln Re]^{10} + [0.5 + 0.43\beta^2]^{10}\}^{0.1}$
Sahin and Ceyhan (1996)	0.5	$1 \leq Re_D \leq 150$	$C_d = \frac{1}{2\sqrt{2}}\left(\frac{1}{\beta}\right)^2 (1-\beta^4)^{\frac{1}{2}}\left(\frac{\rho V_{max}^2}{\Delta P}\right)^{\frac{1}{2}}$

Table 2.5: Summary of pressure loss coefficient correlations for short orifices

Reference	Range of geometrical parameters	Range of flow parameters	Equation
Carnot-Borda formula	$0 \leq \beta \leq 1$	Turbulent flow	$k_{or} = \left(\frac{1}{C_c\beta^2} - 1\right)^2 = \left(\frac{1}{C_c \propto} - 1\right)^2$
Benedict (1977)	$0 \leq \beta \leq 1$	Turbulent flow	$Eu = \left(\frac{1-\beta^4}{C_d^2}\right) - 2\beta^2\left(\frac{1}{C_c} - \beta^2\right)$
Ginsburg (1963)	$0.1 \leq \beta \leq 0.8$	Turbulent flow	$Eu = (1-\beta^2)^2 + \frac{1}{2}(1-\beta^2) + 1.41\sqrt{1-\beta^2}(1-\beta^2)$
Ward-Smith (1971)	$0 < \beta < 0.87$	$Re_D \geq 10^4$	$k_{or} = \left[\frac{1}{0.608\beta^2(1-\beta^{5.2}) + \beta^{7.2}} - 1\right]$
McNeil and Stuart (2005)	$\beta = 0.5$	$10 \leq Re_D \leq 200$	$k_{0r} = 91.1Re_D^{-0.384}$
Samanta et al. (1999)	0.4646, 0.5984, and 0.7087	Laminar flow	For liquids: $Eu_l = 0.601Re_l^{-0.048\pm0.044}\left(\frac{d}{D}\right)^{-4.380\pm0.248}$

2.11 CONCLUSION

It has been shown from the literature reviewed in this chapter that many researchers have investigated flow through orifice plates. Some provided equations and others correlations predicting pressure loss coefficients and discharge coefficients numerically, analytically or experimentally. The review of data for incompressible flow through an orifice plate published by ESDU (2007) stipulates that although some work has been done for flow through orifice plates, deficiencies still exist for a certain geometries and flow conditions. The review reports that the majority of the data available in the literature are in the turbulent flow regime using Newtonian fluids. There is:

- Insufficient data for orifice beta ratio 0.2;
- no data in the literature for orifice ratio 0.3;
- data for orifice ratio 0.57 only in turbulent flow;
- non-existent data for fractal-shaped orifice using liquids

Little data is available for non-Newtonian fluids despite their use in the field of polymer processing flow of petroleum products, biomedical engineering, food processing, mineral processing plants, where orifice plates are used as flow meters, choking devices etc.

There is therefore a need for further investigation of flow through orifices under the above mentioned conditions.

2.12 RESEARCH TOPIC IDENTIFIED

It is evident that, from the literature survey done, some aspects need further investigation. The following research topics were identified:

- The determination of non-Newtonian loss coefficients through short square-edged orifice plates. This is based on determination of experimental pressure loss coefficients and discharge coefficients for short square-edged orifice plates with diameter ratio of 0.2, 0.3, 0.57 and 0.7 respectively.
- The determination of pressure loss and discharge coefficients for fractal-shaped orifice plates.
- The development of a correlation for predicting the pressure loss coefficients for regular short square-edged orifices from laminar to turbulent flow.

CHAPTER 3

3.1. INTRODUCTION

The experimental investigation work for this project was conducted on the fittings test rig in slurry laboratory at the Material Science and Technology Group at the Cape Peninsula University of Technology. In this chapter the details of the fittings test rig and how it was used to collect loss coefficient data are described. Two straight pipe lines with inside diameter (ID) 46 mm were installed on the rig.

The following aspects of the experimental work are presented in this chapter.

- Description of the experimental rig;
- instrumentation;
- experimental procedures;
- short square-edged orifice plates tested;
- material tested and,
- experimental errors.

3.2. DESCRIPTION OF EXPERIMENTAL RIG

The experimental rig shown in Figure 3.1 below consists of five lines of PVC pipes with diameters ranging from 25 mm to 80 mm ID. Each line is 25 m long. This length was chosen to allow a fully developed flow upstream and downstream of each fitting.

Test fluids were mixed in a 1.7 m^3 storage tank. The tank was rubber-lined to avoid chemical reactions of fluid with metal. The fluids were circulated in a continuous loop, as follows: From the storage tank, fluids were pumped out with a positive displacement pump before passing through a heat exchanger. After the heat exchanger, the fluid was divided in two lines. Passing through a valve the first line directed the flow to the high part of the rig (which contained two straight pipes with 46 mm ID, where short square-edged orifice plates were inserted). The second line went to the lower part (which contained a bigger pipe, 80 mm ID).

Each of the two routes was fitted with a flow meter (a KROHNE of 50 mm ID [5 l/s] and a SAFMAG of 100 mm ID [80 l/s]). After the flow meters the fluids could enter any of the five test sections. An on/off valve was situated at the beginning of each line for isolation, so that only one line was tested at a time. After a fluid had passed a test section, it was collected via a common

pipe and directed to the storage tank. Another flow meter was installed on the common pipe (65 mm ID, KROHNE flow meter [11 l/s]). At the outlet it was possible to send the fluid through a weigh tank used for calibration purposes.

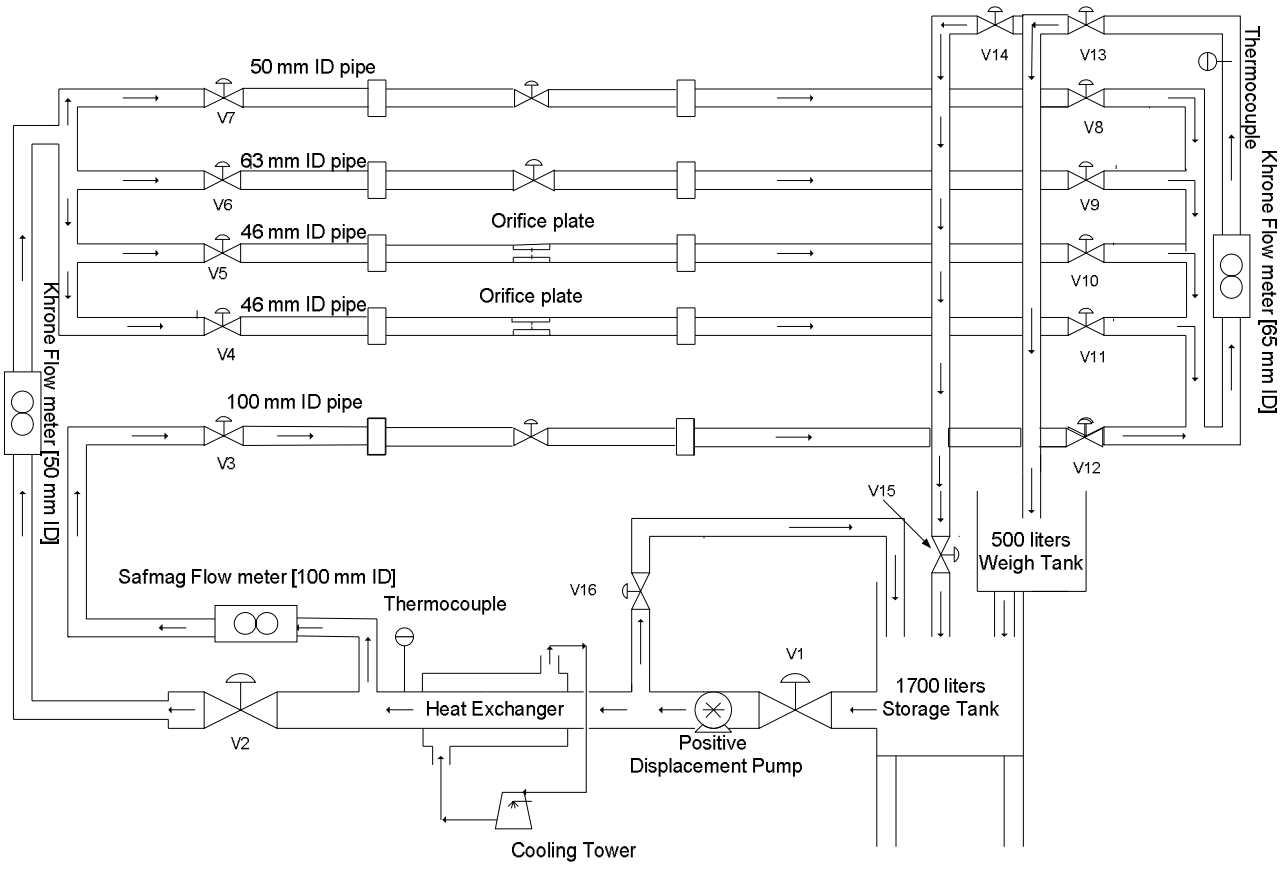

Figure 3.1: Fittings test rig

3.3. INSTRUMENTATION

This section presents all the instruments connected to the rig or used to collect experimental data.

3.3.1 Pressure transducers

In order to measure the pressure, two types of pressure transducers were used: the point pressure transducer and differential pressure transducer.

3.3.1.1 Point pressure transducers (PPT)

A point pressure transducer (PPT) was used to measure the static pressure at a given point in the line test.

The pressure gradients were measured with a pressure transducer of the type PHPWO1V1-AKAYY-OY [GP] version 25.0 Fuji Electric with maximum range of 500 kPa and a precision of 0.25%. The output of this instrument was a DC current ranging from 4 to 20 mA, proportional to the pressure applied. The range and span of this instrument was adjusted by a handheld communicator (HHC).

3.3.1.2 Differential pressure transducer (DP cell)

Differential Pressure Transducers (DP Cell) were used to measure the difference of static pressure between two points.

Two DP cells of the type IKKW35VI-AKCYYAA [DP], version 25.0 Fuji Electric, were used to measure differential pressures. The maximum ranges were 6 kPa and 130 kPa respectively. They had the same characteristics as the PTT, i.e., a precision of 0.25 %, and could be adjusted with a handheld communicator (HHC).

3.3.2 The handheld communicator (HHC)

A Fuji electric handheld communicator, type FXY 10AY A3, was used. This portable instrument was connected to the PPT or DP cell to change parameters such as: data display, range, span, time constant, units, calibration, etc. It was mainly used to change the ranges and to calibrate the transducers.

3.3.3 Data acquisition unit (DAU)

A Hewlett Packard (HP) data acquisition unit (DAU) of the type HP 34970A was connected to a computer. This instrument received, through various channels, analogue signals from different parts of the rig (DP cell, PTT, temperature probes, load cell) and converted them to digital signals compatible with a PC.

3.3.4 Computer

All processes were controlled by a central PC, a Celeron 300. This was coupled with the DAU as an interface and was used to capture and process the experimental data automatically. Test programs were written in Visual Basic 6.

3.3.5 Flow meters

Two Krohne magnetic flow meters were used during test work and were mounted vertically.

- A Krohne IFC 010D of 50 mm internal diameter with a maximum flow rate output of 5 l/s and,
- a Krohne Optilux flow meter of 65 mm internal diameter with a maximum flow rate output of 11 l/s.

3.3.6 Pumps

A progressive cavity positive displacement pump (B9602-C1 EN8N1T), driven by a 15 kW electric motor, was used to circulate the fluid in the test loop. It had a maximum capacity of 11 l/s (39.6 m^3/h). The pump was connected to a Yaskawa variable speed drive (VSD) of type (V100) to obtain desirable flow rates.

3.3.7 Weigh tank and load cell

The weigh tank, similar to the bucket and stopwatch method, was used to determine the mass slurry distribution between the two vessels. This method was used during the calibration or when running a test at low flow rate, i.e, < 1 l/s. The operation of the weigh tank is quite simple. It consisted of a 500 l weigh tank installed above the storage tank. It was suspended to the ceiling via a load cell. The output voltage of the load cell varied linearly with the applied force, and was proportional to the input voltage. The resistors were connected to a power supply which was connected to the DAU. The input voltage divided by the output voltage gave a non-dimensional load cell reading which was independent of the input voltage.

3.3.8 Heat exchanger

A double pipe heat exchanger was installed at the inlet of the rig to keep the test fluids at a constant temperature.

3.3.9 Temperature probes

Two temperature probes were installed to measure the temperature before and after a fluid had entered a test section. One of the temperature probes was located at the exit point of the heat exchanger and the other one before the diversion point between the weigh tank and the mixing tank. The temperature probes information was used to regulate the temperature of the test fluid, using the heat exchanger, and by either reducing or increasing the flow rate of water.

3.3.10 Mixer

A mixer driven by a 3 kW electrical motor, was fitted to the storage tank to mix the test fluids at the preparation stage. At times, the mixer was run during a test to keep the fluid particles suspended.

3.3.11 Valves board

A switchboard made of small ball valves, as shown in Figure 3.2, was used to select a particular test section and direct its pressure readings to specific pressure transducers, so that different test modes could be possible.

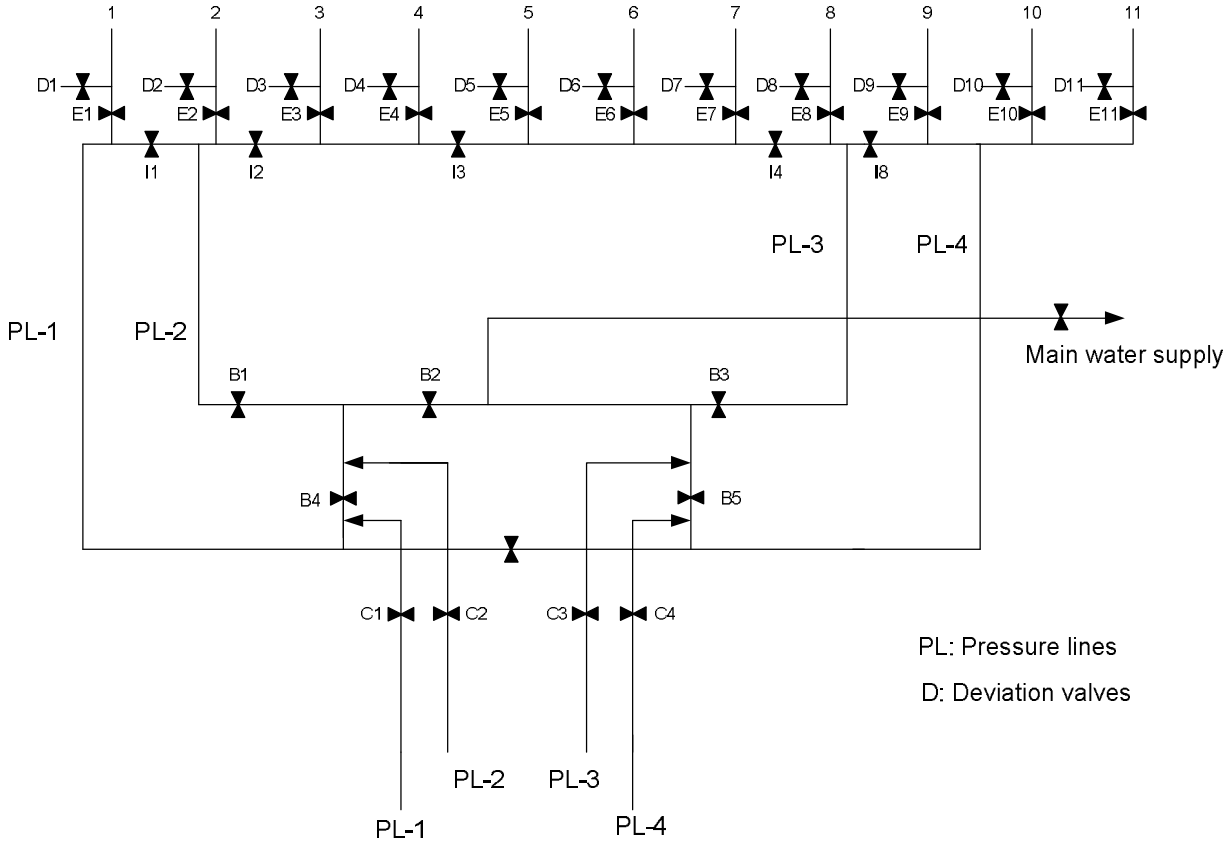

Figure 3.2 : Pressure lines board of the orifice test rig

Figure 3.2 presents schematically the connection of pressure lines on the valves board. These pressure lines were made of nylon tubes of 3 mm internal diameter filled with water. Deviation valves (D1, D2… D11) were on-off valves giving access to pressure transducers. Pressure lines [(PL1… PL4) and (1, 2… 11)] were connected to the test sections' pressure tappings via solid pods filled with water. The purpose of the pods was to collect any solid particles that might

come from the test fluid, preventing them from entering the pressure lines. Each pod had a valve on top and at the bottom. The top valve was for flushing away any air bubbles and the bottom valve was used for flushing away any solid particles.

3.4 EXPERIMENTAL PROCEDURES

This section describes the procedure used to collect the experimental data. It gives the calibration procedures for transducers, load cell and flow meters. This is followed by the measuring procedures for the pipe internal diameter, density, running determination of viscous properties of fluids, and orifice loss coefficients.

3.4.1 Calibration procedures

The aim of the calibration was two-fold:

- Firstly, to ensure that the measuring instrument readings were valid (normally this is done by double checking the measurement with other devices).
- Secondly, to ensure that the readings appearing on the PC via the DAU were as close as possible to actual readings.

3.4.1.1 Load cell

To calibrate load cell, the weigh tank should be empty. It was ensured that nothing disturbed the tank. The calibration procedure was as follows:

1. Switch on the computer and load the calibration program.
2. Select an appropriate channel on the DAU (channel 118); assigned to capture the voltage induced on the load cell.
3. Divert the water flow into the weigh tank and fill it to a certain level.
4. Re-direct the water to the mixing tank.
5. Records the voltage indicated on the DAU and use the bucket to collect all water from the weigh tank, and weigh it on the portable scale.
6. Repeat the exercise for 3 to 5 different water levels and record both the voltage and the weight.
7. Plot the weight versus the voltage and determine the slope and the intercept of the linear relationship.

The linear relationship of the weight versus the voltage for load cell calibration is given in Figure 3.3

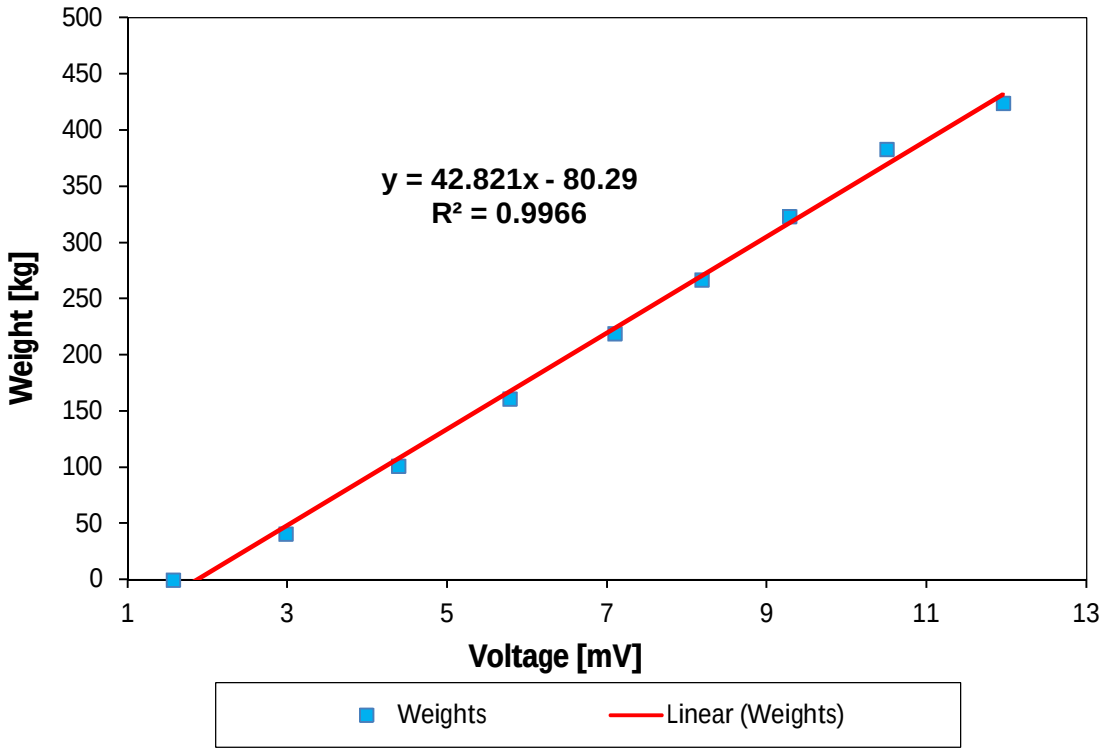

Figure 3.3 : Load cell calibration line

3.4.1.2 Flow meter

The flow meters were calibrated using the weigh tank. The weigh tank was used to record the mass of the water, the DAU was used to record the voltage induced by the flow meter, while the program was used to record both the mass and the time in order to determine the flow rate. The calibration procedure was as follows:

1. Open the computer program and select channel 118 on the DAU for the Krohne IFC 010D of 50 mm internal diameter flow meter.
2. Choose the time interval at which the weight of the tank should be recorded by the computer program.
3. Pump water through the the rig and close valve V3, V12 and V14 (Figure 3.1) to divert the flow through the Krohne IFC 010D flow meter and into the weigh tank.
4. Close the valve at the bottom of the weigh tank to accumulate water in the tank.
5. Start the computer program; stop it when the tank is almost full.
6. Record the voltage reading on the DAU.
7. Empty the weigh tank by opening the valve at the bottom of the tank.
8. Vary the speed of the pump to change the flow rate of water through the rig.

9. Repeat step 4 to 8 to record another set of data.
10. Repeat the same procedure to acquire at least 5 sets of data at differing flow rates.
11. Follow the same procedure to calibrate the Krohne Optilux flow meter of 65 mm internal diameter.

The mass flow rate through the flow meter was determined as the ratio of the recorded mass of the weigh tank to the time it took to fill it. It was converted to the volumetric flow rate by dividing the ratio with the density of water at its recorded temperature.

The linear relationship of the flow rate versus the voltage for the Krohne IFC 010D of 50 mm internal diameter flow meter is given in Figure 3.4 and Figure 3.5 gives the linear relationship of bucket and stopwatch test.

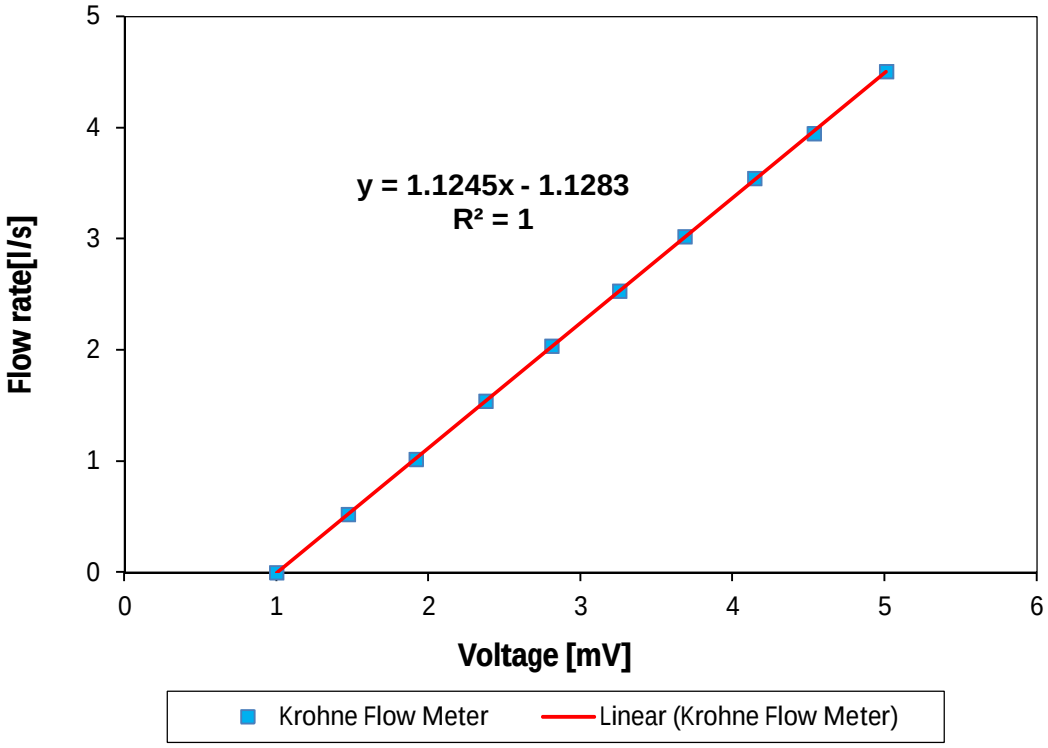

Figure 3.4: Krohne flow meter calibration constants

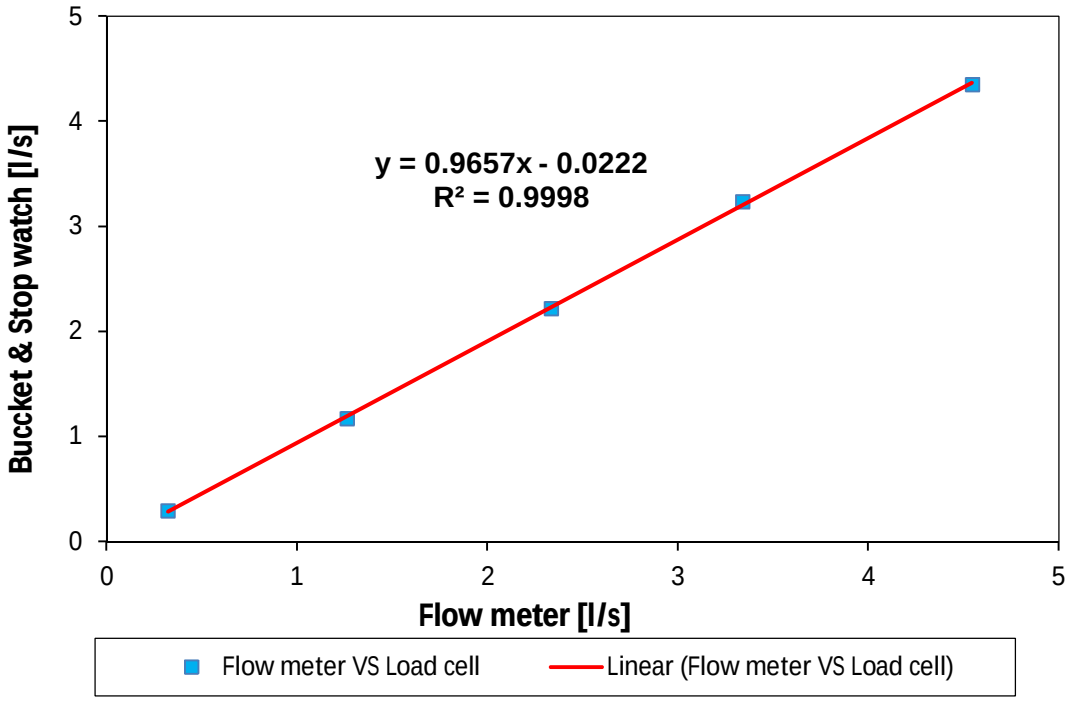

Figure 3.5 : Flow rate comparison between two different methods

3.4.1.3 Transducers

The PPT and DP cells were calibrated using the handheld communicator (HHC). A known pressure was applied directly to the transducers using a hydraulic pump connected to a digital manometer.

The calibration procedure was as follows:

1. Open the calibration computer program and switch on the DAU to channel 101.
2. Open the transducer's cap and set it to zero.
3. Open the pipe valves leading to the transducers and expose them to the atmosphere, to release any pressure induced by the system.
4. Connect the handheld communicator to the transducers and switch it on.
5. Set the handheld communicator to the desired pressure range, either 0-40 kPa or 0–130 kPa, and set it on data recording mode.
6. Read the pressure recorded by the handheld communicator and the voltage recorded by the DAU. This was considered as the zero mark.

7. Apply pressure on the transducers and record both the pressure and the voltage reading on the handheld communicator and the DAU, respectively.
8. Continue to increase the pressure on the transducers, recording the pressure and voltage readings to acquire at least 6 different readings.
9. Plot the pressure readings against the voltage readings to determine the linear relationship between them. The slope and the intercept of this linear relationship were used to relate the pressure applied by the test fluid in the rig to the voltage recorded by the DAU.

The linear relationship of the pressure versus the voltage for the point pressure transducer calibration is given in Figure 3.6:

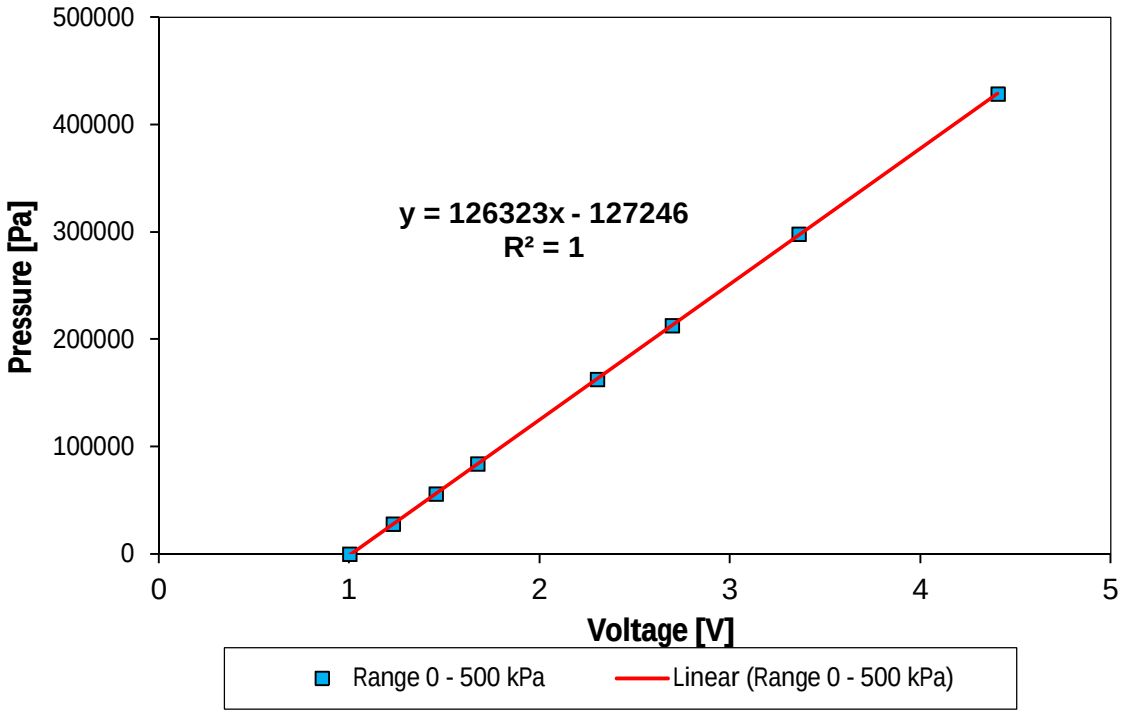

Figure 3.6 : Calibration curve of the pressure transducer

In similar manner the calibration of the DP cell was conducted. The only difference was the channel used on the DAU to record the voltage produced by the pressure in the system. Channel 115 and 116 of the DAU were used to calibrate the DC cells for a pressure drop range of 6 kPa and 130 kPa respectively. The linear relationship of the pressure versus the voltage for the 130 kPa differential pressure transducer calibration is given in Figure 3.8 and, in Figure 3.7 is shown the calibration curve of the 6 kPa differential pressure transducers.

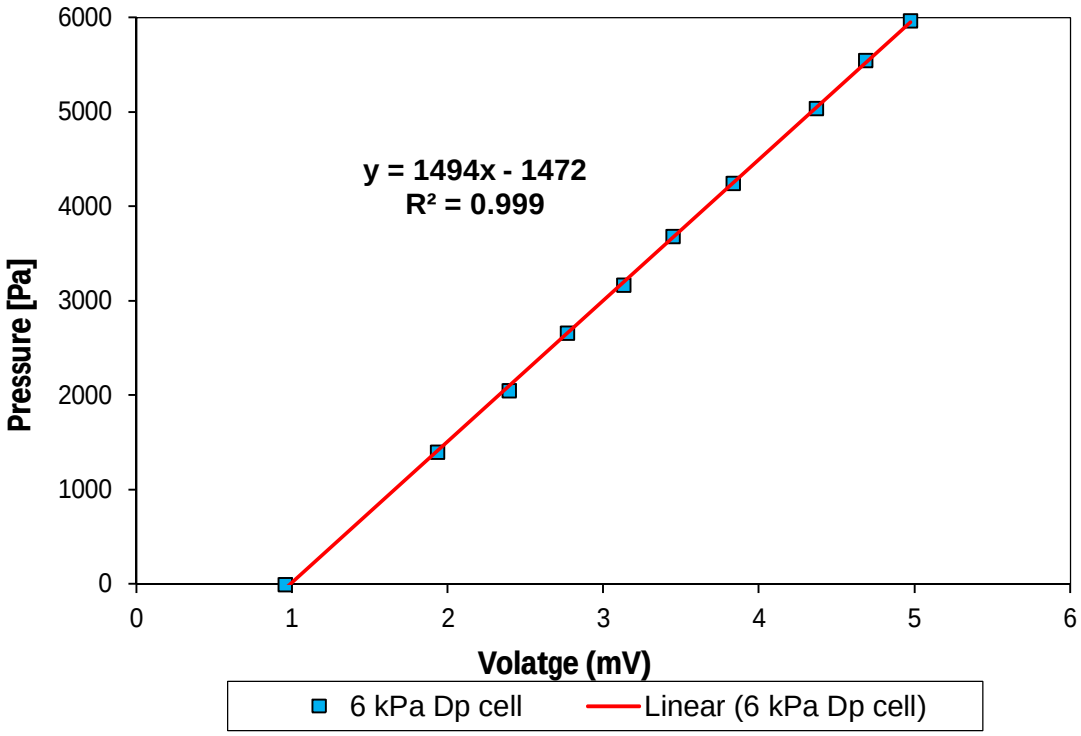

Figure 3.7 : The calibration curve of 6 kPa DP cell

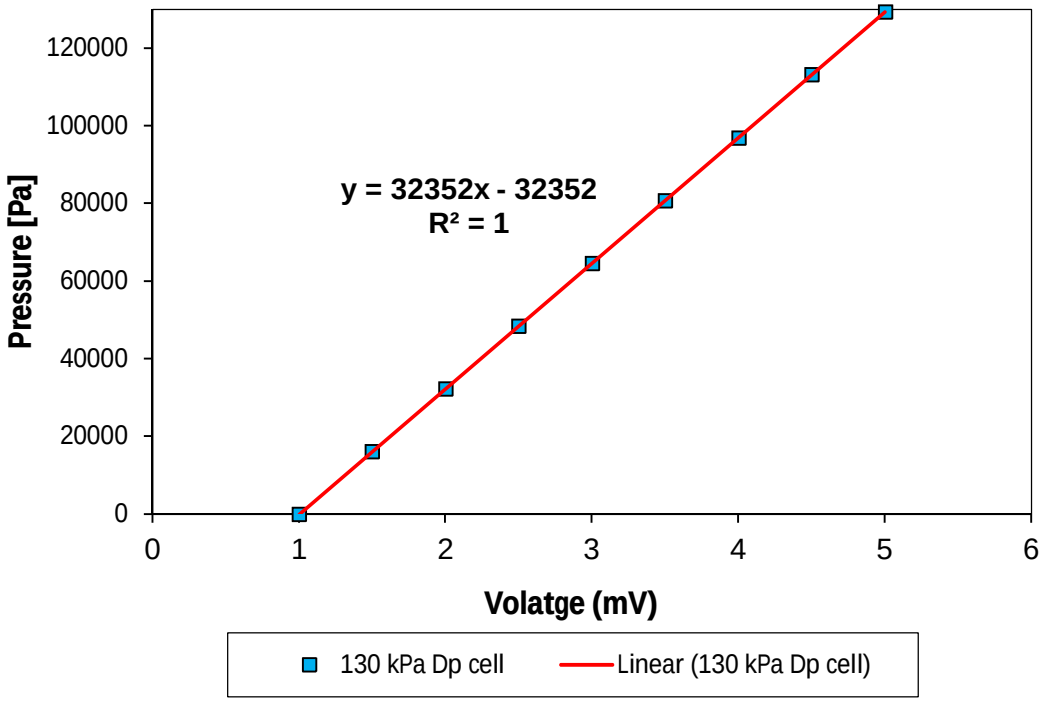

Figure 3.8 : The calibration curve of 130 kPa DP cell

3.4.2 Measurement of the pipe internal diameter

The measurement of the internal diameter of the pipe used in the test section was very important, as the value was needed to calculate the velocity in the pipe line.

The internal diameter was measured by weighing the mass of water (M_w) filling a known length of pipe (L). The pipe diameter was calculated from the Equation 3.1 below:

$$D = \sqrt{\frac{4M_w}{\pi\rho_w L}} \qquad \text{Equation 3.1}$$

where ρ_w is the water density.

The method used to determine the diameter of the test section on the fitting test rig is as follows:

1. A pipe was unscrewed at the flanges and removed from the rig.
2. The pipe was fitted with a rubber plug or valve (ball valve) mounted on the flanges at the end of the pipe.
3. The pipe was positioned into an upright position, with a valve at the bottom of the pipe, and filled with water.
4. The next step was to measure the temperature of the water and determine its density at that temperature from the literature.
5. The water level in vertically positioned pipe was marked as point A_0.
6. Water was drained out of the pipe to the level A_1 by opening the valve at the bottom of the pipe. The distance between A_0 and A_1 was measured and the water drained was weighed and recorded.
7. Water was again drained to another level, A_2. The mass of the drained water was recorded and the distance of the drained water measured. This was repeated three more times to obtain a set of four readings of drained mass and the drainage distance.
8. Using the measured mass of water, M_w, drainage length, L, and known water density, Equation 3.1 was applied to determine the internal diameter of the pipe.

The result of the measurement is shown in Table 3.1.

Table 3.1: **Internal diameter of the pipe test results**

Pipe 1								
	Weight							
	Empty [kg]	Empty + water [kg]	Water [kg]	Length [m]	Temp. [°C]	Density [kg/m^3]	Diameter [m]	Average diameter [m]
Bucket 1	0.7	3.9	3.2	1.86	21	998.6	0.0468	
Bucket 2	0.7	4.46	3.76	2.296	21	998.6	0.0457	
Bucket 3	0.7	3.9	3.2	1.86	21	998.6	0.0468	
Bucket 4	0.7	4.46	3.76	2.296	21	998.6	0.0457	
Pipe 2								
	Weight							
	Empty [kg]	Empty + water [kg]	Water [kg]	Length [m]	Temp. [°C]	Density [kg/m^3]	Diameter [m]	
Bucket 1	0.7	5.42	4.72	2.865	21	998.6	0.0458	
Bucket 2	0.7	3.9	3.2	1.965	21	998.6	0.0456	
Bucket 3	0.7	5.42	4.72	2.865	21	998.6	0.0458	
Bucket 4	0.7	3.9	3.2	1.965	21	998.6	0.0456	
Pipe 3								
	Weight							
	Empty [kg]	Empty + water [kg]	Water [kg]	Length [m]	Temp. [°C]	Density [kg/m^3]	Diameter [m]	
Bucket 1	0.7	1.14	0.44	0.276	21	998.6	0.0451	
Bucket 2	0.7	3.7	3	1.835	21	998.6	0.0457	
Bucket 3	0.7	4.46	3.76	2.3	21	998.6	0.0457	
Bucket 4	0.7	1.16	0.46	0.276	21	998.6	0.0461	
Bucket 5	0.7	3.7	3	1.835	21	998.6	0.0457	
Bucket 6	0.7	4.48	3.78	2.3	21	998.6	0.0458	
Pipe 4								
	Weight							
	Empty [kg]	Empty + water [kg]	Water [kg]	Length [m]	Temp. [°C]	Density [kg/m^3]	Diameter [m]	
Bucket 1	0.7	4.18	3.48	2.116	21	998.6	0.04579	
Bucket 2	0.7	2.94	2.24	1.375	21	998.6	0.04558	
Bucket 3	0.7	2.2	1.5	0.92	21	998.6	0.04559	
Bucket 4	0.7	4.18	3.48	2.116	21	998.6	0.04579	
Bucket 5	0.7	2.96	2.26	1.375	21	998.6	0.04578	
Bucket 6	0.7	2.2	1.5	0.92	21	998.6	0.04559	0.0458

3.4.3 Measurement of the fluid relative density

The slurry relative density (RD) and the slurry density (ρ) were determined carefully for each fluid tested. It was measured from a slurry sample collected from a sampling valve on the rig. About one litre of fluid was collected; half of it was retained and labelled for future reference. The test was performed according to a standard procedure as follows:

1. Three clean, dry 250 ml volumetric flasks were weighed (M_1).
2. A slurry sample was taken from a tapping in the pipe wall. The slurry was poured into those flasks (approximately half of the volume) and was weighed (M_2).
3. The volumetric flasks were filled up to the graduated mark of the flasks (250 ml level) with clear water and weighed again (M_3).
4. The flasks were emptied, filled with clear water to the same graduated mark of the flasks and each was weighed again (M_4).
5. The relative density RD was defined as $RD = \rho/\rho_w$

Calculations

Mass of slurry: M_2-M_1

Mass of water filling the flask: M_4-M_1

Mass of water filling the space left by the fluid: M_3-M_2

Mass of water having volume equal to that of the fluid: (M_4-M_1)-(M_3-M_2).

$$RD = \frac{\text{Mass of fluid}}{\text{Mass of equal volume of water}} = \frac{(M_2 - M_1)}{(M_4 - M_1) - (M_3 - M_2)} \qquad \text{Equation 3.2}$$

3.4.4 Orifice test procedures

The aim of a test on the orifice line on the fittings rig was to obtain a set of pressure drops across the orifice plate. These set of pressure drops were further transformed into a set of pressure loss coefficient k_{or} (Equation 2.7) versus Reynolds number and discharge coefficient C_d (Equation 2.18) versus Reynolds number. In general, this section explains step by step the operation mode of the orifice test rig. The operation was as follows:

3.4.4.1 General mode

1. Switch on the computer and open the desired program of test operation, i.e., the HGL manual mode, the straight pipe test.
2. Switch on the mixer to mix the slurry evenly.
3. Open fully the by-pass valve V16, positioned immediately after the pump, to ensure that there is no build-up of pressure in the rig if the wrong valves are open or if all outlet valves are closed.
4. Switch on the pump and set it at the desired speed to achieve a certain flow rate.
5. Open all the diaphragm valves in the system to circulate the test fluid left in the rig.
6. Close the by-pass valve V16 and let the rig run for an hour to thoroughly mix the test fluid.
7. As the orifice line test is on the top of the rig, to conduct the test on this line, ensure that valve V2 is open and valve V3 is closed. Then close all other valves on the top of the rig except the one that is leading the fluid into the 46 mm internal diameter which contain short orifice.
8. Flush the pressure pods and the pressure line board and fill them with tap water, ensuring that there are no bubbles in the tubes.
9. Decide on the required pressure tappings on the test section and record their distances in the appropriate columns of the spreadsheet on the computer program.
10. Open the valves of the tappings leading to the pressure pods.
11. Use the handheld communicator to set the pressure range to be used during the test.
12. Set the computer program to the determined pressure range and the chosen pipe diameter, and indicate the type of fluid to be tested.
13. connect the pressure tapping to the transducers by opening or closing the appropriate valves on the pressure lines board
14. Take a sample of the fluid and conduct RD tests, and record the information on the computer program.
15. Start the test.
16. Change the flow rate of the fluid by increasing or decreasing the pump speed.

17. Perform the flow stability control test and take a reading only if the flow has stabilised.

The test liquid was circulated from the tank to the test section using a positive displacement pump. The flow rate was controlled by a by-pass valve V16 and measured with two different flow meters. The liquid discharge from the test section was returned to the liquid storage tank. The test section was 25 m long and consists of a horizontal upstream straight pipe, an orifice plate and a downstream straight pipe. The test section was provided with pressure taps at various points of the upstream and downstream sections of the pipe. The static pressure at different points was measured by using the point pressure transducers or differential pressure transducers. The fluids were maintained at a temperature between 25°C and 30°C.

3.4.4.2 Pressure grade line test

The pressure grade line test was conducted by reading the static pressure using only one point pressure transducer for all eleven tapping points. The procedure was as follows referring to pressure lines board (Figure 3.2):

1. The exit valve E1 is open to read the pressure on tapping 1.
2. E2 to E11 are closed.
3. The deviation valves (D1 to D11) are closed. The isolation valves are open.
4. The bypass valves (B1 to B6) are closed, also closed are the connecting ball valves except C1.
5. C1 is connected to the point pressure transducer 1.
6. Record the pressure reading.
7. Close valve E1 and open E2.
8. Read the pressure, close E2 and open E3.
9. Continue the procedure described in Step 1 for E2 etc… until E11 is open.

3.4.4.3 Straight pipe test or rheology mode

The straight pipe test can be conducted simultaneously on the downstream and upstream legs of the orifice test section. It was used to measure the viscous properties of the slurries. The test consisted of measuring pressure drop over a straight part of the test section at least 50D away from the bend or test orifice. The pressure drops were measured with two DP cells separately, but simultaneously. This test was conducted in at least three different diameter pipes to evaluate the wall slip effect.

The procedure is as follows referring to Figures 3.2:

1. Choose the straight pipe section on which the pressure drop will be measured and record the tapping distance.
2. On the pressure lines board close the isolating valves I1, I3 and I4.
3. Open the valves E according to the test sections chosen. All deviation valves and the other E valves must be closed.
4. Close the by-pass valves B2, B4, B5, and B6
5. Use the pressure line PL-1 and PL-2 to measure the pressure drop upstream of the test orifice by opening the connecting valves C1 and C2.
6. Ensure that the pressure line PL-1 is connected to the high side of the DP cell and PL-2 to the low side of the DP cell.
7. Use the pressure line PL-3 and PL-4 to measure the pressure drop downstream of the test orifice by opening the connecting valves C3 and C4.

3.5. ORIFICES TESTED

The orifices tested in this study were concentric orifice plates mounted between a pair of flanges. The orifice is equidistant to the inside diameter of the pipe. These orifices are suitable for slurry applications. A photograph of a circular orifice is shown in Figure 3.10. A drawing of a circular orifice and triangular orifice with sharp apex and with round apex of these orifices are shown in Figures 3.11, 3.12 and Figure 3.13. Table 3.2 presents in detail the dimension of orifices tested.

Table 3.2 : Dimension of orifices tested

Orifice bore diameter, d [mm]	β ratio	Orifice bore thickness, t [mm]
9.2	0.2	6
13.8	0.3	6
26.2	0.57	6
32.2	0.7	6

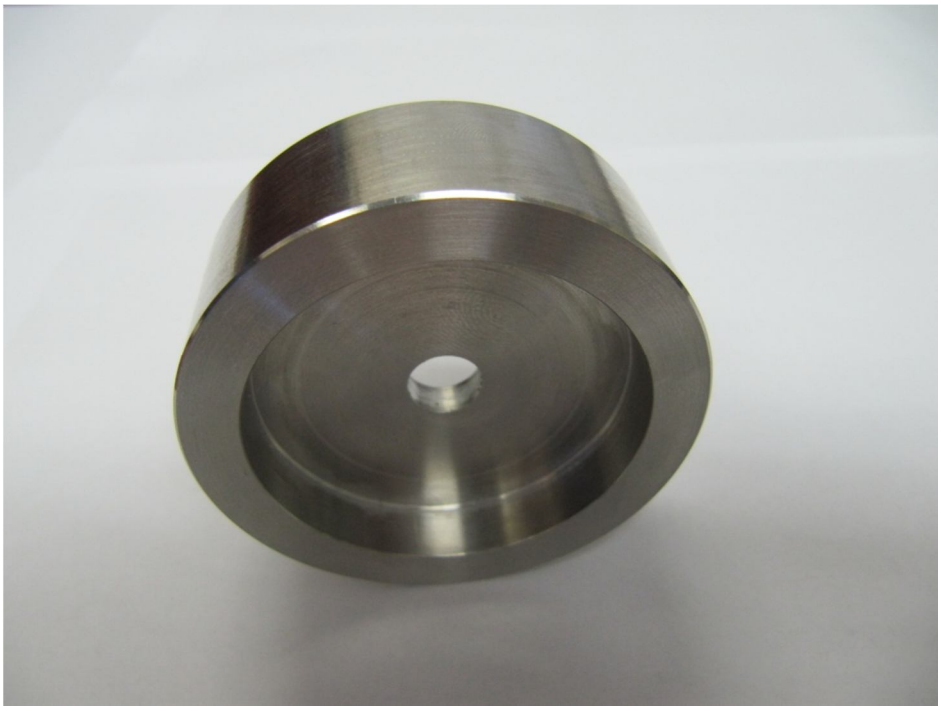

Figure 3.9 : Photograph of short orifice plate with β ratio 0.2

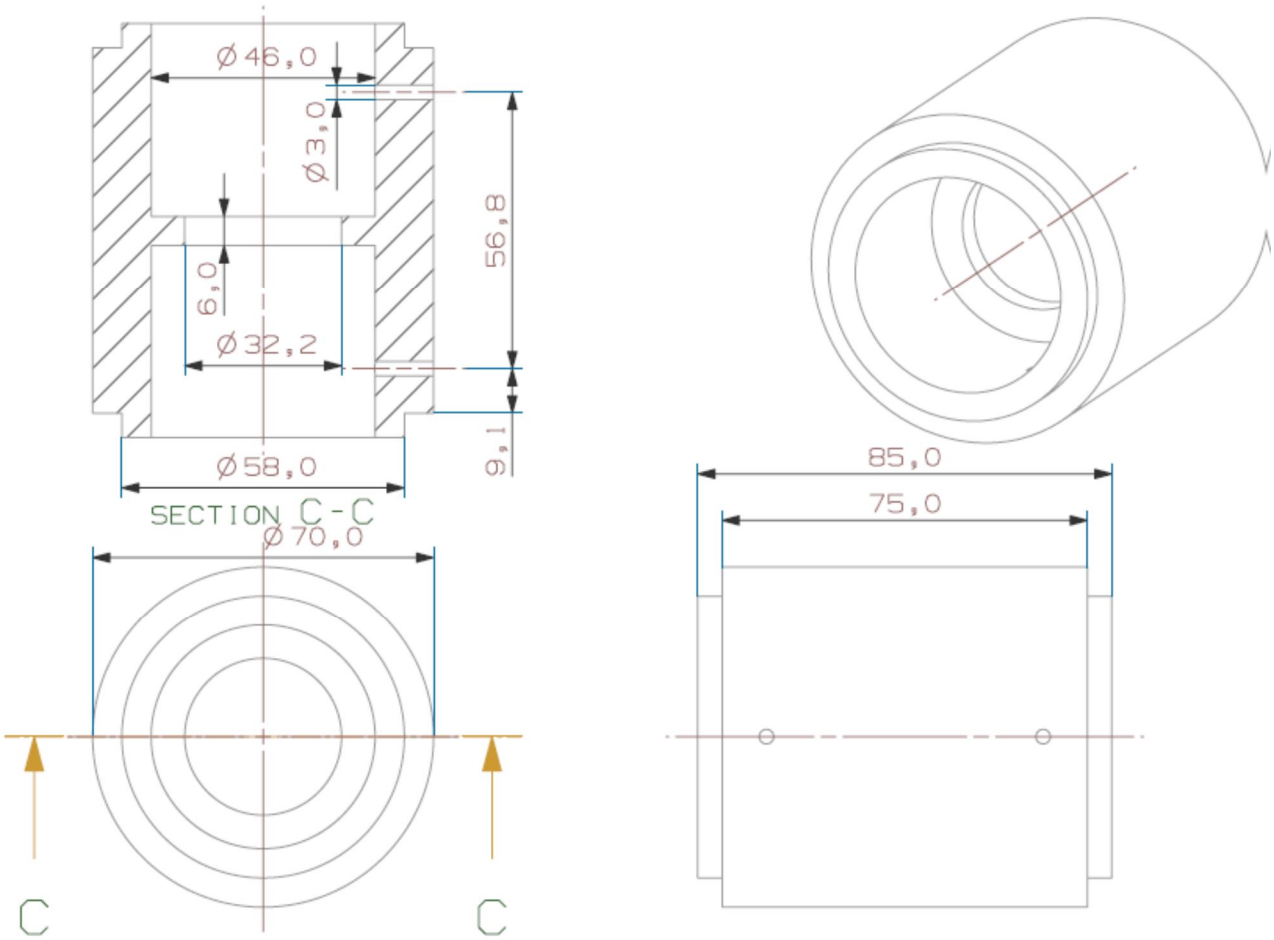

Figure 3.10 : Drawing of short orifice plate with β ratio 0.7

Two more generation 0 Von Koch fractal-shaped orifice plates were tested. These orifices consist on triangular shaped orifices with round apex and sharp apex. The equivalent diameters of the two orifices were the same as that of the regular circular orifice with beta ratio 0.57. Figure 3.11 and 3.12 show the drawing of the generation 0 of Von Koch fractal-shaped orifice plates.

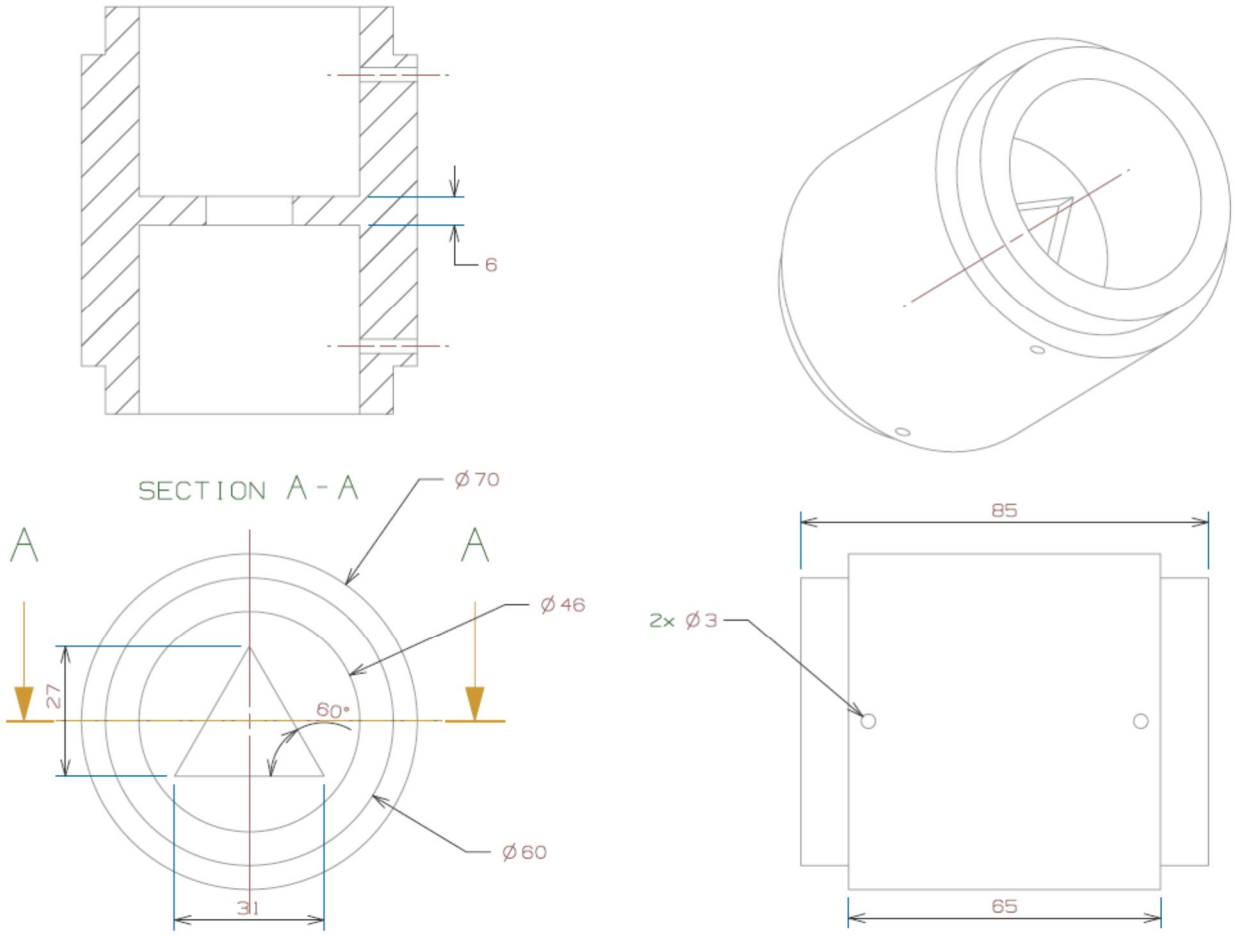

Figure 3.11 : Drawing of triangular short orifice plate with sharp apex (equivalent diameter, β = 0.57)

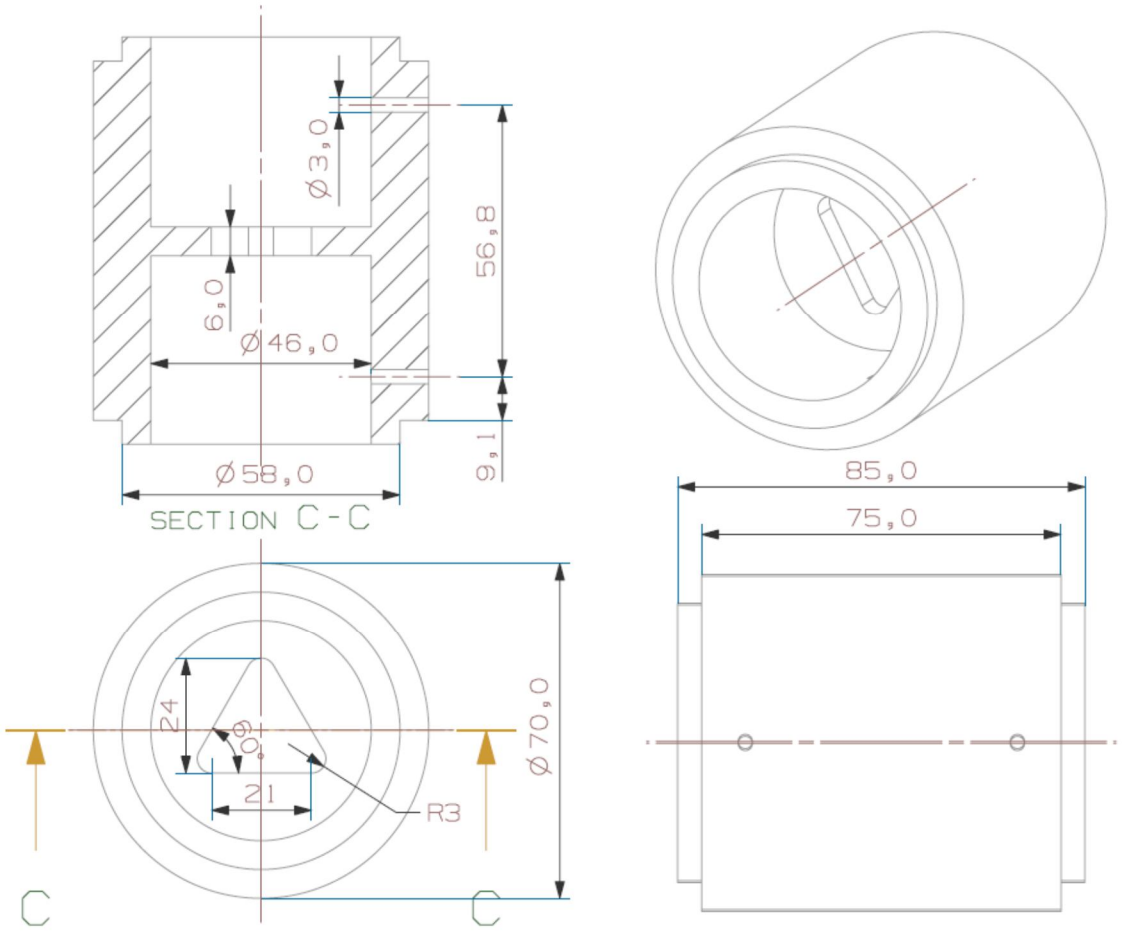

Figure 3.12 : Drawing of triangular short orifice plate with round apex (equivalent diameter, β = 0.57)

3.6. FLUIDS TESTED

In order to perform the tests, fluids were selected to represent a wide range of rheological behaviour associated with industrial slurries. The Newtonian fluid (water) was used for the calibration of the orifice test section. Non-Newtonian fluids (carboxymethyl cellulose, bentonite and kaolin at different concentrations) were tested to derive and to provide loss coefficient data, which will be useful for designing pipelines in industries. A detailed description of these fluids is given below.

3.6.1 Water

Ordinary municipal tap water was tested in straight pipes to establish credibility, accuracy and precision of the procedure and apparatus. It was also used in the mixture to make up other fluids. The typical properties of water are as follows: a pH of 9 with a total alkalinity of 35 mg/l as $CaCO_3$ and an ionic strength of less than 0.01 molar scale.

3.6.2 Kaolin

Kaolin slurries used were prepared using tap water with kaolin powder. A mixer, in the mixing tank, was used to mix the suspension thoroughly. The kaolin slurry was mixed in volumetric concentrations of 8%, 14%, 19%, 20%, 21%and 24%.

3.6.3 Carboxy methyl cellulose (CMC)

The carboxy methyl cellulose was supplied in granular form in bags of 20 kg. Solutions of this material at 4%, 5%, 6%, 7% and 8% were prepared. Solutions were then mixed for at least 48 hours before being pumped into the rig. Care was taken to avoid formations of lumps. Solutions of CMC are stable between pH of 2 and 10. Below pH 2, precipitation of the solids occurs, and above pH 10 the 'viscosity' decreases rapidly. The pH of the solutions tested for this study was pH 9.0 at 20ºC.

CMC is used for industrial applications such as in drilling mud, in detergents as a soil-suspending agent, in resin emulsion paints, adhesives, printing inks, as protective colloid in general and as a stabiliser in foods.

3.6.4 Bentonite

Bentonite suspensions used were prepared by mixing tap water with bentonite powder. A mixer, in the mixing tank was used to mix the solution thoroughly. It was supplied in powder form in bags of 40 kg and was mixed in mass concentrations of 6% and 9%.

3.7 EXPERIMENTAL ERRORS

In research it is of utmost importance to be aware of the sources of errors and to minimise them. Even though care has been taken to minimise errors, absolute accuracy in measuring is not always achieved, unless the data are discrete numbers. There are three types of error: Gross errors, systematic errors and random errors (Benziger & Aksay, 1999).

3.7.1 Gross errors

Gross errors are due to blunders, equipment failure and power failure. A gross error is immediate cause for rejection of a measurement (Benziger & Aksay, 1999).

3.7.2 Systematic or cumulative errors

Systematic errors result in constant bias in an experimental measurement. Systematic errors are those that are due to known conditions. These conditions might be:

- natural (temperature, pressure, humidity, etc.);
- instrumental (calibration, graduation, range, etc.) ; and,
- operator (poor sight of the experimenter, inability of the experimenter to take correct reading, etc.) (Barry, 1991).

In this work precautions were taken to prevent those errors occurring, e.g, checking the calibration of instruments by another instrument not related to the instrument, or independent calibration, and also by checking the reproducibility of the results.

3.7.3 Random errors

Random errors are statistical fluctuations (in either direction) in the measured data due to the precision limitations of the measurements device. Most experiments proceed with minor variations that change from event to event and follow no systematic trend. The same quantity may be measured many times, giving close but not identical results. The fluctuations in the measurement are assumed to be random and lead to a distribution of values (Barry, 1991).

3.8 ERRORS IN MEASURED VARIABLES

Normally an absolute error equivalent to the resolution or the least increment of the instrument can be assumed to occur on any measurement done. The errors of measurable variables may be associated with the precision of the instrument used to measure them.

3.8.1 Axial distance

The axial distances were measured using a measuring tape divided up in mm. The absolute error on measurements of ± 0.001 m can be assumed on axial distance measured to locate the pressure tapping.

3.8.2 Weight

The mass of all samples was measured using an electronic balance (Denver Instrument) graduated in grams. The absolute error on measurements was 0.001 kg.

3.8.3 Flow rate

The flow rates were measured with Krohne flow meters accurate to 0.001 l/s (1 ml/s), which can be assumed as the absolute error.

3.8.4 Pressure

The pressure transducers used were accurate to 0.25%. Care should be taken in calibration to obtain a correlation coefficient of 0.999.

3.8.5 Evaluation of errors

The absolute error is the difference between the true value of any number or quantity and the value obtained or used for that number or quantity in a given circumstance. If the true value of a number or quantity is X, the value obtained or used for that number or quantity is A, and the absolute uncertainty is ΔA then:

$$X = A \pm \Delta A \qquad \text{Equation 3.3}$$

This means that X is between $A - \Delta A$ and $A + \Delta A$. ΔA is called the maximum error. If X is a quantity, ΔA is expressed in the same unit. ΔA is here the smallest division of the instrument, and the smallest value detected by the instrument (Barry, 1991). ΔA is calculated from the standard deviation of a set repeated measurement as well. The absolute error for A at 99,9% confidence interval is given by the equation:

$$A = 3.29\sigma \qquad \text{Equation 3.4}$$

where σ is the standard deviation

If a 95% confidence level is considered, then the absolute error may be approximated by:

$$\Delta A = 2\sigma \qquad \text{Equation 3.5}$$

The relative or percentage error of a number or quantity is calculated by:

$$\delta A = \frac{\Delta A}{A} \qquad \text{Equation 3.6}$$

3.8.6 Errors in computed variables

When a variable is a result of a computation of other variables with their subsequent errors, the resulting error is the combination of the independent variable errors (mean quadratic value of the independent errors). Errors are unavoidable when analogue signals from instruments such as a flow meter, a pressure transducer etc are converted into a digital signal by the DAU. Quantities such as inner pipe diameter, shear stress, shear rate, Reynolds number, pressure loss coefficient and discharge coefficient are dependent on more than one measurement. If a variable X is a function of n other variables, i.e., X = F (a, b, c,…n), the expected highest error (Brinkworth, 1968) can be calculated from:

$$\left(\frac{\Delta X}{X}\right)^2 = \sum \left(\frac{\partial X}{\partial n}\right)^2 \left(\frac{n}{X}\right)^2 \left(\frac{\Delta n}{n}\right)^2 \qquad \text{Equation 3.7}$$

where X is the computed result

ΔX, is the computed result absolute error.

n are the independent variables involved

Δn are the independent absolute errors.

3.8.7 Errors of derived variables

In this section errors analysis has been used to quantify the errors for pipe diameter, wall shear stress, pressure loss coefficient, discharge coefficient, Reynolds number (Re_3).

3.8.7.1 Pipe diameter error

The highest expected error in calculating the pipe diameter is obtained by applying Equation 3.7 to 3.1 that yields Equation 3.8.

$$\frac{\Delta D}{D} = \pm \frac{1}{2}\sqrt{\left(\frac{\Delta M_w}{M_w}\right)^2 + \left(\frac{\Delta L}{L}\right)^2} \qquad \text{Equation 3.8}$$

Table 3.3 presents the summary of combined errors for a pipe diameter.

Table 3.3 : Expected highest error for 46 mm ID diameter pipe

ID pipe diameter (mm)	Expected error (ΔD/D) %
46	0.40

3.8.7.2 Velocity errors

The velocity in pipes can be accurately established using Equation 2.59. The highest expected error for the velocity estimation can be found by using the Equation 3.9 below:

$$\frac{\Delta V}{V} = \pm \sqrt{\left(\frac{\Delta Q}{Q}\right)^2 + 4\left(\frac{\Delta D}{D}\right)^2} \qquad \text{Equation 3.9}$$

3.8.7.3 Pseudo shear rate errors

The highest expected errors for pseudo shear rate are calculated as follows:

$$\frac{\Delta \dot{\gamma}_0}{\dot{\gamma}_0} = \pm \sqrt{\left(\frac{\Delta Q}{Q}\right)^2 + 5\left(\frac{\Delta D}{D}\right)^2} \qquad \text{Equation 3.10}$$

3.8.7.4 Wall shear stress errors

The wall shear stress is given by the Equation 2.29.

$$\tau_0 = \frac{D.\Delta P}{4L} \qquad \text{Equation 2.29}$$

The combined errors of the wall shear stress were determined by applying Equation 3.7 in Equation 2.29 and the error analysis yields the following equation:

$$\frac{\Delta \tau_0}{\tau_0} = \pm \sqrt{\left(\frac{\Delta(\Delta P)}{\Delta P}\right)^2 + \left(\frac{\Delta D}{D}\right)^2 + \left(\frac{\Delta L}{L}\right)^2} \qquad \text{Equation 3.11}$$

3.8.7.4 Reynolds number errors

In this investigation the Slatter Reynolds number Re_3 has been used; the error on Reynolds was then evaluated on Re_3 which is given by Equation 2.70:

$$Re_3 = \frac{8\rho V_{ann}^2}{\tau_y + K\left(\frac{8V_{ann}}{D_{shear}}\right)^n} \qquad \text{Equation 2.70}$$

The highest expected error for wall shear stress was found by using the following equation:

$$\frac{\Delta R_3}{Re_3} = \pm\sqrt{\left(\frac{\Delta\rho}{\rho}\right)^2 + 4\left(\frac{\Delta Q}{Q}\right)^2 + \left(\frac{\Delta L}{L}\right)^2 + 25\left(\frac{\Delta D}{D}\right)^2 + \left(\frac{\Delta(\Delta P)}{\Delta P}\right)^2} \qquad \text{Equation 3.12}$$

3.8.7.5 Pressure loss coefficient

The orifice pressure loss coefficient is obtained using Equation 2.7. The highest expected error in calculating the pressure loss coefficients was found by means of the following equation:

$$\frac{\Delta k_{or}}{k_{or}} = \pm\sqrt{\left(\frac{\Delta(\Delta P_{or})}{\Delta P_{or}}\right)^2 + \left(\frac{\Delta\rho}{\rho}\right)^2 + 4\left(\frac{\Delta Q}{Q}\right)^2 + 16\left(\frac{\Delta D}{D}\right)^2} \qquad \text{Equation 3.13}$$

3.8.7.6 Discharge coefficient

The discharge coefficient of the orifice plate was found by using Equation 2.18. Using Equation 3.7 for the highest expected error analysis yields the following equation:

$$\left(\frac{\Delta C_d}{C_d}\right)^2 = \left(\frac{\Delta Q}{Q}\right)^2 + 0.25\left(\frac{\Delta(\Delta P)}{\Delta P}\right)^2 + \left(\frac{\Delta A_2}{A_2}\right)^2 + 0.25\left(\frac{\Delta\rho}{\rho}\right)^2 + \left(\frac{4\beta^6\Delta\beta^2}{(1-\beta^4)^2}\right) \qquad \text{Equation 3.14}$$

It could be seen that the error in diameter will propagate more than the others in the overall errors of k_{or}, Re_3 and C_d followed by error in flow rate.

A set of 25 readings at same flow rate was collected in order to evaluate the accuracy of the test rig in data capturing for pressure and discharge coefficient.

Typical expected highest errors in calculating pressure loss coefficient data and discharge coefficient data for a short square-edged orifice plate with diameter ratio 0.2, 0.3, 0.57, 0.7 are given in Table 3.4.

Table 3.4 : Highest expected errors in calculating k_{or} and C_d

β	$\left(\frac{\Delta k_{or}}{k_{or}}\right)$ calc %	$\left(\frac{\Delta k_{or}}{k_{or}}\right)$ Exp %	$\left(\frac{\Delta C_d}{C_d}\right)$ calc %	$\left(\frac{\Delta C_d}{C_d}\right)$ Exp %
0.2	15.23	9.25	12.36	1.78
0.3	19.98	13.27	10	2.06
0.57 (circ)	30.06	29.87	15.33	0.93
0.57 (sharp)	56.31	56.25	28.16	2.33
0.57 (round)	53.86	53.62	26.93	7.80
0.7	76.36	52.32	38.18	3.76

3.9. CONCLUSION

The experimental procedure and related aspects presented in Chapter 3 may be summarised as followed:

- The test section was 25 m long and consists of a horizontal upstream straight pipe, an orifice plate and a downstream straight pipe (Figure 3.1).
- Detailed dimensions and drawings of the orifices tested were presented (Table 3.2; Figures 3.10 to 3.12).
- The experimental equipment has been described. It is reliable and can be used to measure the loss coefficient through short orifice plates.
- Experimental procedures such as test, calibration, measurement of density and pipe internal diameter were explained. The basic operation used to provide useful data of loss coefficient for different purposes has been outlined.
- The proprieties of fluids tested (kaolin slurries, carboxyl methyl cellulose, bentonite and water) as well as their particular purposes have been described.
- The relative experimental errors were evaluated, analysed and quantified (Table 3.3 and Table 3.4).
- The water test results will be correlated to the Colebrook & White equation and the rheogram of rheological characterisation of the non-Newtonian fluids will also be presented in Chapter 4.
- The orifice pressure loss and discharge coefficient results will be presented in Chapter 4.

CHAPTER 4

4.1 INTRODUCTION

The aim of this investigation was to measure pressure loss and discharge coefficients for short square-edged orifice plates. In this chapter, the procedure followed to obtain and analyse experimental data is explained. The results are presented as follows:

- The friction factor water results obtained in straight pipe test was compared to the calculated friction factor (Equation 2.54) to ascertain the precision of the experimental procedure.
- The rheological characterisation of non-Newtonian fluids tested is explained.
- The method for validating the measured pressure loss and discharge coefficients, based on the evaluation of the hydraulic grade line is explained.
- Finally, based on pressure drop across the orifice plate, the laminar and turbulent pressure loss coefficients and discharge coefficients were calculated.
- The output of the experimental work is summarised in:
  - plots of pressure loss coefficients versus Slatter Reynolds numbers for short square-edged orifice plates at different beta ratios;
  - plots of discharge coefficients versus Slatter Reynolds numbers for short square-edged orifice plates at different beta ratios.

4.2 STRAIGHT PIPE RESULTS

The straight pipe test results obtained in this investigation are presented in this section for both water and non-Newtonian fluids. The straight pipe results are important in order to establish the credibility of the test rig, as well as for the rheological characterisation of non-Newtonian fluids.

4.2.1. Clear water test

In order to establish the accuracy and the credibility of the equipment, water tests were conducted in a straight pipe section. The pipe roughness was determined by measuring the pressure drop across a known length of pipe and by comparing it with the Colebrook - White equation, Equation 2.54 (Massey, 1990). Figure 4.1 shows the comparison of the experimentally obtained shear stress (τ_0) with the calculated shear stress using the friction

factor obtained from the Colebrook-White equation. The value of k was found to be 10 µm, which is acceptable for smooth wall pipes.

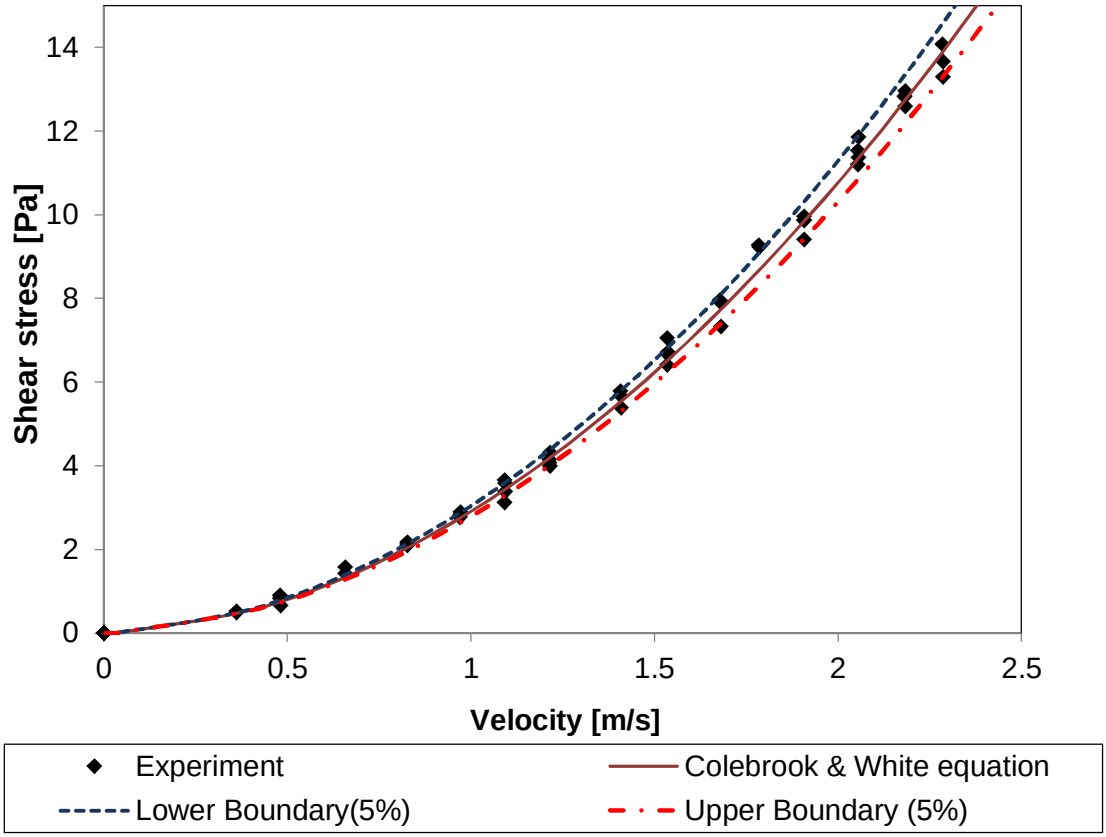

Figure 4.1 : Water test comparison with Colebrook-White equation

From Figure 4.1, it can be seen that 80% of the data were within ± 5% of the calculated prediction for the 46 mm ID pipe. Such agreement indicates the validity and degree of accuracy of the experimental technique and equipment used in the current investigation.

4.2.2 Non-Newtonian fluids

The objective of this section is to explain how the rheological constants were obtained. The non-Newtonian fluids tested were kaolin suspensions, bentonite suspensions and CMC solutions. Rheological constants obtained for non-Newtonian fluids will be presented for CMC at 4%, 5%, 6%, and 8% concentration by mass and kaolin of 8%, 14%, 19%, 20% and 24% and bentonite at 6% and 9% concentration by volume (C_v).

4.2.2.1 Fitting the pseudoplastic model

The power-law model was fitted to wall shear stress (τ_0) against pseudo shear rate (8V/D) data to determine the rheological constants of CMC. The data consisted of both upstream and downstream sections of three different pipes. The viscous flow data in the laminar region should be coincident for the three different pipes, if not; there is probably a wall slip effect that should first be corrected. Chhabra and Richardson (1999) warn that serious errors could occur when the wall slip is not accounted for. To account for the wall slip, more than one diameter tube should be tested. Only laminar data were considered in the determination of rheological constants. A power law trend curve was fitted to the data to obtain the constant n' (apparent flow behaviour index) and K' (apparent fluid consistency index).

$$\tau_0 = K' \left(\frac{8V}{D}\right)^{n'} \qquad \text{Equation 2.50}$$

A typical pseudo-shear diagram is shown in Figure 4.2.

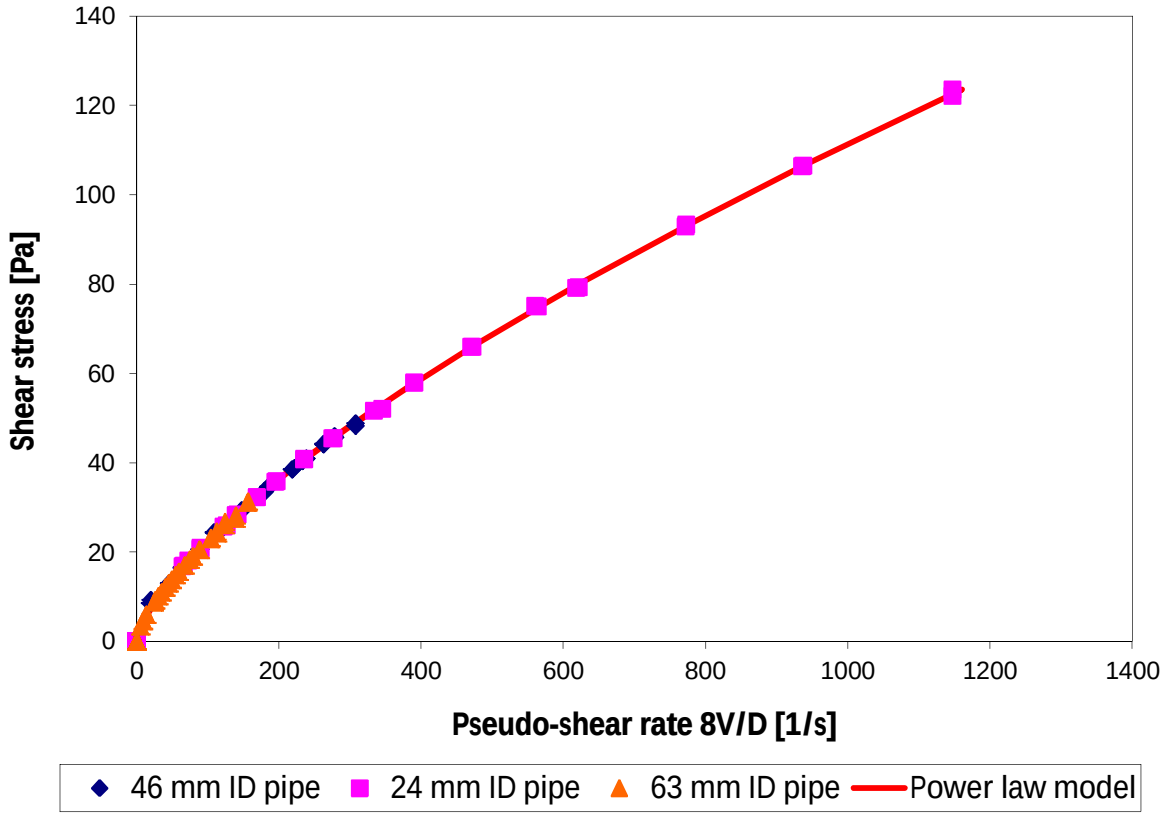

Figure 4.2 : Pseudo-shear diagram for straight pipe test of CMC 6%

A combined flow curve of all CMC's concentration tested is presented in Figure 4.3 below. In addition Table 4.1, gives the rheological constants obtained for CMC at 4%, 5%, 6%, 7% and 8%.

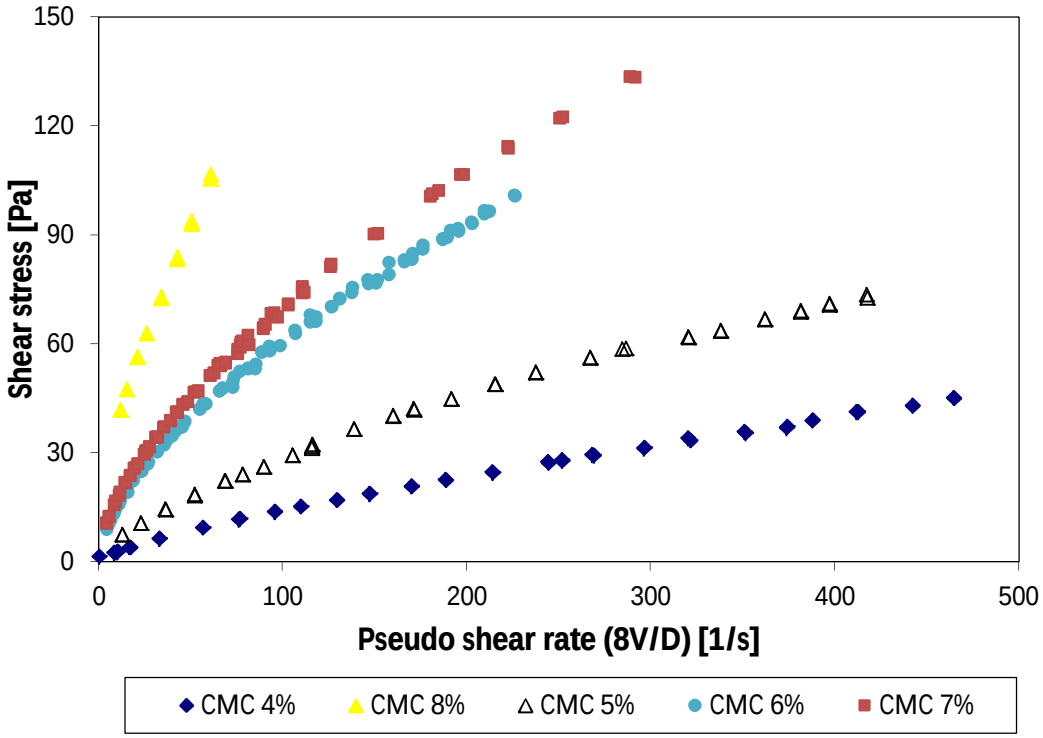

Figure 4.3 : Pseudo-shear diagram of CMC at different concentrations

The Rabinowitsch-Mooney relation (Equations 2.50 and 2.51) were used for the transformation of the rheological constants to the true values.

Table 4.1 : Rheological constants of CMC

%Concentration [m]	Density [kg/m^3]	n'= n [-]	K' [Pa.s$^{n'}$]	K [Pa.s^n]
4	1023	0.75	0.5	0.48
5	1029	0.64	1.38	1.26
6	1036	0.62	3.40	3.11
7	1041	0.60	3.85	3.50
8	1043	0.60	8.30	7.56

4.2.2.2 Rheological characterisation of kaolin suspensions

Kaolin suspensions from two different batches were tested in this study. The first batch of kaolin "A" was tested at concentrations of 8%, 14% and 20%. The second batch of kaolin "B" was at 14%, 19%, 21% and 24%. The yield pseudoplastic model (Equation 2.46) was used to determine the flow behavior of the two types of kaolin suspensions. An example of the yield pseudo plastic model fit is given in Figure 4.4 for kaolin suspension from three different straight pipes.

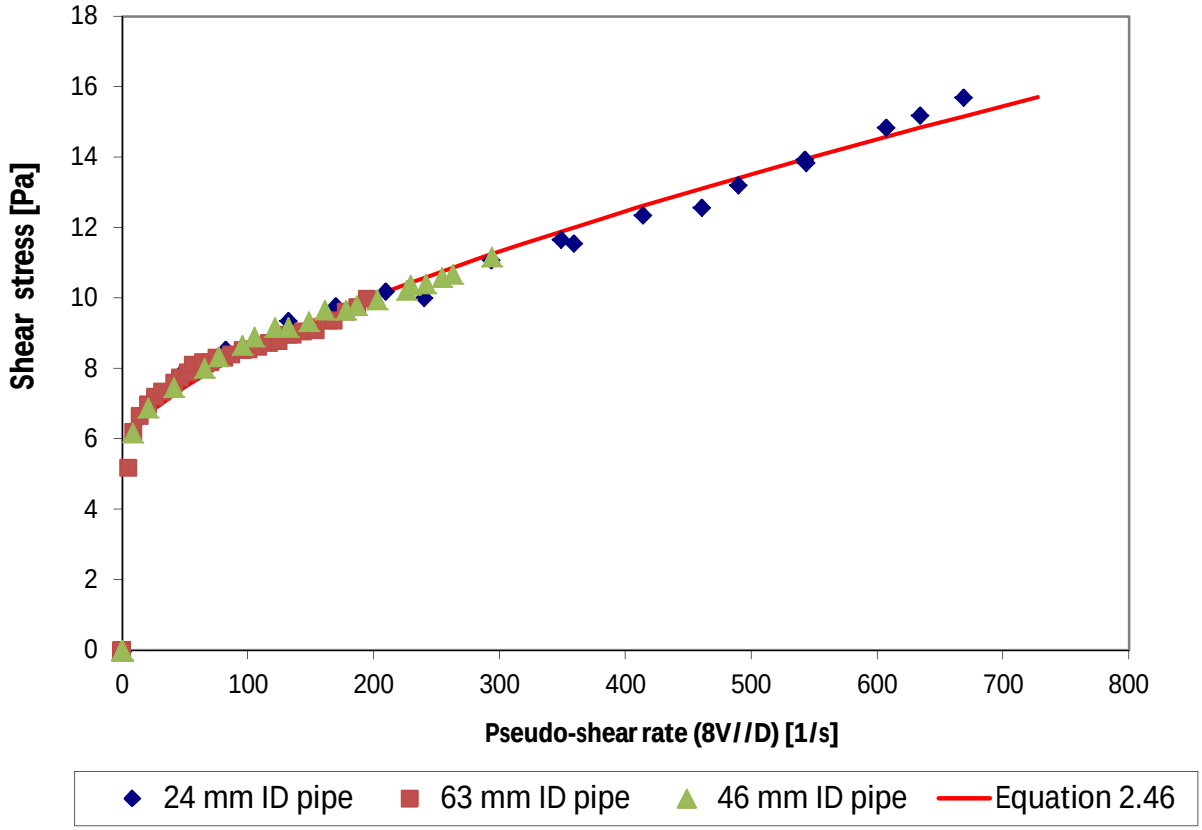

Figure 4.4 : Pseudo-shear diagram for straight pipe test of 14% kaolin suspension

A combined flow curve of both types of kaolin suspensions tested at different volume concentrations is presented in Figure 4.5. Table 4.2 gives the rheological constants used in this investigation for kaolin suspension at different volume concentrations. It was observed that the yield stress (τ_y), increased with the increasing slurry concentration. No difference was seen between kaolin 14% A and B; also between kaolin (19%) B, and kaolin 20% (A).

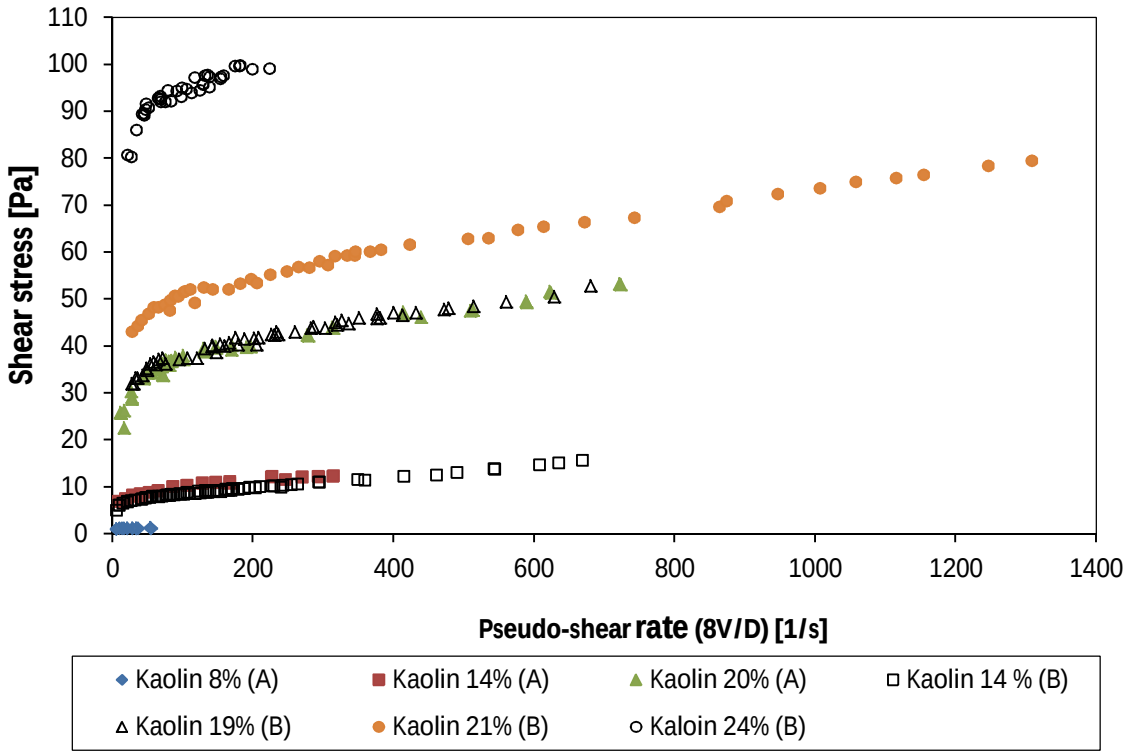

Figure 4.5 : Pseudo-shear diagram of kaolin suspensions at different concentrations

Table 4.2 : Rheological constants of kaolin suspensions

Concentration (v) [%]	Density [kg/m^3]	τ_y [Pa]	K [Pa.s^n]	n [-]
8 (A)	1140	0.6	0.6	0.5
14 (A)	1242	6.2	0.2	0.4
20 (A)	1324	19.1	2.4	0.4
14 (B)	1227	5.2	0.08	0.7
19 (B)	1319	25.4	0.8	0.5
21 (B)	1349	37.0	0.4	0.6
24 (B)	1393	63.0	5.1	0.3

4.2.2.3 Rheological characterisation of bentonite suspensions

Equation 2.46, assuming Bingham plastic behavior, was used to determine the rheological parameters of the bentonite suspensions. The model was fitted to the laminar shear stress and shear rate data from all straight pipes to determine τ_y and K, as the apparent flow behaviour index (n) is known to be equal to one for a fluid showing a Bingham plastic behaviour. The bentonite tested might have a time dependent behaviour or thixotropic behavior. It was therefore sheared over a long time to reduce time dependant effects before the tests were conducted and

then it behaved reasonably well as was also noted by Haldenwang (2003). Figure 4.6 shows a typical straight pipe test for 6% bentonite.

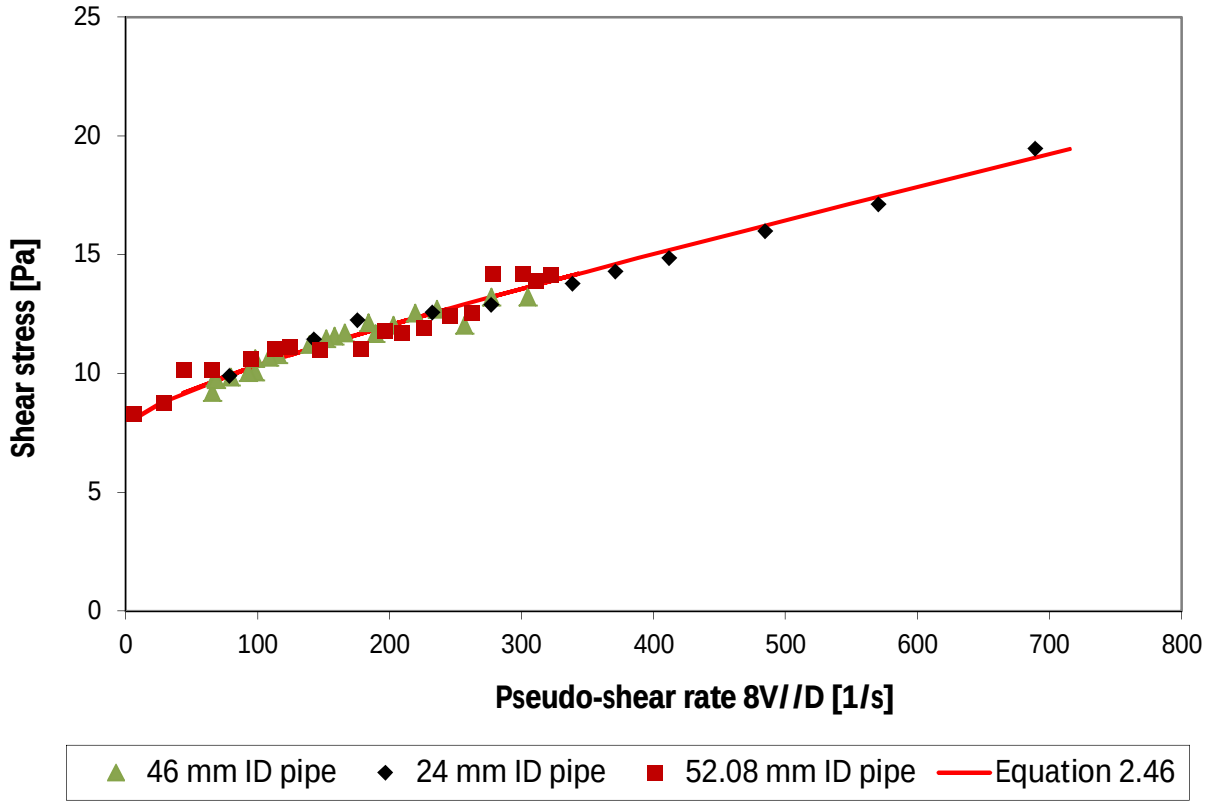

Figure 4.6 : Pseudo-shear diagram for straight pipe test of 6% bentonite

A combined flow curve of the two different concentrations of bentonite tested in this work is given in Figure 4.7 below. In addition, Table 4.3 gives the rheological constants used in this investigation for bentonite at 6% and 9% concentration by volume.

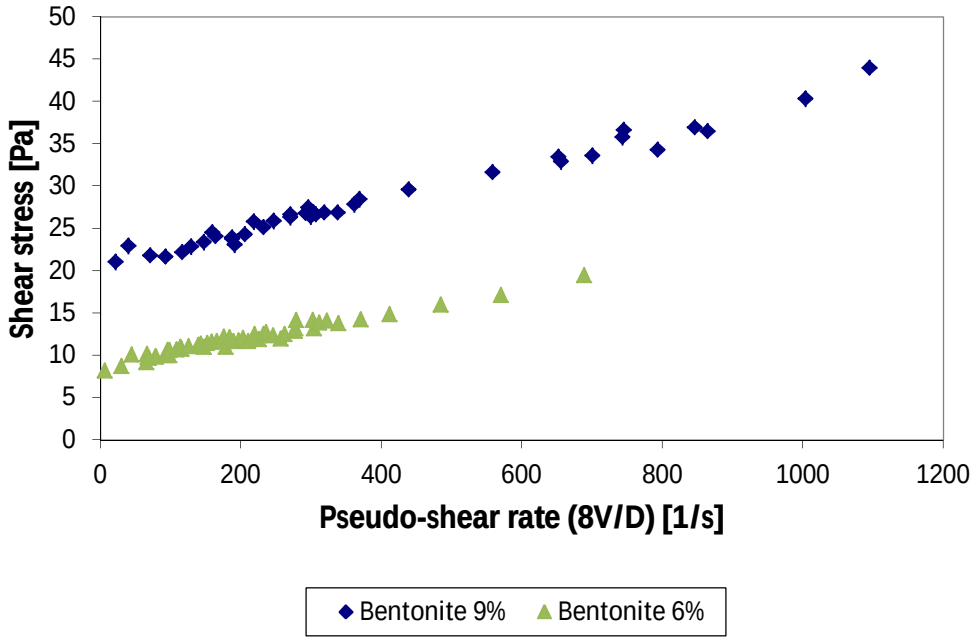

Figure 4.7 : Pseudo-shear diagram of bentonite at 6% and 9%

Table 4.3 : Rheological constants of bentonite suspensions

Concentration (m) [%]	Density [kg/m^3]	τ_y [Pa]	K [Pa.s^n]	n [-]
9	1058.2	17.24	0.017	1
6	1040.1	6.70	0.014	1

A wide range of rheological parameters were obtained for the selected fluids with yield stress data ranging from 0.6 - 63 Pa, K values from 0.014 – 10 Pa.s^n and n ranged from 0.3 -1.

4.2.2.4 Friction factor chart evaluation

To evaluate the accuracy of the rheological parameters, friction factor values were calculated using Re_3 which accommodates the rheological constants. The calculated friction factor was compared to the theoretical friction factor, Equation 2.35, for laminar flow and Equation 2.55 for turbulent flow. Figures 4.8 to 4.10 show charts of friction factor respectively for CMC solution, kaolin suspension and bentonite suspension at different concentrations.

Figure 4.8 presents a friction factor chart comparison for CMC solutions tested in this investigation with the theoretical friction factor. It can be seen from Figure 4.8 that the majority of CMC experimental friction factor data agree well with the theoretical friction factor, 85% of experimental data fell within +/- 15% of the calculated friction factor.

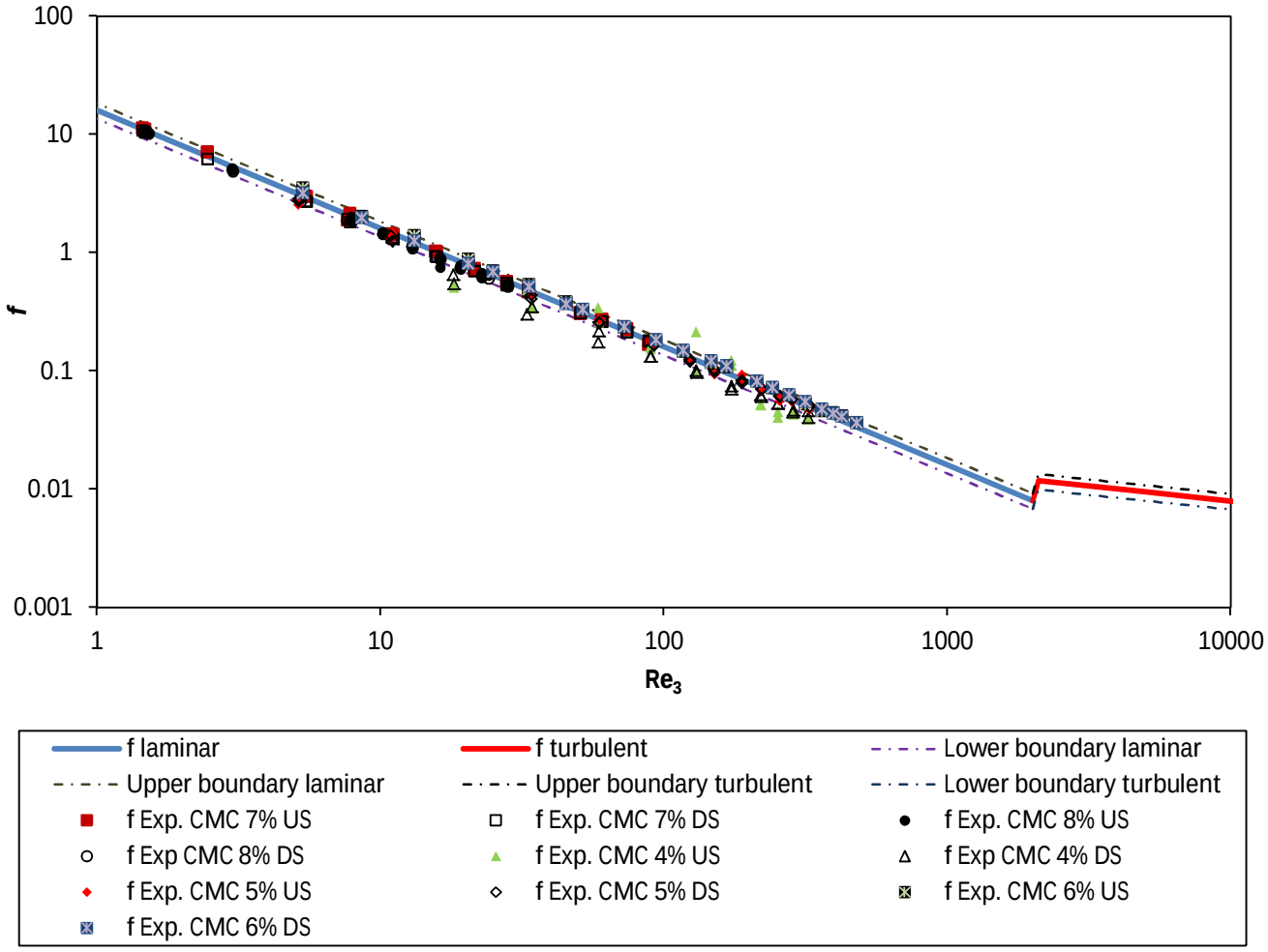

Figure 4.8 : Friction factor comparison for CMC at 4%, 5%, 6%, 7% and 8%

Figure 4.9 shows the comparison of experimental data of a combined two types of kaolin suspension with the theoretical friction factor. The figure shows a good agreement between experimental and calculated friction factor. Seventy percent (70%) of experimental data were within ± 15% of the theoretical friction factor.

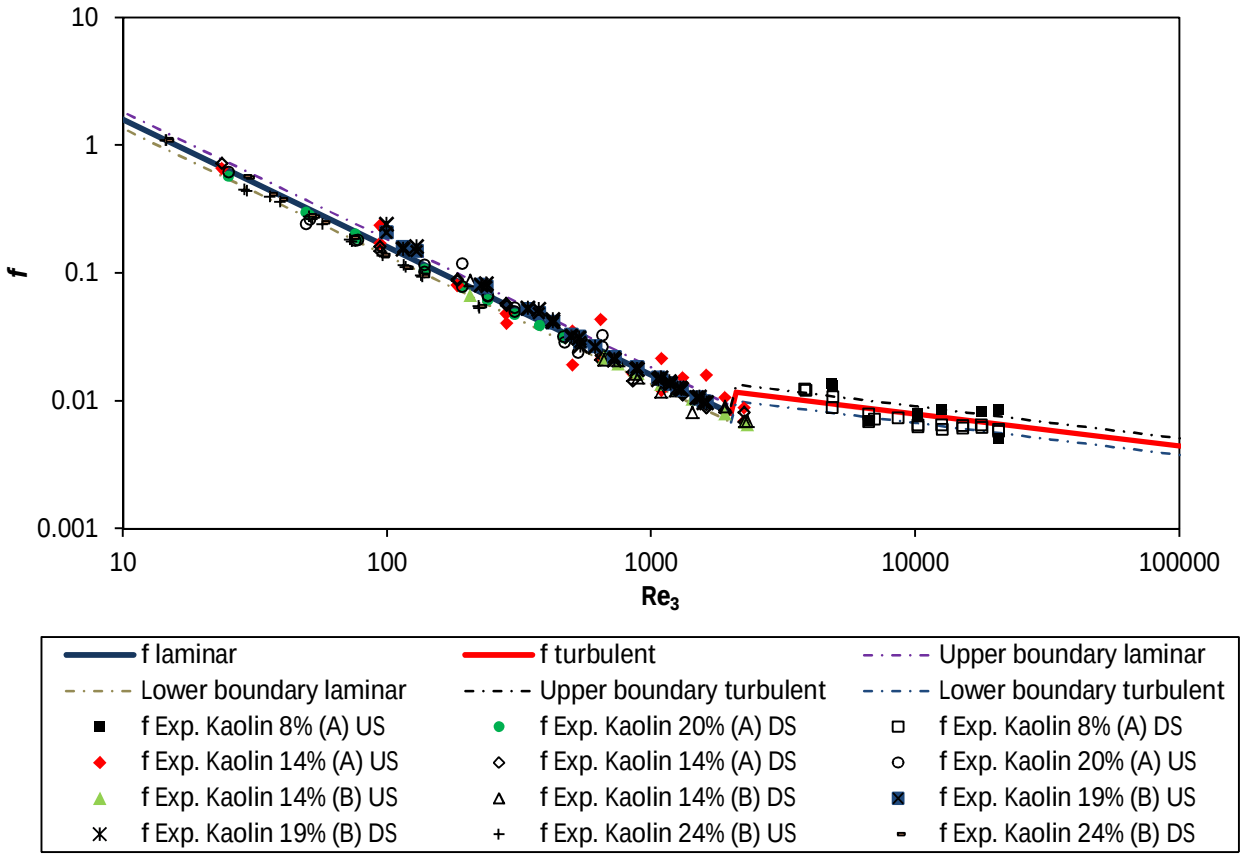

Figure 4.9 : Friction factor comparison for kaolin suspensions

Figure 4.10 shows a comparison between the theoretical friction factor and the experimental friction factor for bentonite suspension at different concentrations. It can be seen from Figure 4.10 that 70% of the experimental data fell within ± 15% of the calculated friction factor.

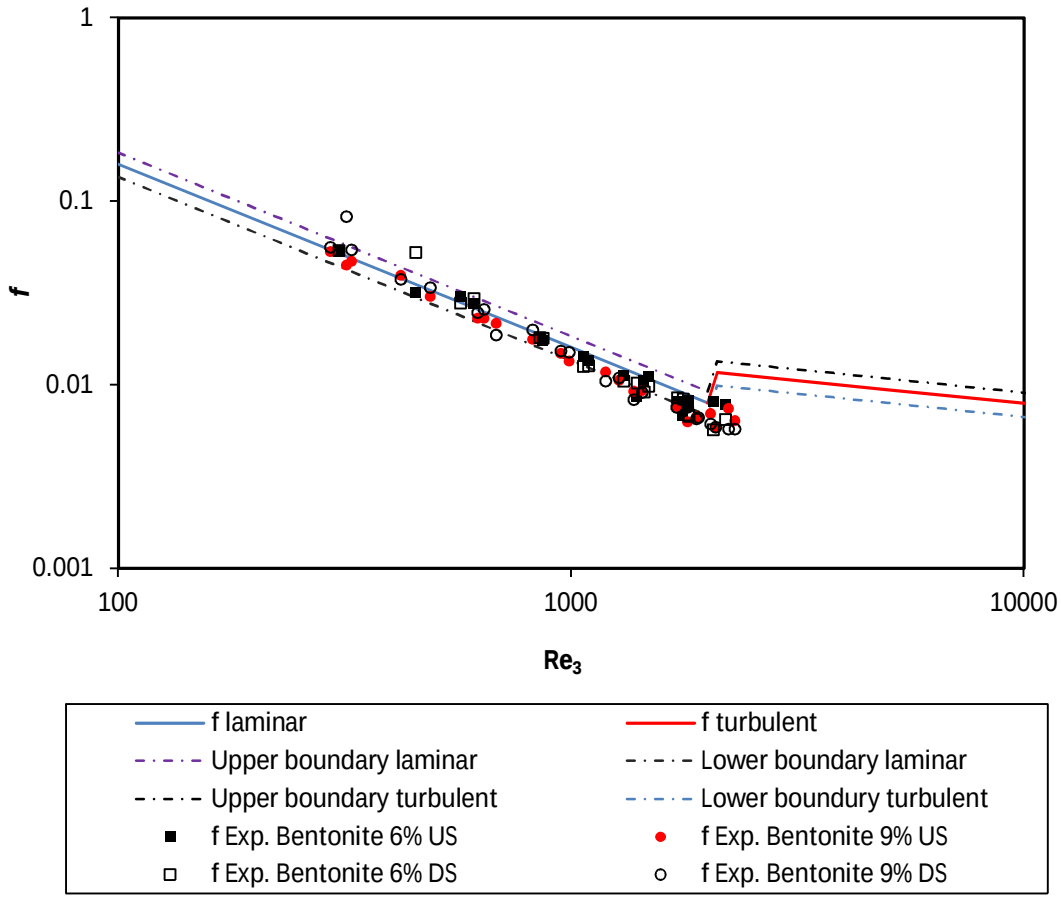

Figure 4.10 : Friction factor comparison for bentonite suspension at 6% and 9%

It can be seen from Figure 4.8 – 4.10 above that the experimental friction factor agrees well with the theoretical friction factor. This type of agreement indicates the validity and degree of accuracy of the equipment, experimental and analytical techniques used in this investigation.

4.3 PRESENTATION OF PRESSURE LOSS COEFFICIENT RESULTS

Orifice plates with different beta ratios have been tested. Head loss data for non-Newtonian fluid in pipe fittings can be meaningfully correlated as plots of loss coefficient versus Reynolds number (Edwards et al., 1985*).* In this case, the Slatter Reynolds number which can accommodate the rheological parameters obtained in this work was used to correlate the pressure loss coefficient.

4.3.1 Orifice pressure loss coefficient determination

The pressure drop across the orifices was determined as the difference between the upstream intercept and downstream intercept as shown in Figure 4.11. It should be noted that the abscissa origin was set at the centre of the orifice. The coordinates of the static pressure versus the tapping distances (measured from the orifice centre line as origin) was used to determine the slopes and the intercepts of the grade lines upstream and downstream of the orifices. Some data points close to the test orifice might be in the region where the flow was distorted due the presence of the orifice; those data points were excluded. Therefore, the first four data points and the last three data points only were selected in the linear regression respectively upstream and downstream of the orifice. Once the pressure drop across the orifice was obtained, the orifice pressure loss coefficient was calculated using Equation 2.7.

$$k_{or} = \frac{\Delta P_{or}}{\frac{1}{2}\rho V_1^2}$$ Equation 2.7

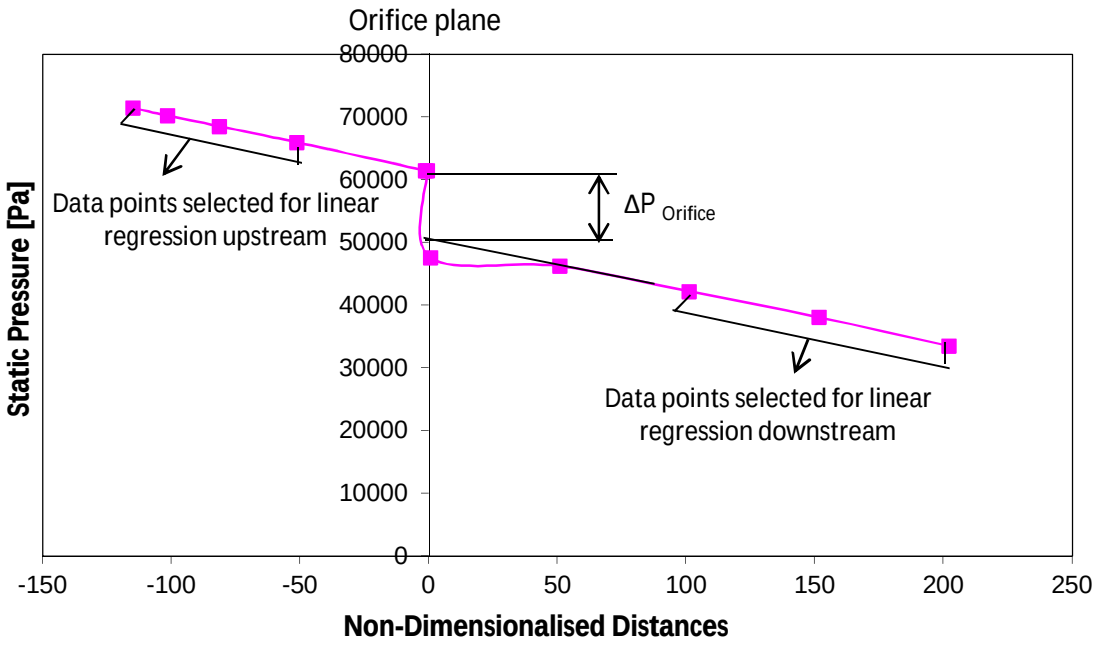

Figure 4.11 : Selection of data points for extrapolation of the orifice pressure drop (ΔP_{or})

In order to give to the operator from the onset of the test runs an indication of the validity of the tests, the first major output of the experimental rig was the static pressure at each tap and flow rate. To proceed with the test work it is very important that the hydraulic grade line be linear and the difference between the upstream and downstream slope be less than 4% (Kabwe et al.,

2010). Otherwise, the operator must stop running the test and check what the problem is. Figure 4.12 below shows a typical plot of pressure grade lines.

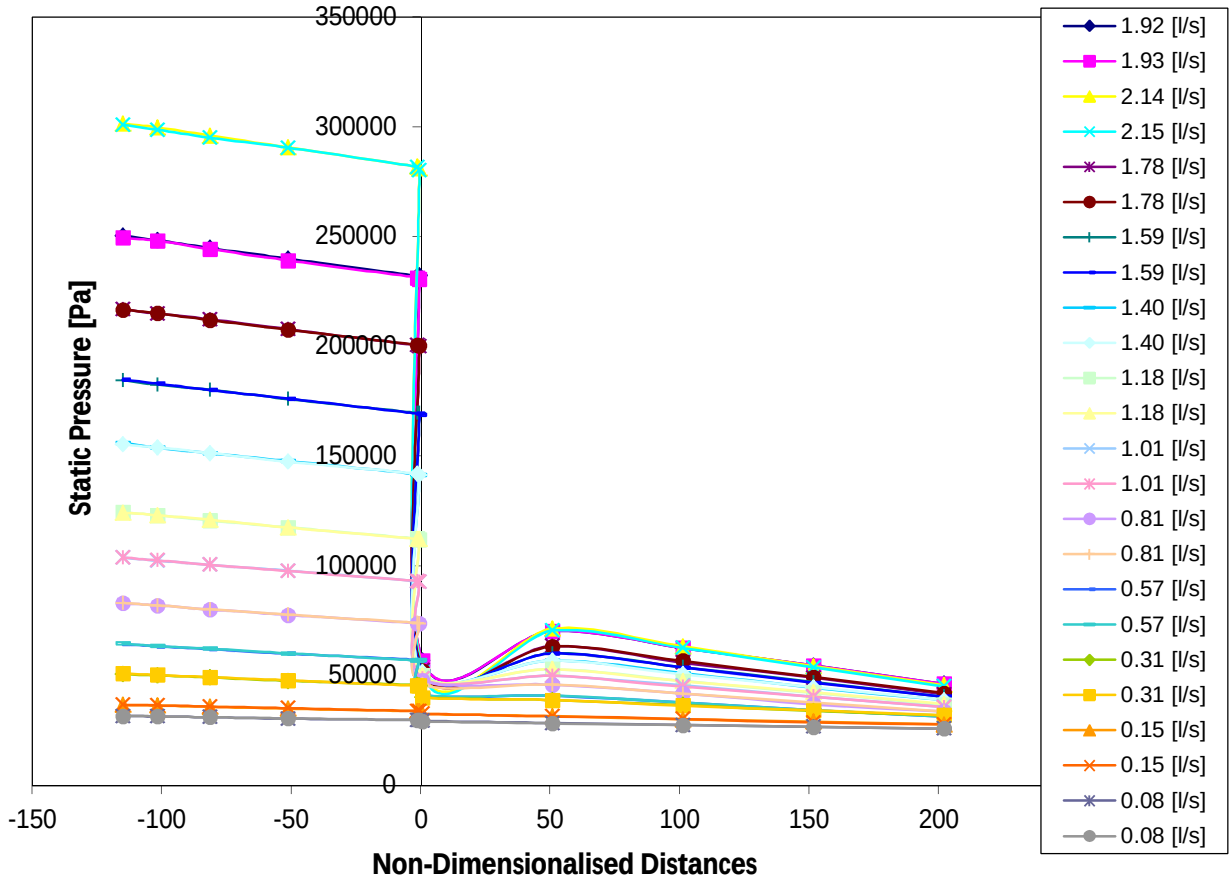

Figure 4.12 : Typical pressure grade lines, CMC 5%

In laminar flow the pressure loss coefficient depends on the Reynolds number and can be correlated using the following equation;

$$k_{or} = \frac{C_{or}}{Re_3} \qquad \text{Equation 4.1}$$

where C_{or} is the laminar flow loss coefficient constant. This value of C_{or} is determined using a logarithmic least square error where E_c is minimised to obtain a value of C_{or}.

$$E_c = \sum \left(\ln \frac{C_{or}}{Re_3} - \ln k_{or\,obs} \right)^2 \qquad \text{Equation 4.2}$$

The pressure loss coefficients for each orifice tested are given below as plots of k_{or} versus Reynolds number.

4.3.2. Orifice diameter ratio, $\beta = 0.2$

Two distinct flow regimes can be observed in Figure 4.13. At Reynolds numbers less than 10 the flow is purely laminar. The pressure loss coefficient increases significantly with decreasing Reynolds number. It means that the flow is dominated by viscous force. This result is qualitatively similar and can be compared to the behaviour found in pipe flow (friction factor). The lowest value k_{or} is 826 for Re_3 equals to 6. As can be observed, the transition starts at Reynolds number equals 4, where the loss coefficient decreases significantly until it reaches its lowest value. It then increases until it reaches a value of 1 213 at a Reynolds number = ±500. Above a Reynolds number of 500, the loss coefficient k_{or} remains constant at an average value of 1 213. It can be said, then, that already at Reynolds number 1 000 the flow is dominated by the inertial forces.

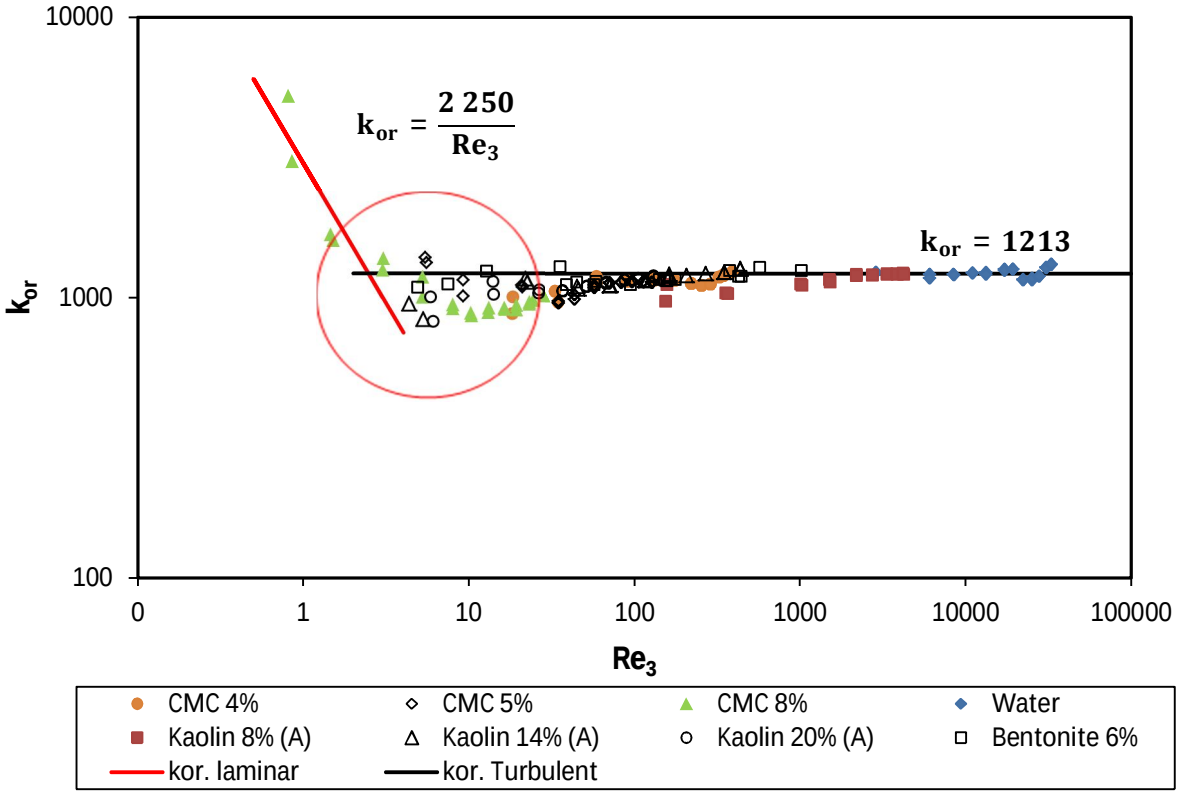

Figure 4.13 : Loss coefficients data for square-edged orifice plate with diameter ratio, β = 0.2

For orifice diameter ratio, β = 0.2, the orifice laminar flow loss coefficient constant, C_{or} has been found to be 2 250.

4.3.3 Orifice diameter ratio, $\beta = 0.3$

Pressure loss coefficients obtained for all fluids tested through an orifice plate of ratio β = 0.3 is shown in Figures 4.14. The observation for orifice plate with diameter ratio β = 0.3 is similar to that of orifice plate with diameter ratio β = 0.2. The pressure loss coefficient k_{or} has been found constant at an average value of 226.9 from Reynolds number Re_3= ± 1 000 and above. Below Re_3 = 1 000, the pressure loss coefficient started decreasing and reached its lowest value of 150 at Re_3 ± 50, after which the pressure loss coefficient started increasing significantly with further decreases in Reynolds number. In the region of 50 < Re_3 < 150, the loss coefficient data are very scattered typically of the transitional regime. The laminar flow loss coefficient constant was found to be 1 111 for orifice with diameter ratio β = 0.3.

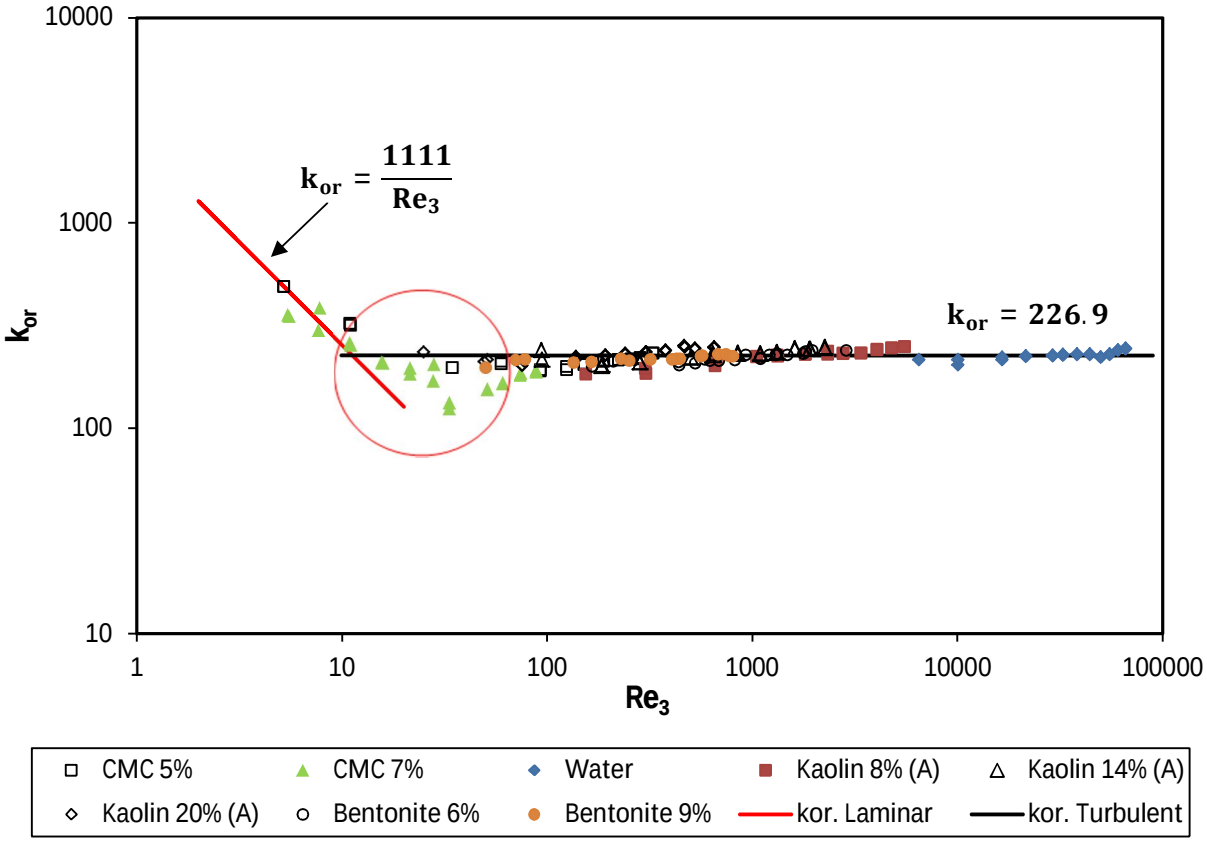

Figure 4.14 : Loss coefficient data for square-edged orifice plate with diameter ratio, β = 0.3

4.3.4 Orifice diameter ratio, $\beta = 0.57$

Two different categories of orifice with diameter ratio β = 0.57 have been tested. The first category was a circular orifice and the second category was a generation 0 of Von Koch fractal-shaped orifice which consists of two triangular orifices with round apex and sharp apex.

4.3.4.1 Circular orifice diameter ratio, $\beta = 0.57$

Figure 4.15 shows experimental pressure loss coefficient for circular orifice diameter ratio β = 0.57 versus Slatter Reynolds number. The pressure loss coefficient k_{or} has been found constant at an average value of 14.24 from Reynolds number Re_3 = ± 3 500 and above. That region can be surely considered as a turbulent regime because the flow is dominated by the inertial forces. Below Re_3 = 1 000, the pressure loss coefficient started decreasing and reached its lowest value of 3 at Re_3 = ± 150, after which the pressure loss coefficient started increasing significantly with further decreases in Reynolds number. In this region the pressure loss coefficient becomes dependent on the Reynolds number. The laminar flow loss coefficient constant was found to be 340 for a circular orifice with diameter ratio β = 0.57.

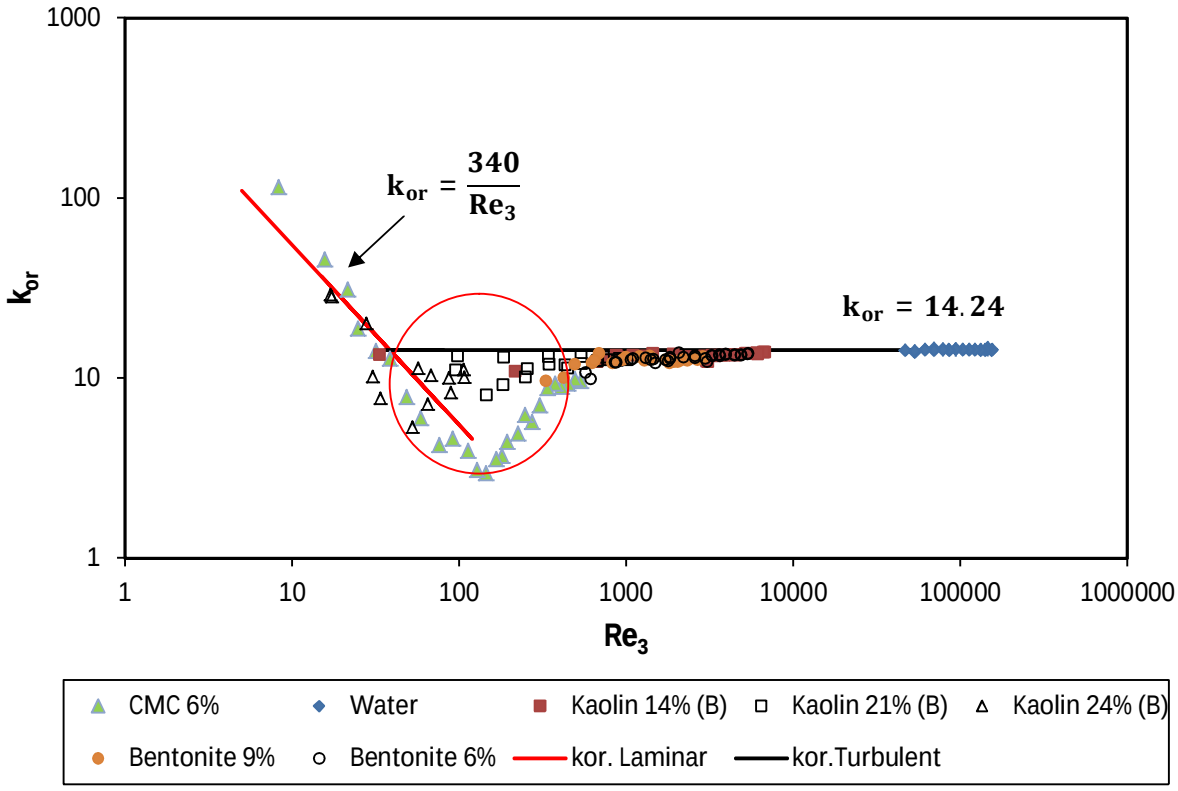

Figure 4.15 : Loss coefficient data for circular square-edged orifice plate with diameter ratio, β = 0.57

4.3.4.2 Triangular orifice with sharp apex (Equivalent diameter, $\beta = 0.57$)

The pressure loss coefficient, k_{or}, for triangular orifice with sharp apex and diameter ratio $\beta = 0.57$ is presented in Figure 4.16. The laminar regime, where the flow is dominated by viscous fluid, can be described by Equation 4.1. It was noticed from Figure 4.16 that the transition from laminar to turbulent flow occurs at around the same Reynolds number as it was observed in a circular orifice with the same flow area. The turbulent regime occurs at $Re_3 = \pm 150$. An average value of 13.36 was obtained in turbulent flow. As for the circular orifice with diameter ratio $\beta = 0.57$, which has the same flow area, the laminar flow loss coefficient constant was found to be 340.

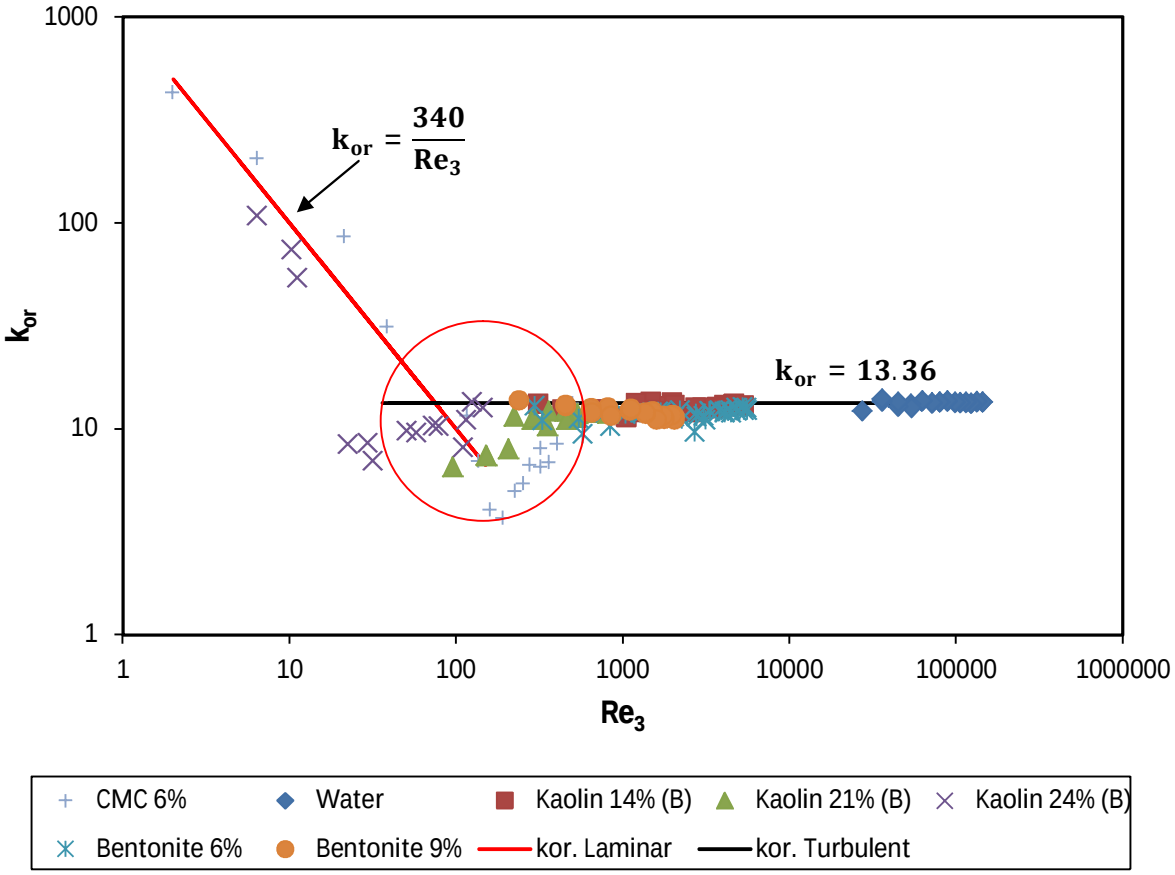

Figure 4.16 : Loss coefficient data for triangular square-edged orifice (sharp apex) plate with equivalent diameter ratio $\beta = 0.57$

4.3.4.3 Triangular orifice with round apex (Equivalent diameter, $\beta = 0.57$)

Figure 4.17 presents the pressure loss coefficient of a generation 0 Von Koch fractal-shaped orifice plate which consists of a triangular orifice with round apex. The orifice has the same flow area as a circular orifice with diameter ratio, $\beta = 0.57$. It was found that except for minor differences in the turbulent flow regime where the value for the current orifice was found to be equal to 14.17, the laminar flow loss coefficient constant was found to be 340, the same as for the circular orifice with the same flow area.

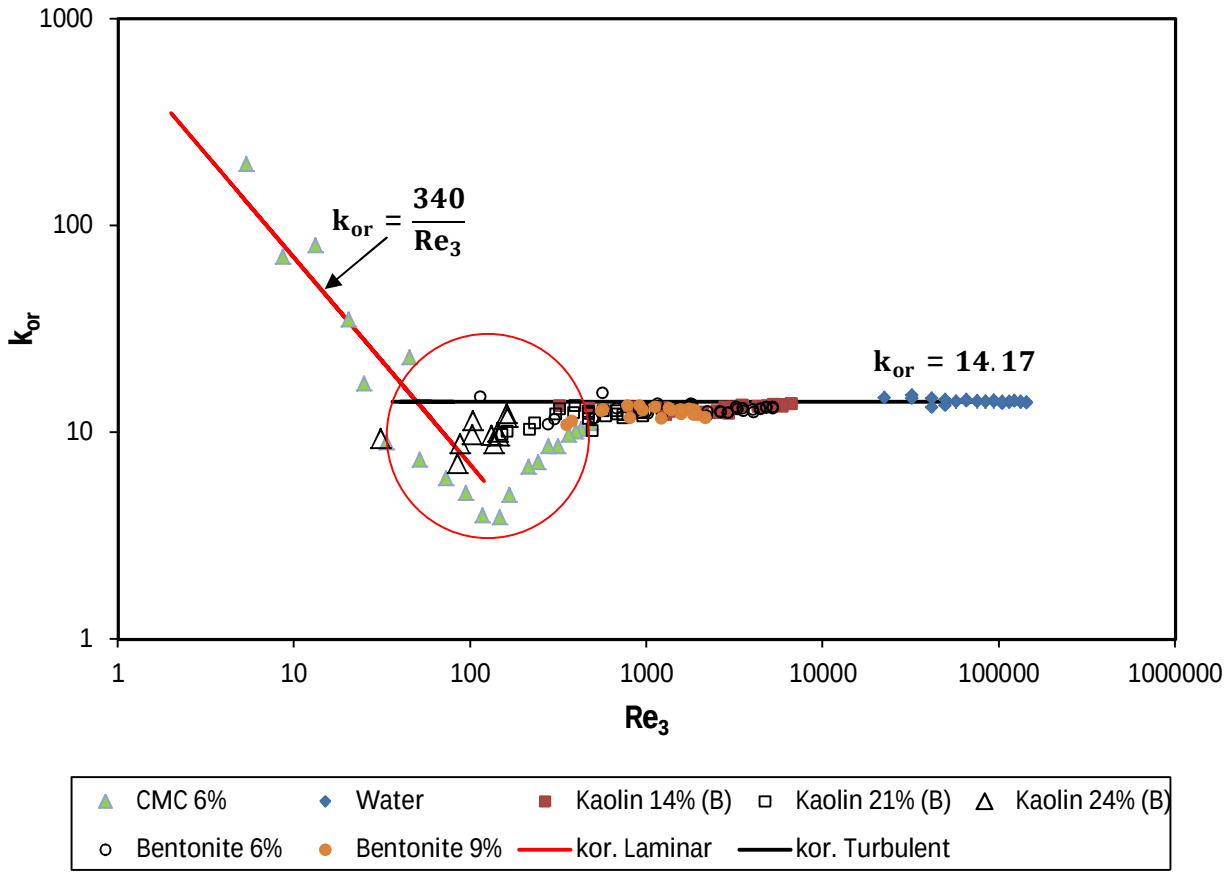

Figure 4.17 : Loss coefficient data for triangular square-edged orifice (round apex) plate with equivalent diameter ratio β = 0.57

4.3.5 Orifice diameter ratio, $\beta = 0.7$

The pressure loss coefficient increase significantly with decreasing of the Reynolds number as it can be observed in Figure 4.18. This corresponds to a truly laminar flow regime where the flow is dominated by viscous force. For an orifice with diameter ratio, β = 0.7, the laminar flow loss coefficient constant has been found to be 122. The transition zone occurs early at around a

$Re_3 = \pm 80$. In the transition regime the pressure loss coefficient reached its lowest value which was 1.45. Above a Reynolds number of 6 000, the pressure loss coefficients become constant at an average value of 3.85 and this result is independent of the Reynolds number.

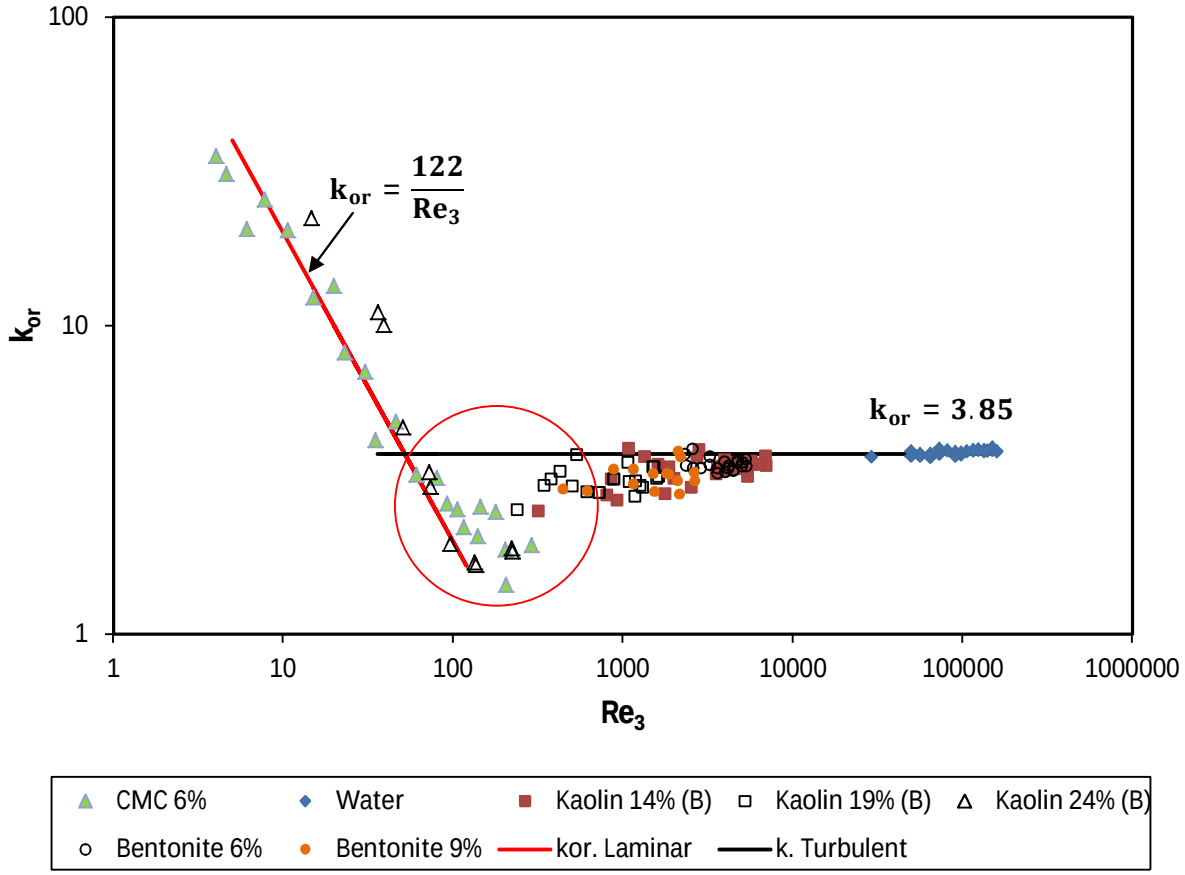

Figure 4.18 : Loss coefficient data for square-edged orifice plate with diameter ratio, β = 0.7

Table 4.5 presents pressure loss coefficients for β = 0.2, 0.3, 0.57 and 0.7 orifices. The pressure loss coefficient decreases with increasing orifice diameter ratio β.

Table 4.4 : Pressure loss coefficient for all β- ratios tested

β	0.2	0.3	0.57 (circ)	0.57 (triang. Sharp)	0.57 (triang. Round)	0.7
C_{or}	2250	1111	340	340	340	122
k_{or} turbulent	1213.0	226.9	14.24	13.36	14.17	3.85
k_{or} Std Dev	± 15.8	± 12.3	± 0.68	± 0.84	± 0.75	± 0.31

4.4. DISCHARGE COEFFICIENTS

Two different methods were used in this work to determine the discharge coefficient data: the flange tapping measurement and D & D/2 tapping measurement. For each of the measurements made, the value of discharge coefficient C_d is the same using either the D & D/2 tapping arrangement method or flange tapping arrangement method for all fluids tested at different concentrations. Therefore, for the rest of the work, only the flange tapping arrangement will be considered. A comparison of experimental discharge coefficient data obtained using the D & D/2 tapping arrangement and flange tapping arrangement is shown in Figure 4.19.

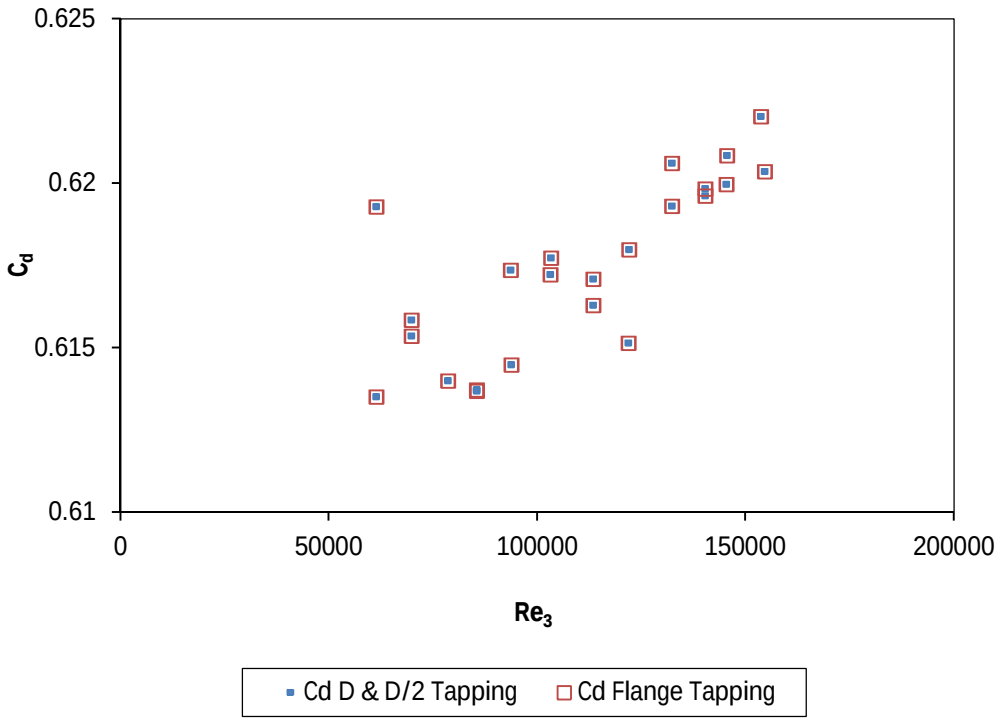

Figure 4.19 : Comparison between discharge coefficients obtained using D&D2 tapping arrangement and flange tapping arrangement for water (β = 0.57)

4.4.1 Orifice diameter ratio, $\beta = 0.2$

The discharge coefficient of a short orifice plate with diameter ratio β = 0.2 was seen to approach a constant average value of 0.71 for Re_3 > 100. This can be assimilated to a pure turbulent flow regime. From Reynolds number Re_3 equals 100 to a Reynolds number Re_3 equals ± 6, there is a transition zone and data are very scattered. For Reynolds number Re_3 equals to 10, the discharge coefficient reaches a peak at a value of 0.83. After reaching a peak,

the discharge coefficient starts decreasing with decreasing Reynolds number Re_3 as shown in Figure 4.20.

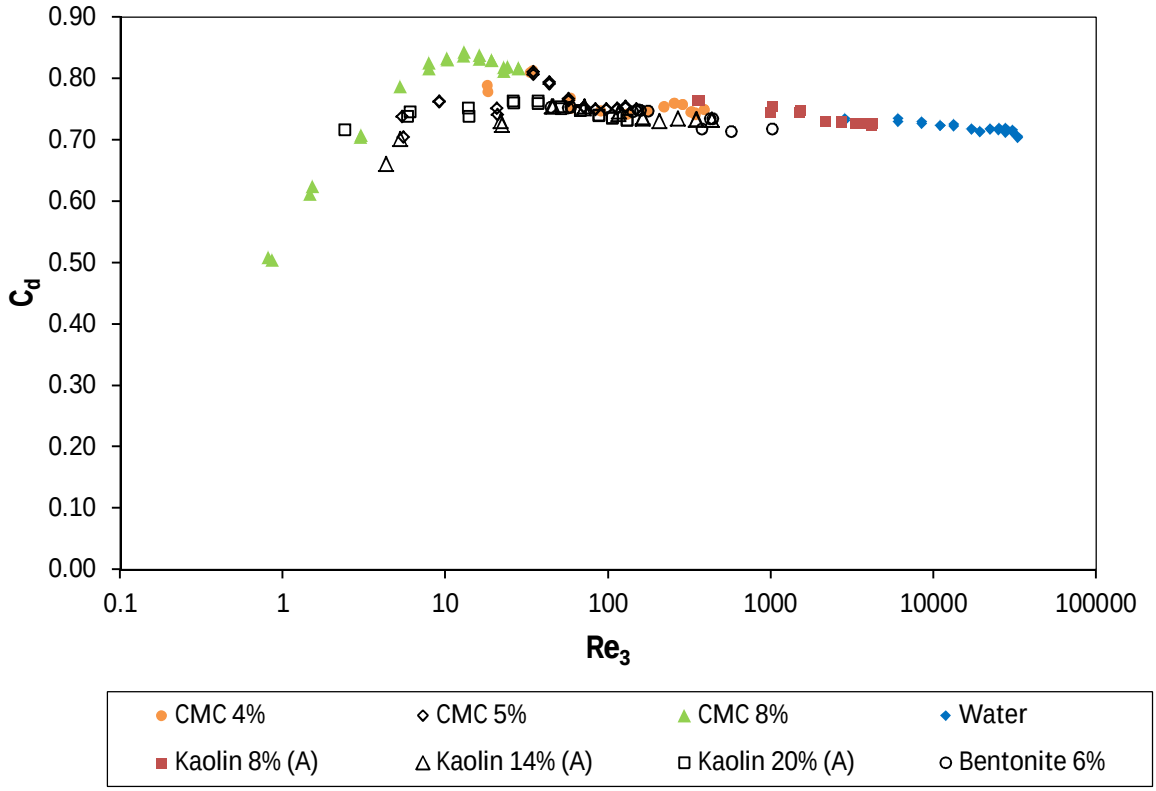

Figure 4.20 : Discharge coefficient data for square-edged orifice plate with diameter ratio, β = 0.2

4.4.2 Orifice diameter ratio, $\beta = 0.3$

Figures 4.21 shows discharge coefficient data for a square-edged orifice plate with diameter ratio, β = 0.3. It was observed from Figure 4.21 that the trend for discharge coefficient in the laminar flow regime increases with the Reynolds number. The discharge coefficients reach a peak in the transition zone which in this case occurs $10 < Re_3 < 250$. In turbulent flow, above $Re_3 > 250$, the discharge coefficient became nearly constant. An average C_d value of 0.67 was determined.

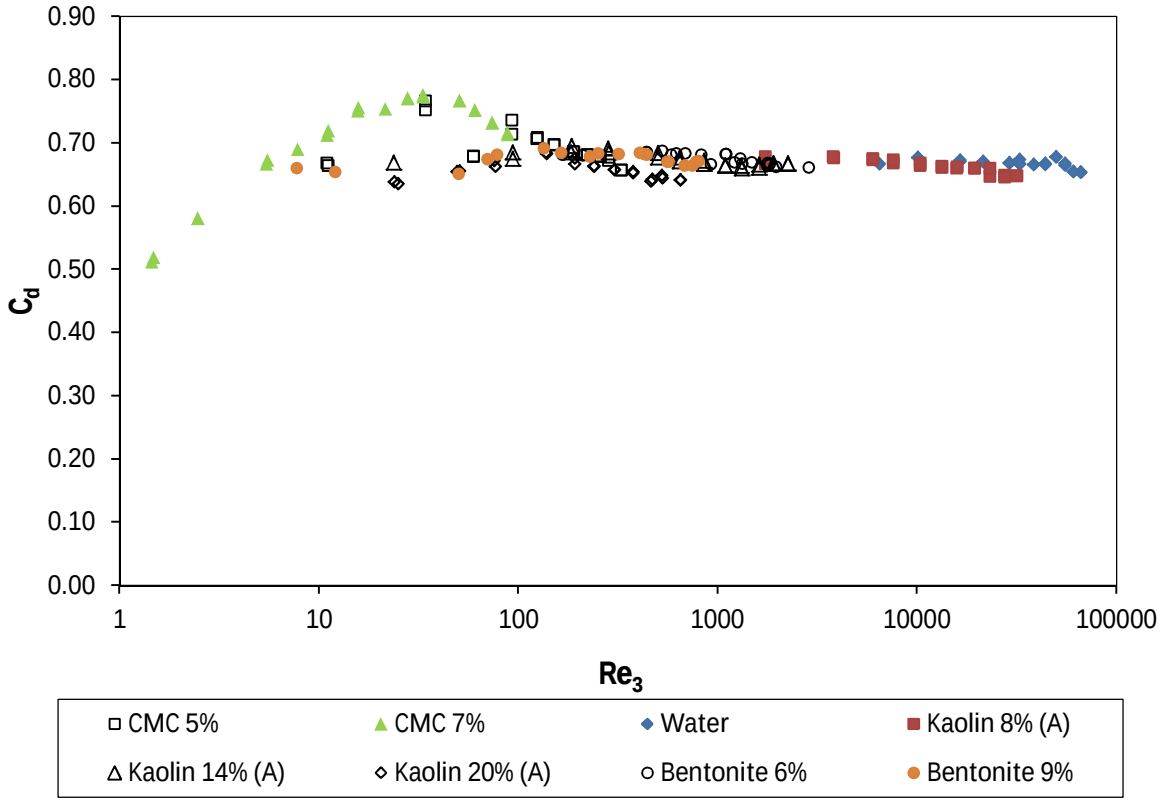

Figure 4.21 : Discharge coefficient data for square-edged orifice plate with diameter ratio, β = 0.3

4.4.3 Orifice beta ratio, $\beta = 0.57$

Figures 4.22 – 4.24 present experimental discharge coefficient data for short orifice plates with diameter β = 0.57 respectively for circular, triangular with sharp apex and round apex triangular orifice. In the laminar flow regime the discharge coefficient, C_d, increases with the Reynolds numbers until it reaches a peak. The transition zone occurs over a range of Reynolds number from 400 to 1 000. In turbulent flow, above Re_3 > 1 000, the discharge coefficients were independent of the Reynolds number. An average C_d value of 0.63, 0.65 and 0.64, was determined for β = 0.57 respectively for circular, triangular with sharp apex and round apex triangular orifice in the turbulent flow regime.

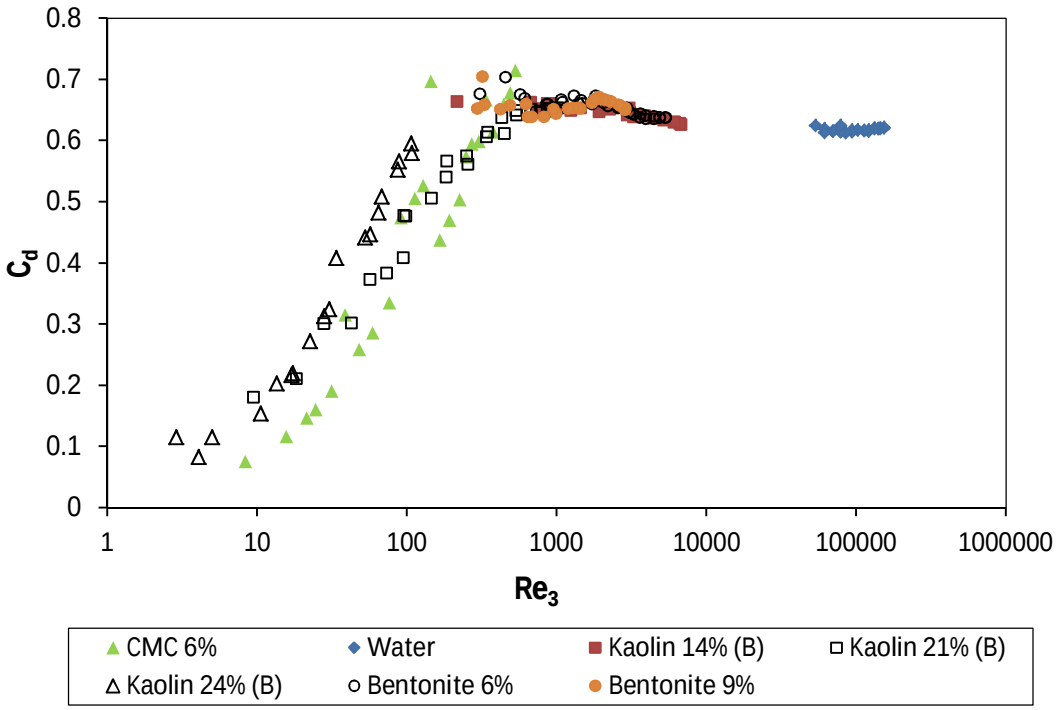

Figure 4.22 : Discharge coefficient data for regular circular square-edged orifice plate with diameter ratio β = 0.57

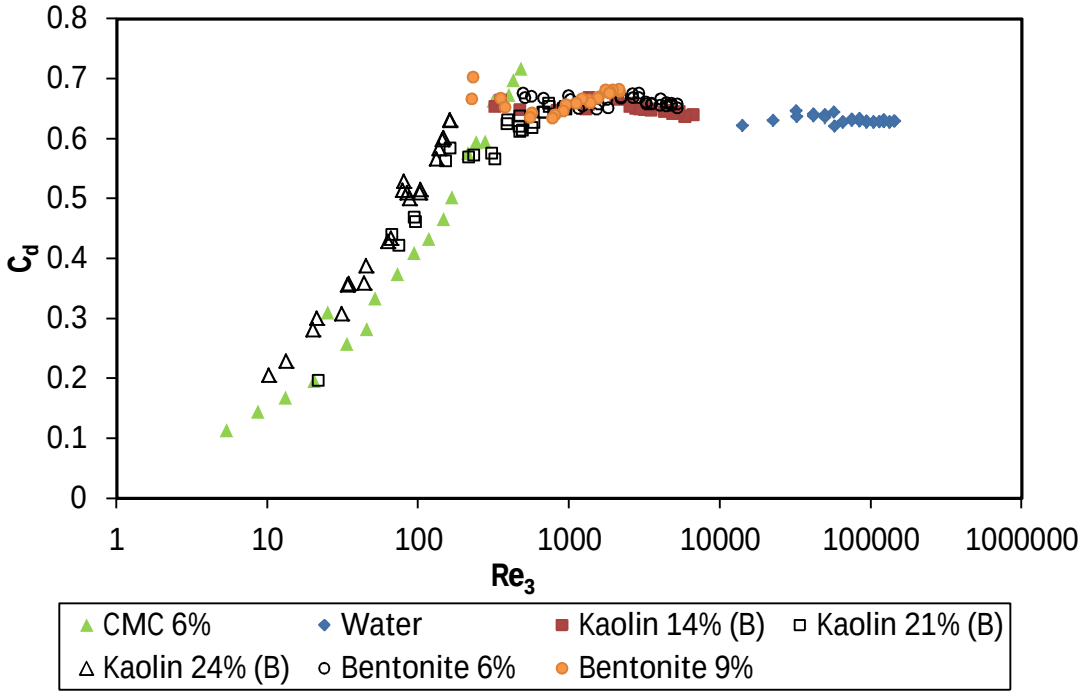

Figure 4.23 : Discharge coefficient data for sharp apex triangular square-edged orifice plate with equivalent diameter ratio β = 0.57

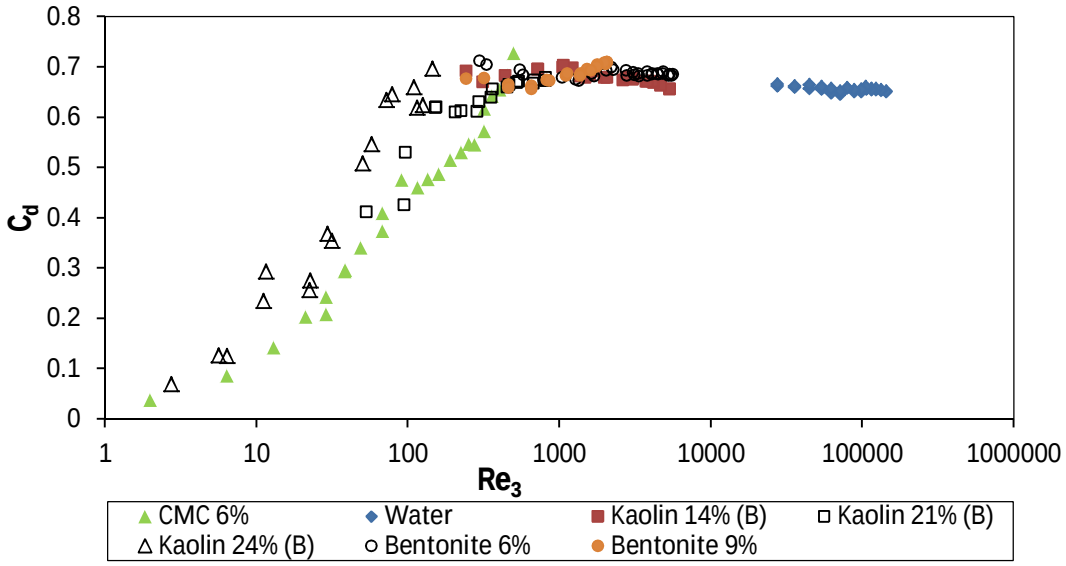

Figure 4.24 : Discharge coefficient data for round apex triangular square-edged orifice plate with equivalent diameter ratio β = 0.57

4.4.4 Orifice diameter ratio, $\beta = 0.7$

It can be seen in Figure 4.25, that the discharge coefficient is dependent on the Reynolds number in the laminar flow regime. The transition zone occurs at Reynolds number between 1 000 and 10 000, where the discharge coefficient reaches its peak value. Above the transition, the discharge coefficient becomes constant with an average value of 0.64.

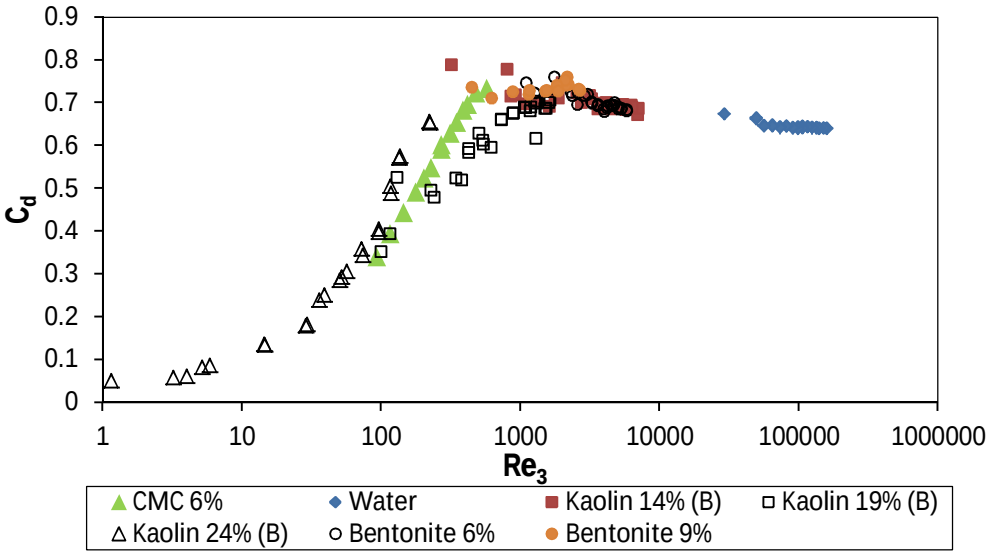

Figure 4.25 : Discharge coefficient data for square-edged orifice plate with equivalent diameter ratio β = 0.7

4.5. CONCLUSION

Results obtained from the orifice test rig have been outlined in this chapter. To ascertain the credibility of the equipment, water tests were conducted in a straight pipe. Friction factor versus Reynolds number, correlated to the theoretical prediction, was shown to illustrate the efficiency of the system.

The rheological characteristics of different fluids tested in this work were determined using a tube viscometer. Carboxymethyl cellulose, bentonite and kaolin slurries were used at different concentrations to obtain laminar, transitional and turbulent flow loss coefficient data. Good agreement was found between the theoretical and experimental friction factors, thus validating the rheological parameters used.

Finally, the pressure loss coefficients and discharge coefficient data for different beta ratios were calculated and presented from laminar to turbulent flow regimes. The pressure loss coefficient reached a constant value at a Reynolds number around 500, 1 000, 3 500 and 6 000 respectively for β = 0.2, 0.3, 0.57 and 0.7. The constant value of pressure loss coefficient decreases with the increasing beta ratio. Unlike the pressure loss coefficient, the discharge coefficient increases with increasing Reynolds number in laminar flow. It, however, remains nearly constant in the turbulent flow regime as the pressure loss coefficient. A comparison of the data presented in this chapter with the existing data in the literature will be presented in the following chapter.

CHAPTER 5

5.1 INTRODUCTION

The objective of this work is to provide laminar to turbulent pressure loss and discharge coefficients. The experimental work obtained in this investigation will be compared with experimental data and models found in the literature. This chapter will present:

- A comparison of experimental pressure loss coefficient and discharge coefficient data obtained in this work with those available in the literature.
- A comparison of the experimental data in this work with models in the literature.
- A comparison of circular shape and generation 0 fractal-shaped orifices.
- A new correlation that can predict pressure loss coefficients from laminar to turbulent flow since all correlations found in the literature can only predict turbulent flow or laminar flow separately.

5.2 PRESSURE LOSS COEFFICIENTS' COMPARISON WITH OTHER EXPERIMENTAL DATA

One of the important objectives of this work is to compare the results obtained in the current experimental investigation with data found in the literature. The relative errors were calculated for pressure loss coefficients in the turbulent flow regime for $Re_3 > 10\ 000$. The following data from the literature review were used for comparison, namely:

- Alvi et al. (1978) using Figure 2.26
- Lakshmana and Shridharam (1972) using Figure 2.26
- Rangaraju and Jain (1976) using Figure 2.26
- Shima (1984) using Figure 2.26
- Humpherys (1987) using Figure 2.26
- Miller (1996) using Figure 2.26
- Ginsburg's (1963) equation in Table 2.5
- Ward-Smith's (1971) equation in Table 2.5

5.2.1. Orifice diameter ratio, $\beta = 0.2$

5.2.1.1 Comparison with experimental data

Figure 5.1 shows the k_{or} versus Re_3 graphs for orifice plate with beta ratio 0.2 obtained in this investigation with the available values from the literature. Although they generated data ranging from a flow condition of 1 to 1 000 only, Figure 5.1 shows good agreement between data from the current study and those of Alvi et al. (1978). The result from Alvi et al. (1978) in for $15 \leq Re_3 \leq 1000$ flow is 10% greater than that found in this work. The experimental data of Lakshmana and Shridharan (1972) were found to be 2% greater than those published in the current investigation, while experimental data provided by Rangaraju and Jain (1976) were found to be 6% lower than data obtained in the current study.

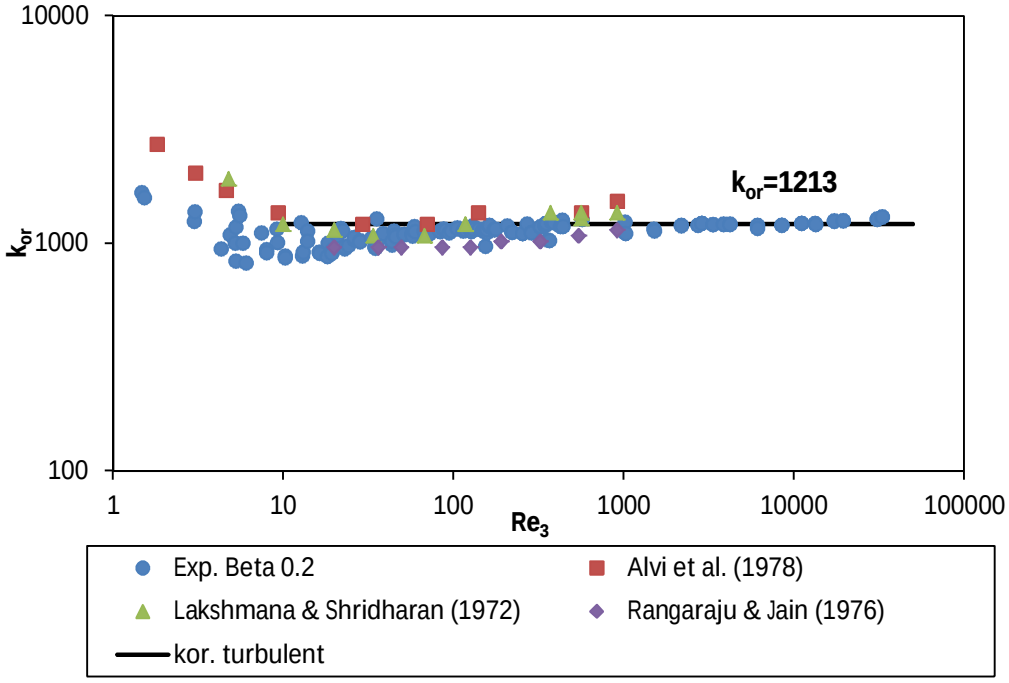

Figure 5.1 : Comparison between β = 0.2 with experimental data obtained by Alvi et al. (1978), Lakshmana & Shridharan (1972) and Rangaraju & Jain (1976)

5.2.1.2 Comparison with models

Figure 5.2 presents the comparison of experimental pressure loss coefficient found in the current work with the model proposed by Ward-Smith (1971) and Ginsburg (1963) in turbulent flow for Re > 10 000. It was noticed that the Ward-Smith and Ginsburg models over-predict the experimental data found in this investigation by 33% and 40% respectively.

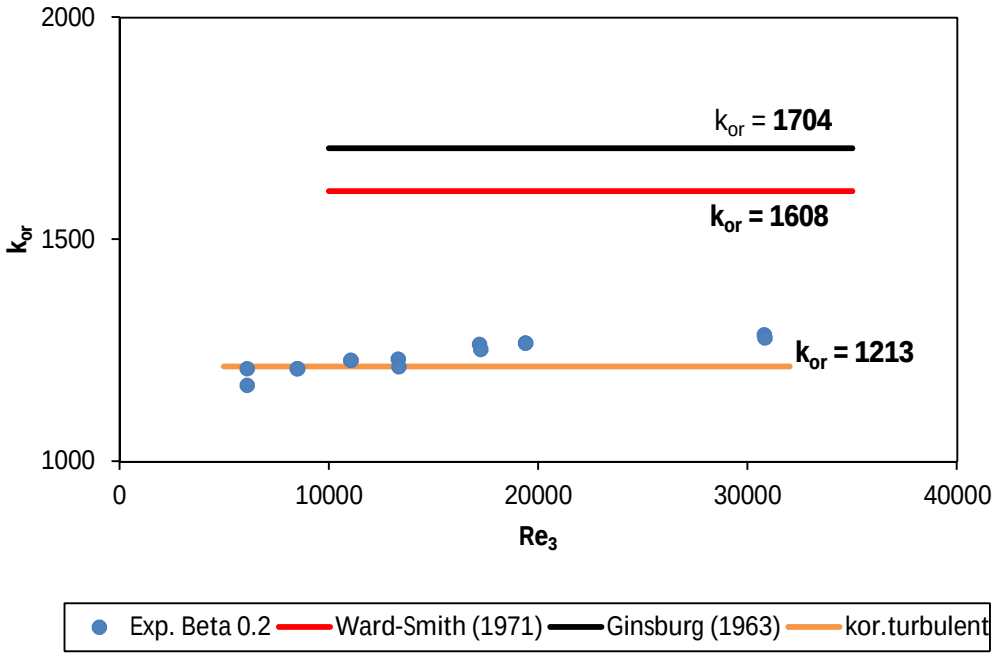

Figure 5.2 : Comparison between β = 0.2 data and models proposed by Ward-Smith (1971) and Ginsburg (1963)

Table 5.1 presents the difference between mean average value from the models and mean average value from the experimental data that was determined using Equation 3.6 between the pressure loss coefficients found in this work and those found in the literature for the turbulent flow regime. A negative result means that the results from the model were lower than those obtained in this work, and positive result means that they were higher than those obtained for this work.

Table 5.1: Comparison of k_{or} with literature for β = 0.2

	Experimental (This work)	Alvi et al (1978)	Lakshmana and Shridharan (1972)	Rangaraju and Jain (1976)	Ward-Smith model (1971)	Ginsburg model (1963)
k_{or}	1213	1336	1234	1145	1608	1704
Difference (%)	0	10	2	-6	33	40

5.2.2 Orifice diameter ratio, $\beta = 0.3$

5.2.2.1 Comparison with models

The two models, Ward-Smith (1971) and Ginsburg (1963), over-predict the experimental pressure loss coefficient data obtained in this work by 24% and 30% respectively in turbulent flow for Re > 10 000. Figure 5.3 below presents the comparison between the experimental data found in this study with the models.

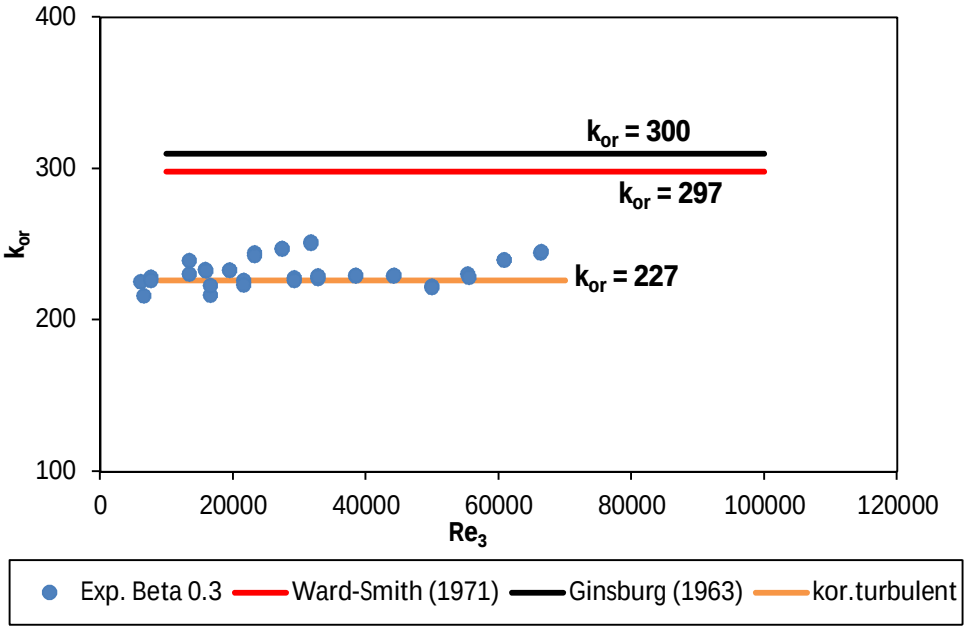

Figure 5.3 : Comparison between β = 0.3 data and models proposed by Ward-Smith (1971) and Ginsburg (1963)

Table 5.2 gives the difference between the experimental data compared with the Ward-Smith and Ginsburg models.

Table 5.2 : Comparison of k_{or} with literature for β = 0.3

	Experimental (This work)	Ward-Smith model (1971)	Ginsburg model (1963)
k_{or}	227	297	300
Difference (%)	0	24	30

5.2.3 Orifice diameter ratio, $\beta = 0.57$ circular

5.2.3.1 Comparison with experimental data

Figure 5.4 presents the comparison of experimental pressure loss coefficient data obtained in this study for circular orifice with diameter ratio 0.57, with experimental data provided by Shima (1984). Good agreement between data from the current study and those from Shima was observed in the turbulent flow regime.

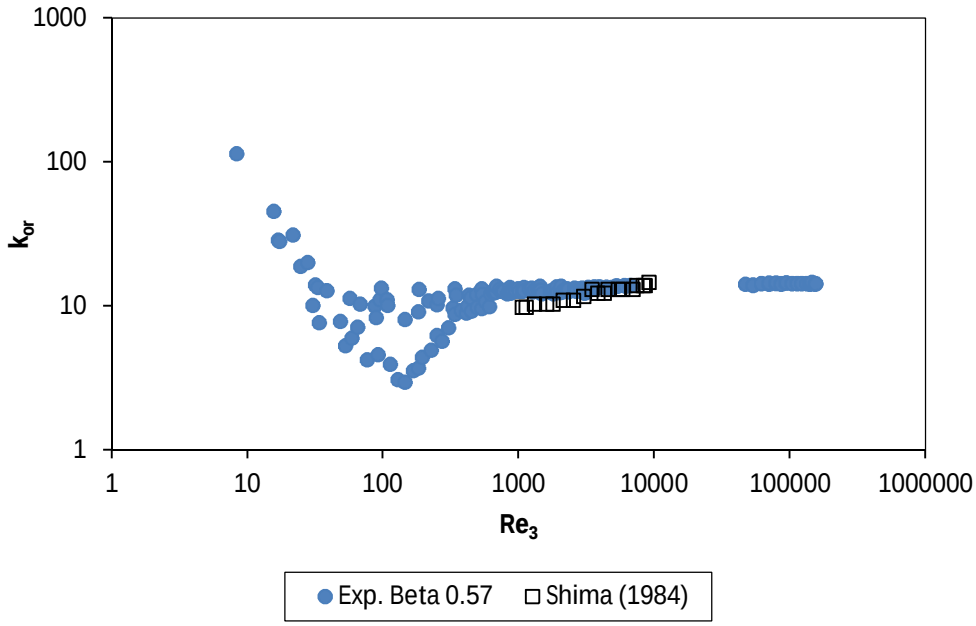

Figure 5. 4 : Comparison between circular orifice with diameter ratio, β = 0.57, and experimental data obtained by Shima (1984)

5.2.3.2 Comparison with models

The experimental orifice pressure loss coefficient data for regular circular orifice with diameter ratio 0.57 was compared with Ward-Smith (1971) and Ginsburg (1963) models. It was found that the pressure loss coefficient data obtained in this investigation were approximately 7.3%

and 5.7% lower than the values predicted by Ward-Smith (1971) and Ginsburg (1963) models. Figure 5.5 shows the comparison between experimental data and the two models.

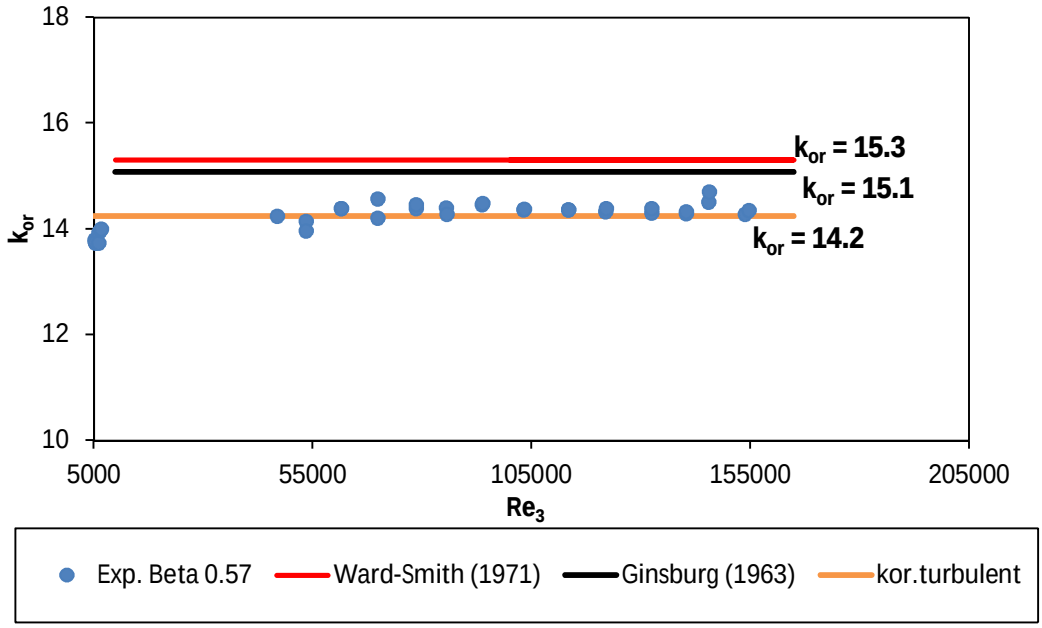

Figure 5.5 : Comparison between β = 0.57 and models proposed by Ward-Smith (1971) and Ginsburg (1963)

In addition, Table 5.3 presents the difference between the experimental pressure loss coefficient data for orifice ratio 0.57 and the data and models in literature.

Table 5.3 : Comparison of k_{or} with literature for β = 0.57

	Experimental (This work)	Shima (1984)	Ward- Smith model (1971)	Ginsburg model (1963)
k_{or}	14.2	12.5	15.3	15.1
Difference (%)	0	-12.5	7.3	5.7

5.2.4 Orifice diameter ratio, $\beta = 0.7$

5.2.4.1 Comparison with experimental data

The pressure loss coefficients obtained in the current study for orifice ratio 0.7 agree well with experimental data published by Humpherys (1987) in the turbulent flow regime. The comparison between experimental data from the current investigation and data published by Miller (1996) shows good agreement in the turbulent flow regime as can be seen in Figure 5.6 below. But a

discrepancy has been observed in the laminar flow regime. This could be due to the fluctuation in pressure in the pipe. As stated by Husain et al. (1984), the pressure fluctuation increases with the orifice diameter ratio β. Figure 5.6 shows the comparison between Humpherys (1987) and Miller (1996) experimental data with those obtained in this work.

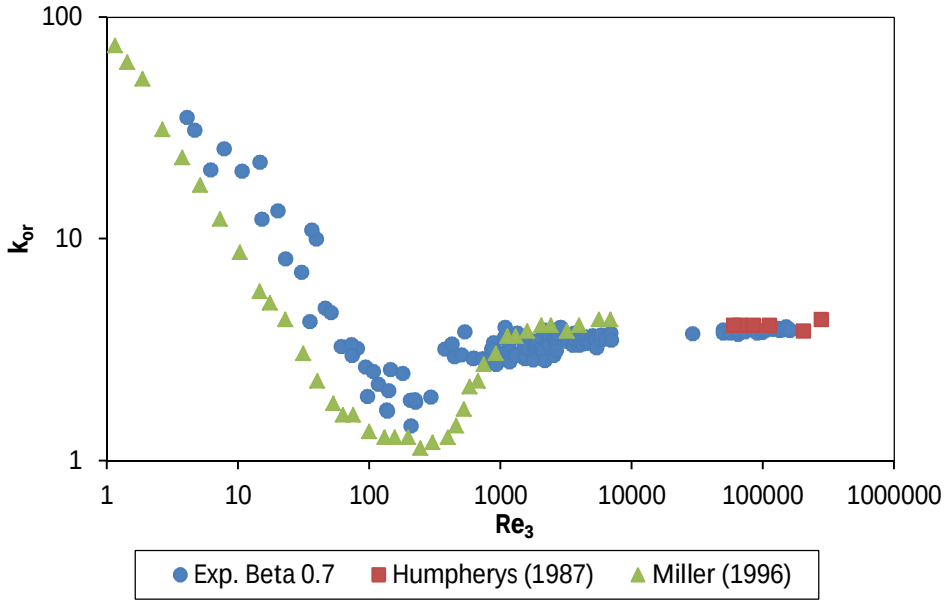

Figure 5.6 : Comparison between β = 0.7 data and experimental data obtained by Humpherys (1987) and Miller (1996)

5.2.4.2 Comparison with models

Figure 5.7 presents a comparison between models proposed by the Ward-Smith model (1971) and by Ginsburg (1963) and experimental data from this work for orifice ratio 0.7. The two models over-predict the experimental data obtained in the current investigation. The pressure loss coefficient data were found to be 11% and 9% lower than predicted by Ward-Smith (1971) and Ginsburg (1963) models.

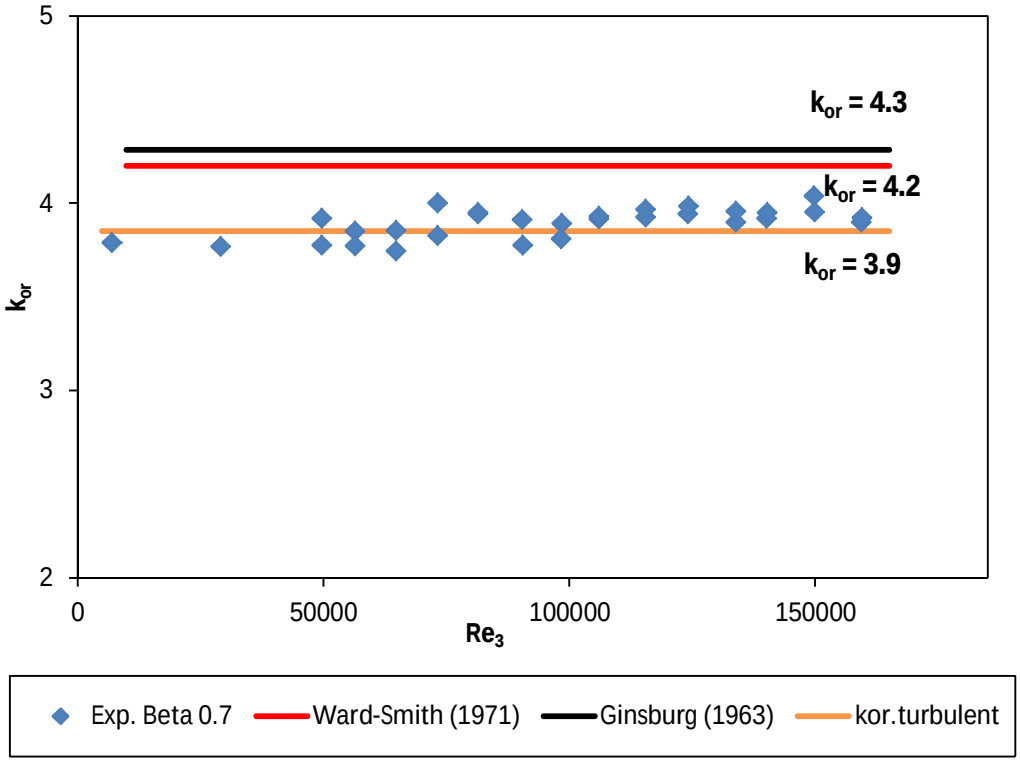

Figure 5.7 : Comparison between β = 0.7 and model proposed by Ward-Smith (1971) and Ginsburg (1963)

Table 5.4 gives the difference between the experimental data obtained in this investigation for orifice ratio 0.7 compared to those available in the literature and from the models.

Table 5.4 : Comparison of k_{or} with literature for β = 0.7

	Experimental (This work)	Humpherys (1987)	Miller (1996)	Ward-Smith model (1971)	Ginsburg model (1963)
k_{or}	3.9	4.1	3.9	4.2	4.3
Difference %	0	6.7	1.8	9	11

Figure 5.8 presents the difference between the model and experimental data versus beta ratio. It can be seen that for the two models used, the difference decreased with increasing beta ratio up to β = 0.57 after which it increased for β = 0.7.

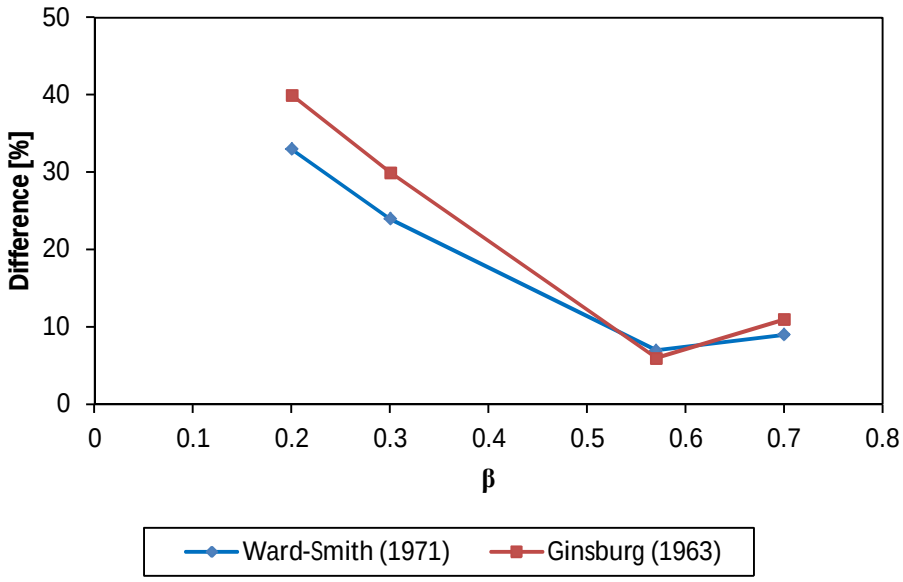

Figure 5.8 : Pressure loss coefficients difference versus diameter ratio

5.2.5 Summary of pressure loss coefficient data

The conclusions from this section are summarised below.

- For orifice diameter ratio, β = 0.2, there was excellent agreement between the experimental data of different authors and this work. However, Ward-Smith (1971) and Ginsburg (1963) models over-predict the experimental data obtained in this investigation by approximately 30% - 40%.
- For orifice diameter ratio, β = 0.3, no experimental data were found to be compared with experimental data obtained in this investigation. Compared to the Ward-Smith (1971) and Ginsburg (1963) models, the models over-predicted the experimental data by 25 -35%.
- For orifice diameter ratio, β = 0.57, there was good agreement between experimental data obtained by Shima (1984) and the current work. At this diameter ratio, the models of Ward-Smith (1971) and Ginsburg (1963) compared much better and were within 10% of the experimental data obtained in this work.
- Finally, experimental data for diameter ratio, β = 0.7, obtained in this work, agree well with experimental data found in the literature in turbulent flow, but not in the laminar flow regime. The two models over-predict the data by 11% in the turbulent flow regime.

- According to the literature the Ward-Smith and Ginsburg models are applicable for $\beta = 0.1 - 0.8$ and $\beta = 0 - 0.87$ respectively. The analysis shows, however, they are more applicable to $\beta > 0.5$, as the errors between the models and the experimental data are within more acceptable limits in this case, i.e., less than 15% which falls within the overall experimental error of this work for the straight pipe tests.
- The fact that the experimental results of this work agrees with other data sets in literature shows clearly a need to, not only improve the existing turbulent flow models, but to also extend them to include laminar and transitional flow.

5.3 DISCHARGE COEFFICIENT COMPARISON WITH OTHER EXPERIMENTAL DATA

There is no experimental data available in the literature to compare with the experimental data obtained in this investigation. Referring to Figure 2.25 presented in Section 2.10 of Chapter 2, the experimental data found in the literature for short or thin square-edged orifice plates are for 30º or 45º back-level short square-edged orifices, for knife-edged thin orifices, for quadrant-edged thin orifices and chamfer-edged thin orifices. There are no data for square-edged thin orifices (ESDU, 2007).

The discharge coefficient is affected by the orifice geometry and the flow regime. Based on the factors that affect the discharge coefficient, many correlations have been proposed to quantify the discharge coefficient over the years. They can be grouped in two: those based on the loss factor across the orifice, such as that of Benedict and Wyler (1973) and those based on the boundary-layer thickness such as that of Hall (1963). The latter method ignores the diameter ratio effect, overlooks losses and velocity profile effects upstream of the orifice plate, and fails to predict adequately the experimental discharge coefficient. However, the correlation proposed by Benedict and Wyler (1973), derived from the 1-D analysis of the energy and continuity equations (generalised friction factor-kinetic energy coefficient formulation), is based on a loss-factor rational method with due account of diameter ratio, upstream velocity profile and pressure loss (ESDU, 2007). In this investigation, experimental data will be compared to the correlation proposed by Benedict and Wyler (1973) shown in Table 2.4.

The model proposed by Benedict and Wyler is valid only in the turbulent flow regime, not in the transitional and the laminar flow regime. Benedict and Wyler's model used the pressure drop from D & D/2 tapping arrangement. However, data presented in this work were obtained using the flange tapping arrangement. It was shown in Chapter 4 that no significant difference was

observed in the pressure drop between the two tapping arrangement methods. So, the use of the model to evaluate the experimental data found in this investigation is justified.

5.3.1. Orifice diameter ratio, $\beta = 0.2$

Figure 5.9 shows the comparison between experimental data and the model for orifice diameter ratio β = 0.2. The discharge coefficient was found to be 0.72 in turbulent flow. Benedict and Wyler's model under-predicts the experimental discharge coefficient data obtained in this investigation by 15%.

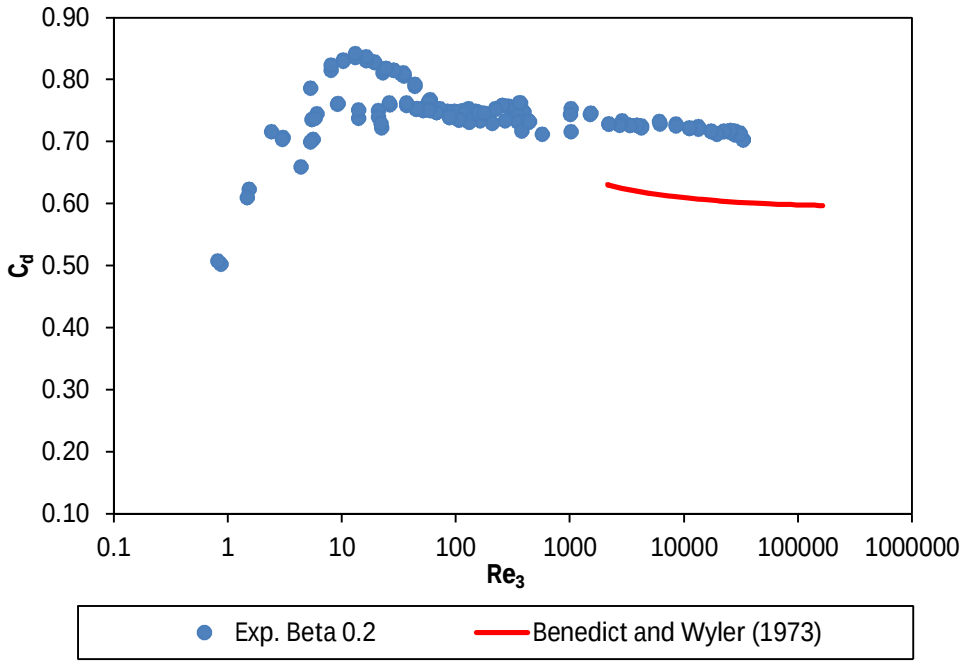

Figure 5.9 : Comparison between discharge coefficient data and Benedict & Wyler (1973) model

Table 5.5 gives the difference between experimental data obtained in this investigation compared with the model proposed by Benedict and Wyler (1973) for β = 0.2. The difference was calculated using Equation 3.6 based on the data in the turbulent flow regime. The negative value means that the results predicted by the model were lower than those obtained in this work.

Table 5.5 : Comparison of C_d with literature for β = 0.2

	Experimental	Benedict and Wyler (1973)
C_d	0.72	0.61
Difference [%]	0	-15

5.3.2 Orifice diameter ratio, $\beta = 0.3$

For orifice diameter ratio β = 0.3, the experimental discharge coefficient data found in this work were also compared with the Benedict and Wyler (1973) model. Once again the model under-predicts the experimental data in the turbulent flow regime, but this time by 9%. Figure 5.10 presents the comparison between the model and experimental discharge coefficient data obtained in this work for orifice diameter ratio β = 0.3.

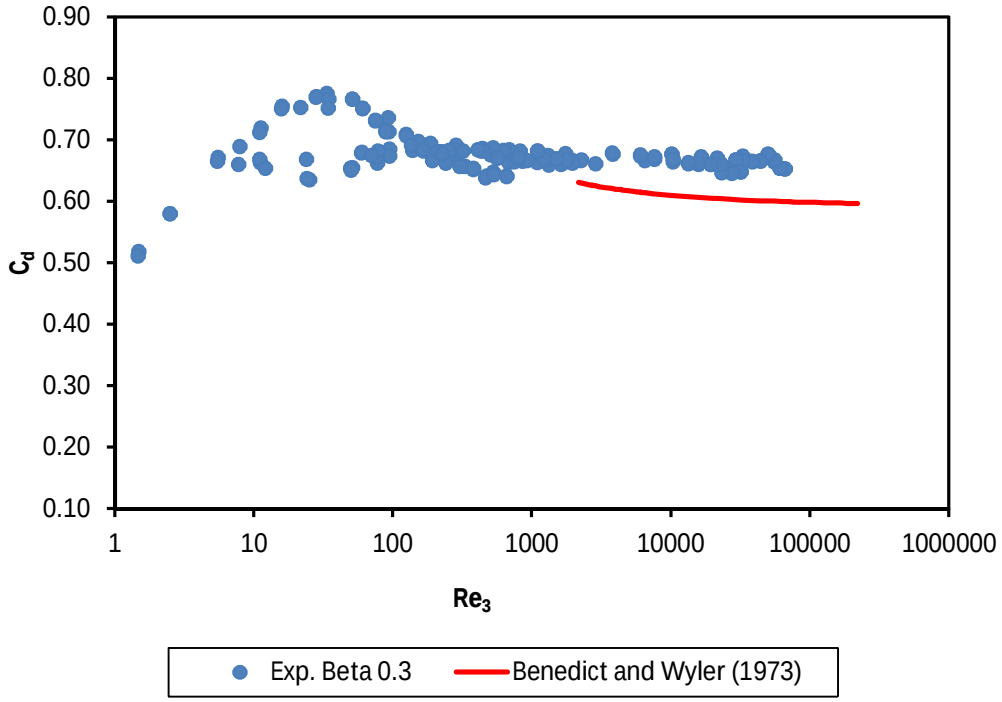

Figure 5.10 : Comparison between discharge coefficient data for beta ratio 0.3 and Benedict & Wyler model (1973)

Table 5.6 gives the difference between discharge coefficient data found in this current work compared with the model of Benedict and Wyler (1973).

Table 5.6 : Comparison of C_d with literature for β = 0.3

	Experimental	Benedict and Wyler (1973)
C_d	0.67	0.61
Difference [%]	0	-9

5.3.3 Orifice diameter ratio, $\beta = 0.57$ [circular]

Figure 5.11 presents the comparison of discharge coefficient data obtained for the circular orifice with diameter ratio, β = 0.57 with the model published by Benedict and Wyler (1973). The discharge coefficient values agree well with the model and were found to be within 2% in the turbulent flow regime.

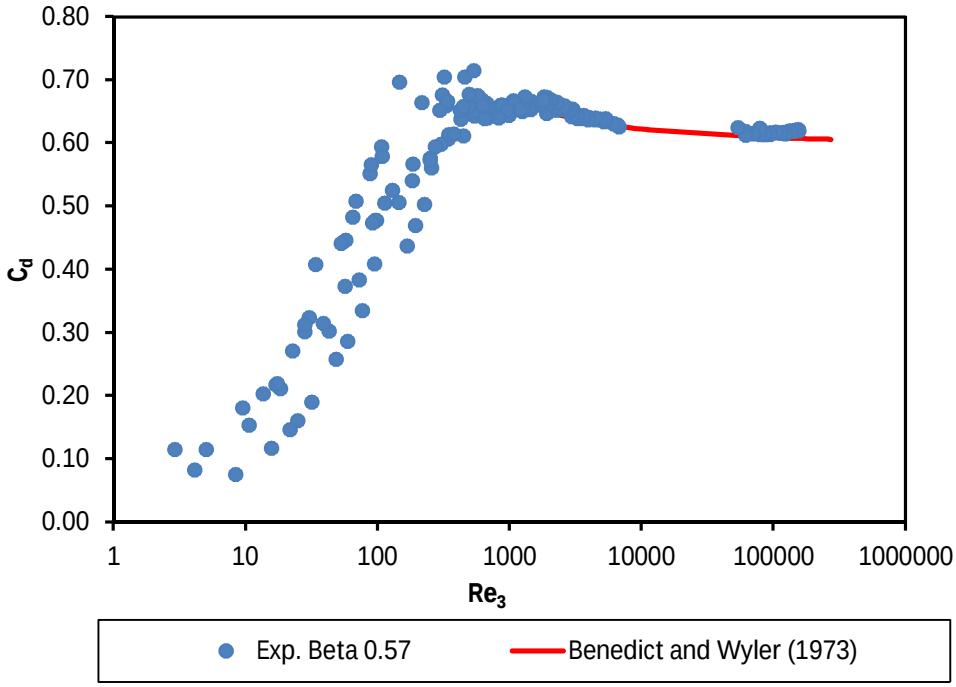

Figure 5.11 : Comparison between discharge coefficient data for beta ratio 0.57 circular and Benedict & Wyler model (1973)

In Table 5.7, the difference between the experimental discharge coefficients obtained for orifice diameter ratio, β = 0.57, and the value obtained using the model published by Benedict and Wyler (1973) is given.

Table 5.7 : Comparison of C_d with literature for β = 0.57

	Experimental	Benedict and Wyler (1973)
C_d	0.63	0.62
Difference [%]	0	-2

5.3.4 Orifice diameter ratio, β = 0.7

For orifice diameter ratio β = 0.7, the experimental discharge coefficient has been compared with the Benedict and Wyler (1973) model. The data were ±5% greater than values obtained using the model in turbulent flow. Figure 5.12 shows the comparison between the experimental discharge coefficient data obtained in the current investigation for orifice diameter ratio β = 0.7 and the Benedict and Wyler (1973) model. Table 5.8 presents the difference between the model and the discharge coefficient data obtained in this work.

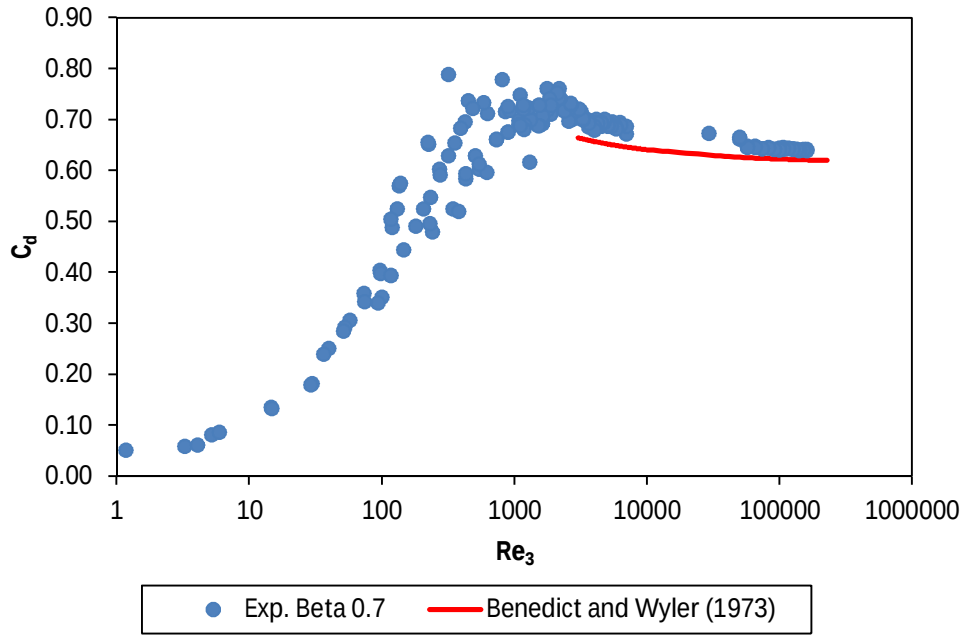

Figure 5.12 : Comparison between discharge coefficient data for beta ratio 0.7 and Benedict & Wyler model (1973)

Table 5.8 : Comparison of C_d with literature for β = 0.7

	Experimental	Benedict and Wyler (1973)
C_d	0.68	0.65
Difference [%]	0	-4.4

Figure 5.13 presents the discharge coefficient difference as a function of beta ratio. It can be seen that the difference increases with decreasing diameter ratio.

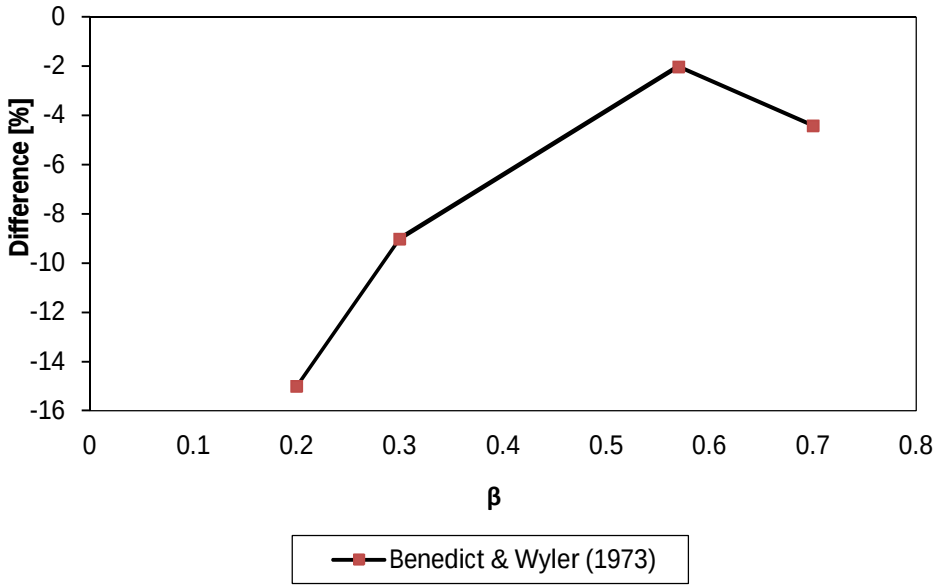

Figure 5.13 : Discharge coefficient difference versus diameter ratio

5.3.5 Summary of discharge coefficient data

The conclusion of this section can be summarised as follows:

- No experimental discharge coefficient data has been found in the literature for short square-edged orifice plate to be compared with the discharge coefficient data obtained in the current work.
- The experimental data was compared with the model presented by Benedict and Wylie (1973).
- Experimental data obtained from the beta ratio 0.3, 0.57 and 0.7 were found to be less than 10% of values predicted by the model.
- However, the experimental data for orifice diameter ratio 0.2 were found to be 15% higher than what the model predicted.
- A similar trend was found for the pressure loss coefficient comparison. In this case, it can either be that there are problems regarding some assumptions in the models or inherent experimental errors for these low orifice ratios and this issue should be resolved in future.

5.4 COMPARISON BETWEEN CIRCULAR ORIFICE AND TRIANGULAR ORIFICE

5.4.1 Introduction

Two generation 0 Von Koch fractal-shaped short square-edged orifices, i.e., triangular short square-edged orifice with round apex and triangular orifice with sharp apex were designed, manufactured and tested for comparison with the circular short square-edged orifice. The triangular orifice plate has the same flow area as the circular orifice of equivalent diameter D_{eq}= 26.2 mm (β = 0.57). Fractal-shaped orifices have been tested by Abou El-Azem Aly et al. (2010) using air. The objective of this investigation was to evaluate fluids, both Newtonian and non-Newtonian, in these types of orifices plates.

5.4.2 Pressure loss coefficient

It can be seen from Figure 5.14 that the difference between the circular orifice and the two triangular orifices can be neglected in both laminar and turbulent flow regimes. The fact that the triangular orifice introduces sharp edges in contrast to the smooth circle edges for circular orifice does not affect the pressure loss coefficient. It can therefore, be concluded that the generation 0 fractal-shaped orifice plate is topologically the same as a circular orifice as was also noticed by Abou El-Azem Aly et al. (2010).

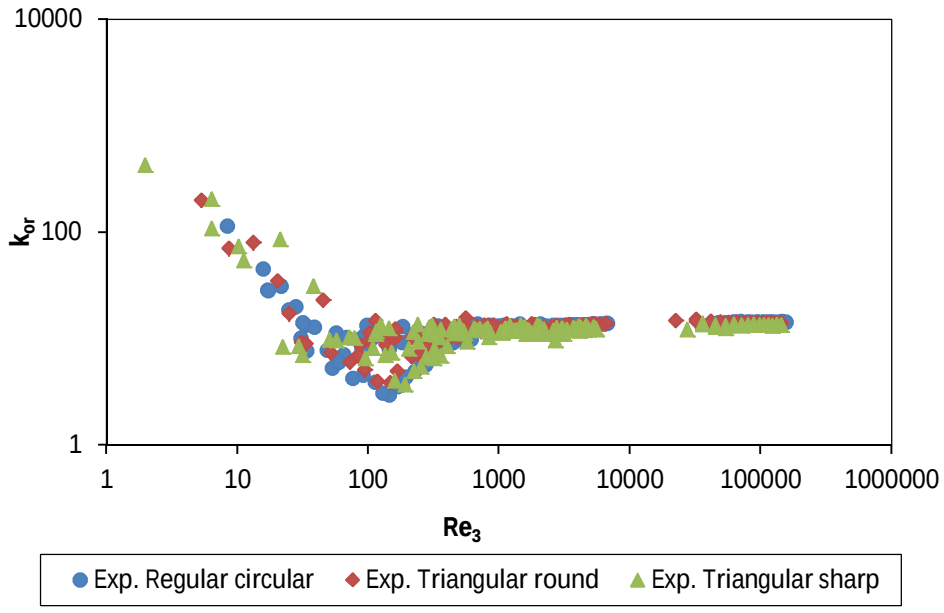

Figure 5.14 : Comparison between circular and triangular orifices

5.4.3 Discharge coefficient

Figure 5.15 presents the discharge coefficient comparison between the circular orifice and the triangular orifice with sharp and round apex. It can be seen from the figure that there is no difference between the three different experimental data in the laminar flow regimes. It can therefore be concluded that the difference between the three pressure drops can be neglected. Small discrepancies have been observed in turbulent flow regimes where the average value of the circular orifice was 0.63 and 0.65 for the triangular orifice with sharp apex; finally an average value of 0.64 was observed for the triangular orifice with round apex. This agrees with the work of Abou El-Azem Aly et al. (2010) that stated that results for triangular and circular orifice were the same. However, with the increase of the fractal generations, from the first to third generation, the difference between the two pressure drops becomes more significant. The pressure drops measured for the fractal-shaped orifices are lower than those of the corresponding circular orifices. These differences can be explained as a fractal-shaped orifice is expected to create a larger range of velocities than the simple orifice shape. This is because the fractal geometry introduces constraints at different scales, rather than just at the diameter scale that characterises the jet from the circular orifice (Abou El-Azem Aly et al., 2010).

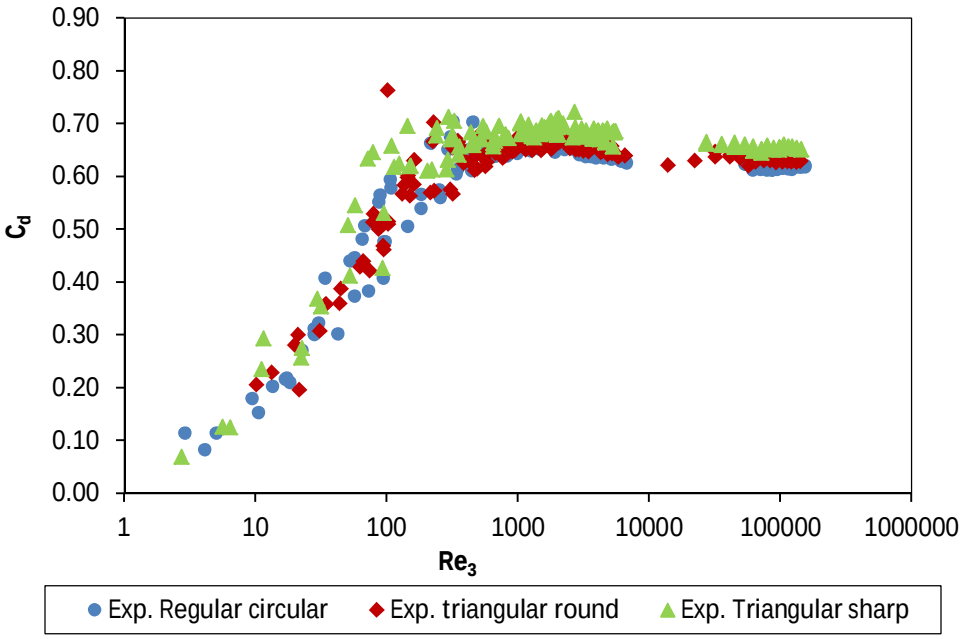

Figure 5.15 : Discharge coefficient comparison between circular and triangular orifices

.

5.5 DEVELOPMENT OF THE NEW CORRELATION TO PREDICT PRESSURE LOSS COEFFICIENTS

5.5.1 Introduction

Many authors have developed correlations to predict pressure loss coefficients; however, none of those correlations found in the literature can predict data from the laminar to the turbulent flow regime. The lack of adequate correlations to predict the pressure loss coefficient from laminar to turbulent flow necessitated the development of a new correlation for short square-edged orifice plates. The purpose of this section is to present the derivation of the new correlation and comparison with the experimental data found in this work and the literature.

5.5.2 Dimensional analysis

Dimensional analysis is a good method for understanding the properties of physical quantities autonomous of the units used to measure them. The following variables were identified as important in influencing the pressure loss coefficient:

$$\Delta P = (V, \mu_{eff}, \rho, D, d) \qquad \text{Equation 5.1}$$

5.5.3 Functional relationship

The relationship between the variables (Equation 5.1) can be obtained through a method called Buckingham's π theorem, which states that (Simons, 2007):

If there are n variables in a problem and these variables contain m primary dimensions for example M, L, T, the equation relating all the variables will have (n-m) dimensionless groups.

Buckingham referred to these groups as π groups.

The final equation obtained is in the form of:

$$\pi = f(\pi 2, \pi 3, \ldots \pi(n-m)) \qquad \text{Equation 5.2}$$

$$f(\Delta P, V, \mu_{eff}, \rho, D, d) = 0 \qquad \text{Equation 5.3}$$

Applying π groups theory to Equation 5.3, this can be expressed as:

$$f\left(\Delta P/\rho V^2, d/D, \mu_{eff}/V\rho d\right) = 0 \qquad \text{Equation 5.4}$$

Equation 5.4 can be rewritten as:

$$(k_{or}, \beta, Re^{-1}) = 0 \qquad \text{Equation 5.5}$$

5.5.4 Laminar flow

It can be seen from experimental data in Figure 5.16 that in the laminar flow region the pressure loss coefficient depends on the Reynolds number and the orifice diameter ratio β. As shown in Figure 5.16, for $Re_3 < 60$, the pressure loss coefficient is a function of the Reynolds number. The Slatter Reynolds number, Re_3, was used because it can accommodate Newtonian and non-Newtonian behaviours. Equation 5.5 can be explicitly formulated in terms of Reynolds number and orifice beta ratio in laminar flow as:

$$k_{or} = C_1 \beta Re_3^{-1} \qquad \text{Equation 5.6}$$

where $C_1$is a constant.

In Equation 5.6 $C_1\beta$ expresses the laminar flow loss coefficient constant C_{or} (Equation 4.1).

It can be seen in Figure 5.16 that the laminar flow loss coefficient constant C_{or} changes with orifice diameter ratio β.

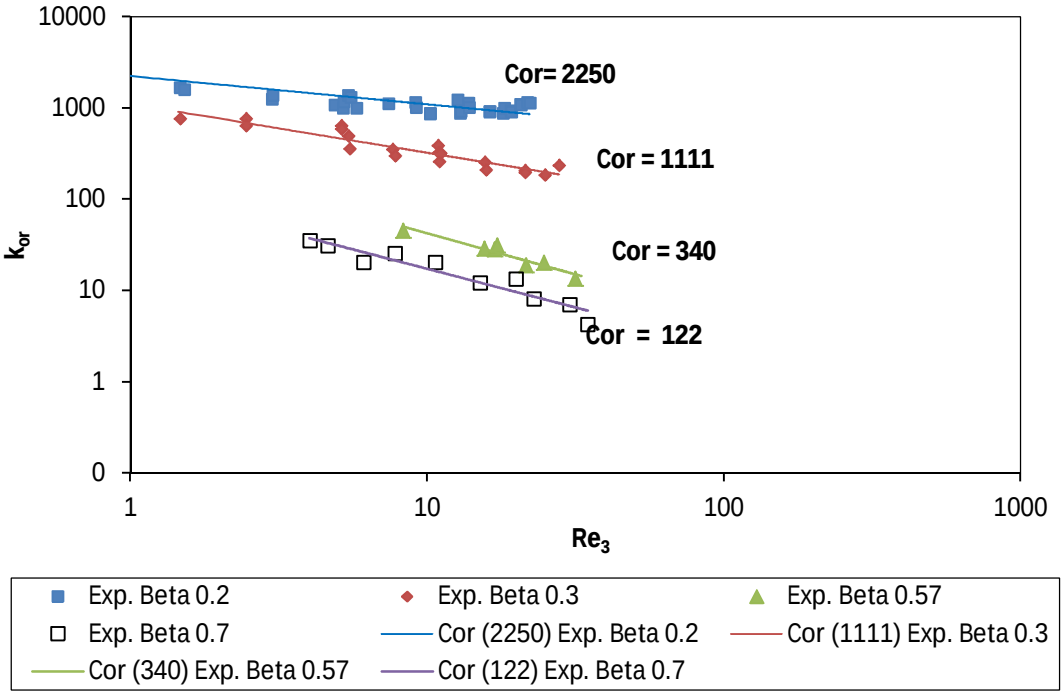

Figure 5.16 : Laminar flow pressure loss coefficients C_{or} versus Reynolds number

A plot of C_{or} versus β is shown in Figure 5.17. A power law model was fitted to describe the relationship between the two variables. A value of R^2 of 0.949 was observed which represented a good fit of experimental data (Benziger and Askay, 1999).

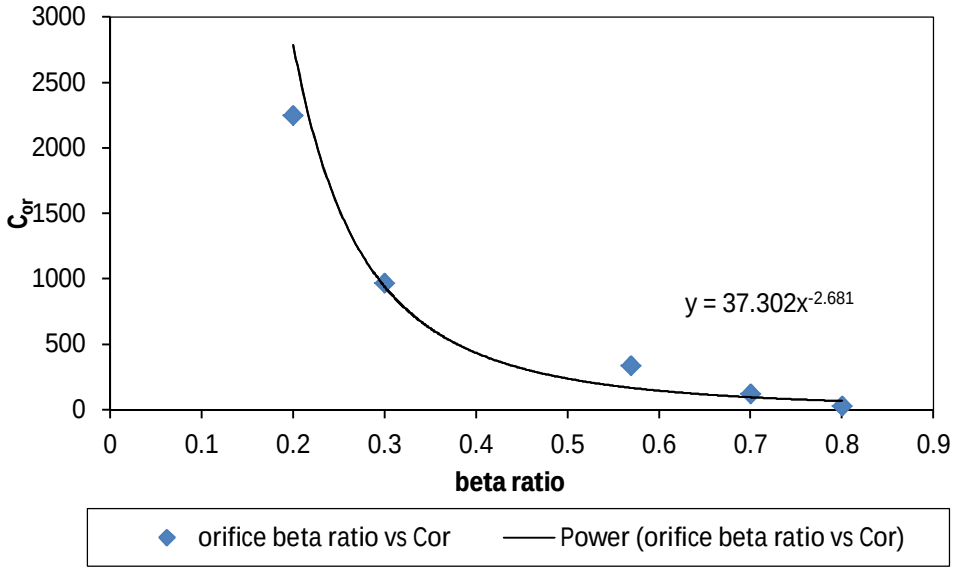

Figure 5.17 : Plot of C_{or} against orifice diameter beta ratio β

Therefore, the laminar flow pressure loss coefficient constant can be expressed as a function of diameter ratio as:

$$C_{or} = 37.3\beta^{-2.68} \quad \text{Equation 5.7}$$

Substituting Equation 5.7 in Equation 5.6 the latest can be re-written as:

$$k_{or} = 37.3\beta^{-2.68}Re_3^{-1} \quad \text{Equation 5.8}$$

Equation 5.8 is only valid to predict the pressure loss coefficient for the laminar flow regime, preferably $Re_3 < 60$.

5.5.5 Turbulent flow

The loss coefficient does not depend on the Reynolds number in the turbulent flow regime. It does, however, depend on the orifice diameter ratio β (Turian et al., 1998). The pressure loss coefficient is a constant value in turbulent flow. Using Equation 5.5, pressure loss coefficient in turbulent flow regime can be given by the Equation 5.9 below, where C_3 is a turbulent constant.

$$K_{or} = C_3\beta \quad \text{Equation 5.9}$$

The following initial assumptions have been taken into account in the analysis of the orifice pressure loss coefficients in turbulent flow at different orifice diameter ratios:

- The roughness of the orifice wall has been neglected as the orifice wall used was smooth.
- The thickness of the orifice has been neglected.
- The pressure loss coefficient is constant in turbulent flow and depends on the orifice diameter ratio.

Experiments were performed to obtain pressure loss coefficients for orifice diameter ratio β of 0.2, 0.3, 0.57 and 0.7. As was noted before, the pressure loss coefficient remains constant in turbulent flow from a Reynolds number above 1 000 and has a specific value for each orifice diameter ratio. Table 5.9 and Figure 5.18 show the pressure loss coefficient obtained for each orifice diameter ratio in the turbulent flow regime.

Table 5.9 : Pressure loss coefficient value in turbulent flow regime

β	k_{or}
0.20	1213
0.30	226.9
0.57	13.32
0.70	3.570

A power law model was fitted to describe the relationship between the two variables.

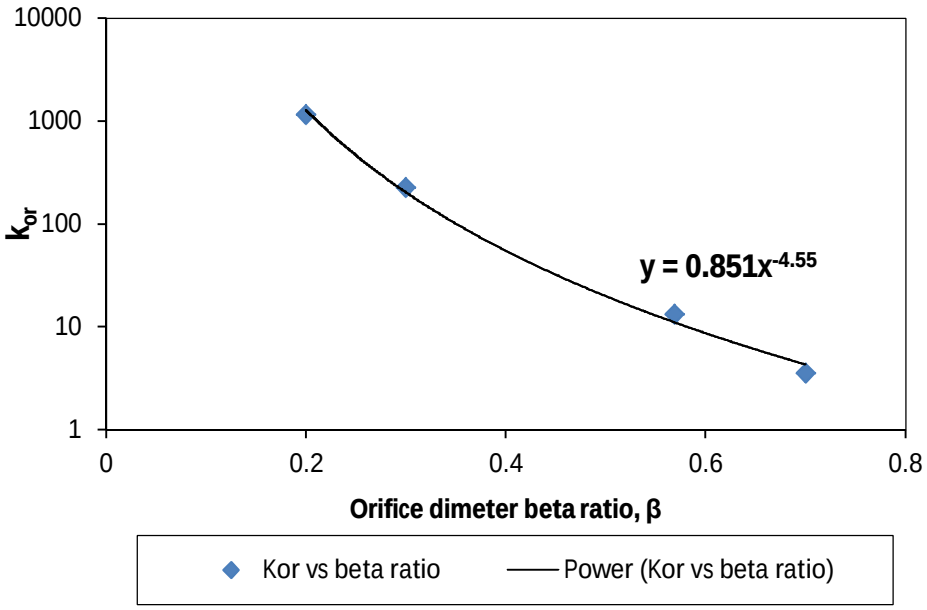

Figure 5.18 : k_{or} versus orifice diameter beta ratio

The pressure loss coefficient can be correlated as shown below by replacing C_3 in Equation 5.9:

$$k_{or} = 0.851\beta^{-4.55} \qquad \text{Equation 5.10}$$

The aim of this section was to provide a correlation which could predict pressure loss coefficient from laminar to turbulent flow. The work of Hooper (1981) showed that the laminar and turbulent values can be added to give a prediction over the entire flow range (Hooper, 1981); combining Equation 5.8 and Equation 5.10, gives Equation 5.11 which can predict the pressure loss coefficient from laminar to turbulent flow.

$$k_{or} = 37.3\beta^{-2.68}Re_3^{-1} + 0.851\beta^{-4.55} \qquad \text{Equation 5.11}$$

5.6 COMPARISON BETWEEN NEW CORRELATION AND EXPERIMENTAL DATA

This section presents a comparison of the new correlation derived with experimental data obtained in this current work and to those found in the literature.

5.6.1 Orifice diameter ratio, $\beta = 0.2$

Figure 5.19 presents a comparison between experimental data obtained in this work and data from literature with the new correlation derived for orifice diameter ratio 0.2. It can be seen that the majority of the experimental data were within 40% in the laminar flow regime. Good agreement between the new correlation and experimental data has been observed in the turbulent flow regime where the data were within ± 10%.

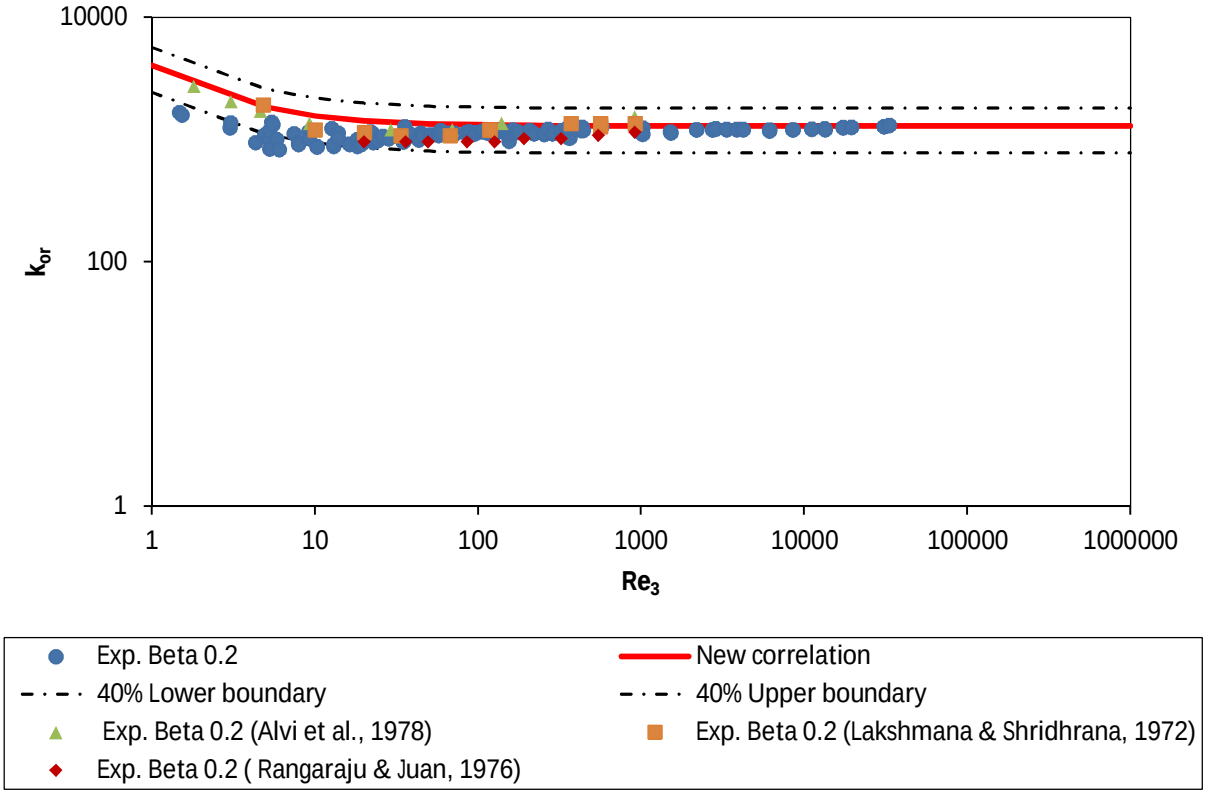

Figure 5.19 : Comparison between the new correlation and experimental data for β = 0.2

5.6.2 Orifice diameter ratio, $\beta = 0.3$

Figure 5.20 below shows the comparison between the model derived and the experimental data obtained for orifice ratio 0.3. Approximately 97% of data fall within 40%. Good agreement

between experimental data for β = 0.3 and the new model has been observed for both laminar and in turbulent flow regimes.

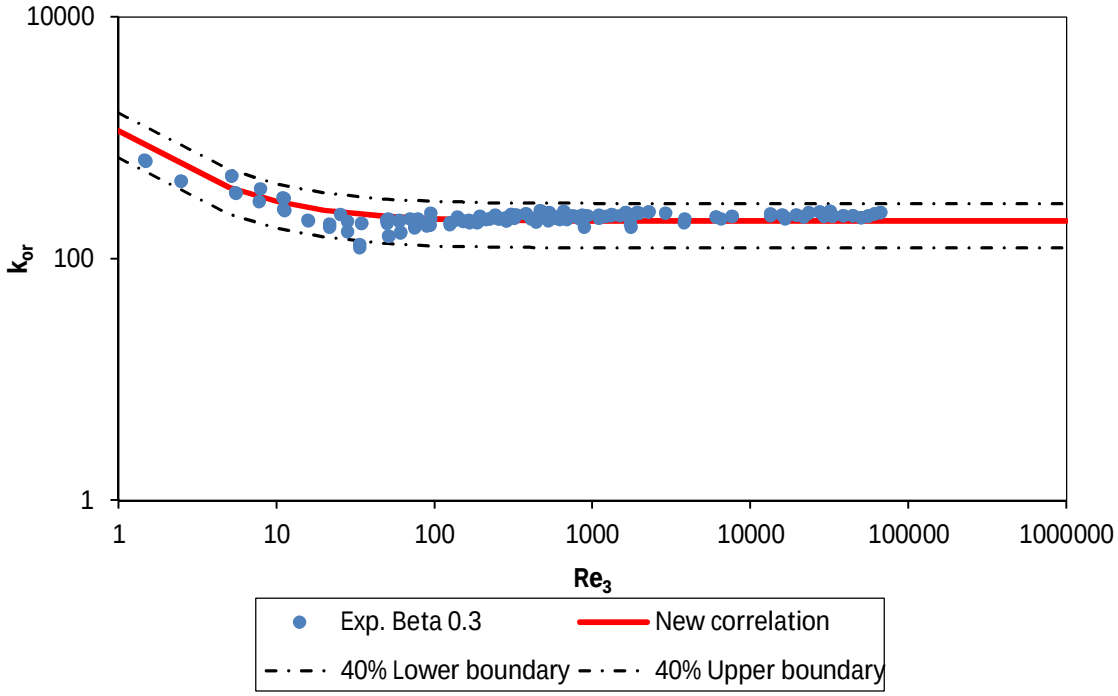

Figure 5.20 : Comparison between the new correlation and experimental data for β = 0.3

5.6.3 Orifice diameter ratio, $\beta = 0.4$

It can be seen from Figure 5.21 that in the laminar flow regime the experimental data obtained from the literature for orifice ratio 0.4 agree well with the new correlation. The experimental data shows an increase at Re > 1 000 that is higher than the model predicts. It is not clear if this is experimental error or true behaviour of the fluid.

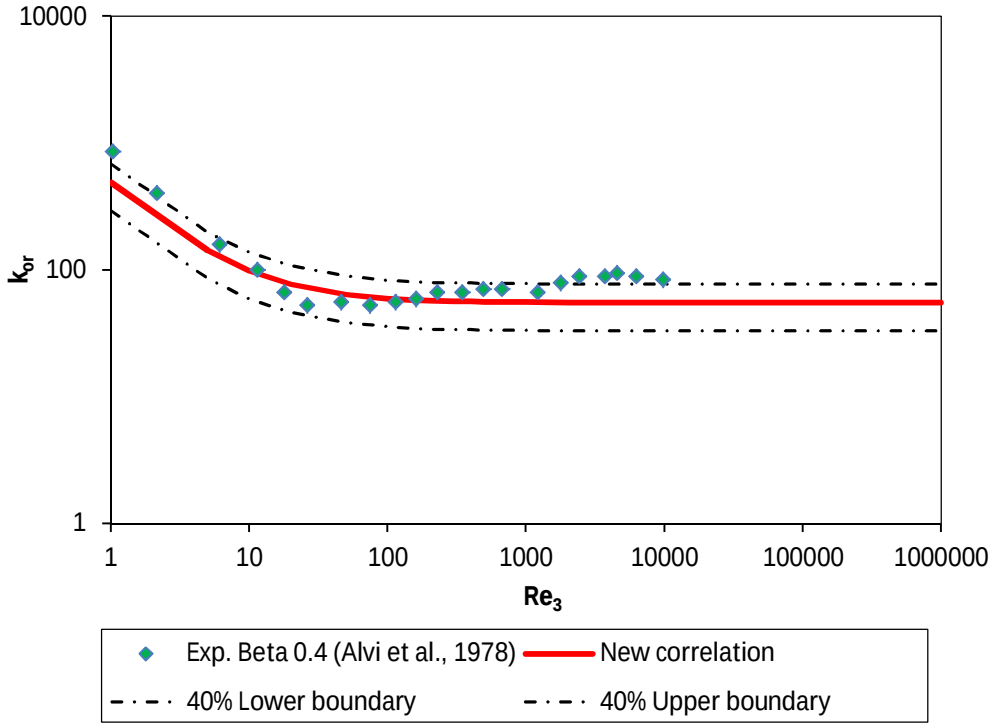

Figure 5.21 : Comparison between the new correlation and experimental data provided by Alvi et al., 1978, for β = 0.4

5.6.4 Orifice diameter ratio, $\beta = 0.57$

Figure 5.22 presents a comparison between experimental data obtained in this work and data from literature with the new correlation derived for orifice diameter ratio 0.57. The new model under-predicts the experimental data 40% for Re > 10 000. The majority of data falls within 40% in the laminar flow and the turbulent flow regime. In this case there is also an increasing trend in the data from Re > 1 000 as was found for β = 0.4

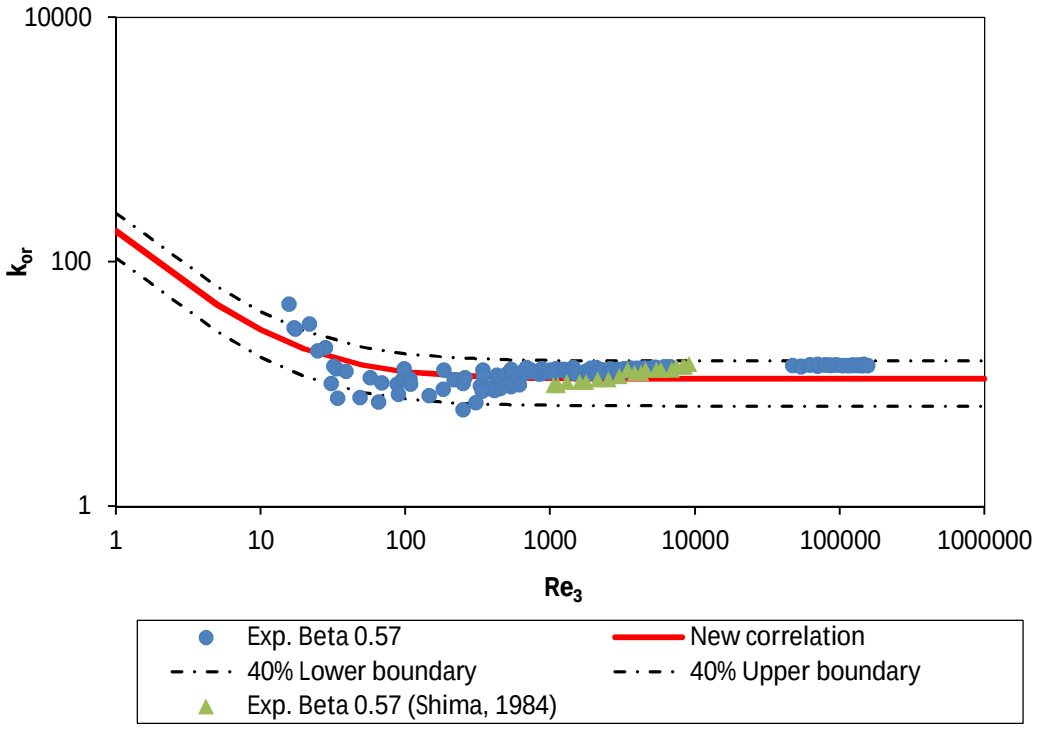

Figure 5.22 : Comparison between the new correlation and experimental data for β = 0.57

5.6.5 Orifice diameter ratio, $\beta = 0.7$

Figure 5.23 presents a comparison between experimental data obtained in the current work and those available in the literature with the new correlation derived for orifice diameter ratio 0.7. It can be seen that the experimental data is within 40% error in both the turbulent flow regime and laminar flow. However, the agreement between the new correlation and experimental is greater than 40% in the transitional flow regime, where a minimum of k_{or} is obtained.

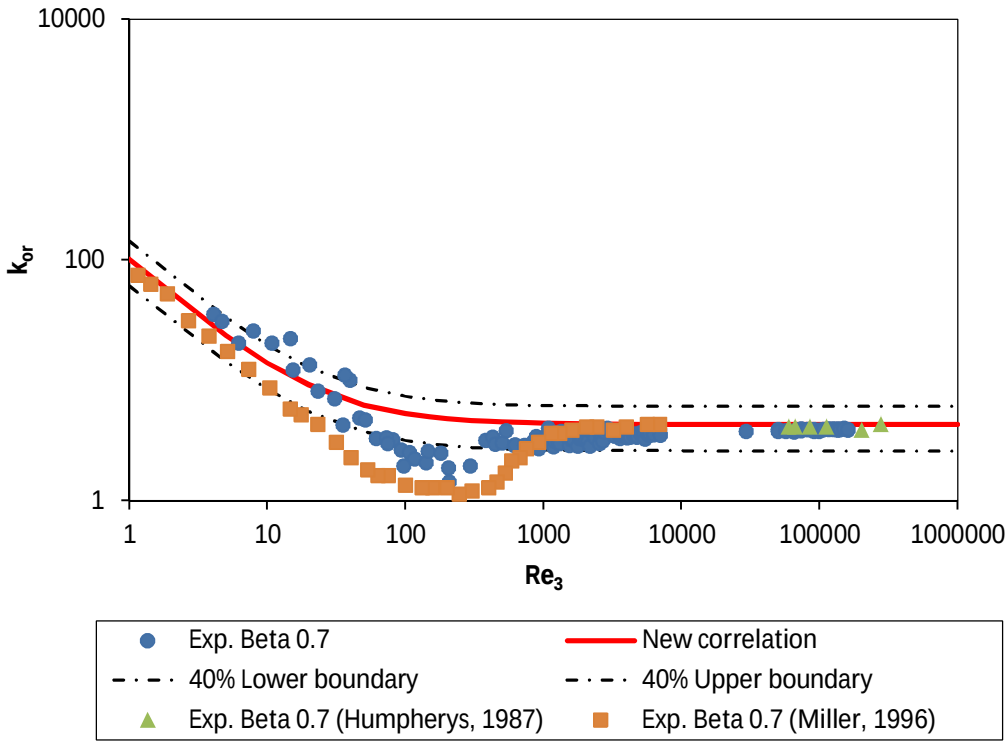

Figure 5.23 : Comparison between the new correlation and experimental data for β = 0.7

5.6.6 Orifice diameter ratio, $\beta = 0.8$

The new correlation over predicts experimental results for β = 0.8 provided by Miller (1996) and Alvi et al., (1978). In the transitional regime the data reached the lower boundary. It can be seen that the majority of data available for beta ratio 0.8 are in the transitional zone. There is no data to establish the ability of the correlation to predict the loss coefficient in turbulent flow. According to literature and the observation made experimentally in this work, the loss coefficient only reach a constant value at a Reynolds number above 10 000.

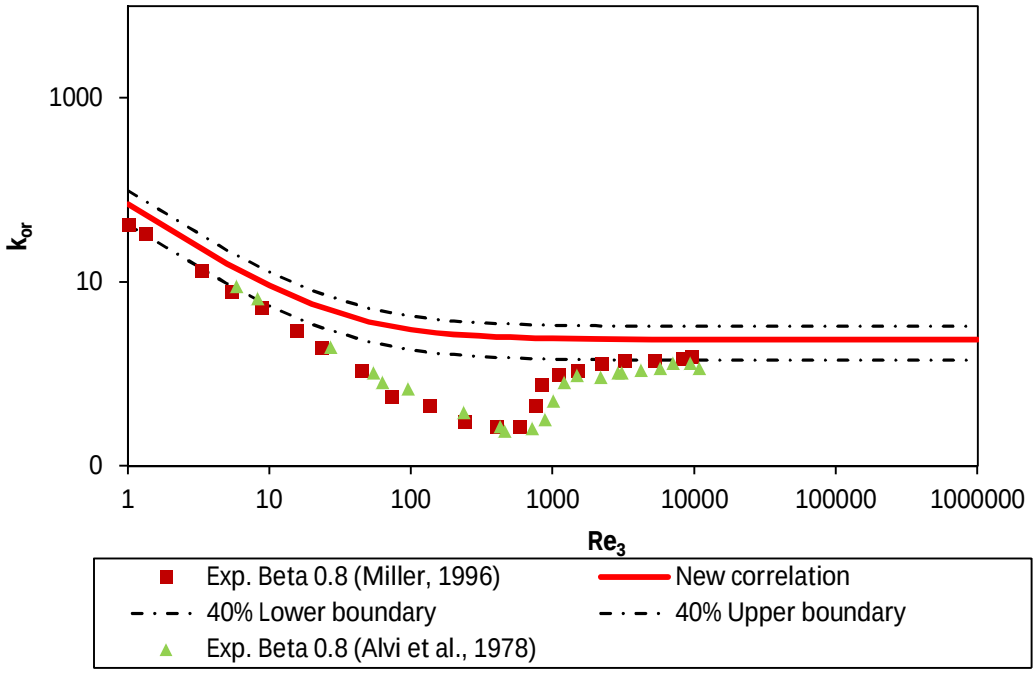

Figure 5.24 : Comparison between the new correlation and experimental data provided by Miller (1996) for β = 0.8.

Table 5.10 presents the overall relative percentage uncertainty of the new correlation compared to the literature and experimental data in the turbulent flow regime.

Table 5.10 : Pressure loss coefficient uncertainty in turbulent flow regime for new correlation

β	% Uncertainty
0.2	9
0.3	10
0.4	29
0.57	19
0.7	17
% average	17.5

From the comparison of the new correlation with experimental data obtained in this investigation and data available in the literature, it can be concluded that the applicability of the new correlation is:

- $0.2 \leq \beta \leq 0.7$
- $5 \leq Re_3 \leq 10^6$

5.7 CONCLUSION

The aim of this work was to determine pressure loss and discharge coefficient for short square-edged orifice plates. After comparison of experimental data obtained in this investigation with experimental data found in the literature, it was seen that there was a lack of correlations to predict pressure loss coefficients from the laminar to turbulent flow regimes. A summary of the conclusions are:

- Pressure loss coefficient data for different diameter ratios obtained in this work were compared with experimental data and Ginsburg (1963) and Ward-Smith (1971) models found in the literature. The experimental data obtained in this work agree well with the experimental data found in the literature. The two models over-predict the experimental data obtained in this work by 25-40% for orifice diameter ratios 0.2 and 0.3. The models performed much better for orifice diameter ratio 0.57 and 0.7 where experimental data obtained in this work were within 11%.
- Discharge coefficient data for different diameter ratios were compared with Benedict and Wyler (1973) in turbulent flow. As was observed for the pressure loss coefficient comparison, the model under-predicts the experimental data for orifice diameter ratios 0.2 and 0.3. Good agreement of the model with the experimental data was seen for orifice diameter ratio 0.57.
- A comparison between experimental data for orifice diameter ratio 0.57 with different shapes (circular orifice and generation 0 Von Koch fractal-shaped orifice plates), but with the same orifice flow areas, has been completed and discrepancies quantified.
- A new correlation to predict pressure loss coefficients was derived from experimental data. The new correlation was compared with existing data and experimental data obtained in this investigation. The correlation shows a good agreement and can be used from laminar to turbulent flow regimes for regular circular short square-edged orifices.

This will provide input data to enable more efficient pipeline designs.

CHAPTER 6

6.1 INTRODUCTION

Orifice plates have been used for a while and will continue to be used for a long time. They are cheap, robust (no moving part is involved) and easy to implement (Abou El-Azm Aly et al., 2010). This explains their popularity across a wide range of industries. This work is an addition to a relatively small body of information on short square-edged orifice plates related to pressure loss and discharge coefficients. The objective of this work was to provide experimental data and derive a correlation able to predict pressure loss coefficients from the laminar to turbulent flow regime. This section will give a summary of the work done, its main contribution, and recommendations for future research.

6.2 SUMMARY

Experiments were done in the slurry laboratory at the Cape Peninsula University of Technology. Four circular short square-edged orifices with orifice diameter ratio β = 0.2, 0.3, 0.57, 0.7 were separately horizontally mounted in a straight pipe and tested. Two generation 0 Von Koch fractal-shaped orifice plates with the same flow areas as a circular orifice with diameter ratio β = 0.57 were also tested. A Newtonian fluid (water) and non-Newtonian fluids (carboxymethyl cellulose solutions, kaolin and bentonite suspensions) at different concentrations were used as test fluids. Pressure loss and discharge coefficients were calculated for laminar, transitional and turbulent flow regimes for all six short square-edged orifices tested. The experimental data were compared with experimental data and correlations available in the literature, such as Ginsburg (1963), Ward-Smith (1971), Lakshmana Rao and Shridharan (1972), Benedict and Wyler (1973), Ragaraju and Jain (1976), Alvi et al. (1978), Shima (1984), Humpherys (1987), and Miller (1996). The fractal-shaped orifices were compared to the circular orifices with the same flow areas. The following important points have been highlighted in this current investigation:

- Experimental data has been extended in laminar and turbulent flow for orifice diameter ratios β = 0.2, 0.57 and 0.7. Experimental data has been provided from laminar to turbulent flow for orifice diameter ratio β = 0.3.
- The generation 0 Von Koch fractal-shaped orifice plate is topologically the same as a circular orifice and no significant difference has been observed for pressure loss

coefficients and discharge coefficients between the two shapes of orifices tested. However, the apex does make a difference.

- The comparison between experimental data and models found in the literature revealed the models performed well only for orifice diameter ratio $\beta > 0.57$ for both pressure loss coefficient and discharge coefficient in the turbulent regime. Therefore, a new correlation has been developed, based on experimental data obtained in this study for pressure loss coefficients. The new correlation takes in account both the laminar and turbulent flow regime and was within 40%.

6.2 CONTRIBUTIONS

The current investigation added pressure loss coefficients and discharge coefficients to the literature. A design correlation for pressure loss coefficient was developed for a circular short square edged orifice plate, which will be useful for designing pipeline systems in industries.

6.3 CONCLUSION

Experimental data have been provided to the literature for orifice diameter ratio $\beta = 0.2$, 0.3, 0.57 and 0.7 for circular orifices and for generation 0 Von Koch fractal-shaped orifices with same flow area as a circular orifice with orifice diameter ratio $\beta = 0.57$. A new correlation has been developed to predict the pressure loss coefficient from the laminar to turbulent regimes and has been proved to be successful for orifice diameter ratio ranging from 0.2 to 0.7.

6.4 FUTURE RESEARCH RECOMMENDATIONS

Although this study covered a wide range of fluids (both Newtonian and non-Newtonian), more data are required, especially in the laminar flow regimes. Therefore the following is recommended:

- Further experiment work should be done for highly viscous and time-dependent fluids
- More experimental work must be conducted for first, second and third generation fractal-shaped orifice plates using liquids.
- Finally a correlation to predict discharge coefficients from the laminar to turbulent flow regime should be developed.

REFERENCES

Abou El-Azem Aly, A., Chong, A., Nicolleau, F. & Beck, S. 2010. Experimental study of the pressure drop after fractal-shaped orifices in turbulent pipe flows. *Experimental Thermal and Fluid Science*, 34(1):104-111, January.

Alvi, S.H., Shridharan, K. & Lakshmana Rao, N.S. 1978. Loss characteristics of orifices and nozzles. *Journal of Fluids Engineering,* 100(3):300-307, September.

ANSI/API. 1995. Manual of petroleum measurement standards. Chapter 14 – Natural gas fluids measurement, section 3 – concentric, square-edged orifice meters. AGA Report No. 3, Part 1, GPA 8185-90, ANSI/API 2530-1991, Parts 1, 2, 3 & 4.

ASME. 2004. Measurement of fluid flow in pipe using orifice, nozzle, and Venturi MFC-3MO. American Society of Mechanical Engineers Standard, ASME MFC-3M-2004, Part 1 &2.

Banerjee, T.K., Das, M., Das & Das, S.K. 1994. Non-Newtonian liquid flow through globe and gate valves. *Canadian Journal of Chemical Engineering*, 72(2):207-211, April.

Barry, B.A. 1991. *Errors in practical measurement in surveying, engineering and technology*. Rancho Cordova, CA: Landmark Enterprises.

Baudouin, M.M. 2003. Contractions and expansion losses for non-Newtonian fluids. Unpublished Mtech thesis, Cape Technikon, Cape Town.

Beck, C. 1944. Laminar flow friction losses through fittings, bends and valves. *Journal of the American Society for Naval Engineers*, 56(2):235-271, May.

Benedict, R.P. & Wyler, J.S. 1973. A generalised discharge coefficient for differential pressure fluid meters. *American Society of Mechanical Engineering*, Winter Annual Meeting Detroit, Michigan, 73:6-9.

Benedict, R.P. 1977. Loss coefficients for fluid meters. *Journal of Fluids Engineering*, 99(1):245-248, March.

Benziger, J.B & Aksay, I.A. 1999. Notes on data analysis: Chemical Engineering 346*, Spring term. Department of Chemical Engineering*, Princeton University, Princeton.

Boger, D.V. & Walters, K. W. 1993. *Rheological phenomena in focus*. New York: Elsevier Science Pub.

Bohra, L.K. 2004. Flow and pressure drop of highly viscous fluids in small aperture orifices. Unpublished MS thesis, School of Mechanical Engineering, Georgia Institute of Technology.

Bohra, L.K., Mincks, L.M. & Garimella, S. 2004. Pressure drop characteristics of viscous fluid flow through orifices. *ASME Heat Transfer/Fluids Engineering.* Summer Conference, Charlotte, North Carolina, USA, Technical Presentation, July 2004

References

Buckingham, E. 1914. On physically similar systems: illustrations of the use of dimensional equations. *Physical Review*, 4 :345-376.

Brinkworth, BJ. 1968. An *introduction to experimentation*. London: English Universities Press.

Chadwick, A.J., Morfett, J.C. & Borthwick, M. 2004*. Hydraulics in civil and environmental engineering*. 4th ed. London: Spon Press.

Chhabra, R.P. & Richardson, J.F. 1999. *Non-Newtonian fluids in the process industries: fundamentals and engineering applications*. Oxford: Butterworth-Heinemann.

Della Valle, D., Tanguy P. A. & Carreau. P.J. 2000. CharacteriZation of the extensional properties of complex fluids using an orifice flowmeter. *Journal of Non-Newtonian Fluid Mechanics*, 94(1):1-13, November.

Douglas, J.F., Gasiorek, J.M. & Swaffield, J.A. 2000. *Fluid mechanics*. 4th ed. Harlow: Prentice-Hall.

Edwards, M.F., Jadallah, M.S.M. & Smith, R. 1985. Head losses in pipe fittings at low Reynolds numbers. *Chemical Engineering Research and Design.* 63:43-50, January.

ESDU TN 07007. 2007. Incompressible flow through orifice plates – a review of the data in the literature.

ESDU 81039. 1981. Pressure losses across orifices plates, perforated plates and thick orifice plates in ducts-flow of liquids.

Ginsburg, I.P. 1963. *Applied fluid dynamics*. Jerusalem: Israel Program for Scientific Translations.

Haldenwang, R. 2003. Flow of non-Newtonian fluids in open channels. Unpublished DTech (Civil Engineering) thesis, Cape Technikon, Cape Town.

Hall, G.W. 1963. Analytical determination of the discharge characteristics of cylindrical-tubes orifices. *Journal of Mechanical engineering Science*, 5(1):91-97.

Hasegawa, T., Suganuma, M. & Watanabe, H. 1997. Anomaly of excess pressure drops of the flow through very small orifices. *Physics of Fluids,* 9(1):1-3.

Heywood, N.I. & Brown, N.P. (eds). 1991. *Slurry handling: design of solid-liquid systems*. London: Elsevier Applied Science.

Hooper, W.B. 1981. The two-k method predicts head losses in pipe fittings. *Chemical Engineering*: 96-100, August.

Humpherys, A.S. 1987. Energy dissipation in low pressure irrigation pipelines: II orifices. *Transactions of the ASAE,* 30(1):176-182.

Husain, Z.D. 1995. The theoretical uncertainty of flow measurement. *Sixty – Sixth International School of Hydrocarbon Measurements.* Houston, TX, Daniel Flow Products, Inc.

References

ISO. 2002. *Measurement of fluid flow by means of pressure differential devices inserted in circular-cross section conduits running full.* BS EN ISO 5167-2:2002(E).

Johansen, F.C. 1930. Flow through pipe orifices at low Reynolds number. *Proceedings of the Royal Society of London, Series A, Containing Papers of a Mathematical and Physical Character*, 126(801):231-245, January.

Kabwe, A.M., Fester, V.G. & Slatter, P.T. 2010. Prediction of non-Newtonian head losses through diaphragm valves at different opening positions. *Chemical Engineering Research and Design,* 88(8):959-970.

Kim, B.-C., Pak, B.-C., Cho, N.-H., Chi, D.-S., Choi, H.-M., Choi. Y.-M. & Park, K.-A. 1998. Effects of cavitation and plate thickness on small diameter ratio orifice meters. *Flow Measurement and Instrumentation,* 8(2):85-92, June.

Lakshmana Rao, N.S. & Shridharan, K. 1972. Orifice losses for laminar approach flow*. ASCE: Journal of Hydraulics Division*, 98(11):2015-2034, Novembre.

Lakshmana Rao, N.S., Shridharan, K & Alvi, S.H. 1977. Critical Reynolds number for orifice and nozzle flows in pipes. *ASCE: Journal of Hydraulics Division*, 15(2):167-178.

Lazarus, J.H. & Slatter, P.T. 1988. A method for the rheological characteristisation of tube viscometer data. *Journal of Pipelines*, 7:1759-1765, November.

Liu, H. 2003. *Pipeline engineering*. Boca Raton, FL: Lewis Publishers.

Malkin, A. Ya. 1994. *Rheology fundamentals*. Toronto: ChemTec Pub.

Massey, B.S. 1975. *Mechanics of fluids*. 3rd ed. New York: Van Nostrand Reinhold.

Massey, B.S. 1990. *Mechanics of fluids*: *Solutions manual*. 6th ed. London: Chapman & Hall.

McNally Institute. 2010. Pump, centrifugal pumps, PD pumps, seals & mechanical seals data. Retrieved 214. www.mcnallyinstitute.com.

McNeil, D.A., Addlesee, J. & Stuart, A.D. 1999. An experimental study of viscous flows in contractions. *Journal of Loss Prevention in the Process Industries,* 12(4):249-258.

Medaugh, F.W. & Johnson, G.D. 1940. Investigation of the discharge and coefficients of small circular orifices. *Civil Engineering*, 7(7):422-424, July.

Metzner, A.B & Reed, J.C. 1955. Flow of non-Newtonian fluids – correlation of the laminar, transition, and turbulent flow regions. *AIChE Journal,* 1(4):434-440, december.

Miller, D.S. 1990. *Internal flow systems*. 2nd ed. Cranfield, Bedfordishire: BHRA Information Services.

Miller, D.S. 1996. *Internal flow: a guide to losses in pipe and duct systems*. Cranfield, Bedfordishire: BHRA Group.

Mincks, L.M. 2002. Pressure drop characteristics of viscous fluid flow across orifices. Unpublished MS thesis, Mechanical Engineering, Iowa State University.

Morrison, G.L. 2003. Euler number based orifice discharge coefficient relationship. *Journal of Fluids Engineering,* 125(1):189-191, January.

Morrison, G.L., DeOtte, R.E., Moen, M., Hall, K.R. & Holste, J.C. 1990. Beta ratio, swirl, and Reynolds number dependence of wall pressure in orifice flowmeters. *Flow Measurement and Instrumentation,* 1(5):269-277, October.

Murdock, J.W. 1976. *Fluid mechanics and its applications*. Boston, MA: Houghton Mifflin.

Nigro, F.E.B., Strong, A.B. & Alpay, S.A. 1978. A numerical study of the laminar, viscous, incompressible flow through a pipe orifice. *Journal of Fluids Engineering*, 100(4):467-472, December.

Paterson, A. & Cooke, R. 1999. The design of slurry pipeline systems. Short course presented at the Cape Technikon, Cape Town, 24─26 March.

Prabu, S.V., Mascomani, R., Balakrishnan, K., & Konnur, M. S. 1996. Effects of upstream pipe fittings on the performance of orifice and conical flow meters*. Flow Measurement and Instrumentation,*7(1):49-54, March.

Rabinowitsch, B. 1929. Über die viskosität und elastizität van solen. *Zeitschrift fur Physikalische Chemie*, A145:1-26.

Rangaraju, K.G & Jain, A.K. 1976. Energy loss due to sharp edged orifice meters. *Irrigation and Power*, 35(3):401-406.

Sahin, B. & Ceyhan, H. 1996. Numerical and experimental analysis of laminar flow through square-edged orifice with variable thickness. *Transactions of the Institute of Measurement and Control*, 18(4):166-174, October.

Salas-Valerio, W.F. & Steffe, J.F. 1990. Orifice discharge coefficients for power-law fluids. *Journal of Food Process Engineering*, 12(2):89-98, February.

Samanta, A.K., Banerjee, T.K. & Das, S.K. 1999. Pressure losses in orifices for the flow of gas-non-Newtonian liquids. *Canadian Journal of Chemical Engineering*, 77(3):579-583, June.

Serway, R.A. 1992. *Physics for scientists and engineers, with moderns physics*. 3rd ed. Philadephia, PA: Saunders College Pub.

Shima, N. 1984. Loss and discharge characteristics of a flow of polymer solutions through pipes orifices. *Bulletin of JSME*, 27(225):443-449.

Simons, S.J. (ed). 2007. *Concepts of chemical engineering 4 chemists*. Cambridge: Royal Society of Chemistry.

Skelland, A.H.P. 1967. *Non-Newtonian flow and heat transfer*. New York: Wiley.

References

Smith, D. & Walker, W.J. 1923. Orifice flow. *Proceedings of the Institution of Mechanical Engineers,* 104:23-36.

Smith, H.Jr. 1886. *Hydraulics, the flow of water through orifices, over weirs, and through open conduits and pipes*. New York: Wiley and sons.

Streeter, V.L. & Wylie, E.B. 1975. *Fluid mechanics*. 6th ed. New York: McGraw-Hill.

Swamee, P.K. 2005. Discharge equations for venturimeter and orificemeter. *Journal of Hydraulic Research*, 43(4):417-420.

Turian, R.M., Ma, T.W., Hsu, F.L.G., Sung, M.D.J & Plackmann, G.W. 1998. Flow of concentrated non-Newtonian slurries: 2. Friction losses in bends, fittings, valves and Venturi meters. *International Journal of Multiphase Flow*, 24(2):243-269.

Von Koch, H. 1904. Sur une courbe continue sans tangente, obtenue par une construction géométrique élémentaire, *Arkiv fur Matematik*, 1:681-704.

Ward-Smith, A.J. 1971. *Pressure losses in ducted flows*. London: Butterworths.

Ward-Smith, A.J. 1979. Critical fowmetering: the characteristics of cylindrical nozzles with sharp upstream edges. *International Journal of Heat and Fluid Flow*, 1(3):123-132, September.

Ward-Smith, A.J. 1980. *Internal fluid flow*: *the fluid dynamics of flow in pipes and ducts*. Oxford: Clarendon Press.

Wu, D., Burton, R. & Schoenau, G. 2002. An empirical discharge coefficient model for orifice flow. *International Journal of Fluid Power*, 3(3):13-18, December.

Zampaglione, D. 1969. Sul moto di una corrente laminare attraverso diaframmi. *Energia Electrica*, 46:821-828.

Zhang, Z. & Cai, J. 1999. Compromise orifice geometry to minimize pressure drop. *Journal of Hydraulic Engineering*, 125(11):1150-1153.

APPENDICES

ORIFICE DIAMETER RATIO, $\beta = 0.2$

CMC 4%

Orifice Type:	Short	
Orifice thickness[m]:	0.0069	Area[m^2]
Orifice dimension[m]:	0.009	6.36173E-05
Pipe Diameter [m]:	0.046	0.001661903
Diameter ratio	0.20	
Aspect ratio	0.77	
g[m/s^2]	9.81	
Material Type:	CMC	
Density[kg/m^3]:	1023.2	
Concentration[%]:	4%	
τ_y[Pa]:	0	
K [Pa.s]:	0.5	
n:	0.676	
PPT used:	110	
Range selected:	0-500	

1/n	n/(n+1)	(n+1)/n	$K^{1/n}$
1.48	0.40	2.48	0.36

	Pod 1	Pod 2	Pod3	Pod 4	Pod 5	Pod 6	Pod 7	Pod 8	Pod 9	Pod10	Pod 11
Axial distances	-5.20	-4.60	-3.68	-2.31	-0.05	-0.03	0.03	2.30	4.61	6.91	9.21
N-D distances incl.[L/D]:	-113.13	-99.98	-80.07	-50.17	-1.04	-0.54	0.54	50.00	100.11	150.26	200.26
Distances[m]:	0.00	0.60	1.52	2.90	5.16	5.18	5.23	7.51	9.81	12.11	14.41

Pod 1	Pod 2	Pod 3	Pod 4	Pod 5	Pod 6	Pod 7	Pod 8	Pod 9	Pod 10	Pod 11	Average Q
[Pa]	[Pa]	[Pa]	[Pa]	[Pa]	[Pa]	[Pa]	[Pa]	[Pa]	[Pa]	[Pa]	[l/s]
355729	355160	354350	352668	350943	350159	18309	34399	31884	29610	27591	1.20
355200	354225	353427	352575	350593	349870	18290	34419	32215	29606	27379	1.19
476188	476469	475629	474357	472053	470989	13435	35712	33401	30725	28143	1.37
474618	475948	475331	474308	470705	470757	13444	35002	33463	30524	27943	1.37
391986	390988	391613	389901	387865	386660	16808	32280	32308	29876	29241	1.25
391002	388949	390626	389399	387509	386184	30686	24984	32415	29954	27599	1.25
285817	284545	284451	283463	281322	280429	20905	33223	31005	28957	27042	1.09
285676	285577	284410	283307	281334	280824	20609	33349	30947	28882	26857	1.09
241858	241098	240755	239018	237640	237185	22084	32354	30191	28246	26302	0.99

Pod 1 [Pa]	Pod 2 [Pa]	Pod 3 [Pa]	Pod 4 [Pa]	Pod 5 [Pa]	Pod 6 [Pa]	Pod 7 [Pa]	Pod 8 [Pa]	Pod 9 [Pa]	Pod 10 [Pa]	Pod 11 [Pa]	Average Q [l/s]
241630	240814	240638	239036	237415	237162	21976	32335	30428	28269	26555	0.99
204130	202895	203108	201717	200110	199337	23126	31474	29534	27694	25933	0.89
203960	203017	202935	201710	200257	199431	23150	31425	29587	27701	25856	0.89
154711	153222	153011	152074	150720	150065	24262	29900	28239	26676	25147	0.75
154470	152928	152941	152164	150684	149982	24251	29804	28189	26693	25282	0.75
111576	109522	109655	108781	107757	106755	24839	28270	27073	25541	24368	0.60
110610	109955	109746	108926	107943	107212	24817	28054	27110	25575	24491	0.60
73656	73074	72868	72176	71419	70704	24635	26102	25269	24181	23238	0.45
73446	72857	72633	72049	71247	70709	24610	26085	25281	24143	23253	0.45
50439	49933	49521	49125	48627	47933	23578	24194	23452	22664	22050	0.33
50443	49853	49742	49404	48752	48031	23662	24282	23700	22653	21927	0.33
32633	32320	32091	32015	31795	31199	22144	22171	21551	20969	20533	0.21
33053	32919	32652	32098	31556	31015	22359	22384	21773	21194	20528	0.22
25369	25289	25136	24967	24619	24492	20769	20765	20332	19963	19586	0.14
25388	25253	25147	24956	24493	24497	20791	20795	20533	20016	19649	0.14

CMC 5%

Orifice Type:	Short	
Orifice thickness[m]:	0.0069	Area[m^2]
Orifice dimension[m]:	0.009	6.36173E-05
Pipe Diameter [m]:	0.046	0.001661903
Diameter ratio	0.20	
Aspect ratio	0.77	
g[m/s^2]	9.81	
Material Type:	CMC	
Density[kg/m^3]:	1029.09	
Concentration[%]:	5%	
τ_y[Pa]:	0	
K [Pa.s]:	1.38	
n:	0.64	
PPT used:	110	
Range selected:	0-500	

1/n	n/(n+1)	(n+1)/n	$K^{1/n}$
1.55	0.39	2.55	1.65

	Pod 1	Pod 2	Pod3	Pod 4	Pod 5	Pod 6	Pod 7	Pod 8	Pod 9	Pod10	Pod 11
Axial distances	-5.20	-4.60	-3.68	-2.31	-0.05	-0.03	0.03	2.30	4.61	6.91	9.21
N-D distances incl.[L/D]:	-113.13	-99.98	-80.07	-50.17	-1.04	-0.54	0.54	50.00	100.11	150.26	200.26
Distances[m]:	0.00	0.60	1.52	2.90	5.16	5.18	5.23	7.51	9.81	12.11	14.41

Pod 1	Pod 2	Pod 3	Pod 4	Pod 5	Pod 6	Pod 7	Pod 8	Pod 9	Pod 10	Pod 11	Average Q
[Pa]	[Pa]	[Pa]	[Pa]	[Pa]	[Pa]	[Pa]	[Pa]	[Pa]	[Pa]	[Pa]	[l/s]
418215	415516	413973	410456	404534	402930	38851	53838	47709	42504	36204	1.27
416259	414851	413475	408961	402936	403034	38795	53741	48258	41338	36055	1.27
340041	339288	336619	332904	326903	326916	40099	51131	45400	39853	35152	1.13
339385	337963	336606	333103	327083	327508	39983	50823	45740	39866	35090	1.13
296631	296670	294281	290579	286238	285869	40400	49085	44155	39151	34289	1.04
296187	296027	294989	291117	286122	285294	40394	48359	43690	39010	34279	1.04
246187	244813	243221	240352	234730	234394	40645	45956	43044	37755	33353	0.93
245879	244477	243011	240024	235156	234686	40670	45963	42432	37864	33166	0.93
205845	204420	202838	199924	195880	195569	40560	43595	40940	36460	32021	0.83
204128	203626	202747	200299	195730	195794	40565	43560	41311	36342	32724	0.83
170626	169230	167674	165368	160999	160878	39951	41626	39407	35432	31341	0.74
170533	168634	168091	165168	161280	160983	40182	41890	39531	35195	31614	0.73
133093	131740	130596	128484	125023	124607	39468	39853	37476	33939	30094	0.63
133075	132093	130725	128383	124744	124705	39456	40262	37555	33780	30639	0.63
98988	97407	96679	94848	91519	91493	38341	38530	35865	32315	29019	0.51
98911	97719	96621	94727	91528	91400	38342	38519	35437	32184	29318	0.51
80283	79516	78262	76582	73704	73858	37151	37175	33991	31063	28261	0.43
80210	79368	78378	76606	73683	73771	37267	37266	34087	31107	28269	0.43
59134	58446	57421	56157	54158	54064	33639	33638	31465	28604	26811	0.30
58986	58357	57553	55973	54007	53896	34196	34024	31367	28789	26844	0.30
38075	37737	37041	36188	34752	34831	29061	28115	26886	25158	23935	0.16
38253	37888	37261	36386	35151	34985	29251	28273	26844	25361	24122	0.16
32269	31828	31446	30785	30152	29891	26693	25992	25039	23888	23097	0.11
32330	32111	31632	31061	30078	29859	27015	25914	24980	23975	23001	0.11

CMC 8%

Orifice Type:	Short	
Orifice thickness[m]:	0.0069	Area[m^2]
Orifice dimension[m]:	0.009	6.36173E-05
Pipe Diameter [m]:	0.046	0.001661903
Diameter ratio	0.20	
Aspect ratio	0.77	
g[m/s^2]	9.81	
Material Type:	CMC	
Density[kg/m^3]:	1043	
Concentration[%]:	8	
τ_y[Pa]:	0	
K [Pa.s]:	8.3	
n:	0.6	
PPT used:	110	
Range selected:	0-500	

1/n	n/(n+1)	(n+1)/n	$K^{1/n}$
1.82	0.35	2.82	46.39

	Pod 1	Pod 2	Pod3	Pod 4	Pod 5	Pod 6	Pod 7	Pod 8	Pod 9	Pod10	Pod 11
Axial distances	-5.20	-4.60	-3.68	-2.31	-0.05	-0.03	0.03	2.30	4.61	6.91	9.21
N-D distances incl.[L/D]:	-113.13	-99.98	-80.07	-50.17	-1.04	-0.54	0.54	50.00	100.11	150.26	200.26
Distances[m]:	0.00	0.60	1.52	2.90	5.16	5.18	5.23	7.51	9.81	12.11	14.41

Pod 1	Pod 2	Pod 3	Pod 4	Pod 5	Pod 6	Pod 7	Pod 8	Pod 9	Pod 10	Pod 11	Average Q
[Pa]	[Pa]	[Pa]	[Pa]	[Pa]	[Pa]	[Pa]	[Pa]	[Pa]	[Pa]	[Pa]	[l/s]
317244	311405	304763	296171	285558	277342	129519	124595	106333	89486	70058	0.86
316806	311613	305449	296032	284386	277013	123234	124608	105469	88651	70146	0.86
274011	269316	263333	253328	235160	234495	125375	117887	100966	83833	66867	0.76
274227	270237	263381	252340	235005	234644	125662	117361	101192	82909	68192	0.76
242702	239273	232634	222858	206454	207240	121048	113015	96049	79941	64911	0.68
241314	238796	232614	222951	206479	205943	120965	112145	96332	79938	65407	0.68
210407	206362	200734	191716	177172	176788	114639	106848	91285	76474	62044	0.58
210787	206265	200793	191886	176690	176434	114608	106683	91553	76423	63384	0.58
185017	182180	175809	167270	154678	154381	108996	100866	87340	73155	60408	0.49
185179	182233	176132	167770	154372	154376	108652	100770	87147	73332	59875	0.50
164500	160311	155747	147421	135863	136333	103016	94075	82368	70037	57946	0.42
164505	161379	156439	147912	135666	136407	103871	94675	82845	70210	58841	0.41
139545	135432	131116	123644	113697	115412	92364	86150	74258	65110	54151	0.31
139150	136102	132197	125505	115038	108302	94469	86012	76283	64353	55232	0.31
115668	112966	109971	104225	95485	95956	84250	76409	67995	58623	51149	0.21
116106	113161	110245	104886	95730	96160	84490	76063	68817	58913	51557	0.21
94477	92558	89890	85474	79265	78807	72974	66271	60036	52612	46314	0.13
94477	92558	89890	85474	79265	78807	72974	66271	60036	52612	46314	0.13
78417	75930	74094	70220	66077	65379	61322	57051	52959	48068	43328	0.09
78290	76880	74922	71858	65907	66010	62313	56957	51927	46374	42880	0.09
388179	382499	374613	363582	343613	342195	136551	131976	112395	91665	73370	0.99
388266	381152	375115	363257	342948	342319	135702	130890	112006	91021	72165	1.00
333009	326869	320035	309010	291424	290106	128868	124896	105498	87514	68864	0.89

Kaolin 8%

Orifice Type:	Short	
Orifice thickness[m]:	0.007	Area[m^2]
Orifice dimension[m]:	0.009	6.36173E-05
Pipe Diameter [m]:	0.046	0.001661903
Diameter ratio	0.20	
Aspect ratio	0.77	

g[m/s^2]	9.81	
Material Type:	Kaolin	
Density[kg/m^3]:	1133.22	
Concentration[%]:	8%	
τ_y[Pa]:	0	
K [Pa.s]:	0.06	
n:	0.5	
PPT used:	110	
Range selected:	0-500	

1/n	n/(n+1)	(n+1)/n	K1/n
2	0.33	3	0.004

	Pod 1	Pod 2	Pod3	Pod 4	Pod 5	Pod 6	Pod 7	Pod 8	Pod 9	Pod10	Pod 11
Axial distances	-5.20	-4.60	-3.68	-2.31	-0.05	-0.03	0.03	2.30	4.61	6.91	9.21
N-D distances incl.[L/D]:	-113.13	-99.98	-80.07	-50.17	-1.04	-0.54	0.54	50.00	100.11	150.26	200.26
Distances[m]:	0.00	0.60	1.52	2.90	5.16	5.18	5.23	7.51	9.81	12.11	14.41

Pod 1 [Pa]	Pod 2 [Pa]	Pod 3 [Pa]	Pod 4 [Pa]	Pod 5 [Pa]	Pod 6 [Pa]	Pod 7 [Pa]	Pod 8 [Pa]	Pod 9 [Pa]	Pod 10 [Pa]	Pod 11 [Pa]	Average Q [l/s]
213931	213890	213774	213669	213580	213358	21129	31564	31505	31225	30840	0.85
213793	213278	214576	213693	213993	213363	21481	31423	31291	30879	30715	0.85
192286	191995	191999	191921	191893	192035	21943	30581	30844	30616	30219	0.80
192361	191713	191930	191710	191399	191653	21990	30900	30779	30612	30349	0.80
163871	163340	163454	163851	163290	163161	22999	30334	30187	30003	29777	0.73
163554	163652	163252	163696	163306	163077	22493	30095	29994	29862	29590	0.73
130856	130600	130504	130620	130562	130711	23411	29082	28977	28940	28669	0.64
130637	130308	130520	130292	130443	129963	23150	28901	28850	28749	28466	0.64
103201	103238	103145	103034	102742	102899	23693	28149	27893	27870	27646	0.55
102885	102420	102819	102897	102859	102795	23670	27505	27808	27779	27523	0.55
67469	67398	67440	67453	67340	67456	21241	23527	23422	23573	23303	0.43
67775	67672	67641	67742	67611	67537	21184	23545	23470	23334	23039	0.43
47086	47095	47053	47026	46897	46853	19958	21405	21365	21192	21032	0.33
47018	46960	46977	46913	46949	46819	20000	21367	21342	21247	20905	0.33
26696	26732	26689	26657	26557	26562	19900	20253	20254	20169	19993	0.17
26661	26672	26662	26591	26517	26527	20420	20321	20314	20234	20026	0.16
22313	22232	22273	22319	22245	22207	19769	19893	19877	19825	19717	0.09
22372	22377	22384	22368	22314	22235	19738	19744	19716	19460	19292	0.09

Kaolin 14%

Orifice Type:	Short	
Orifice thickness[m]:	0.0069	Area[m^2]
Orifice dimension[m]:	0.009	6.36173E-05
Pipe Diameter [m]:	0.046	0.001661903
Diameter ratio	0.20	
Aspect ratio	0.77	
g[m/s^2]	9.81	
Material Type:	Kaolin	
Density[kg/m^3]:	1239	
Concentration[%]:	14%	
τ_y[Pa]:	0	
K [Pa.s]:	3.91	
n:	0.18	
PPT used:	110	
Range selected:	0-500	

1/n	n/(n+1)	(n+1)/n	$K^{1/n}$
5.56	0.15	6.56	1949.26

	Pod 1	Pod 2	Pod3	Pod 4	Pod 5	Pod 6	Pod 7	Pod 8	Pod 9	Pod10	Pod 11
Axial distances	-5.20	-4.60	-3.68	-2.31	-0.05	-0.03	0.03	2.30	4.61	6.91	9.21
N-D distances incl.[L/D]:	-113.13	-99.98	-80.07	-50.17	-1.04	-0.54	0.54	50.00	100.11	150.26	200.26
Distances[m]:	0.00	0.60	1.52	2.90	5.16	5.18	5.23	7.51	9.81	12.11	14.41

Pod 1	Pod 2	Pod 3	Pod 4	Pod 5	Pod 6	Pod 7	Pod 8	Pod 9	Pod 10	Pod 11	Average Q
[Pa]	[Pa]	[Pa]	[Pa]	[Pa]	[Pa]	[Pa]	[Pa]	[Pa]	[Pa]	[Pa]	[l/s]
353121	353273	352487	351243	350161	350267	19170	35038	33699	31891	30242	1.05
354396	352117	352436	351992	351757	350090	18506	34400	33110	31406	29785	1.05
278308	276995	276680	275528	273792	273347	20738	33141	31606	30071	28492	0.93
276784	276482	276432	274437	272810	272664	19836	32591	31459	29511	28164	0.93
214998	214779	214438	213651	212334	212252	23122	32058	30640	29073	27655	0.81
167778	167249	166654	165366	163853	164081	25312	31750	30502	28909	27320	0.70
136209	134969	134908	133773	132211	132319	26874	31440	30051	28471	27241	0.61
139131	135051	134947	133766	132816	132740	26838	30730	30223	28550	27200	0.61
102812	102661	102030	101247	99650	99574	27969	30752	29654	27965	26593	0.51
103243	102450	102045	101525	99453	99547	28011	30775	29637	28002	26680	0.51
72858	72376	72036	71517	70130	69957	29096	30234	29042	27586	26091	0.39
72981	72423	72071	71324	69603	69573	28888	30111	29052	27283	26085	0.39
57150	56702	56412	55528	54379	54207	29391	29621	28836	27383	26110	0.31
57424	57025	56519	55912	54507	54191	30024	30191	29223	27628	26497	0.30
42967	42794	42476	41689	40700	40486	28426	28040	27144	25715	24732	0.21
43037	42777	42397	41729	40538	40407	28776	28408	27194	25774	24775	0.20

Pod 1 [Pa]	Pod 2 [Pa]	Pod 3 [Pa]	Pod 4 [Pa]	Pod 5 [Pa]	Pod 6 [Pa]	Pod 7 [Pa]	Pod 8 [Pa]	Pod 9 [Pa]	Pod 10 [Pa]	Pod 11 [Pa]	Average Q [l/s]
32970	32816	32551	31878	31106	30930	28425	27627	26713	25550	24528	0.09
33598	33188	32677	32072	31057	30954	28626	27718	26877	25460	24399	0.08

Kaolin 20%

Orifice Type:	short	Area[m^2]
Orifice thickness[m]:	0.0069	6.36173E-05
Orifice dimension[m]:	0.009	0.001661903
Pipe Diameter [m]:	0.046	
Diameter ratio	0.20	
Aspect ratio	0.77	
g[m/s^2]	9.81	
Material Type:	Kaolin	
Density[kg/m^3]:	1324	
Concentration[%]:	20%	
τ_y[Pa]:	0	
K [Pa.s]:	15	
n:	0.15	
PPT used:	110	
Range selected:	0-500	

1/n	n/(n+1)	(n+1)/n	$K^{1/n}$
6.67	0.13	7.67	69280082

	Pod 1	Pod 2	Pod3	Pod 4	Pod 5	Pod 6	Pod 7	Pod 8	Pod 9	Pod10	Pod 11
Axial distances	-5.20	-4.60	-3.68	-2.31	-0.05	-0.03	0.03	2.30	4.61	6.91	9.21
N-D distances incl.[L/D]:	-113.13	-99.98	-80.07	-50.17	-1.04	-0.54	0.54	50.00	100.11	150.26	200.26
Distances[m]:	0.00	0.60	1.52	2.90	5.16	5.18	5.23	7.51	9.81	12.11	14.41

Pod 1 [Pa]	Pod 2 [Pa]	Pod 3 [Pa]	Pod 4 [Pa]	Pod 5 [Pa]	Pod 6 [Pa]	Pod 7 [Pa]	Pod 8 [Pa]	Pod 9 [Pa]	Pod 10 [Pa]	Pod 11 [Pa]	Average Q [l/s]
375473	373921	373321	368932	363029	362735	52670	64827	59528	53255	47491	1.01
375846	374312	373023	369443	363247	362866	52722	64885	58788	53597	47609	1.01
313259	311254	309594	306697	301111	301173	55545	64299	58899	52722	47276	0.90
312686	311460	309573	306120	300863	299607	55837	64371	59039	52902	47191	0.90
267514	265107	264845	261426	255273	254573	57537	63719	58253	52303	46843	0.81
267613	265224	264169	260712	254891	254245	57626	63771	58637	52671	47292	0.81
218059	215669	214875	211283	205134	205112	58761	62507	57461	51580	46032	0.71
218568	214930	214232	211078	205501	204504	59626	62692	57810	51715	46613	0.71
178657	177089	175852	172353	167474	166520	60187	61698	56337	51054	45412	0.61
178824	176898	176047	172333	168111	156876	60532	61774	56867	50985	45548	0.61

Pod 1	Pod 2	Pod 3	Pod 4	Pod 5	Pod 6	Pod 7	Pod 8	Pod 9	Pod 10	Pod 11	Average Q
[Pa]	[Pa]	[Pa]	[Pa]	[Pa]	[Pa]	[Pa]	[Pa]	[Pa]	[Pa]	[Pa]	[l/s]
146086	144494	143383	140700	134878	134816	60944	60785	56269	50518	45168	0.51
145843	144720	143238	140121	134688	134540	61472	61096	56033	50653	45198	0.51
123999	122165	120367	117488	112697	112304	61729	60164	55430	49600	44934	0.42
123888	121429	119870	117392	112027	112059	61822	60228	55660	50037	44801	0.42
94254	92911	91719	89297	86080	85763	58832	56070	51798	47042	42480	0.30
96057	94328	93242	90469	86253	85800	60139	57455	52252	48116	43490	0.30
79950	78407	77564	77152	70733	70572	59887	56341	51898	47081	42284	0.19
80006	78388	77830	75127	70386	70461	59800	56396	51719	47257	42624	0.19
68996	67349	66545	64224	62956	62969	58625	54749	50798	46149	42171	0.12
69013	67322	66426	64029	60872	60631	58182	54245	49957	45659	40975	0.11

Bentonite 6%

Orifice Type:	Short	
Orifice thickness[m]:	0.006	Area[m^2]
Orifice dimension[m]:	0.009	6.36173E-05
Pipe Diameter [m]:	0.046	0.001661903
Diameter ratio	0.20	
Aspect ratio	0.77	
g[m/s^2]	9.81	
Material Type:	Bentonite	
Density[kg/m^3]:	1035.9	
Concentration[%]:	6%	
τ_y[Pa]:	2.9	
K [Pa.s]:	0.035	
n:	1	
PPT used:	110	
Range selected:	0-500	

1/n	n/(n+1)	(n+1)/n	$K^{1/n}$
1	0.5	2	0.04

	Pod 1	Pod 2	Pod3	Pod 4	Pod 5	Pod 6	Pod 7	Pod 8	Pod 9	Pod10	Pod 11
Axial distances	-5.20	-4.60	-3.68	-2.31	-0.05	-0.03	0.03	2.30	4.61	6.91	9.21
N-D distances incl.[L/D]:	-113.13	-99.98	-80.07	-50.17	-1.04	-0.54	0.54	50.00	100.11	150.26	200.26
Distances[m]:	0.00	0.60	1.52	2.90	5.16	5.18	5.23	7.51	9.81	12.11	14.41

Pod 1	Pod 2	Pod 3	Pod 4	Pod 5	Pod 6	Pod 7	Pod 8	Pod 9	Pod 10	Pod 11	Average Q
[Pa]	[Pa]	[Pa]	[Pa]	[Pa]	[Pa]	[Pa]	[Pa]	[Pa]	[Pa]	[Pa]	[l/s]
531154	531153	531151	531148	531152	531152	-3937	31474	29270	27855	25940	1.58

Pod 1 [Pa]	Pod 2 [Pa]	Pod 3 [Pa]	Pod 4 [Pa]	Pod 5 [Pa]	Pod 6 [Pa]	Pod 7 [Pa]	Pod 8 [Pa]	Pod 9 [Pa]	Pod 10 [Pa]	Pod 11 [Pa]	Average Q [l/s]
428148	426493	425446	425475	422644	422465	11751	31367	29109	27930	25910	1.27
425965	426881	425587	424836	422367	421506	15186	30967	29146	27579	25998	1.27
357707	358185	356632	354915	353779	351909	13913	31070	28959	27732	25825	1.17
356871	357104	357105	354915	353779	351814	13808	31011	28969	27287	25757	1.17
277838	278302	277279	275481	274502	271293	17718	29714	28745	27216	25597	1.04
278251	277923	277825	276369	274496	271170	17328	30182	28705	26549	25551	1.04
230339	229502	228821	227413	225199	222409	19915	29760	28680	27260	25573	0.95
230711	229856	229116	227751	225315	222054	21194	29183	28672	26972	25348	0.95
187137	186430	185870	184334	181867	178374	21532	28916	28418	27239	25270	0.84
186244	185566	185034	184256	181682	176780	23627	29136	28424	26870	25173	0.83
145137	144288	143659	141323	140140	136158	23819	28112	28226	26406	25227	0.72
145010	145037	143625	141769	140159	135598	24335	28618	28231	27095	25275	0.72
108075	107864	106820	106151	104694	100999	25493	29483	28006	26789	24851	0.59
108332	107539	106740	106054	104761	101036	26112	29253	27979	25920	26048	0.59
88572	88020	87436	86388	84859	84529	26091	29164	27681	26110	24699	0.51
89166	88404	87250	86402	85050	84210	26497	29262	27758	26372	24646	0.51
62854	62305	61702	60345	59499	58630	27664	28674	27484	26115	24346	0.37
62612	62278	61332	60348	59769	58382	31099	28708	27506	25975	24303	0.37
47167	46780	46380	45150	43817	43220	29476	28435	27130	25706	24269	0.24
37079	36845	36407	35133	34163	33477	29205	28157	26785	25142	23718	0.14

Water

Orifice Type:	Short	
Orifice thickness[m]:	0.0069	Area[m^2]
Orifice dimension[m]:	0.009	6.36173E-05
Pipe Diameter [m]:	0.046	0.001661903
Diameter ratio	0.20	
Aspect ratio	0.77	
g[m/s^2]	9.81	

Material Type:	Water
Density[kg/m^3]:	1000
Concentration[%]:	100%
τ_y[Pa]:	0
K [Pa.s]:	0.001
n:	1
PPT used:	110
Range selected:	0-500

1/n	n/(n+1)	(n+1)/n	$K^{1/n}$
1	0.5	2	0.001

	Pod 1	Pod 2	Pod3	Pod 4	Pod 5	Pod 6	Pod 7	Pod 8	Pod 9	Pod10	Pod 11
Axial distances	-5.20	-4.60	-3.68	-2.31	-0.05	-0.03	0.03	2.30	4.61	6.91	9.21
N-D distances incl.[L/D]:	-113.13	-99.98	-80.07	-50.17	-1.04	-0.54	0.54	50.00	100.11	150.26	200.26
Distances[m]:	0.00	0.60	1.52	2.90	5.16	5.18	5.23	7.51	9.81	12.11	14.41

Pod 1 [Pa]	Pod 2 [Pa]	Pod 3 [Pa]	Pod 4 [Pa]	Pod 5 [Pa]	Pod 6 [Pa]	Pod 7 [Pa]	Pod 8 [Pa]	Pod 9 [Pa]	Pod 10 [Pa]	Pod 11 [Pa]	Average Q [l/s]
239003	237219	237962	238197	237109	237065	11603	19988	19922	19766	19335	1.00
237012	238064	237396	237654	237021	237461	9360	18837	18588	18514	18223	1.00
357209	357077	356698	357188	356136	356552	4185	17712	17779	17414	17017	1.19
357768	357063	357240	357390	356518	356516	2571	18313	17487	17313	16939	1.19
305398	306044	305444	305560	305344	305565	7010	17969	17685	17232	17019	1.11
305792	306388	305364	306239	304879	305300	4755	17617	17472	16925	17116	1.11
192789	192539	192840	192721	192299	192358	7881	15397	17030	16806	16621	0.91
193095	192422	192489	192577	192238	192242	8754	16603	16225	16712	16496	0.91
153457	152959	153056	152409	152572	152608	9611	15881	16436	16301	16184	0.81
153130	153092	152875	152541	152559	152510	8997	14979	16450	16338	16169	0.81
128544	128690	128573	128609	128544	128551	9972	14071	15666	15535	15428	0.70
128439	128374	128294	128737	128638	128249	10021	13900	15703	15536	15427	0.70
104049	103759	103955	103681	103717	103196	11248	14379	15238	15147	15033	0.62
103739	103567	104048	103728	103585	103727	10913	14381	15268	15156	15058	0.62
70755	70260	70503	71052	70962	70990	16605	19467	19428	19357	19326	0.48
71064	71231	70952	71209	71135	71028	16567	18996	19460	19373	19308	0.48
54521	54541	54699	54507	54503	54758	17094	18987	19093	19035	19016	0.40
54645	54686	54285	54721	54729	54564	17224	18696	19129	19073	19025	0.40
39313	39597	39547	39507	39385	39287	17571	18619	18731	18714	18706	0.31
39382	39270	39584	39658	39401	39178	17586	18352	18749	18733	18703	0.31
28674	28918	29028	28923	28977	28889	17789	18232	18394	18367	18362	0.22
28982	28913	28995	28968	29001	28988	17995	18272	18397	18241	18366	0.22
20572	20621	20640	20597	20596	20576	18123	18162	18218	18134	18215	0.10
20572	20621	20640	20597	20596	20576	18123	18162	18218	18134	18215	0.10

ORIFICE DIAMETER RATIO, $\beta = 0.3$

CMC 5%

Orifice Type:	Short	
Orifice thickness[m]:	0.006	Area[m^2]
Orifice dimension[m]:	0.014	0.000153938
Pipe Diameter [m]:	0.046	0.001661903
Diameter ratio	0.30	
Aspect ratio	0.43	

g[m/s^2]	9.81	
Material Type:	CMC	
Density[kg/m^3]:	1028.1155	
Concentration[%]:	5%	
τ_y[Pa]:	0	
K [Pa.s]:	0.95	
n:	0.7	
PPT used:	110	
Range selected:	0-500	

1/n	n/(n+1)	(n+1)/n	$K^{1/n}$
1.43	0.41	2.43	0.93

	Pod 1	Pod 2	Pod3	Pod 4	Pod 5	Pod 6	Pod 7	Pod 8	Pod 9	Pod10	Pod 11
Axial distances	-5.29	-4.68	-3.74	-2.36	-0.06	-0.03	0.03	2.34	4.65	6.97	9.29
N-D distances incl.[L/D]:	-115.05	-101.68	-81.38	-51.27	-1.38	-0.62	0.62	50.83	101.16	151.60	201.92
Distances[m]:	0.00	0.62	1.55	2.93	5.23	5.26	5.32	7.63	9.95	12.27	14.58

Pod 1	Pod 2	Pod 3	Pod 4	Pod 5	Pod 6	Pod 7	Pod 8	Pod 9	Pod 10	Pod 11	Average Q
[Pa]	[Pa]	[Pa]	[Pa]	[Pa]	[Pa]	[Pa]	[Pa]	[Pa]	[Pa]	[Pa]	[l/s]
250332	248391	244801	239988	232180	232402	56982	70424	62612	54543	46324	1.92
249495	248158	244327	239189	231346	230666	56982	70424	62612	54543	46324	1.93
301509	299776	296036	290639	281843	281177	52442	71447	63375	54369	45694	2.15
300912	298710	295067	290514	281769	280199	51518	70526	62639	53706	45190	2.15
216848	214921	212381	207833	200484	200131	52522	63505	55989	49091	41435	1.78
216771	215071	212040	207669	200638	200277	52203	63313	56737	49328	42108	1.78
184558	182574	180237	176052	169675	169582	52129	60189	53881	47045	40467	1.59
184783	183123	180105	176213	169371	168824	52104	60157	53748	46698	40419	1.59
155964	153851	151358	147848	141801	141555	51605	56981	51171	44549	38894	1.41
155361	153896	151461	147510	142078	141382	51544	56931	50633	44639	38849	1.41
124495	123132	120731	117556	112427	112028	50307	53061	47540	42251	36692	1.19
124357	123112	121031	117526	112297	112143	50223	52994	47422	42482	37059	1.19
103789	102431	100571	97825	93024	92807	48749	49935	45500	40391	35763	1.02
103843	102499	100531	97638	93165	92775	48678	49929	44915	40531	35586	1.02
83010	82059	80172	77689	73896	73712	47784	45927	41903	36998	33702	0.81
83125	82068	80198	77810	74067	73790	46081	45973	41815	37635	33564	0.81
64341	63367	62051	60064	57229	57007	41502	40858	37683	34304	31225	0.58
64599	63459	62324	60199	56957	57063	41555	40892	37719	34289	31350	0.58
50774	50097	49188	47678	45793	45495	40263	38905	36654	33919	31919	0.38
51025	50312	49317	47886	45365	45467	40046	38931	36344	34174	31970	0.38
36774	36400	35848	34986	33880	33878	32653	31525	30161	29040	27785	0.16
36774	36486	35947	35203	33893	33898	32713	31474	30323	28595	27734	0.16
31635	31441	31067	30455	29832	29703	29409	28435	27533	26789	25831	0.09
31576	31468	31074	30522	29773	29668	29195	28250	27459	26662	25857	0.09

CMC 7%

Orifice Type:	Short	
Orifice thickness[m]:	0.006	Area[m^2]
Orifice dimension[m]:	0.014	0.000153938
Pipe Diameter [m]:	0.046	0.001661903
Diameter ratio	0.304	
Aspect ratio	0.429	
g[m/s^2]	9.81	
Material Type:	CMC	
Density[kg/m^3]:	1041	
Concentration[%]:	7%	
τ_y[Pa]:	0	
K [Pa.s]:	3.85	
n:	0.61	
PPT used:	110	
Range selected:	0-500	

1/n	n/(n+1)	(n+1)/n	$K^{1/n}$
1.64	0.38	2.64	9.12

	Pod 1	Pod 2	Pod3	Pod 4	Pod 5	Pod 6	Pod 7	Pod 8	Pod 9	Pod10	Pod 11
Axial distances	-5.29	-4.68	-3.74	-2.36	-0.06	-0.03	0.03	2.34	4.65	6.97	9.29
N-D distances incl.[L/D]:	-115.05	-101.68	-81.38	-51.27	-1.38	-0.62	0.62	50.83	101.16	151.60	201.92
Distances[m]:	0.00	0.62	1.55	2.93	5.23	5.26	5.32	7.63	9.95	12.27	14.58

Pod 1	Pod 2	Pod 3	Pod 4	Pod 5	Pod 6	Pod 7	Pod 8	Pod 9	Pod 10	Pod 11	Average Q
[Pa]	[Pa]	[Pa]	[Pa]	[Pa]	[Pa]	[Pa]	[Pa]	[Pa]	[Pa]	[Pa]	[l/s]
235510	231115	224220	214501	198271	197096	117387	113375	97573	80373	64829	1.41
235510	230788	223886	214435	197675	197387	116829	112824	96601	79697	64264	1.41
268536	264520	257639	247159	229317	228000	120374	118831	101333	83573	65840	1.60
268536	264173	257171	246087	229749	227772	119636	118208	100963	83100	66205	1.61
199806	196108	189619	180560	166827	166237	109657	104323	90261	74506	60552	1.22
199806	195641	189507	180547	166395	165405	109230	104110	89819	74329	60215	1.22
177675	174103	168735	160295	147347	146559	104573	98746	85590	70703	58225	1.08
177495	174273	168280	160742	147092	146555	104226	98508	85534	71610	58344	1.08
140298	137158	132480	125908	115267	114947	92539	86597	75824	64686	53192	0.79
140370	137625	132920	126178	115358	115038	92508	86805	76237	64686	53192	0.79
132828	130473	125719	119645	110370	109376	85241	81965	71991	60984	52191	0.70
133106	130631	126383	120664	110763	109411	87645	82261	72790	62689	51996	0.70
117379	114885	111095	105171	97281	96517	82665	76242	66843	58076	49075	0.58
117474	115143	111386	105953	96403	96655	82842	76712	67542	58727	49714	0.58
102911	100620	97288	92287	84557	84734	76328	70098	61828	53950	46593	0.46
102911	100620	97288	92287	84557	84734	76328	70098	61828	53950	46593	0.46

Pod 1 [Pa]	Pod 2 [Pa]	Pod 3 [Pa]	Pod 4 [Pa]	Pod 5 [Pa]	Pod 6 [Pa]	Pod 7 [Pa]	Pod 8 [Pa]	Pod 9 [Pa]	Pod 10 [Pa]	Pod 11 [Pa]	Average Q [l/s]
91510	89796	86831	82855	75894	76060	70437	64457	57611	50682	44623	0.36
91510	89796	86831	82855	75894	76060	70437	64457	57611	50682	44623	0.36
81277	79526	77012	73626	67862	67796	64278	58779	52634	46518	41838	0.28
81625	80317	77959	74124	68733	68314	64651	59044	53355	47584	42138	0.28
73686	72306	70120	66925	61922	62079	59647	54509	49760	44773	40043	0.22
73686	72306	70120	66925	61922	62079	59647	54509	49760	44773	40043	0.22
60171	59389	57502	55648	52712	52496	51753	47412	44009	40383	36986	0.12
60171	59389	57502	55648	52712	52496	51753	47412	44009	40383	36986	0.12
54199	53377	52187	50631	47788	47597	47213	43608	41086	38266	35389	0.08
54199	53377	52187	50631	47788	47597	47213	43608	41086	38266	35389	0.08

Kaolin 8%

Orifice Type:	Short	
Orifice thickness[m]:	0.006	Area[m^2]
Orifice dimension[m]:	0.014	0.000153938
Pipe Diameter [m]:	0.046	0.001661903
Diameter ratio	0.30	
Aspect ratio	0.43	
g[m/s^2]	9.81	
Material Type:	Kaolin	
Density[kg/m^3]:	1140	
Concentration[%]:	8%	
τ_y[Pa]:	0	
K [Pa.s]:	0.09	
n:	0.5	
PPT used:	110	
Range selected:	0-500	

1/n	n/(n+1)	(n+1)/n	$K^{1/n}$
2	0.33	3	0.0081

	Pod 1	Pod 2	Pod 3	Pod 4	Pod 5	Pod 6	Pod 7	Pod 8	Pod 9	Pod 10	Pod 11
Axial distances	-5.29	-4.68	-3.74	-2.36	-0.06	-0.03	0.03	2.34	4.65	6.97	9.29
N-D distances incl.[L/D]:	-115.05	-101.68	-81.38	-51.27	-1.38	-0.62	0.62	50.83	101.16	151.60	201.92
Distances[m]:	0.00	0.62	1.55	2.93	5.23	5.26	5.32	7.63	9.95	12.27	14.58

Pod 1 [Pa]	Pod 2 [Pa]	Pod 3 [Pa]	Pod 4 [Pa]	Pod 5 [Pa]	Pod 6 [Pa]	Pod 7 [Pa]	Pod 8 [Pa]	Pod 9 [Pa]	Pod 10 [Pa]	Pod 11 [Pa]	Average Q [l/s]
347181	346292	345694	344898	343558	343387	-6971	20927	20046	18414	16950	2.48
346124	346037	345249	343932	343072	343478	-6976	20985	20068	18424	17075	2.49

Pod 1	Pod 2	Pod 3	Pod 4	Pod 5	Pod 6	Pod 7	Pod 8	Pod 9	Pod 10	Pod 11	Average Q
[Pa]	[Pa]	[Pa]	[Pa]	[Pa]	[Pa]	[Pa]	[Pa]	[Pa]	[Pa]	[Pa]	[l/s]
284380	283038	283214	282573	281056	281052	-6971	19738	18885	17432	16245	2.26
283647	282766	281784	281948	280730	279881	-6971	19485	19026	17562	16276	2.25
227875	227768	227440	226661	225848	225392	-6967	18419	17754	16478	15672	2.02
227917	226057	227550	226511	225861	225567	-6975	18266	17847	16621	15659	2.02
175009	174758	174252	173690	173306	172930	-2225	17223	16791	15831	15054	1.79
174989	174516	174668	173922	173668	173673	-2151	17325	16722	15868	15104	1.79
136543	135827	135999	135625	134995	134790	1506	16491	15986	15269	14700	1.56
136417	135942	135902	135373	135177	134968	1281	16419	15938	15183	14612	1.57
110319	110541	110902	110430	109989	109498	3955	15713	15420	14677	14224	1.39
115161	110467	110743	110393	110052	109930	3947	15722	15399	14688	14227	1.40
82664	82562	82391	82194	81891	81795	6672	15078	14796	14205	13992	1.18
83213	82660	82647	82220	82119	81717	6718	15056	14796	14264	13879	1.18
59045	58763	58694	58507	58117	58099	9202	14532	14265	13904	13584	0.96
59078	58776	58741	58541	58334	58082	9166	14483	14368	13871	13537	0.96
47033	46700	46603	46315	45927	45932	10598	14355	14210	13782	13512	0.82
46569	46442	46539	46248	45957	45866	10616	14333	14156	13745	13475	0.82
32053	31437	31220	31213	30995	30738	12137	14062	13952	13580	13215	0.61
30330	31290	31184	31107	30792	30616	12327	13948	14008	13610	13315	0.60
26886	26803	26725	26611	26328	26156	19896	20376	20226	19912	19427	0.36
26891	26781	26744	26576	26383	26174	19954	20407	20272	19916	19604	0.36
23563	23486	23374	23310	23142	23006	20223	20272	20163	19888	19508	0.23
21623	21587	21460	21378	21219	21059	20195	20068	19951	19752	19317	0.13

Kaolin 14%

Orifice Type:	Short	
Orifice thickness[m]:	0.006	Area[m^2]
Orifice dimension[m]:	0.014	0.000153938
Pipe Diameter [m]:	0.046	0.001661903
Diameter ratio	0.30	
Aspect ratio	0.43	
g[m/s^2]	9.81	
Material Type:	Kaolin	
Density[kg/m^3]:	1242.09	
Concentration[%]:	15%	
τ_y[Pa]:	0	
K [Pa.s]:	3.5	
n:	0.18	
PPT used:	110	
Range selected:	0-500	

1/n	n/(n+1)	(n+1)/n	$K^{1/n}$
5.56	0.15	6.56	1053.42

	Pod 1	Pod 2	Pod 3	Pod 4	Pod 5	Pod 6	Pod 7	Pod 8	Pod 9	Pod 10	Pod 11
Axial distances	-5.29	-4.68	-3.74	-2.36	-0.06	-0.03	0.03	2.34	4.65	6.97	9.29
N-D distances incl.[L/D]:	-115.05	-101.68	-81.38	-51.27	-1.38	-0.62	0.62	50.83	101.16	151.60	201.92
Distances[m]:	0.00	0.62	1.55	2.93	5.23	5.26	5.32	7.63	9.95	12.27	14.58

Pod 1 [Pa]	Pod 2 [Pa]	Pod 3 [Pa]	Pod 4 [Pa]	Pod 5 [Pa]	Pod 6 [Pa]	Pod 7 [Pa]	Pod 8 [Pa]	Pod 9 [Pa]	Pod 10 [Pa]	Pod 11 [Pa]	Average Q [l/s]
366742	365528	365151	363515	361660	360823	-6964	27653	26293	24051	22607	2.44
365687	363917	364439	363040	359755	360573	-6962	27892	26622	24103	22219	2.44
304660	303951	303993	302640	301207	300486	-6967	26562	25513	23308	21836	2.23
305267	303979	303682	302140	300762	300084	-6967	26475	25322	23305	21536	2.22
258989	257813	256995	256316	254405	253176	-1705	26046	24438	22693	21136	2.03
258958	257799	257721	255456	254258	254296	-1981	26012	24654	22688	21154	2.03
204943	203898	203433	202779	201011	200632	4465	25430	24093	22089	20640	1.82
204708	204213	203344	202708	201325	200560	4354	23275	24226	22103	20910	1.81
171048	170142	169297	168653	166870	166455	8113	25017	23713	21897	20386	1.64
170370	169422	169390	169103	166573	166255	8026	24811	23754	22307	20340	1.64
135511	135413	135056	133933	132446	132202	12108	24602	22979	21342	20320	1.43
135682	134956	134679	133809	132240	131504	12124	24613	23425	21618	20299	1.43
106257	105477	105273	104227	102600	102236	15393	24208	22593	21110	19493	1.23
107459	105347	105495	104506	102581	102008	15394	24209	22610	21145	19767	1.23
86447	86191	85788	84758	83127	82718	17735	23888	22723	20711	19532	1.07
86808	86014	85584	84625	83563	82663	17676	23899	22806	21107	19595	1.07
57866	57261	56977	56039	54622	54335	20715	23440	22372	20717	19206	0.78
57754	57205	57005	55850	54737	54517	20768	23475	22345	20771	19247	0.78
45878	45335	44945	44143	42709	42277	21903	23052	22016	20453	18925	0.62
45988	45401	45065	44044	43184	42503	21807	23047	21993	20469	18968	0.62
42290	41664	41350	40575	39258	39031	29016	28998	27690	26246	25022	0.43
42879	41814	41583	40658	39158	39021	28691	29004	27634	26325	25183	0.43
33667	33291	32870	32221	32100	31569	29265	28105	26858	25330	24255	0.20

Kaolin 20%

Orifice Type:	Short	
Orifice thickness[m]:	0.006	Area[m^2]
Orifice dimension[m]:	0.014	0.000153938
Pipe Diameter [m]:	0.046	0.001661903
Diameter ratio	0.30	
Aspect ratio	0.43	
g[m/s^2]	9.81	
Material Type:	Kaolin	
Density[kg/m^3]:	1324	
Concentration[%]:	20%	

τ_y [Pa]:	0
K [Pa.s]:	14.5
n:	0.15
PPT used:	110
Range selected:	0-500

1/n	n/(n+1)	(n+1)/n	$K^{1/n}$
6.67	0.13	7.67	55265403.88

	Pod 1	Pod 2	Pod 3	Pod 4	Pod 5	Pod 6	Pod 7	Pod 8	Pod 9	Pod 10	Pod 11
Axial distances	-5.29	-4.68	-3.74	-2.36	-0.06	-0.03	0.03	2.34	4.65	6.97	9.29
N-D distances incl.[L/D]:	-115.05	-101.68	-81.38	-51.27	-1.38	-0.62	0.62	50.83	101.16	151.60	201.92
Distances[m]:	0.00	0.62	1.55	2.93	5.23	5.26	5.32	7.63	9.95	12.27	14.58

Pod 1	Pod 2	Pod 3	Pod 4	Pod 5	Pod 6	Pod 7	Pod 8	Pod 9	Pod 10	Pod 11	Average Q
[Pa]	[Pa]	[Pa]	[Pa]	[Pa]	[Pa]	[Pa]	[Pa]	[Pa]	[Pa]	[Pa]	[l/s]
321897	320400	318216	314331	308819	305714	40895	66340	60331	54562	48450	1.99
322225	320680	318196	314456	308798	304434	40388	65908	60251	54258	48059	1.97
263716	262351	261017	257397	250433	248961	46505	65192	59278	53465	47551	1.77
262186	261914	259800	256558	250718	248258	46699	65199	59303	53405	47563	1.77
222694	220512	218709	215507	209496	208731	51265	64625	59055	53233	47551	1.57
222680	220229	218363	215680	209628	208924	51024	64046	58764	53050	47413	1.57
189061	186893	184950	181897	176462	175035	54760	64028	58444	52663	47074	1.38
189187	186685	185020	181866	176122	174894	54610	63981	58644	52758	47137	1.38
163632	161111	159814	156801	151004	150657	56910	63406	57721	52386	46555	1.22
165211	161228	159373	157247	151294	150380	56935	63371	58110	52204	46554	1.23
135783	133785	132258	129285	124194	123506	59164	62464	57139	51380	46139	1.03
136202	133530	132220	129090	123713	123195	59199	62483	56725	51665	46174	1.03
106194	103995	102886	100046	95008	95902	60605	60511	55288	50453	45126	0.75
105897	104172	102670	99783	94752	94678	60996	60904	56011	50473	45225	0.74
93779	92246	90736	88111	83176	83113	60180	59230	54151	49314	44349	0.60
93867	92520	91156	88134	83521	82990	60707	59535	54661	49716	44594	0.59
82300	80573	78943	76597	72075	71600	60226	57990	52818	48339	43548	0.41
80428	79757	78824	75811	71653	71207	60509	57977	53464	48507	43605	0.40
423070	419089	417082	413975	407376	406406	26606	65410	59240	53364	47518	2.38
422132	418037	417260	412512	407684	405097	26518	64930	59626	53376	47270	2.37
348610	346943	345129	342051	335512	333325	34788	64528	59070	52714	46794	2.12
347485	346155	345092	341640	335200	332715	37994	63959	58963	53024	46677	2.12

Bentonite 6%

Orifice Type:	Short	
Orifice thickness[m]:	0.006	Area[m^2]
Orifice dimension[m]:	0.014	0.000153938
Pipe Diameter [m]:	0.046	0.001661903
Diameter ratio	0.30	
Aspect ratio	0.43	
g[m/s^2]	9.81	
Material Type:	Bentonote	
Density[kg/m^3]:	1040.1	
Concentration[%]:	6%	
τ_y[Pa]:	2.7	
K [Pa.s]:	0.0251	
n:	1	
PPT used:	110	
Range selected:	0-500	

1/n	n/(n+1)	(n+1)/n	$K^{1/n}$
1	0.5	2	0.03

	Pod 1	Pod 2	Pod 3	Pod 4	Pod 5	Pod 6	Pod 7	Pod 8	Pod 9	Pod 10	Pod 11
Axial distances	-5.29	-4.68	-3.74	-2.36	-0.06	-0.03	0.03	2.34	4.65	6.97	9.29
N-D distances incl.[L/D]:	-115.05	-101.68	-81.38	-51.27	-1.38	-0.62	0.62	50.83	101.16	151.60	201.92
Distances[m]:	0.00	0.62	1.55	2.93	5.23	5.26	5.32	7.63	9.95	12.27	14.58

Pod 1 [Pa]	Pod 2 [Pa]	Pod 3 [Pa]	Pod 4 [Pa]	Pod 5 [Pa]	Pod 6 [Pa]	Pod 7 [Pa]	Pod 8 [Pa]	Pod 9 [Pa]	Pod 10 [Pa]	Pod 11 [Pa]	Average Q [l/s]
383062	383030	381543	378643	377224	374518	-5446	28400	26192	24087	21542	2.79
382408	381718	381049	379930	377192	374842	-2849	28029	26099	24027	21638	2.79
439448	439970	439541	437263	434673	431205	-6652	24194	26715	24805	22171	2.98
439904	440281	438196	437661	434188	429286	-6306	16310	27001	24762	22184	2.98
313342	311987	311209	309360	306810	306653	-3806	27903	24992	23041	20780	2.52
311835	312134	311246	309205	306805	306172	-3389	27986	25332	23278	21023	2.52
265508	265719	263924	262555	260983	258442	3531	26417	24202	22506	20117	2.32
265270	265223	264316	262596	260704	258323	-947	26039	24055	22168	20083	2.32
227638	226888	225449	224909	222282	218421	1641	24365	23813	21870	19786	2.13
226758	226359	225453	223638	221830	218535	3246	18464	23857	22188	19810	2.12
175041	175138	174179	172135	170891	168122	9026	22821	23415	21326	19791	1.86
175098	174738	174113	172162	170959	166820	9193	21621	23508	21512	19475	1.86
139261	139110	138038	136765	135273	132751	12318	20206	23502	21745	19489	1.62
139742	138769	137826	136322	134939	132434	11890	19206	23195	21507	19299	1.62
114453	113810	113319	111672	110273	108122	15108	16518	23607	21186	19745	1.43
114897	114468	113444	111563	110345	106873	15088	16921	23689	21070	19556	1.43

Pod 1 [Pa]	Pod 2 [Pa]	Pod 3 [Pa]	Pod 4 [Pa]	Pod 5 [Pa]	Pod 6 [Pa]	Pod 7 [Pa]	Pod 8 [Pa]	Pod 9 [Pa]	Pod 10 [Pa]	Pod 11 [Pa]	Average Q [l/s]
83306	83224	82384	81322	79121	78366	19268	19220	23931	22118	20089	1.14
83741	83340	82502	81198	79393	78392	19101	19347	23834	21267	19938	1.14
70022	69596	69188	68064	66234	64996	20829	20380	24005	21965	20161	0.99
70915	70466	69368	68428	66643	65523	20813	21042	23712	22357	20077	0.99
53635	54000	53529	52183	50790	49741	24216	22866	24132	22473	20360	0.75
45483	45203	44532	43245	41697	40732	24328	23580	23207	21513	20286	0.58
43130	42412	41831	41060	38605	38141	29725	27737	27558	25824	24794	0.43

Bentonite 9%

Orifice Type:	Short	
Orifice thickness[m]:	0.006	Area[m^2]
Orifice dimension[m]:	0.014	0.000153938
Pipe Diameter [m]:	0.046	0.001661903
Diameter ratio	0.30	
Aspect ratio	0.43	
g[m/s^2]	9.81	
Material Type:	Bentonite	
Density[kg/m^3]:	1058.2	
Concentration[%]:	9%	
τ_y[Pa]:	6.58	
K [Pa.s]:	0.03	
n:	1.00	
PPT used:	110	
Range selected:	0-500	

1/n	n/(n+1)	(n+1)/n	$K^{1/n}$
1	0.5	2	0.034

	Pod 1	Pod 2	Pod 3	Pod 4	Pod 5	Pod 6	Pod 7	Pod 8	Pod 9	Pod 10	Pod 11
Axial distances	-5.29	-4.68	-3.74	-2.36	-0.06	-0.03	0.03	2.34	4.65	6.97	9.29
N-D distances incl.[L/D]:	-115.05	-101.68	-81.38	-51.27	-1.38	-0.62	0.62	50.83	101.16	151.60	201.92
Distances[m]:	0.00	0.62	1.55	2.93	5.23	5.26	5.32	7.63	9.95	12.27	14.58

Pod 1 [Pa]	Pod 2 [Pa]	Pod 3 [Pa]	Pod 4 [Pa]	Pod 5 [Pa]	Pod 6 [Pa]	Pod 7 [Pa]	Pod 8 [Pa]	Pod 9 [Pa]	Pod 10 [Pa]	Pod 11 [Pa]	Average Q [l/s]
375923	374789	371638	369167	364957	361123	9469	48321	43224	38882	34033	2.66
375004	373626	371191	368732	363374	359295	9839	48473	43152	39023	34173	2.66
303822	302630	301083	297556	292923	288966	18346	47683	42534	38280	33714	2.36
302330	301944	299777	296377	292298	286984	18705	47951	42921	38671	34211	2.36
251263	249637	248190	244985	240141	236114	24367	46793	41994	37684	33218	2.10

Pod 1	Pod 2	Pod 3	Pod 4	Pod 5	Pod 6	Pod 7	Pod 8	Pod 9	Pod 10	Pod 11	Average Q
[Pa]	[Pa]	[Pa]	[Pa]	[Pa]	[Pa]	[Pa]	[Pa]	[Pa]	[Pa]	[Pa]	[l/s]
250950	250008	248006	245027	240455	235217	24794	46915	41959	37754	33417	2.10
211595	209763	208402	205398	200666	199174	29293	46374	41657	37382	32973	1.90
211288	210074	208158	205126	200763	196959	29387	45908	41742	37363	33009	1.90
181394	179946	178625	175404	170660	169353	32966	46221	41467	37263	32777	1.71
181263	180038	178105	175497	170911	168063	32495	46135	41441	37277	33036	1.71
140766	139540	138006	135080	130650	129903	37464	45678	41173	37494	32714	1.40
140322	139744	137427	135051	130401	128833	37377	45646	41087	37092	32538	1.39
116539	115413	113595	110939	106143	105722	40270	45385	40950	37257	32513	1.19
116654	115533	113880	110991	106553	105325	40334	45322	41098	36927	32468	1.18
97796	96687	95032	92106	87807	86156	43814	45222	41010	37064	32570	0.96
97949	96523	95068	92338	87967	83681	43060	45548	41134	36966	32557	0.96
76614	75703	73943	71625	67241	66597	46100	44927	40885	36714	32351	0.64
76828	75714	74079	71311	67176	65670	46561	44730	41034	36889	32519	0.64
64389	63658	62396	60011	56581	55843	52112	47552	43717	39854	35941	0.33
66706	65373	63783	61102	57102	56125	51582	48020	44323	40462	35853	0.33

Water

Orifice Type:	Short	
Orifice thickness[m]:	0.006	Area[m^2]
Orifice dimension[m]:	0.014	0.000153938
Pipe Diameter [m]:	0.046	0.001661903
Diameter ratio	0.30	
Aspect ratio	0.43	
g[m/s^2]	9.81	
Material Type:	Water	
Density[kg/m^3]:	998.8	
Concentration[%]:	100%	
τ_y[Pa]:	0	
K [Pa.s]:	0.001	
n:	1	
PPT used:	110	
Range selected:	0-500	

1/n	n/(n+1)	(n+1)/n	$K^{1/n}$
1	0.5	2	0.001

	Pod 1	Pod 2	Pod 3	Pod 4	Pod 5	Pod 6	Pod 7	Pod 8	Pod 9	Pod 10	Pod 11
Axial distances	-5.29	-4.68	-3.74	-2.36	-0.06	-0.03	0.03	2.34	4.65	6.97	9.29
N-D distances incl.[L/D]:	-115.05	-101.68	-81.38	-51.27	-1.38	-0.62	0.62	50.83	101.16	151.60	201.92
Distances[m]:	0.00	0.62	1.55	2.93	5.23	5.26	5.32	7.63	9.95	12.27	14.58

Pod 1 [Pa]	Pod 2 [Pa]	Pod 3 [Pa]	Pod 4 [Pa]	Pod 5 [Pa]	Pod 6 [Pa]	Pod 7 [Pa]	Pod 8 [Pa]	Pod 9 [Pa]	Pod 10 [Pa]	Pod 11 [Pa]	Average Q [l/s]
276324	275882	275297	274877	274019	274094	-6970	18459	17593	16351	15307	2.40
276927	276302	276365	275311	274355	274441	-6973	18385	17275	16191	15292	2.40
230040	229570	229402	228821	227943	227436	-6975	17395	16598	15475	14656	2.20
230224	229639	229488	228881	228299	228054	-6974	17373	16548	15568	14598	2.20
185032	184850	184788	184110	183441	183766	-4790	16407	15644	14944	14208	2.00
185304	184864	184620	184084	183537	183532	-4617	16418	15828	14739	14252	2.01
148346	147735	147936	147401	146975	146659	-875	15550	15084	14358	13761	1.80
148488	148121	147654	147176	146750	146747	-904	15505	15069	14389	13761	1.80
122231	122287	122014	121592	121014	121139	1542	14852	14403	13889	13455	1.60
122431	122342	122243	121824	121521	121551	1616	14872	14467	13881	13286	1.59
95783	95702	95559	95279	95011	94975	4208	14281	13955	13494	13134	1.39
95674	95643	95530	95387	95101	95131	4230	14256	13996	13520	13125	1.39
72792	72675	72548	72300	72056	71929	6333	13709	13502	13104	12871	1.18
72907	72657	72527	72325	72063	72019	7666	13573	13521	13028	12862	1.18
72752	72656	72714	72365	72124	72218	6384	13676	13505	13113	12786	1.18
59892	59898	59766	59563	59448	59322	7592	13341	13172	12879	12634	1.05
59822	59812	59663	59594	59403	59335	7566	13367	13210	12907	12601	1.05
38355	38225	38068	37980	37848	37823	9673	12833	12724	12515	12350	0.78
38122	38117	38075	37956	37909	37821	9659	12812	12694	12443	12258	0.78
27299	27224	27242	27152	27082	27155	10643	12453	12406	12214	12156	0.60
26700	27174	27244	27199	27139	27039	10641	12472	12411	12268	12185	0.60
23192	23168	23162	23171	23072	23050	16996	17679	17642	17542	17484	0.37
22971	23127	23104	23097	23030	23037	16988	17604	17670	17461	17442	0.36
19945	20000	19975	19967	19960	19949	17369	17655	17645	17615	17570	0.23

ORIFICE DIAMETER RATIO, $\beta = 0.57$ (circular)

CMC 6%

Orifice Type:	Short	
Orifice thickness[m]:	0.006	Area[m^2]
Orifice dimension[m]:	0.0262	0.000539129
Pipe Diameter [m]:	0.046	0.001661903
Diameter ratio	0.57	
Aspect ratio	0.23	
g[m/s^2]	9.81	
Material Type:	CMC	
Density[kg/m^3]:	1036	
Concentration[%]:	6%	
τ_y[Pa]:	0	
K [Pa.s]:	3.40	
n:	0.61	

Appendices

PPT used:	110
Range selected:	0-500

1/n	n/(n+1)	(n+1)/n	$K^{1/n}$
1.64	0.38	2.64	7.48

	Pod 1	Pod 2	Pod 3	Pod 4	Pod 5	Pod 6	Pod 7	Pod 8	Pod 9	Pod 10	Pod 11
Axial distances	-6.96	-4.66	-3.74	-2.36	-0.07	-0.03	0.03	2.51	4.81	7.11	9.41
N-D distances incl.[L/D]:	-151.27	-101.27	-81.27	-51.38	-1.49	-0.62	0.62	54.47	104.47	154.47	204.47
Distances[m]:	0.00	2.30	3.22	4.60	6.89	6.93	6.99	9.46	11.76	14.06	16.36

Pod 1	Pod 2	Pod 3	Pod 4	Pod 5	Pod 6	Pod 7	Pod 8	Pod 9	Pod 10	Pod 11	Average Q
[Pa]	[Pa]	[Pa]	[Pa]	[Pa]	[Pa]	[Pa]	[Pa]	[Pa]	[Pa]	[Pa]	[l/s]
240726	218367	209886	197114	175425	175264	150207	147099	125423	101527	81717	2.44
404055	373703	360186	340563	306913	306238	209349	217016	182265	152241	115691	5.30
386687	354615	341777	322698	291162	291583	203779	208553	175759	143662	111506	5.02
363954	333361	321025	302549	271032	271184	204834	198695	167399	141303	106013	4.67
346421	316795	305348	287539	258044	257350	189709	191552	162072	132009	102637	4.40
326941	299393	288058	271063	243553	242888	181949	183422	154209	125882	98204	4.12
312980	285123	274528	257472	230573	230306	178291	177617	150090	121947	95683	3.82
293195	267498	257201	241675	216258	215758	170708	169615	143208	115765	90874	3.53
277244	252814	243158	228176	203454	203784	164948	162372	138279	113273	88424	3.28
263726	240612	231231	217215	193509	193724	157981	156207	132206	112272	85515	3.07
250445	228653	219279	206262	184024	184592	152637	150606	127524	103926	82256	2.86
233138	212474	203934	191771	171153	171392	143752	141897	120132	98209	77944	2.56
219091	199391	191677	179992	160510	161290	136296	134246	114217	93521	74497	2.31
206796	188557	181200	170308	151945	152497	127702	127219	108838	88692	71294	2.08
194285	177028	170208	159924	142804	143067	121865	120454	103242	84862	68346	1.91
184348	168209	161507	151813	135662	135671	116794	114606	98332	81180	65464	1.74
169028	153990	148182	139327	124331	124727	108489	107491	91158	76259	61466	1.49
157025	143582	138048	129815	115911	116393	101510	99612	85700	72016	58338	1.31
142710	130359	125662	118286	105864	105917	92700	91731	79066	66605	54681	1.09
133197	122116	117670	110927	100574	100134	89349	86443	74393	63003	51891	0.94
119121	108849	105237	99476	89711	89763	79306	78744	68393	58099	49107	0.81
113566	104384	100815	95298	85974	85893	74612	75140	65688	56779	47501	0.70
104753	96498	93043	88122	79588	79522	68513	69843	61443	53027	44951	0.58
98963	91196	87968	83291	75648	65476	74939	66860	58967	51257	43935	0.53
90113	83100	80512	76370	69265	59500	68773	61411	54443	47511	41065	0.42
78476	72811	70724	67538	62343	52484	62511	56494	51375	46261	41376	0.27

Kaolin 14%

Orifice Type:	Short	
Orifice thickness[m]:	0.006	Area[m^2]
Orifice dimension[m]:	0.0262	0.000539129
Pipe Diameter [m]:	0.046	0.001661903
Diameter ratio	0.57	
Aspect ratio	0.23	
g[m/s^2]	9.81	
Material Type:	Kaolin	
Density[kg/m^3]:	1319.4	
Concentration[%]:	19%	
τ_y[Pa]:	25.91	
K [Pa.s]:	0.47	
n:	0.56	
PPT used:	110	
Range selected:	0-500	

1/n	n/(n+1)	(n+1)/n	$K^{1/n}$
1.80	0.36	2.80	0.26

	Pod 1	Pod 2	Pod 3	Pod 4	Pod 5	Pod 6	Pod 7	Pod 8	Pod 9	Pod 10	Pod 11
Axial distances	-5.29	-4.68	-3.74	-2.36	-0.06	-0.03	0.03	2.34	4.65	6.97	9.29
N-D distances incl.[L/D]:	-115.05	-101.68	-81.38	-51.27	-1.38	-0.62	0.62	50.83	101.16	151.60	201.92
Distances[m]:	0.00	0.62	1.55	2.93	5.23	5.26	5.32	7.63	9.95	12.27	14.58

Pod 1	Pod 2	Pod 3	Pod 4	Pod 5	Pod 6	Pod 7	Pod 8	Pod 9	Pod 10	Pod 11	Average Q
[Pa]	[Pa]	[Pa]	[Pa]	[Pa]	[Pa]	[Pa]	[Pa]	[Pa]	[Pa]	[Pa]	[l/s]
174413	172139	167968	161888	152974	150349	41369	72106	62529	53518	44047	4.82
174413	172139	167968	161888	152974	150349	41369	72449	62493	53516	43999	4.81
166459	163840	160029	154085	145312	142505	45658	72444	62552	53667	44288	4.56
166464	163924	160224	154528	145566	142479	45307	72213	62542	53720	44309	4.56
156336	154228	150102	144572	135418	132068	49479	70599	62019	53230	43929	4.24
156646	154270	149906	143558	135517	132755	49341	69866	62088	53014	44090	4.24
146104	143911	139712	133869	125300	121775	51945	68791	60063	51415	42269	3.91
145959	143593	139363	133501	125285	123821	51306	69034	60081	51369	42246	3.91
142099	140093	136299	130328	122145	120396	64287	75376	67896	59760	50484	3.47
142308	140144	136195	130402	122152	118627	64287	76285	67539	59426	49764	3.47
135381	132658	128756	122839	114867	112383	66432	75124	66650	58396	49589	3.17
134751	132892	128818	123199	115111	113339	66435	75391	66974	58753	49622	3.17
130901	128924	124821	119226	111395	108781	71175	77904	69543	60263	52681	2.83
130868	128769	124539	119394	111098	108418	71419	77800	69404	61171	52330	2.84
124679	122827	119300	113705	105839	103122	73823	77552	69613	61317	52894	2.52
125392	123447	119497	114480	106209	104122	73789	77607	70006	62026	52696	2.51
118044	116250	113017	107235	99997	95983	78732	78868	71378	63780	55352	2.00

Pod 1 [Pa]	Pod 2 [Pa]	Pod 3 [Pa]	Pod 4 [Pa]	Pod 5 [Pa]	Pod 6 [Pa]	Pod 7 [Pa]	Pod 8 [Pa]	Pod 9 [Pa]	Pod 10 [Pa]	Pod 11 [Pa]	Average Q [l/s]
118082	116426	112530	107446	99705	96565	77276	78834	71385	63619	54600	2.00
112447	110917	107506	102099	94772	95598	79904	78382	71484	63539	56169	1.66
112757	111048	107574	102309	94817	92264	79716	78376	71401	63937	55183	1.66
108109	106490	103320	98334	90919	89289	80545	77460	70299	63228	55244	1.38
108233	106653	103484	98323	91110	89228	80617	77598	70564	63367	55243	1.38
104769	103053	100322	95046	87991	85640	77893	76763	69681	62810	54790	1.14
105143	103399	100117	95139	88138	86239	79433	76755	69960	62810	54680	1.14
103248	101355	98803	94055	87327	84313	78556	77510	70849	63895	56769	0.88
103287	101788	98662	93778	87049	83362	76579	77103	70537	63845	55995	0.88

Kaolin 21%

Orifice Type:	Short	
Orifice thickness[m]:	0.006	Area[m^2]
Orifice dimension[m]:	0.0262	0.000539129
Pipe Diameter [m]:	0.046	0.001661903
Diameter ratio	0.570	
Aspect ratio	0.229	
g[m/s^2]	9.81	
Material Type:	Kaolin	
Density[kg/m^3]:	1348.9	
Concentration[%]:	21%	
τ_y[Pa]:	23.48	
K [Pa.s]:	5.43	
n:	0.35	
PPT used:	110	
Range selected:	0-500	

1/n	n/(n+1)	(n+1)/n	$K^{1/n}$
2.8750887	0.2580586	3.8750887	129.90777

	Pod 1	Pod 2	Pod 3	Pod 4	Pod 5	Pod 6	Pod 7	Pod 8	Pod 9	Pod 10	Pod 11
Axial distances	-5.29	-4.68	-3.74	-2.36	-0.06	-0.03	0.03	2.34	4.65	6.97	9.29
N-D distances incl.[L/D]:	-115.05	-101.68	-81.38	-51.27	-1.38	-0.62	0.62	50.83	101.16	151.60	201.92
Distances[m]:	0.00	0.62	1.55	2.93	5.23	5.26	5.32	7.63	9.95	12.27	14.58

Pod 1	Pod 2	Pod 3	Pod 4	Pod 5	Pod 6	Pod 7	Pod 8	Pod 9	Pod 10	Pod 11	Average Q
[Pa]	[Pa]	[Pa]	[Pa]	[Pa]	[Pa]	[Pa]	[Pa]	[Pa]	[Pa]	[Pa]	[l/s]
186305	183222	177639	171132	159012	156548	80337	97320	85335	73799	61553	4.00
186285	183553	178491	170594	159224	156107	82399	98259	86333	74763	62680	3.98
181644	178659	173481	165569	154626	153311	85928	98754	87010	75479	63240	3.76
181339	178583	173479	166177	154446	153537	85058	98817	86828	75173	63422	3.76
171362	168225	162747	154805	144271	141707	84945	94529	83058	71402	59701	3.46
169877	166821	161960	154065	144431	142490	85731	95016	83431	71934	60358	3.45
162920	159858	155168	147382	136815	134343	87419	94095	82908	71691	59829	3.16
163192	160223	155626	147736	136937	135102	88503	95275	83631	72644	60859	3.15
156969	153473	148942	141080	130691	128242	89669	94033	83435	72677	60568	2.86
157473	154455	149334	141650	130922	128583	90846	94414	83004	71904	60625	2.86
151261	148026	143195	135751	125534	122922	92677	94106	83953	73127	61399	2.54
151566	149022	143894	136595	126443	123048	90954	94838	84843	73794	62056	2.53
146410	143922	138900	131647	121816	118736	95469	95527	85370	74525	63850	2.16
146156	144065	138870	131478	121581	119045	95965	95163	85545	75043	63578	2.16
139214	136243	131815	125179	115138	111833	94148	94309	83995	74179	62330	1.83
139021	136243	131744	124797	115157	110766	93064	93575	84097	74321	62931	1.83
133725	130764	126612	119746	110389	106556	95628	93065	82689	73799	62543	1.51
133354	130755	126342	119973	110174	107119	94118	92249	83010	73513	62044	1.51
129584	127286	123181	116827	107244	104476	94040	91344	81868	72080	61180	1.28
130906	127440	122697	116228	107037	103072	92188	91157	82135	71517	61475	1.28
125314	123504	118895	112553	103444	100989	93972	89983	80775	71312	61499	1.02
125561	123680	119068	112313	103463	100825	90541	89720	80956	71775	60786	1.02
122391	120612	116326	109908	101087	98475	90794	88867	80028	70881	60411	0.86
123406	120471	116374	110245	101194	97793	90524	87611	80439	70627	60092	0.85
119378	116970	113022	106453	98119	93374	88004	86232	78274	69944	59252	0.67
119930	117130	112670	106439	98476	95769	88792	86034	78689	70148	59111	0.65
110748	109226	105957	101054	94142	92343	88267	83409	75501	66908	58067	0.36
111803	108877	105536	100871	93300	91110	86332	82675	75490	66255	58126	0.33

Kaolin 24%

Orifice Type:	Short	
Orifice thickness[m]:	0.006	Area[m^2]
Orifice dimension[m]:	0.026	0.000539129
Pipe Diameter [m]:	0.046	0.001661903
Diameter ratio	0.570	
Aspect ratio	0.229	
g[m/s^2]	9.810	
Material Type:	Kaolin	
Density[kg/m^3]:	1393	
Concentration[%]:	0.24	
τ_y[Pa]:	35.28	

K [Pa.s]:	10.04
n:	0.41
PPT used:	110
Range selected:	0-500

1/n	n/(n+1)	(n+1)/n	$K^{1/n}$
2.46	0.29	3.46	292.34

	Pod 1	Pod 2	Pod 3	Pod 4	Pod 5	Pod 6	Pod 7	Pod 8	Pod 9	Pod 10	Pod 11
Axial distances	-5.29	-4.68	-3.74	-2.36	-0.06	-0.03	0.03	2.34	4.65	6.97	9.29
N-D distances incl.[L/D]:	-115.05	-101.68	-81.38	-51.27	-1.38	-0.62	0.62	50.83	101.16	151.60	201.92
Distances[m]:	0.00	0.62	1.55	2.93	5.23	5.26	5.32	7.63	9.95	12.27	14.58

Pod 1	Pod 2	Pod 3	Pod 4	Pod 5	Pod 6	Pod 7	Pod 8	Pod 9	Pod 10	Pod 11	Average Q
[Pa]	[Pa]	[Pa]	[Pa]	[Pa]	[Pa]	[Pa]	[Pa]	[Pa]	[Pa]	[Pa]	[l/s]
213874	208882	202599	190482	173800	169965	156803	146994	129196	111189	93481	1.68
213806	209361	202342	190756	173988	169309	155659	147604	129480	110592	93450	1.69
209231	205296	197592	186847	169737	169196	153993	145960	128180	110739	92961	1.50
209262	204860	198010	186451	169164	166674	153959	146353	128685	110610	93297	1.51
203327	199314	192301	181606	165130	161045	150782	143407	126530	109583	92036	1.25
203625	199047	192653	182066	164980	162891	151419	143561	126412	109615	92492	1.28
199373	195645	189065	177957	162386	161284	148540	142273	124886	108704	91882	1.14
199033	194520	188309	178492	161988	159584	148713	142780	125347	108968	91871	1.10
191046	187611	180685	171410	155924	150929	146860	138117	121806	106225	90098	0.84
190688	188262	181715	171330	156509	148263	144493	138481	121840	105952	90238	0.77
188437	185432	178895	169299	153937	148682	141523	136389	120786	104947	89318	0.65
188490	185380	179086	168720	153902	147680	142200	136050	119686	104383	88802	0.73
183136	179120	173067	163188	149308	142200	135068	131411	116666	101639	86753	0.56
183136	179120	173067	163188	149308	142200	135068	131411	116666	101639	86753	0.57
178538	175180	169216	159207	146907	141404	131741	128029	112860	99263	85589	0.41
170863	168098	163048	154725	141898	138268	131511	127911	112848	99685	85446	0.45
166120	162462	155934	146718	133649	131822	125107	122531	108391	95027	82079	0.23
168573	164734	157934	147943	134705	131751	119619	117492	104595	91946	80715	0.31
159379	155755	149402	140439	129236	120325	114057	107054	95882	86193	78736	0.22

Bentonite 6%

Orifice Type:	Short	
Orifice thickness[m]:	0.006	Area[m^2]
Orifice dimension[m]:	0.026	0.000539129
Pipe Diameter [m]:	0.046	0.001661903
Diameter ratio	0.570	
Aspect ratio	0.229	
g[m/s^2]	9.81	
Material Type:	Bentonite	
Density[kg/m^3]:	1040.1	
Concentration[%]:	6%	
τ_y[Pa]:	2.4	
K [Pa.s]:	0.0241	
n:	1	
PPT used:	110	
Range selected:	0-500	

1/n	n/(n+1)	(n+1)/n	$K^{1/n}$
1	0.5	2	0.0241

	Pod 1	Pod 2	Pod 3	Pod 4	Pod 5	Pod 6	Pod 7	Pod 8	Pod 9	Pod 10	Pod 11
Axial distances	-5.29	-4.68	-3.74	-2.36	-0.06	-0.03	0.03	2.34	4.65	6.97	9.29
N-D distances incl.[L/D]:	-115.05	-101.68	-81.38	-51.27	-1.38	-0.62	0.62	50.83	101.16	151.60	201.92
Distances[m]:	0.00	0.62	1.55	2.93	5.23	5.26	5.32	7.63	9.95	12.27	14.58

Pod 1	Pod 2	Pod 3	Pod 4	Pod 5	Pod 6	Pod 7	Pod 8	Pod 9	Pod 10	Pod 11	Average Q
[Pa]	[Pa]	[Pa]	[Pa]	[Pa]	[Pa]	[Pa]	[Pa]	[Pa]	[Pa]	[Pa]	[l/s]
150500	148035	145048	140874	134367	133614	8333	44893	38084	30926	24453	5.67
150351	147614	144623	140329	133750	133226	7972	44757	38123	31511	24603	5.66
132248	130368	128285	124600	118346	116994	9915	42324	35399	29685	23175	5.25
132060	130524	127931	124074	117969	116748	9431	42516	35466	29854	23065	5.25
118710	117233	114756	110991	105520	104596	9450	38190	32774	27569	21717	4.93
118459	116801	114294	111340	105733	106103	10245	38473	33124	27447	22242	4.94
102834	100759	98558	96131	91858	90142	11059	34338	29571	24891	20172	4.56
102584	100949	98666	95855	92273	90543	9895	34139	29075	25074	20010	4.57
91024	89343	87687	85179	80731	80437	9961	30629	26506	22375	18087	4.25
90340	89002	87372	84484	80423	79937	10369	30786	26347	22387	17969	4.27
81358	80022	78255	75930	72178	71607	10993	28711	24868	21286	17208	3.98
81404	79562	78076	75553	72066	72185	10908	29239	24774	21044	17211	3.98
71959	71125	69800	67714	64890	64509	12632	28054	24188	20272	16785	3.70
71569	70683	69305	67205	64045	63646	12942	27995	24289	21038	17746	3.70
62849	61826	60622	58744	55752	55740	12855	25477	22106	19233	16419	3.40
62660	61991	60775	59039	56132	55751	12800	25329	22038	19736	16754	3.40
55726	55048	53820	51850	49633	49399	13961	24477	21659	19666	16903	3.10
55408	54653	53433	51895	49606	49172	14568	24208	21466	18949	17275	3.10

Pod 1 [Pa]	Pod 2 [Pa]	Pod 3 [Pa]	Pod 4 [Pa]	Pod 5 [Pa]	Pod 6 [Pa]	Pod 7 [Pa]	Pod 8 [Pa]	Pod 9 [Pa]	Pod 10 [Pa]	Pod 11 [Pa]	Average Q [l/s]
51503	50803	49904	48681	46281	46308	19340	27060	24105	22606	20109	2.77
51544	51286	50006	48720	46572	45956	19125	26758	24197	22615	20252	2.77
48415	47897	47084	45582	43471	43299	19804	26183	23981	21921	19800	2.54
47925	47392	46802	45246	43283	43192	20023	26050	23785	22056	19675	2.54
45383	44643	43897	42584	40636	40531	20632	25688	23728	21577	19865	2.36
45359	44764	43801	42696	40550	40353	20248	25403	23563	21803	19405	2.36
41939	41586	40902	39734	37794	37498	20604	24545	22798	21155	19138	2.17
42601	41995	41252	40002	37698	37874	21140	24596	22962	21269	19207	2.17
39802	39245	38462	37323	35193	35004	21908	24400	23184	21631	19616	1.92
40145	39621	38877	37718	35554	35425	22131	24677	23574	21494	19989	1.92
37528	37133	36331	35114	33259	33141	23707	24451	23732	22180	20129	1.61
37574	37116	36421	35125	33304	32983	23737	24388	23748	22342	20177	1.61
34428	34117	33251	32210	30362	30169	24421	24396	23294	21630	19557	1.29
34678	34220	33372	32335	30450	30268	24472	24436	23400	21663	19766	1.31
31389	31335	30672	29685	27847	27737	24989	24522	22798	21144	19223	0.94
31842	31526	30677	29669	27960	27808	24988	24760	22805	20994	19311	0.92
34788	33819	33188	32228	30546	30207	29768	28981	26789	25096	23226	0.62

Bentonite 9%

Orifice Type:	Short	
Orifice thickness[m]:	0.006	Area[m^2]
Orifice dimension[m]:	0.0262	0.000539129
Pipe Diameter [m]:	0.046	0.001661903
Diameter ratio	0.570	
Aspect ratio	0.229	
g[m/s^2]	9.81	
Material Type:	Bentonite	
Density[kg/m^3]:	1058.2	
Concentration[%]:	9%	
τ_y[Pa]:	7.18	
K [Pa.s]:	0.04	
n:	1.00	
PPT used:	110	
Range selected:	0-500	

1/n	n/(n+1)	(n+1)/n	$K^{1/n}$
1	0.5	2	0.0377361

	Pod 1	Pod 2	Pod 3	Pod 4	Pod 5	Pod 6	Pod 7	Pod 8	Pod 9	Pod 10	Pod 11
Axial distances	-5.29	-4.68	-3.74	-2.36	-0.06	-0.03	0.03	2.34	4.65	6.97	9.29
N-D distances incl.[L/D]:	-115.05	-101.68	-81.38	-51.27	-1.38	-0.62	0.62	50.83	101.16	151.60	201.92
Distances[m]:	0.00	0.62	1.55	2.93	5.23	5.26	5.32	7.63	9.95	12.27	14.58

Pod 1 [Pa]	Pod 2 [Pa]	Pod 3 [Pa]	Pod 4 [Pa]	Pod 5 [Pa]	Pod 6 [Pa]	Pod 7 [Pa]	Pod 8 [Pa]	Pod 9 [Pa]	Pod 10 [Pa]	Pod 11 [Pa]	Average Q [l/s]
175269	173035	169568	165346	157075	153699	18069	57889	50418	43205	35034	6.01
175174	173454	168982	164636	157393	153271	18808	57961	50980	43266	34935	6.03
156340	154768	151813	147872	140334	139333	19297	55449	47649	41058	33497	5.66
156880	154716	151916	147205	140105	138744	20424	54988	47656	41472	33674	5.65
139483	137033	134110	129605	123957	123477	21365	51478	44151	38019	31662	5.29
138608	136571	133999	129818	123831	121889	21281	51473	44583	38632	32212	5.27
123272	121703	119605	115978	110192	109429	22649	48252	41824	36267	30914	4.90
123483	121562	119142	115488	109869	108821	22651	47599	41811	36383	30430	4.89
114510	113242	110904	107173	101282	100902	25374	46052	40952	35900	30134	4.59
114265	113195	110603	107519	101905	100758	24974	46461	40641	35742	29970	4.59
106719	105575	103140	99752	94565	93321	27126	45556	39797	34606	29190	4.26
106026	104716	103088	99750	94145	93197	28120	46464	40647	35955	30007	4.26
97374	95963	93869	90683	85354	84580	30122	45320	39638	34669	29468	3.81
96810	95472	93344	89782	84806	83472	29722	44699	39550	35393	30201	3.81
91565	90488	88279	84901	79804	78655	34242	45777	40705	35973	30538	3.46
91494	89995	87856	84281	79133	78143	33384	45024	40155	35274	30411	3.46
87832	86861	84949	81589	76647	75504	44289	50997	46328	41672	36707	2.87
87809	86770	84634	81533	76823	75728	45217	51791	46754	42003	36974	2.87
84108	83030	81114	77872	73067	72321	47155	51902	47218	42343	37143	2.55
84796	83242	81133	77863	73064	72244	47147	52044	47273	42227	37811	2.55
80205	79161	77302	74370	69473	69829	51313	53545	49022	44111	39721	2.20
81553	80750	78664	75452	70606	69701	51274	53566	49038	44200	39313	2.20
79159	78288	76346	73205	68369	67841	54868	55115	50630	46408	41231	1.90
80263	78540	76580	73278	68693	68154	54875	54797	50466	45830	39974	1.90
75795	74898	72980	70014	65320	64972	56654	54918	50652	45863	40912	1.52
76033	74935	72838	69898	65429	64376	56587	54744	50653	45689	40538	1.52
70257	69973	68569	66026	61607	60898	56837	54111	49638	45118	40303	1.21

Water

Orifice Type:	Short	
Orifice thickness[m]:	0.006	Area[m^2]
Orifice dimension[m]:	0.0262	0.000539129
Pipe Diameter [m]:	0.046	0.001661903
Diameter ratio	0.570	
Aspect ratio	0.229	

g[m/s^2]	9.81	
Material Type:	Water	
Density[kg/m^3]:	998.5	
Concentration[%]:	100%	
τ_y[Pa]:	0	
K [Pa.s]:	0.001	
n:	1	
PPT used:	110	
Range selected:	0-500	

1/n	n/(n+1)	(n+1)/n	$K^{1/n}$
1	0.5	2	0.001

	Pod 1	Pod 2	Pod 3	Pod 4	Pod 5	Pod 6	Pod 7	Pod 8	Pod 9	Pod 10	Pod 11
Axial distances	-5.29	-4.68	-3.74	-2.36	-0.06	-0.03	0.03	2.34	4.65	6.97	9.29
N-D distances incl.[L/D]:	-115.05	-101.68	-81.38	-51.27	-1.38	-0.62	0.62	50.83	101.16	151.60	201.92
Distances[m]:	0.00	0.62	1.55	2.93	5.23	5.26	5.32	7.63	9.95	12.27	14.58

Pod 1	Pod 2	Pod 3	Pod 4	Pod 5	Pod 6	Pod 7	Pod 8	Pod 9	Pod 10	Pod 11	Average Q
[Pa]	[Pa]	[Pa]	[Pa]	[Pa]	[Pa]	[Pa]	[Pa]	[Pa]	[Pa]	[Pa]	[l/s]
128355	127006	125429	122012	117258	117832	-5691	32061	27253	22523	17428	5.56
130060	128440	127009	123143	118735	118981	-6454	32344	27491	22911	17716	5.60
116412	114754	112866	110103	105834	106421	-4836	30616	25075	20817	16918	5.27
116266	114754	112970	109900	105879	106097	-4927	29623	25054	20712	16464	5.26
108518	107321	105633	102984	99210	99390	-4009	28057	23946	19879	15599	5.08
108500	107199	105562	102801	99158	99380	-4099	27971	23878	19781	15629	5.08
97978	96299	95040	92627	88894	89294	-2748	25680	22117	18326	14697	4.79
97728	96213	94935	92641	89074	89395	-2902	25627	22069	18473	14573	4.79
84642	83558	82402	80295	77068	77493	-1444	22945	19861	16752	13383	4.42
84522	83400	82208	80323	77300	77564	-1802	23176	19878	16717	13318	4.41
74188	73240	72262	70262	67688	67866	-319	20947	18119	15306	12419	4.10
74246	73334	72273	70408	67832	67826	-371	20834	18069	15234	12323	4.11
62829	61994	61028	59523	57272	57507	963	18430	16103	13764	11249	3.74
62733	61979	61202	59575	57232	57375	979	19208	16164	13676	11388	3.74
52976	52369	51816	50406	48443	48669	2078	16423	14334	12544	10386	3.39
53130	52386	51678	50337	48480	48557	1548	16877	14377	12685	10463	3.40
45551	44903	44319	43156	41484	41550	2369	15235	13098	11415	9636	3.10
45447	44928	44147	43190	41509	41603	2368	15195	13163	11572	9682	3.10
39562	38849	38551	37333	36041	36082	3021	13909	12002	10645	9100	2.85
39579	38879	38393	37433	35926	36081	4031	13891	12096	10599	9142	2.85

Pod 1	Pod 2	Pod 3	Pod 4	Pod 5	Pod 6	Pod 7	Pod 8	Pod 9	Pod 10	Pod 11	Average Q
[Pa]	[Pa]	[Pa]	[Pa]	[Pa]	[Pa]	[Pa]	[Pa]	[Pa]	[Pa]	[Pa]	[l/s]
32642	32157	31814	30936	29661	29942	3773	12312	10779	9680	8467	2.53
32311	32156	31730	30921	29828	29979	3903	11894	10832	9553	8439	2.53
26635	26342	26025	25371	24388	24586	4563	10931	9729	9025	7890	2.22
26735	26338	26057	25440	24448	24534	4250	10943	9746	8834	7854	2.22
21424	20828	20525	20120	19478	19435	5060	9632	8774	7889	7314	1.94
21424	20765	20557	20069	19404	19424	4654	9673	8723	8197	7354	1.94
17682	17475	17235	16818	16316	16355	5082	8709	8090	7489	7067	1.70

ORIFICE DIAMETER RATIO, $\beta = 0.57$ (round apex)

CMC 6%

Orifice Type:	Short	
Orifice thickness[m]:	0.006	Area[m^2]
Orifice dimension[m]:	0.026	0.000539129
Pipe Diameter [m]:	0.046	0.001661903
Diameter ratio	0.570	
Aspect ratio	0.229	
g[m/s^2]	9.81	
Material Type:	CMC	
Density[kg/m^3]:	1036	
Concentration[%]:	6%	
τ_y[Pa]:	0	
K [Pa.s]:	3.40	
n:	0.61	
PPT used:	110	
Range selected:	0-500	

1/n	n/(n+1)	(n+1)/n	$K^{1/n}$
1.64	0.38	2.64	7.48

	Pod 1	Pod 2	Pod 3	Pod 4	Pod 5	Pod 6	Pod 7	Pod 8	Pod 9	Pod 10	Pod 11
Axial distances	-6.95	-4.65	-3.73	-2.36	-0.06	-0.03	0.03	2.34	4.64	6.94	9.24
N-D distances incl.[L/D]:	-151.16	-101.16	-81.16	-51.27	-1.38	-0.62	0.62	50.83	100.83	150.83	200.83
Distances[m]:	0.00	2.30	3.22	4.60	6.89	6.93	6.98	9.29	11.59	13.89	16.19

Pod 1	Pod 2	Pod 3	Pod 4	Pod 5	Pod 6	Pod 7	Pod 8	Pod 9	Pod 10	Pod 11	Average Q
[Pa]	[Pa]	[Pa]	[Pa]	[Pa]	[Pa]	[Pa]	[Pa]	[Pa]	[Pa]	[Pa]	[l/s]
399696	366508	353178	332862	299731	298785	219093	217769	183519	150282	117532	4.91
370817	338703	326213	306866	275175	275088	204115	205084	172475	141072	109511	4.51
356002	325360	313082	294618	264417	264304	207925	199209	167624	137676	106801	4.29
334913	307806	296136	278390	249493	248988	192535	191050	161119	131821	103719	4.01
311190	285761	274668	258144	230578	232173	183477	180434	152609	124363	97979	3.64
291882	266252	255953	240139	214357	214002	174563	170713	144637	118466	93128	3.31
273510	248893	239112	224366	200186	200294	166075	162103	137163	112178	87848	3.01
256795	233430	224030	210266	189243	188986	157621	154253	130099	107229	83695	2.75
239805	218516	209555	196234	176469	176541	149415	145651	123621	102000	79514	2.30
219698	199881	192159	180311	160879	161900	137850	133727	114408	94531	73962	2.11
197242	179733	172610	161890	144383	145467	125856	121971	104422	86080	68478	1.79
179562	163601	157251	147680	132092	132478	116146	112733	96614	80712	64596	1.53
163035	148795	143087	134613	120208	121070	106242	103689	88907	74402	60189	1.27
143515	131045	126412	118980	106881	107359	93964	92737	79950	67387	55257	0.99
137525	125487	120972	113827	102286	102934	89992	88957	77190	65493	54609	0.90
126498	115720	111555	105457	95134	95863	83842	83865	73825	63394	53264	0.73
114897	105840	102195	96750	87581	88280	76602	77808	68580	59382	50613	0.59
105202	96651	93255	88543	80883	81143	69502	71943	63793	56023	48051	0.51
93219	85978	83081	78947	72757	72974	61495	64596	58021	51543	44893	0.37
82617	76874	74566	71190	65422	65979	54914	59292	53415	47584	42193	0.27
73216	68059	66204	63391	58845	59193	48271	53409	48767	44069	39619	0.19
288422	292627	252118	268431	285452	334847	204449	253298	254282	261862	279429	0.10

Kaolin 14%

Orifice Type:	Short	
Orifice thickness[m]:	0.006	Area[m^2]
Orifice dimension[m]:	0.0262	0.000539129
Pipe Diameter [m]:	0.046	0.001661903
Diameter ratio	0.570	
Aspect ratio	0.229	
g[m/s^2]	9.81	
Material Type:	Kaolin	
Density[kg/m^3]:	1227.2	
Concentration[%]:	14%	
τ_y[Pa]:	3.20	
K [Pa.s]:	0.09	
n:	0.77	
PPT used:	110	
Range selected:	0-500	

1/n	n/(n+1)	(n+1)/n	$K^{1/n}$
1.297	0.435	2.297	0.041

	Pod 1	Pod 2	Pod 3	Pod 4	Pod 5	Pod 6	Pod 7	Pod 8	Pod 9	Pod 10	Pod 11
Axial distances	-5.29	-4.68	-3.74	-2.36	-0.06	-0.03	0.03	2.34	4.65	6.97	9.29
N-D distances incl.[L/D]:	-115.05	-101.68	-81.38	-51.27	-1.38	-0.62	0.62	50.83	101.16	151.60	201.92
Distances[m]:	0.00	0.62	1.55	2.93	5.23	5.26	5.32	7.63	9.95	12.27	14.58

Pod 1 [Pa]	Pod 2 [Pa]	Pod 3 [Pa]	Pod 4 [Pa]	Pod 5 [Pa]	Pod 6 [Pa]	Pod 7 [Pa]	Pod 8 [Pa]	Pod 9 [Pa]	Pod 10 [Pa]	Pod 11 [Pa]	Average Q [l/s]
165154	162473	159750	155475	149250	149553	3880	44985	38261	31371	24473	5.62
165154	162473	159750	155475	149250	149553	3880	44985	38261	31371	24473	5.62
142533	140382	138097	134056	128457	128739	2795	39595	34559	28488	22767	5.20
142385	140399	137600	133984	128465	128666	3119	39937	34190	28054	21463	5.20
128868	126802	124608	121249	116368	116474	5787	38228	31926	27121	21463	4.93
128594	126725	124715	121353	115927	116249	5955	38193	31904	26836	21469	4.93
113450	112058	110319	107110	102755	102746	5678	35046	29453	24892	20205	4.61
113542	112050	110302	107165	102479	102846	5315	34396	29615	24827	20144	4.61
101316	99950	98289	95534	91429	91198	6840	32403	27498	23360	19199	4.32
101249	99874	98425	95617	91468	91215	7308	32451	27571	23406	19123	4.33
94006	92506	91004	88680	85266	85152	16017	36624	32170	28524	25085	3.94
94006	92506	91004	88680	85266	85152	16017	36624	32170	28524	25085	3.93
82510	81358	80175	78078	74830	75009	16516	33533	30275	27097	23910	3.64
82510	81358	80175	78078	74830	75009	16516	33533	30275	27097	23910	3.61
70937	69961	68660	66613	63582	63610	12505	27974	24298	21483	18477	3.39
70937	69696	68660	66227	63536	64052	12505	28275	24887	21598	18269	3.38
65777	64931	63948	61960	59629	59441	17163	29216	27155	24294	21862	3.13
65777	64931	63948	61960	59629	59441	17163	29216	27155	24294	21862	3.10
58713	58072	56946	55509	53243	52843	21344	29838	27182	24999	22204	2.76
58591	57890	56931	55235	52860	52410	20547	29642	26876	24255	21955	2.76
52659	52011	50804	49038	46454	46649	24375	30215	27905	25771	23293	2.29
52509	51616	50512	48930	46781	46348	24059	29609	27102	25263	22593	2.30
48139	47778	46926	45483	43367	42841	26820	30622	28445	26143	23943	1.92
47315	46947	46065	44691	42439	41990	25862	29708	27339	24797	22418	1.95
43048	42974	42015	40768	38661	38509	29119	30611	28595	27080	24798	1.46
43544	42738	41832	40512	38385	38066	28853	30362	28631	26640	24610	1.46
39464	38945	38253	37168	35199	35230	30648	30600	28810	27177	25109	1.03
39855	39442	38613	37316	35498	35110	30805	30596	28836	27588	25266	1.03
34583	34293	33630	32550	30915	30604	30020	28526	26899	25346	23622	0.57

Kaolin 21%

Orifice Type:	Short	
Orifice thickness[m]:	0.006	Area[m^2]
Orifice dimension[m]:	0.0262	0.000539129
Pipe Diameter [m]:	0.046	0.001661903

Diameter ratio	0.570	
Aspect ratio	0.229	
g[m/s^2]	9.81	
Material Type:	Kaolin	
Density[kg/m^3]:	1348.9	
Concentration[%]:	21%	
τ_y[Pa]:	23.48	
K [Pa.s]:	5.43	
n:	0.35	
PPT used:	110	
Range selected:	0-500	

1/n	n/(n+1)	(n+1)/n	$K^{1/n}$
2.88	0.26	3.88	129.91

	Pod 1	Pod 2	Pod 3	Pod 4	Pod 5	Pod 6	Pod 7	Pod 8	Pod 9	Pod 10	Pod 11
Axial distances	-5.23	-4.63	-3.71	-2.33	-0.06	-0.03	0.03	2.34	4.65	6.97	9.29
N-D distances incl.[L/D]:	-113.77	-100.62	-80.62	-50.73	-1.38	-0.62	0.62	50.94	101.16	151.60	201.92
Distances[m]:	0.00	0.61	1.53	2.90	5.17	5.21	5.26	7.58	9.89	12.21	14.52

Pod 1	Pod 2	Pod 3	Pod 4	Pod 5	Pod 6	Pod 7	Pod 8	Pod 9	Pod 10	Pod 11	Average Q
[Pa]	[Pa]	[Pa]	[Pa]	[Pa]	[Pa]	[Pa]	[Pa]	[Pa]	[Pa]	[Pa]	[l/s]
182837	179352	174426	166857	156998	153516	80105	96243	85582	74283	61863	3.96
182677	179581	174139	166538	157192	153856	81534	96167	85052	73545	62432	3.95
175829	172953	168511	160579	150192	146370	82519	94978	84994	73383	62384	3.72
176167	172985	168530	161060	150340	144444	82424	95844	85044	73672	62228	3.72
169297	165885	161000	154065	143840	141095	88019	96107	85950	74902	63345	3.42
169180	165885	161000	154065	143840	142701	87412	95942	85802	75098	62636	3.42
162302	159640	154894	148846	137795	134455	89887	96087	85725	75013	63910	3.10
162302	159640	155177	148342	137597	135539	89644	96455	85991	75184	63777	3.10
158218	155472	150837	143570	133490	131865	89718	96151	86193	75294	63964	2.88
158451	155804	150759	143300	133705	132576	88908	96484	85908	75131	64002	2.88
153007	150547	145297	138382	128515	127451	88567	94970	85020	74363	61731	2.70
153170	150405	144987	138503	128549	124737	88343	94865	85240	74073	63087	2.70
148447	146166	141209	134332	124867	118799	90886	94472	84481	73301	63481	2.51
148763	146656	141661	134983	125194	119076	93001	93547	84128	73725	62731	2.51
144873	142414	137822	130689	121255	118281	94319	94408	84401	74212	63337	2.25
144586	142338	137522	131094	121129	117264	94777	93749	84609	74208	64233	2.25
139552	137428	133040	126086	117068	109876	92365	94232	84800	74200	64689	1.96
139873	137383	132998	125881	116633	115664	92686	94163	84853	74344	64372	1.96

Pod 1	Pod 2	Pod 3	Pod 4	Pod 5	Pod 6	Pod 7	Pod 8	Pod 9	Pod 10	Pod 11	Average Q
[Pa]	[Pa]	[Pa]	[Pa]	[Pa]	[Pa]	[Pa]	[Pa]	[Pa]	[Pa]	[Pa]	[l/s]
134274	132133	127763	120856	111771	112235	94618	93559	83898	74093	63708	1.65
134640	132334	127654	120932	111985	110036	94682	93617	84103	74044	63588	1.65
127752	125766	121806	114995	106113	105070	95825	91799	81919	72422	62392	1.30
127915	125405	121425	115049	106070	103122	95006	91840	82316	72547	62827	1.30
122476	120322	116266	110142	101797	99172	92536	89501	80954	71390	61596	0.99
122976	121352	117015	110554	102326	99913	92877	89661	81229	71203	61748	0.99
118929	117252	113421	107170	99220	96961	91936	87489	79506	70389	62185	0.79
118408	116685	112623	106650	98875	96804	92293	87280	79518	70572	61276	0.78
107490	106272	103566	98852	91927	88927	84773	81124	74282	65727	57755	0.37

Kaolin 24%

Orifice Type:	Short	
Orifice thickness[m]:	0.006	Area[m^2]
Orifice dimension[m]:	0.0262	0.000539129
Pipe Diameter [m]:	0.046	0.001661903
Diameter ratio	0.570	
Aspect ratio	0.229	
g[m/s^2]	9.81	
Material Type:	Kaolin	
Density[kg/m^3]:	1392.9	
Concentration[%]:	24%	
τ_y[Pa]:	35.28	
K [Pa.s]:	10.04	
n:	0.41	
PPT used:	110	
Range selected:	0-500	

1/n	n/(n+1)	(n+1)/n	$K^{1/n}$
2.46	0.29	3.46	292.34

	Pod 1	Pod 2	Pod 3	Pod 4	Pod 5	Pod 6	Pod 7	Pod 8	Pod 9	Pod 10	Pod 11
Axial distances	-5.29	-4.68	-3.74	-2.36	-0.06	-0.03	0.03	2.34	4.65	6.97	9.29
N-D distances incl.[L/D]:	-115.05	-101.68	-81.38	-51.27	-1.38	-0.62	0.62	50.83	101.16	151.60	201.92
Distances[m]:	0.00	0.62	1.55	2.93	5.23	5.26	5.32	7.63	9.95	12.27	14.58

Pod 1	Pod 2	Pod 3	Pod 4	Pod 5	Pod 6	Pod 7	Pod 8	Pod 9	Pod 10	Pod 11	Average Q
[Pa]	[Pa]	[Pa]	[Pa]	[Pa]	[Pa]	[Pa]	[Pa]	[Pa]	[Pa]	[Pa]	[l/s]
215398	209618	202671	192821	175121	174808	149875	143181	125777	108140	90687	2.17
215398	209907	202786	191994	175217	173597	150173	143037	125528	108599	90585	2.16
209971	204909	198446	187990	171451	171142	147653	142309	125339	107680	90493	2.01
210013	205966	198802	188531	170998	169228	147640	142585	125506	108274	90691	1.98
207165	203187	196048	185421	169387	168430	146001	141796	124993	107942	90654	1.87
206800	203274	196528	186088	169406	166502	146828	142572	125336	108154	90993	1.90
201526	198744	191686	180941	164594	162032	143797	141119	123915	107377	90467	1.59
202547	198107	191984	181147	164798	163417	144042	140525	124055	107548	90994	1.61
197808	193740	187459	177063	161353	158636	143493	139710	123237	106916	90643	1.45
197157	193536	187242	177265	161349	160655	144922	139710	123432	106943	90660	1.41
194758	191563	185542	175640	160277	159116	145617	139108	123242	106267	90404	1.34
195274	191914	185948	175891	160040	160445	145979	139285	123362	106837	90809	1.36
191949	188362	181857	172385	157554	157785	140539	137641	122238	106085	90183	1.22
191949	188912	182591	173079	157652	157463	141489	137240	121718	105353	89708	1.18
187800	184289	177634	168156	152679	139504	139008	134800	119519	103749	87971	0.98
187180	183623	177611	167623	152857	142795	137881	134578	119420	104166	87906	0.95
183110	180013	174220	164782	150304	145179	137160	131471	116762	101689	86420	0.76
178168	174578	168858	160405	145610	136782	134646	128383	113831	98786	84008	0.81
178168	174578	168531	160091	145697	134851	134506	128383	113831	98786	84008	0.82
167465	163346	159430	151078	138286	132272	130026	123659	109528	95099	81056	0.59
164095	160998	156705	149204	137119	132272	128587	123636	109166	94994	81201	0.56
163008	160887	156702	148300	136384	129124	128628	121998	108404	94619	80902	0.44
150374	146763	142193	136225	127121	124949	120728	113284	100298	88105	76297	0.36

Bentonite 6%

Orifice Type:	Short	
Orifice thickness[m]:	0.006	Area[m^2]
Orifice dimension[m]:	0.0262	0.000539129
Pipe Diameter [m]:	0.046	0.001661903
Diameter ratio	0.570	
Aspect ratio	0.229	
g[m/s^2]	9.81	
Material Type:	Bentonite	
Density[kg/m^3]:	1040.1	
Concentration[%]:	6%	
τ_y[Pa]:	2.4	
K [Pa.s]:	0.024	
n:	1	
PPT used:	110	
Range selected:	0-500	

1/n	n/(n+1)	(n+1)/n	$K^{1/n}$
1	0.5	2	0.024

	Pod 1	Pod 2	Pod 3	Pod 4	Pod 5	Pod 6	Pod 7	Pod 8	Pod 9	Pod 10	Pod 11
Axial distances	-6.95	-4.65	-3.73	-2.35	-0.06	-0.03	0.03	2.33	4.63	6.93	9.23
N-D distances incl.[L/D]:	-151.05	-101.05	-81.05	-51.05	-1.27	-0.62	0.62	50.62	100.62	150.62	200.62
Distances[m]:	0.00	2.30	3.22	4.60	6.89	6.92	6.98	9.28	11.58	13.88	16.18

Pod 1	Pod 2	Pod 3	Pod 4	Pod 5	Pod 6	Pod 7	Pod 8	Pod 9	Pod 10	Pod 11	Average Q
[Pa]	[Pa]	[Pa]	[Pa]	[Pa]	[Pa]	[Pa]	[Pa]	[Pa]	[Pa]	[Pa]	[l/s]
147477	140008	136837	132974	126463	125526	12514	44694	37197	30417	24107	5.56
146152	139174	136175	132221	126507	126324	12104	44137	37084	30776	23792	5.51
131151	125572	122871	119044	113855	114177	14298	41155	34645	28953	23181	5.20
131478	126089	123274	119448	113789	113077	13768	41179	34776	29033	23189	5.19
116886	111869	109504	106172	101352	100731	13267	37176	32011	26660	21676	4.90
116323	112142	109811	106034	101223	100676	13354	37229	31982	27198	21565	4.86
103898	98658	97351	94471	89717	89901	15074	34401	29951	24947	20175	4.56
104274	98807	97431	94792	89825	89715	12829	34600	29654	24985	20243	4.55
88803	84872	83260	80486	76611	76417	12876	30514	26392	22509	18539	4.15
88265	84325	82927	80629	76707	76549	13351	31065	26395	22615	18413	4.15
82368	78602	76866	74527	70779	71178	13157	28960	25205	22180	17872	3.95
81676	77780	76339	74253	70731	70271	13640	29539	25190	21621	18321	3.95
75052	72414	70944	69305	65824	65334	19187	31689	28497	25695	22294	3.61
75295	72456	70978	69291	65749	64302	20148	31662	28668	25439	22315	3.61
64359	61795	60889	58949	56462	55267	14801	25802	22928	20622	17583	3.42
64653	61603	60709	58952	56226	56275	15208	26334	22844	20157	17407	3.42
56542	53799	52444	51155	49544	48917	16479	25563	22841	19403	17721	3.05
56485	53824	53013	51419	48754	48197	15552	25588	22691	19095	17929	3.05
52889	50960	49778	48434	46091	45864	20111	26947	24726	21081	20738	2.69
53647	51275	50390	49152	46781	46209	19813	27741	24938	21130	20670	2.68
49223	47212	46087	45086	42855	42707	21772	26796	24831	21714	20449	2.39
49057	46982	45851	44893	42584	42357	20927	26380	24632	22468	20527	2.39
44309	42241	41412	40096	38082	38047	23113	26427	24362	22514	20177	2.01
44402	42259	41372	40131	38042	37964	23049	26498	24253	22343	20404	2.01
41588	39763	38886	37718	35714	35691	24586	26714	24631	22736	20855	1.77
41989	39974	39413	38023	36187	35996	24894	26822	24876	22843	20998	1.77
38777	36727	36109	34874	32829	32723	25711	26324	24522	22684	20826	1.41
39248	36876	35980	34766	32726	32672	25701	26279	24466	22592	20896	1.41
36393	34602	33968	32654	30857	30662	26038	25872	24168	22210	20491	1.16
36218	34338	33711	32660	30743	30589	26012	25759	24100	22087	20453	1.16
34229	32503	31826	30682	28908	28805	26269	25663	23610	21589	20060	0.90
34479	32695	31839	30667	28862	28757	26485	25754	23696	21897	20065	0.90
36682	35209	34585	33537	31683	31625	31323	29572	27679	25913	24463	0.59

Bentonite 9%

Orifice Type:	Short	
Orifice thickness[m]:	0.006	Area[m^2]
Orifice dimension[m]:	0.0262	0.000539129
Pipe Diameter [m]:	0.046	0.001661903
Diameter ratio	0.570	
Aspect ratio	0.229	
g[m/s^2]	9.81	

Appendices

Material Type:	Bentonite
Density[kg/m^3]:	1058.2
Concentration[%]:	9%
τ_y[Pa]:	7.18
K [Pa.s]:	0.04
n:	1.00
PPT used:	110
Range selected:	0-500

1/n	n/(n+1)	(n+1)/n	$K^{1/n}$
1	0.5	2	0.038

	Pod 1	Pod 2	Pod 3	Pod 4	Pod 5	Pod 6	Pod 7	Pod 8	Pod 9	Pod 10	Pod 11
Axial distances	-6.95	-4.65	-3.73	-2.35	-0.06	-0.03	0.03	2.33	4.63	6.93	9.23
N-D distances incl.[L/D]:	-151.05	-101.05	-81.05	-51.05	-1.27	-0.62	0.62	50.62	100.62	150.62	200.62
Distances[m]:	0.00	2.30	3.22	4.60	6.89	6.92	6.98	9.28	11.58	13.88	16.18

Pod 1 [Pa]	Pod 2 [Pa]	Pod 3 [Pa]	Pod 4 [Pa]	Pod 5 [Pa]	Pod 6 [Pa]	Pod 7 [Pa]	Pod 8 [Pa]	Pod 9 [Pa]	Pod 10 [Pa]	Pod 11 [Pa]	Average Q [l/s]
130273	124105	121150	117269	111905	111921	23987	48464	42853	37230	30573	5.00
130540	123804	121150	117621	111955	111252	24848	48053	43066	36935	30868	5.00
120477	114777	111923	108518	103086	101855	27191	46582	41069	35925	29737	4.66
120477	114404	112148	108379	102536	102634	26029	46741	40614	35882	30181	4.65
114347	108943	106843	103323	97028	96806	28750	46491	40981	36172	31251	4.42
114242	108682	106843	103289	97611	96066	28370	46971	40981	35673	30041	4.42
107231	100913	98883	95363	90211	89419	30565	46184	40773	35372	29871	4.06
106590	101017	98941	95616	90049	89392	29994	45809	40149	35033	30044	4.06
99662	94108	91917	88496	82968	82112	32495	44358	39646	35027	29570	3.70
99403	94038	91915	88297	83100	82052	31915	45042	39597	34710	29307	3.70
96278	91053	88593	85241	79150	79151	38975	47398	42925	38061	31616	3.31
96664	91006	88599	85201	80016	78695	39042	47578	42861	38074	32682	3.31
90399	85499	83653	80631	75395	74634	44172	50076	45191	40311	35358	2.88
91792	86491	84501	81193	76240	74913	44056	50440	45582	40071	35665	2.88
87663	82787	80706	77770	72816	71941	46493	51413	46550	41684	36217	2.58
88218	83255	81306	78121	73178	72438	46356	51506	46493	41587	36753	2.58
84491	79803	77995	74885	69916	69613	52196	53641	49019	44322	39392	2.12
84563	79893	77780	74633	69919	69296	51818	53613	49051	44256	39312	2.12
78736	73945	72114	69160	64192	63877	53817	52958	48601	43689	38987	1.69
78574	74262	72426	69234	64665	63942	53870	52786	48631	43850	39178	1.68
74988	70671	68960	66003	61429	60899	55789	52908	48409	43811	38688	1.31
75210	71029	69139	66081	61559	60947	55289	52716	48493	44471	38805	1.31
72244	68423	66840	64123	59736	59183	57392	53350	48974	44851	38805	0.92

Water

Orifice Type:	Short	
Orifice thickness[m]:	0.006	Area[m^2]
Orifice dimension[m]:	0.0262	0.000539129
Pipe Diameter [m]:	0.046	0.001661903
Diameter ratio	0.570	
Aspect ratio	0.229	
g[m/s^2]	9.81	
Material Type:	Water	
Density[kg/m^3]:	998.5	
Concentration[%]:	100%	
τ_y[Pa]:	0	
K [Pa.s]:	0.001	
n:	1	
PPT used:	110	
Range selected:	0-500	

1/n	n/(n+1)	(n+1)/n	$K^{1/n}$
1	0.5	2	0.001

	Pod 1	Pod 2	Pod 3	Pod 4	Pod 5	Pod 6	Pod 7	Pod 8	Pod 9	Pod 10	Pod 11
Axial distances	-5.29	-4.68	-3.74	-2.36	-0.06	-0.03	0.03	2.34	4.65	6.97	9.29
N-D distances incl.[L/D]:	-115.05	-101.68	-81.38	-51.27	-1.38	-0.62	0.62	50.83	101.16	151.60	201.92
Distances[m]:	0.00	0.62	1.55	2.93	5.23	5.26	5.32	7.63	9.95	12.27	14.58

Pod 1	Pod 2	Pod 3	Pod 4	Pod 5	Pod 6	Pod 7	Pod 8	Pod 9	Pod 10	Pod 11	Average Q
[Pa]	[Pa]	[Pa]	[Pa]	[Pa]	[Pa]	[Pa]	[Pa]	[Pa]	[Pa]	[Pa]	[l/s]
111104	109316	108029	105131	100791	101344	-2553	28862	24379	20302	15811	5.17
110983	109165	107948	105082	100804	101696	-2740	29411	24631	20080	15811	5.17
97767	96137	94762	92139	88556	89063	-1523	26304	22225	18535	14644	4.81
97260	95743	94676	92042	88522	88713	-1487	26441	22052	18486	14521	4.81
83328	82038	80833	78706	75707	76076	106	23491	19662	16499	13320	4.41
83596	81785	80713	78648	75512	75915	831	22887	19648	16465	13231	4.41
73546	72254	71522	69614	66895	67176	1110	21477	17994	14723	12245	4.12
73390	72333	71230	69461	66758	67253	961	21249	17978	14502	12285	4.12
63102	62164	61105	59554	57259	57425	1668	18627	16439	13666	11270	3.78
62898	62103	61129	59749	57199	57443	1941	19081	16104	13547	11271	3.77
51943	51024	50431	49044	47169	47301	2794	15882	14184	12223	10181	3.37
51969	51108	50447	49092	47158	47348	3054	15957	14084	12112	10168	3.37
43249	42542	42125	40941	39159	39509	3605	14738	12598	10966	9281	3.03
43249	42554	42189	40996	39276	39537	4057	14585	12595	11179	9372	3.03
35829	35314	34915	33930	32693	32817	4576	12984	11300	9881	8650	2.71
35865	35315	34897	33921	32541	32797	4208	12962	11314	9934	8679	2.71

Pod 1	Pod 2	Pod 3	Pod 4	Pod 5	Pod 6	Pod 7	Pod 8	Pod 9	Pod 10	Pod 11	Average Q
[Pa]	[Pa]	[Pa]	[Pa]	[Pa]	[Pa]	[Pa]	[Pa]	[Pa]	[Pa]	[Pa]	[l/s]
28544	28191	27729	27136	26131	26181	4632	11251	9967	8789	7904	2.35
28927	28125	27818	27121	26140	26256	4700	11307	9994	8396	7875	2.35
23440	23193	22969	22329	21526	21646	5784	10067	9041	8181	7401	2.06
23492	23246	22898	22364	21621	21617	4649	10041	9066	8314	7445	2.07
18493	18346	18092	17638	17075	17132	5065	8894	8146	7359	6944	1.79
18788	18308	18128	17680	17080	17161	4917	8846	8021	7516	6949	1.79
14801	14634	14564	14181	13810	13845	5436	8012	7474	7025	6586	1.50
15151	14716	14524	14219	13763	13882	5305	8049	7396	7043	6586	1.50
15453	15033	14888	14689	14405	14415	9482	10939	10648	10378	10157	1.16
15293	15012	14898	14738	14496	14411	9419	10928	10589	10384	10081	1.16
12254	12195	12121	12021	11866	11870	9329	10169	9977	9923	9743	0.81
10493	10560	10416	10356	10326	10300	9312	9602	9526	9540	9512	0.51

ORIFICE DIAMETER RATIO, $\beta = 0.57$ (sharp apex)

CMC 6%

Orifice Type:	Short	
Orifice thickness[m]:	0.006	Area[m^2]
Orifice dimension[m]:	0.0262	0.000539129
Pipe Diameter [m]:	0.046	0.001661903
Diameter ratio	0.570	
Aspect ratio	0.229	
g[m/s^2]	9.81	
Material Type:	CMC	
Density[kg/m^3]:	1036	
Concentration[%]:	6%	
τ_y[Pa]:	0	
K [Pa.s]:	3.40	
n:	0.61	
PPT used:	110	
Range selected:	0-500	

1/n	n/(n+1)	(n+1)/n	$K^{1/n}$
1.64	0.38	2.64	7.48

	Pod 1	Pod 2	Pod 3	Pod 4	Pod 5	Pod 6	Pod 7	Pod 8	Pod 9	Pod 10	Pod 11
Axial distances	-6.96	-4.66	-3.74	-2.36	-0.07	-0.03	0.03	2.51	4.81	7.11	9.41
N-D distances incl.[L/D]:	-151.27	-101.27	-81.27	-51.38	-1.49	-0.62	0.62	54.47	104.47	154.47	204.47
Distances[m]:	0.00	2.30	3.22	4.60	6.89	6.93	6.99	9.46	11.76	14.06	16.36

Pod 1	Pod 2	Pod 3	Pod 4	Pod 5	Pod 6	Pod 7	Pod 8	Pod 9	Pod 10	Pod 11	Average Q
[Pa]	[Pa]	[Pa]	[Pa]	[Pa]	[Pa]	[Pa]	[Pa]	[Pa]	[Pa]	[Pa]	[l/s]
382755	351289	338697	319743	288338	289235	211511	205760	174145	142121	117047	5.05
361891	331933	319792	302218	271649	273751	204528	197172	166124	135656	109104	4.75
335641	307193	295777	278943	250153	250192	196187	186675	158011	129294	100279	4.34
312228	285778	275243	258430	232074	231799	188475	177242	150298	122560	94990	3.99
293813	268302	258030	242803	217208	216970	180686	169191	143412	117669	91126	3.67
293751	267805	257494	241884	216674	216290	180808	168498	142290	116802	91092	3.67
271521	247619	238062	223523	199740	199448	171202	158904	134711	110463	86581	3.31
259113	236088	226701	212938	190087	190273	165709	152986	130111	106767	83499	3.10
243130	221412	212763	199890	178139	178689	158072	145750	123996	102069	80372	2.85
225679	205883	197651	185342	165122	165083	149565	136625	116224	95908	75178	2.53
210368	191854	184282	172878	154074	154858	140577	128361	109589	98546	72623	2.23
194878	177853	170932	160830	143463	144385	132889	120418	102946	85610	68966	1.98
181746	165853	159425	149560	133829	133685	125672	113476	97046	80775	66474	1.77
164021	149761	144138	135508	121345	121105	115693	103414	89020	74749	59699	1.49
147461	134889	129796	122079	109446	110280	105485	94125	81775	68417	55447	1.21
147104	134465	129440	122013	109237	110028	105503	94482	81911	69089	55545	1.21
135290	123670	119319	112496	100933	101929	98100	87863	76012	64250	52429	1.03
129852	118919	114701	108203	97355	97361	94938	84619	73499	62355	51351	0.95
124303	114538	110465	104481	94717	95374	92789	83218	71993	63062	53080	0.80
123401	113319	109446	103598	93985	94562	92232	82508	72768	62743	52917	0.80
113014	104192	100758	95541	86871	86808	85322	77049	68107	58931	50095	0.65
112423	104345	100980	95555	87090	87458	85511	76790	68018	59132	50088	0.65
99359	91869	88821	84499	76919	77601	76301	68826	61585	54251	48438	0.52
87548	81235	78925	75269	69166	69083	68476	62054	56195	49831	43579	0.37
73582	67466	65262	62511	57878	58153	57455	52742	48281	43734	39134	0.22
52933	50329	49164	47617	45195	45519	44790	42299	39646	37265	34738	0.10
87559	81392	78934	75203	68997	69671	69426	62188	56087	50392	43606	0.36

Kaolin 14%

Orifice Type:	Short	
Orifice thickness[m]:	0.006	Area[m^2]
Orifice dimension[m]:	0.0262	0.000539129
Pipe Diameter [m]:	0.046	0.001661903
Diameter ratio	0.570	
Aspect ratio	0.229	
g[m/s^2]	9.81	
Material Type:	Kaolin	
Density[kg/m^3]:	1227.2	
Concentration[%]:	14%	
τ_y[Pa]:	3.10	
K [Pa.s]:	0.08	
n:	0.80	

Appendices

PPT used:	110
Range selected:	0-500

1/n	n/(n+1)	(n+1)/n	$K^{1/n}$
1.25	0.44	2.25	0.05

	Pod 1	Pod 2	Pod 3	Pod 4	Pod 5	Pod 6	Pod 7	Pod 8	Pod 9	Pod 10	Pod 11
Axial distances	-5.29	-4.68	-3.74	-2.36	-0.06	-0.03	0.03	2.34	4.65	6.97	9.29
N-D distances incl.[L/D]:	-115.05	-101.68	-81.38	-51.27	-1.38	-0.62	0.62	50.83	101.16	151.60	201.92
Distances[m]:	0.00	0.62	1.55	2.93	5.23	5.26	5.32	7.63	9.95	12.27	14.58

Pod 1	Pod 2	Pod 3	Pod 4	Pod 5	Pod 6	Pod 7	Pod 8	Pod 9	Pod 10	Pod 11	Average Q
[Pa]	[Pa]	[Pa]	[Pa]	[Pa]	[Pa]	[Pa]	[Pa]	[Pa]	[Pa]	[Pa]	[l/s]
137954	136275	133906	130371	124799	124889	5799	39728	34103	27925	22259	5.22
137955	136275	133906	130371	124799	124889	5799	39728	34103	27925	22259	5.22
122865	120879	118677	115100	110292	110220	8051	36948	31021	25817	20997	4.90
122865	120879	118388	114848	109908	109823	7770	36636	31010	26113	20818	4.89
104611	103296	101682	98618	94462	94544	9621	33340	28139	23698	19422	4.49
104945	103227	101490	98618	94386	94522	9848	33077	27900	23699	19365	4.50
92294	91108	89464	87002	83336	83388	10149	30422	25998	22069	18205	4.18
91959	91119	89493	86808	83220	83076	10068	30578	26105	22283	18160	4.18
84152	83032	81385	79463	76143	76065	17210	33976	29898	26832	23310	3.79
84152	83032	81385	79463	76143	76065	17210	33976	29898	26832	23310	3.78
71755	70526	68984	66318	63324	63334	12748	29545	25883	22223	19664	3.49
74182	73395	72258	70174	67019	67316	18224	31874	28214	25897	22570	3.45
64678	63211	62030	60389	57398	57396	15677	27305	23962	21154	19149	3.19
64678	63211	62030	60389	57398	57396	15508	27060	23918	21367	18874	3.20
58940	57653	56403	54826	52405	51787	20782	28777	26156	23959	21403	2.80
58940	57653	56403	54826	52405	51787	20549	28690	25862	23803	21424	2.80
50793	50245	49526	48141	46167	45817	23635	28696	26099	23930	21777	2.39
50958	50347	49282	47849	45795	45540	22654	27924	25788	24043	21449	2.40
48054	47592	46829	45453	43371	42898	25548	29024	26819	25075	22455	2.10
47343	46738	45889	44330	42131	41736	24976	28238	25864	23841	21982	2.11
44217	43523	42769	41288	39182	39115	25551	27947	26020	24132	21805	1.88
44217	43523	42769	41288	39182	39115	25551	27947	26020	24132	21805	1.89
41740	41144	40480	39120	37225	36807	28693	29464	27629	25025	23779	1.48
41740	41144	40480	39120	37225	36807	28693	29464	27629	25025	23779	1.48
38578	38130	37357	36268	34374	34254	29105	29047	27190	25468	23560	1.14
39093	38257	37566	36322	34475	34097	29005	29010	27288	25727	23652	1.14
34382	34144	33458	32339	30804	30610	28680	27729	26134	24440	22786	0.73

Kaolin 21%

Orifice Type:	Short	
Orifice thickness[m]:	0.006	Area[m^2]
Orifice dimension[m]:	0.0262	0.000539129
Pipe Diameter [m]:	0.046	0.001661903
Diameter ratio	0.570	
Aspect ratio	0.229	
g[m/s^2]	9.81	
Material Type:	Kaolin	
Density[kg/m^3]:	1348.9	
Concentration[%]:	21%	
τ_y[Pa]:	23.48	
K [Pa.s]:	5.43	
n:	0.35	
PPT used:	110	
Range selected:	0-500	

1/n	n/(n+1)	(n+1)/n	$K^{1/n}$
2.9	0.3	3.9	129.9

	Pod 1	Pod 2	Pod 3	Pod 4	Pod 5	Pod 6	Pod 7	Pod 8	Pod 9	Pod 10	Pod 11
Axial distances	-5.29	-4.68	-3.74	-2.36	-0.06	-0.03	0.03	2.34	4.65	6.97	9.29
N-D distances incl.[L/D]:	-115.05	-101.68	-81.38	-51.27	-1.38	-0.62	0.62	50.83	101.16	151.60	201.92
Distances[m]:	0.00	0.62	1.55	2.93	5.23	5.26	5.32	7.63	9.95	12.27	14.58

Pod 1	Pod 2	Pod 3	Pod 4	Pod 5	Pod 6	Pod 7	Pod 8	Pod 9	Pod 10	Pod 11	Average Q
[Pa]	[Pa]	[Pa]	[Pa]	[Pa]	[Pa]	[Pa]	[Pa]	[Pa]	[Pa]	[Pa]	[l/s]
172425	169457	164853	157108	145736	145766	91501	99408	87701	76327	64718	3.48
172425	169457	164853	157108	145736	145766	90465	99569	87548	76066	64487	3.48
165916	163139	158019	150431	139903	138228	93584	98989	87520	77006	65012	3.19
165916	163139	158019	150431	139903	138228	92985	98568	87440	76444	64712	3.18
159118	155884	150741	144443	134049	132783	96321	98795	87766	76592	65113	2.86
159204	156205	151022	144450	132927	132919	95206	98441	87314	75850	64808	2.86
153790	151034	146269	138933	128783	127579	98949	98969	88330	77454	66525	2.51
153414	150922	146307	138319	128490	126955	99026	98649	88113	76297	65560	2.51
149063	146751	142075	135431	124878	123814	101371	99807	89709	78586	67472	2.16
149048	146886	141993	134088	123564	121841	100832	97931	88056	77139	66108	2.18
144499	142074	137261	130027	120304	118066	99504	97526	88137	77238	66559	1.94
143985	141730	136954	129858	120036	118452	100374	97498	87794	77069	66405	1.94
138523	136921	132318	125931	115864	114143	102031	97890	88018	78160	67666	1.58
138935	136604	132208	125188	115577	114106	101634	97833	87884	77192	66332	1.58
134703	132784	128212	121581	112205	110816	102921	97757	87755	78119	67303	1.31
134703	132784	128212	121581	112205	110816	102921	97757	87755	78119	67303	1.31

Pod 1	Pod 2	Pod 3	Pod 4	Pod 5	Pod 6	Pod 7	Pod 8	Pod 9	Pod 10	Pod 11	Average Q
[Pa]	[Pa]	[Pa]	[Pa]	[Pa]	[Pa]	[Pa]	[Pa]	[Pa]	[Pa]	[Pa]	[l/s]
127861	125838	121876	115411	106488	104747	99491	93952	85323	75401	66096	0.98
127883	125910	122003	115493	106946	104463	96216	93593	85542	75532	65680	0.97
123556	121853	117445	111525	103187	101748	96801	91732	83273	74456	64098	0.72

Kaloin 24%

Orifice Type:	Short	
Orifice thickness[m]:	0.006	Area[m^2]
Orifice dimension[m]:	0.0262	0.000539129
Pipe Diameter [m]:	0.046	0.001661903
Diameter ratio	0.570	
Aspect ratio	0.229	
g[m/s^2]	9.81	
Material Type:	Kaolin	
Density[kg/m^3]:	1392.9	
Concentration[%]:	24%	
τ_y[Pa]:	35.28	
K [Pa.s]:	10.04	
n:	0.41	
PPT used:	110	
Range selected:	0-500	

1/n	n/(n+1)	(n+1)/n	$K^{1/n}$
2.46	0.29	3.46	292.34

	Pod 1	Pod 2	Pod 3	Pod 4	Pod 5	Pod 6	Pod 7	Pod 8	Pod 9	Pod 10	Pod 11
Axial distances	-5.29	-4.68	-3.74	-2.36	-0.06	-0.03	0.03	2.34	4.65	6.97	9.29
N-D distances incl.[L/D]:	-115.05	-101.68	-81.38	-51.27	-1.38	-0.62	0.62	50.83	101.16	151.60	201.92
Distances[m]:	0.00	0.62	1.55	2.93	5.23	5.26	5.32	7.63	9.95	12.27	14.58

Pod 1	Pod 2	Pod 3	Pod 4	Pod 5	Pod 6	Pod 7	Pod 8	Pod 9	Pod 10	Pod 11	Average Q
[Pa]	[Pa]	[Pa]	[Pa]	[Pa]	[Pa]	[Pa]	[Pa]	[Pa]	[Pa]	[Pa]	[l/s]
210347	206656	200053	189323	171209	169918	154143	143208	124685	107106	90363	1.97
209919	206130	199094	189206	172093	168571	154045	141862	125045	107725	90606	1.81
203848	200241	193208	182897	166607	165218	150211	142278	123540	106799	89819	1.71
203761	200221	192737	182759	167416	160691	153418	142058	124416	107064	89982	1.68
195692	191579	185023	175511	159601	154297	150046	138977	121125	105038	88626	1.36
195370	191658	184786	175478	159432	154674	150424	138480	121564	105076	89104	1.30
190626	187046	180405	170987	156140	150395	147001	135258	119700	103479	87945	1.13
191135	187654	180405	170987	155809	154106	146464	137025	120355	104652	88550	1.06
184313	181222	174786	165118	150895	143834	140346	132634	117171	102139	86326	0.79

Pod 1	Pod 2	Pod 3	Pod 4	Pod 5	Pod 6	Pod 7	Pod 8	Pod 9	Pod 10	Pod 11	Average Q
[Pa]	[Pa]	[Pa]	[Pa]	[Pa]	[Pa]	[Pa]	[Pa]	[Pa]	[Pa]	[Pa]	[l/s]
176833	173718	169148	160113	146614	140249	134599	130319	114767	100324	86198	0.61
168804	165522	159105	150767	137890	135427	133538	121559	108617	95314	81921	0.41
168856	164881	158995	150020	136885	132551	132151	120471	107769	95816	81516	0.44
163449	160359	154497	146729	133059	130016	129964	119131	107525	94623	81480	0.35
163596	160601	154857	145822	134720	128277	128601	117949	106707	94836	81248	0.40
160162	157056	151381	142919	129526	123998	117879	115567	104087	92480	79109	0.29
160162	157056	151628	142508	130379	124699	121471	114734	103514	91931	80046	0.26
151503	148549	142782	134759	122820	118081	114337	107608	97022	87202	76155	0.13
149330	146072	140702	132563	121449	115310	110979	103932	93857	85043	74842	0.15

Bentonite 6%

Orifice Type:	Short	
Orifice thickness[m]:	0.006	Area[m^2]
Orifice dimension[m]:	0.0262	0.000539129
Pipe Diameter [m]:	0.046	0.001661903
Diameter ratio	0.570	
Aspect ratio	0.229	
g[m/s^2]	9.81	
Material Type:	Bentonite	
Density[kg/m^3]:	1040.1	
Concentration[%]:	6%	
τ_y[Pa]:	2.4	
K [Pa.s]:	0.0241	
n:	1	
PPT used:	110	
Range selected:	0-500	

1/n	n/(n+1)	(n+1)/n	$K^{1/n}$
1	0.5	2	0.0241

	Pod 1	Pod 2	Pod 3	Pod 4	Pod 5	Pod 6	Pod 7	Pod 8	Pod 9	Pod 10	Pod 11
Axial distances	-6.95	-4.65	-3.73	-2.35	-0.06	-0.03	0.03	2.33	4.63	6.93	9.23
N-D distances incl.[L/D]:	-151.05	-101.05	-81.05	-51.05	-1.27	-0.62	0.62	50.62	100.62	150.62	200.62
Distances[m]:	0.00	2.30	3.22	4.60	6.89	6.92	6.98	9.28	11.58	13.88	16.18

Pod 1	Pod 2	Pod 3	Pod 4	Pod 5	Pod 6	Pod 7	Pod 8	Pod 9	Pod 10	Pod 11	Average Q
[Pa]	[Pa]	[Pa]	[Pa]	[Pa]	[Pa]	[Pa]	[Pa]	[Pa]	[Pa]	[Pa]	[l/s]
153656	146067	143704	138507	132479	130777	16712	47415	38833	32042	24602	5.84
153093	145347	142733	137935	131526	130905	16126	46715	38487	31899	24916	5.81
145254	137530	134560	130424	124021	122630	16525	45326	37202	31181	24357	5.60

Pod 1	Pod 2	Pod 3	Pod 4	Pod 5	Pod 6	Pod 7	Pod 8	Pod 9	Pod 10	Pod 11	Average Q
[Pa]	[Pa]	[Pa]	[Pa]	[Pa]	[Pa]	[Pa]	[Pa]	[Pa]	[Pa]	[Pa]	[l/s]
127069	121716	118671	115233	109286	107381	16761	40852	34259	28260	23103	5.23
116022	110107	107513	104186	98689	96386	16630	38009	32318	27275	21472	4.92
115434	109846	107178	104083	98947	97723	16022	37735	32535	27394	21498	4.94
103322	98519	96508	92953	88941	88083	16855	34781	30322	25389	20367	4.62
103502	97948	96023	92705	88808	89034	16451	35586	30083	25557	20276	4.61
94403	89435	87648	84781	80415	79979	15225	32176	27632	23289	18988	4.41
94419	89771	88060	84813	81038	79741	15426	33434	27954	23650	19095	4.38
80031	76514	74735	72217	68671	68285	14968	28646	24810	21184	17328	3.98
80131	76456	74741	72454	68630	68088	13957	29328	24757	20944	17219	3.99
72881	69065	67611	65389	62292	61883	15150	27914	23899	20328	16609	3.75
72444	69356	68183	65954	62425	62810	14543	28404	24188	20195	16642	3.75
69841	66852	65456	63710	60547	59607	19617	30450	27141	24229	21129	3.51
69563	66673	65300	63461	61013	59419	18873	30235	27349	24367	21166	3.51
55901	52914	51972	50258	48422	47706	16498	24969	21470	19323	16868	3.13
54830	52261	50859	50301	47645	47911	15154	24920	21977	19186	17051	3.13
51251	49305	48085	46530	44417	43918	17337	24043	22172	19954	17578	2.85
51274	48651	47584	46315	44209	44244	18164	24081	22323	20024	17724	2.85
48684	46379	45692	44072	42197	41156	20177	25709	23465	21481	19275	2.53
48638	46513	45264	43959	41892	41738	20204	26061	23524	21727	19391	2.53
43265	41280	40595	39283	37325	36669	21391	24987	22914	20999	18928	2.13
43158	41057	40190	38960	37046	36904	21224	24631	23219	21436	19371	2.13
39822	37837	37102	35901	33832	33442	22250	24234	22760	20832	18936	1.83
37167	35423	34726	33688	31719	31398	23559	24004	22954	21293	19404	1.52
37447	35746	35011	33976	32032	31725	23585	24134	23183	21450	19380	1.55
34923	33292	32593	31572	29620	29245	24554	23956	22848	21232	19128	1.22
35050	33328	32526	31578	29602	29314	24556	24235	22741	20981	19129	1.24
32743	31120	30357	29487	27586	27169	24675	24316	22320	20456	18894	0.95
32827	31124	30344	29565	27659	27278	24819	24183	22341	20854	19063	0.95
62034	59682	58875	57221	54880	54938	19032	29304	26449	23658	20792	3.42

Bentonite 9%

Orifice Type:	Short	
Orifice thickness[m]:	0.006	Area[m^2]
Orifice dimension[m]:	0.0262	0.000539129
Pipe Diameter [m]:	0.046	0.001661903
Diameter ratio	0.570	
Aspect ratio	0.229	
g[m/s^2]	9.81	
Material Type:	Bentonite	
Density[kg/m^3]:	1058.2	
Concentration[%]:	9%	

τ_y[Pa]:	7.183
K [Pa.s]:	0.038
n:	1.00
PPT used:	110
Range selected:	0-500

1/n	n/(n+1)	(n+1)/n	$K^{1/n}$
1	0.5	2	0.0377361

	Pod 1	Pod 2	Pod 3	Pod 4	Pod 5	Pod 6	Pod 7	Pod 8	Pod 9	Pod 10	Pod 11
Axial distances	-6.95	-4.65	-3.73	-2.35	-0.06	-0.03	0.03	2.33	4.63	6.93	9.23
N-D distances incl.[L/D]:	-151.05	-101.05	-81.05	-51.05	-1.27	-0.62	0.62	50.62	100.62	150.62	200.62
Distances[m]:	0.00	2.30	3.22	4.60	6.89	6.92	6.98	9.28	11.58	13.88	16.18

Pod 1 [Pa]	Pod 2 [Pa]	Pod 3 [Pa]	Pod 4 [Pa]	Pod 5 [Pa]	Pod 6 [Pa]	Pod 7 [Pa]	Pod 8 [Pa]	Pod 9 [Pa]	Pod 10 [Pa]	Pod 11 [Pa]	Average Q [l/s]
122692	115910	113642	110128	104754	103547	26379	47648	41330	35634	30323	4.90
122599	115971	113642	110151	104498	104023	26977	46947	41347	35043	29936	4.90
117887	111946	110357	106046	100655	100849	27613	46233	41292	35944	30011	4.76
117665	112293	109966	106650	100655	100506	27533	46693	41043	35612	30533	4.75
109498	103712	101500	97993	92638	91845	30397	45462	40968	35177	29834	4.36
109624	103712	101611	97845	92353	91827	29634	45752	40464	35255	29706	4.36
102947	97563	95162	91737	86540	83516	31965	44735	39928	35101	29919	4.04
103118	97543	95460	91938	86904	85561	31888	44735	40976	35432	29975	4.03
96394	91108	88919	85346	80224	79823	33255	44723	39500	34419	29161	3.69
96419	91288	88730	85320	80225	79344	32638	44572	39278	34194	28959	3.69
92236	86627	83917	80617	75909	74929	37338	45142	40650	35602	30423	3.33
92152	86996	84041	81309	76243	74564	37880	45156	39784	34835	29540	3.34
88612	83210	81210	77900	72814	71700	46554	50677	45901	40781	35970	2.71
88362	83210	81064	77885	72983	71622	46622	50602	45868	41059	35484	2.71
83188	78542	76385	73373	68317	66940	48341	50453	45806	40963	36107	2.32
83426	78586	76538	73350	68405	67331	48102	50636	46114	41205	36199	2.32
78957	74215	72212	69171	64496	63632	50302	50488	46006	41341	36693	1.97
79099	74454	72464	69357	64594	64042	50212	50469	46133	42067	36916	1.96
75392	71095	69409	66383	61874	60964	53774	51552	47702	43212	38056	1.52
75965	71209	69359	66379	61694	61110	53712	51671	47578	42934	38623	1.50
71270	67083	65323	62549	58035	57069	55097	51053	46919	42328	37752	1.04
71391	67220	65534	62520	58155	58322	55558	51048	47116	42567	37516	1.04

Water

Orifice Type:	Short	
Orifice thickness[m]:	0.006	Area[m^2]
Orifice dimension[m]:	0.0262	0.000539129
Pipe Diameter [m]:	0.046	0.001661903
Diameter ratio	0.570	
Aspect ratio	0.229	
g[m/s^2]	9.81	
Material Type:	Water	
Density[kg/m^3]:	998.5	
Concentration[%]:	100%	
τ_y[Pa]:	0	
K [Pa.s]:	0.001	
n:	1	
PPT used:	110	
Range selected:	0-500	

1/n	n/(n+1)	(n+1)/n	$K^{1/n}$
1	0.5	2	0.001

	Pod 1	Pod 2	Pod 3	Pod 4	Pod 5	Pod 6	Pod 7	Pod 8	Pod 9	Pod 10	Pod 11
Axial distances	-5.29	-4.68	-3.74	-2.36	-0.06	-0.03	0.03	2.34	4.65	6.97	9.29
N-D distances incl.[L/D]:	-115.05	-101.68	-81.38	-51.27	-1.38	-0.62	0.62	50.83	101.16	151.60	201.92
Distances[m]:	0.00	0.62	1.55	2.93	5.23	5.26	5.32	7.63	9.95	12.27	14.58

Pod 1	Pod 2	Pod 3	Pod 4	Pod 5	Pod 6	Pod 7	Pod 8	Pod 9	Pod 10	Pod 11	Average Q
[Pa]	[Pa]	[Pa]	[Pa]	[Pa]	[Pa]	[Pa]	[Pa]	[Pa]	[Pa]	[Pa]	[l/s]
109252	107514	105895	102851	98956	99370	1884	30063	24946	20710	16364	5.19
109146	107772	105963	103091	99275	99537	1884	29484	25026	20504	16328	5.19
95712	94135	92943	90867	86793	86838	3456	26723	22644	18786	15136	4.82
95302	94197	92943	90386	86533	86608	2778	26621	22090	18406	14668	4.82
82413	81168	79925	78032	74894	74752	3824	23689	20182	16561	13392	4.45
82290	81003	79942	77953	74629	74778	4164	23516	20135	16834	13490	4.45
72575	71570	70441	68619	65774	66023	4613	21765	18389	15326	12604	4.15
72664	71591	70528	68672	65770	65951	4132	21788	18311	15429	12582	4.15
63027	62229	61233	59715	57203	57304	4729	19712	16667	14183	11705	3.83
63097	61973	61116	59553	57244	57122	5763	19607	16639	14115	11664	3.83
55492	54491	53886	52573	50252	50437	4331	18020	15366	13093	11048	3.56
55531	54540	53792	52370	50315	50324	5199	17488	15268	13159	10955	3.56
46594	45911	45329	43892	42189	42457	4879	16037	13666	11817	10110	3.21
46938	45891	45281	44037	42388	42243	5433	15997	13658	11773	10090	3.21
38979	38408	37916	36970	35516	35648	6074	14169	12292	10738	9356	2.88
39111	38356	37960	36876	35512	35510	6038	14232	12286	10938	9353	2.89

Pod 1	Pod 2	Pod 3	Pod 4	Pod 5	Pod 6	Pod 7	Pod 8	Pod 9	Pod 10	Pod 11	Average Q
[Pa]	[Pa]	[Pa]	[Pa]	[Pa]	[Pa]	[Pa]	[Pa]	[Pa]	[Pa]	[Pa]	[l/s]
26566	26159	25809	25128	24286	24375	5745	11274	9963	9201	8086	2.25
26566	26144	25810	25135	24334	24294	6252	11020	9970	9310	8158	2.26
20724	20451	20194	19749	18945	18993	5520	9581	8868	8360	7562	1.94
20724	20405	20183	19753	19096	18950	5830	9776	8955	8231	7498	1.94
16419	16169	15957	15605	15188	15203	5792	8720	8034	7645	7013	1.62
16582	16167	15979	15676	15121	15243	5937	8658	8031	7613	7096	1.62
16605	16470	16357	16156	15772	15784	9846	11603	11278	10964	10720	1.30
16949	16513	16323	16116	15800	15810	9923	11711	11275	11002	10650	1.29
13835	13813	13689	13569	13313	13341	9872	10900	10721	10536	10279	0.99
13826	13791	13698	13561	13375	13369	9975	10977	10714	10498	10223	0.99
16520	16453	16422	16337	16187	16167	14774	15313	15100	15116	15022	0.59

ORIFICE DIAMETER RATIO, $\beta = 0.7$

CMC 6%

Orifice Type:	Short	
Orifice thickness[m]:	0.006	Area[m^2]
Orifice dimension[m]:	0.0322	0.000814332
Pipe Diameter [m]:	0.046	0.001661903
Diameter ratio	0.7	
Aspect ratio	0.19	
g[m/s^2]	9.81	
Material Type:	CMC	
Density[kg/m^3]:	1036	
Concentration[%]:	6%	
τ_y[Pa]:	0	
K [Pa.s]:	3.40	
n:	0.61	
PPT used:	110	
Range selected:	0-500	

1/n	n/(n+1)	(n+1)/n	$K^{1/n}$
1.64	0.38	2.64	7.48

	Pod 1	Pod 2	Pod 3	Pod 4	Pod 5	Pod 6	Pod 7	Pod 8	Pod 9	Pod 10	Pod 11
Axial distances	-6.96	-4.66	-3.74	-2.36	-0.07	-0.03	0.03	2.51	4.81	7.11	9.41
N-D distances incl.[L/D]:	-151.27	-101.27	-81.27	-51.38	-1.49	-0.62	0.62	54.47	104.47	154.47	204.47
Distances[m]:	0.00	2.30	3.22	4.60	6.89	6.93	6.99	9.46	11.76	14.06	16.36

Pod 1	Pod 2	Pod 3	Pod 4	Pod 5	Pod 6	Pod 7	Pod 8	Pod 9	Pod 10	Pod 11	Average Q
[Pa]	[Pa]	[Pa]	[Pa]	[Pa]	[Pa]	[Pa]	[Pa]	[Pa]	[Pa]	[Pa]	[l/s]
383474	348956	335067	313456	277479	276848	232745	231642	195356	159448	123471	5.62
362549	328302	314526	294409	261351	261347	229551	220180	185919	151928	117901	5.19
347027	314369	301084	281415	249043	248756	211733	211130	178697	146082	113310	4.91
326231	295414	283016	264699	234157	233795	199885	199001	167882	137138	106365	4.46
311697	283224	271927	254489	225069	224818	192411	191973	161734	132592	102024	4.22
299421	271046	259869	242889	214831	214855	194114	183355	155263	127273	97509	3.91
297953	271424	260118	243243	215482	216658	184180	182920	154284	125978	97462	3.92
286779	259692	248939	232813	206036	207645	186229	175392	148337	120973	94823	3.63
267337	242588	232701	217925	192382	192645	175053	164882	140071	114168	88404	3.26
266566	241790	232106	217332	192586	192091	174552	164843	139149	114419	88375	3.27
249846	226305	217067	203178	180423	179899	163926	153826	130926	107870	83572	2.89
237736	216129	207264	194177	171991	171772	156723	147263	125216	103415	81058	2.66
224136	204344	196332	183817	163037	162796	148726	140247	119300	99014	77287	2.42
206911	187807	180746	169512	150499	151833	137561	130207	110523	91282	71814	2.08
186511	169277	163111	153366	136468	136597	124503	118560	101527	85175	66710	1.77
171491	156127	150153	141025	125677	125588	114018	109335	93429	78428	62395	1.51
153326	139888	134479	126414	113584	113258	111724	88195	84671	71029	57486	1.21
139781	127481	122619	115531	103462	103298	102337	80295	78229	66423	54166	1.01
133293	122297	118016	111448	100576	100403	99771	78935	77760	67149	55598	0.86
121264	111330	107373	101730	92109	92138	91496	71929	72087	62454	52207	0.72
113610	104681	101413	96071	87244	87165	86587	67745	68459	59866	50129	0.62
97261	89993	87136	82895	75681	75670	75388	58213	60991	54313	46173	0.45
89330	83157	80637	76830	70214	70357	70154	53678	57200	51332	44129	0.36
77711	72812	70844	67834	63181	62842	62775	46771	51621	46933	41379	0.25
60979	56913	55127	52949	49884	49955	49562	35990	42788	39610	36485	0.12
72101	67019	65137	62313	58167	58349	57315	43307	49254	44533	39763	0.21
78631	73535	71496	68334	62966	63348	63624	47072	51849	46423	41057	0.26

Kaolin 14%

Orifice Type:	Short	
Orifice thickness[m]:	0.006	Area[m^2]
Orifice dimension[m]:	0.0322	0.000814332
Pipe Diameter [m]:	0.046	0.001661903
Diameter ratio	0.7	
Aspect ratio	0.19	
g[m/s^2]	9.81	
Material Type:	Kaolin	
Density[kg/m^3]:	1227.2	
Concentration[%]:	14%	
τ_y[Pa]:	3.20	
K [Pa.s]:	0.08	

n:	0.75
PPT used:	110
Range selected:	0-500

1/n	n/(n+1)	(n+1)/n	$K^{1/n}$
1.33	0.43	2.33	0.04

	Pod 1	Pod 2	Pod 3	Pod 4	Pod 5	Pod 6	Pod 7	Pod 8	Pod 9	Pod 10	Pod 11
Axial distances	-5.29	-4.68	-3.74	-2.36	-0.06	-0.03	0.03	2.34	4.65	6.97	9.29
N-D distances incl.[L/D]:	-115.05	-101.68	-81.38	-51.27	-1.38	-0.62	0.62	50.83	101.16	151.60	201.92
Distances[m]:	0.00	0.62	1.55	2.93	5.23	5.26	5.32	7.63	9.95	12.27	14.58

Pod 1 [Pa]	Pod 2 [Pa]	Pod 3 [Pa]	Pod 4 [Pa]	Pod 5 [Pa]	Pod 6 [Pa]	Pod 7 [Pa]	Pod 8 [Pa]	Pod 9 [Pa]	Pod 10 [Pa]	Pod 11 [Pa]	Average Q [l/s]
88376	86186	84000	79709	73523	73892	27323	44753	37297	32068	25379	5.46
88676	86411	84089	80044	74286	73977	29974	45405	38073	31943	25487	5.46
80686	78533	76376	73241	67510	68081	28759	42165	35588	29956	24480	5.16
81020	79160	76788	73535	67882	67990	28607	42225	35869	29665	24613	5.16
75251	73645	71278	68096	62971	63134	27031	39282	33727	28903	23425	4.90
75163	73490	71171	68089	62977	63221	27650	39487	33845	28737	23649	4.89
69458	67787	65896	63216	58241	58308	26347	37421	31966	27157	21991	4.69
69485	68113	65874	63218	58164	58259	25766	37401	31798	26869	22293	4.69
61741	60305	58482	55735	51879	51752	24208	34016	28953	24709	20659	4.31
61432	60072	58463	55923	51735	51461	24228	33273	28955	24738	20543	4.33
57195	55842	54202	51839	47831	47933	24193	32130	27563	23873	19693	4.07
61761	60524	58968	56710	52971	53023	29557	37621	33314	28887	26080	4.00
57189	56128	54745	52762	49459	49052	28371	35986	31942	28491	25321	3.76
57539	56423	54858	52927	49647	49494	29348	35879	32241	28544	25301	3.76
47249	46410	44815	43075	40497	40655	23760	28900	25983	22149	19023	3.47
47521	46149	44815	42969	40034	40042	23655	28799	25675	22392	18442	3.47
44989	44382	43103	41367	39315	38499	24089	27423	24794	22521	19875	3.30
45149	44382	43103	41197	38911	38607	23403	27239	25104	22521	19969	3.30
44619	43920	43146	41309	38609	38897	27804	30874	27969	24993	22688	2.84
45231	44181	42877	40978	38595	38745	27675	30570	27948	25642	22803	2.84
43681	42770	41880	40395	37843	37667	28530	30386	27897	25293	22983	2.59
43319	42695	41658	40013	37453	37277	28982	30548	27719	25708	22751	2.59
41561	40931	40009	38612	36310	36197	28704	29639	27139	24947	22363	2.28
40724	40391	39396	37792	35466	35570	28434	29835	27414	25015	22706	2.28
40724	40012	39044	37633	35333	35143	29520	30129	27785	25648	23449	2.01
40390	39953	39003	37649	35252	34593	29519	29952	27681	24644	23190	2.01
40430	39843	38843	37642	35258	34977	31126	31149	28926	26830	24569	1.74
40452	39890	38899	37534	35224	35096	31119	31003	28775	26644	24201	1.74
39211	38921	38138	36814	34646	34737	32387	31253	29252	27137	25149	1.40
37208	36759	35983	34763	32732	32460	31620	30272	28270	26253	24347	0.99

Kaolin 19%

Orifice Type:	Short	
Orifice thickness[m]:	0.006	Area[m^2]
Orifice dimension[m]:	0.0322	0.000814332
Pipe Diameter [m]:	0.046	0.001661903
Diameter ratio	0.7	
Aspect ratio	0.19	
g[m/s^2]	9.81	
Material Type:	Kaolin	
Density[kg/m^3]:	1319.4	
Concentration[%]:	19%	
τ_y[Pa]:	19.51	
K [Pa.s]:	2.57	
n:	0.40	
PPT used:	110	
Range selected:	0-500	

1/n	n/(n+1)	(n+1)/n	$K^{1/n}$
2.53	0.28	3.53	10.94

	Pod 1	Pod 2	Pod 3	Pod 4	Pod 5	Pod 6	Pod 7	Pod 8	Pod 9	Pod 10	Pod 11
Axial distances	-5.29	-4.68	-3.74	-2.36	-0.06	-0.03	0.03	2.34	4.65	6.97	9.29
N-D distances incl.[L/D]:	-115.05	-101.68	-81.38	-51.27	-1.38	-0.62	0.62	50.83	101.16	151.60	201.92
Distances[m]:	0.00	0.62	1.55	2.93	5.23	5.26	5.32	7.63	9.95	12.27	14.58

Pod 1	Pod 2	Pod 3	Pod 4	Pod 5	Pod 6	Pod 7	Pod 8	Pod 9	Pod 10	Pod 11	Average Q
[Pa]	[Pa]	[Pa]	[Pa]	[Pa]	[Pa]	[Pa]	[Pa]	[Pa]	[Pa]	[Pa]	[l/s]
128245	125562	121746	115171	106487	105711	75227	81386	71750	62919	52827	4.51
127835	125445	121488	115069	106236	105169	75667	81361	71680	62416	52854	4.50
124886	122546	118867	112120	103625	102855	74919	78772	70087	61030	51584	4.24
124874	122467	118725	112313	103644	101617	74919	78772	70087	61030	51584	4.24
120870	118655	114653	108803	100263	98123	76934	78757	70024	61053	51513	3.91
121217	119119	115074	109344	100515	97740	69795	71994	62505	53303	43662	3.94
113111	110749	106932	100622	92011	90429	67775	70278	61746	52365	43042	3.97
110625	108223	104604	98208	89888	87667	68030	69889	61337	52336	43216	3.71
111350	109122	105321	99558	91283	90183	68880	71103	62178	52700	43513	3.71
109785	107673	103715	97679	89320	88030	69699	70877	61705	53364	44298	3.52
110157	108039	104272	97836	89509	87810	69798	70768	61970	53055	43817	3.52
113554	111171	107381	101905	93021	91224	75573	75727	66994	57994	49037	3.25
113554	111171	107381	101905	93021	91224	75573	75727	66994	57994	49037	3.25
113196	110883	106976	101216	93135	91294	77958	76825	68951	60439	51189	2.96
113196	110883	106976	101216	93135	91294	77958	76825	68951	60439	51189	2.97
113298	111325	107011	101373	94095	92214	80058	79999	72208	63417	54541	2.60

Pod 1	Pod 2	Pod 3	Pod 4	Pod 5	Pod 6	Pod 7	Pod 8	Pod 9	Pod 10	Pod 11	Average Q
[Pa]	[Pa]	[Pa]	[Pa]	[Pa]	[Pa]	[Pa]	[Pa]	[Pa]	[Pa]	[Pa]	[l/s]
113647	111558	107818	101962	94041	91392	79700	79944	72012	63394	54754	2.60
112255	110391	106452	100937	93356	90239	82929	80059	72502	64142	55744	2.34
112194	110311	106596	100960	93354	92151	82371	80233	72379	64270	56104	2.34
110059	108603	104824	99554	91973	90330	83155	80266	72707	65142	56167	2.00
110086	108652	104810	99435	92232	90491	83743	80423	72885	65268	56976	1.99
108469	106823	103313	98047	90653	88579	82220	80019	72454	64966	56703	1.75
108543	106826	103757	98104	90913	89809	82362	80227	72832	65899	57372	1.75
106209	104861	101362	96028	89044	87061	82680	79354	72116	64279	56655	1.39
106093	104247	101050	95739	88854	88531	82945	79191	71867	64627	56913	1.39
103441	102187	98813	93951	86916	83654	84269	78227	71235	63547	56124	0.98
103838	102160	98879	93497	86891	83044	82197	77705	71019	63516	56653	0.98
100526	99301	96340	92067	85466	83238	81651	77181	70447	63843	55801	0.79

Kaolin 24%

Orifice Type:	Short	
Orifice thickness[m]:	0.006	Area[m^2]
Orifice dimension[m]:	0.0322	0.000814332
Pipe Diameter [m]:	0.046	0.001661903
Diameter ratio	0.7	
Aspect ratio	0.19	
g[m/s^2]	9.81	
Material Type:	Kaolin	
Density[kg/m^3]:	1392.9	
Concentration[%]:	24%	
τ_y[Pa]:	35.28	
K [Pa.s]:	10.04	
n:	0.41	
PPT used:	110	
Range selected:	0-500	

1/n	n/(n+1)	(n+1)/n	$K^{1/n}$
2.46	0.29	3.46	292.34

	Pod 1	Pod 2	Pod 3	Pod 4	Pod 5	Pod 6	Pod 7	Pod 8	Pod 9	Pod 10	Pod 11
Axial distances	-5.29	-4.68	-3.74	-2.36	-0.06	-0.03	0.03	2.34	4.65	6.97	9.29
N-D distances incl.[L/D]:	-115.05	-101.68	-81.38	-51.27	-1.38	-0.62	0.62	50.83	101.16	151.60	201.92
Distances[m]:	0.00	0.62	1.55	2.93	5.23	5.26	5.32	7.63	9.95	12.27	14.58

Pod 1	Pod 2	Pod 3	Pod 4	Pod 5	Pod 6	Pod 7	Pod 8	Pod 9	Pod 10	Pod 11	Average Q
[Pa]	[Pa]	[Pa]	[Pa]	[Pa]	[Pa]	[Pa]	[Pa]	[Pa]	[Pa]	[Pa]	[l/s]
210868	206084	198239	187213	168529	163633	159036	147918	127233	108664	89075	1.97
210868	206084	198239	187213	168529	163633	159036	147918	127233	108664	89075	1.99
220041	215299	207207	195808	176377	170366	163134	151267	131225	112189	91446	2.66
220377	215105	207162	195205	176139	170409	163079	151461	131658	111997	91928	2.65
207297	202401	194733	183402	166126	161159	155058	145033	126850	108133	89435	1.82
207297	201964	194302	183800	165364	163100	155058	145033	126850	108133	89435	1.82
205582	199381	192360	181346	163069	159889	150041	144202	125711	107346	88898	1.64
205341	200888	193379	181547	164082	155654	151141	144254	125831	107666	89333	1.60
199563	195488	188487	177161	159332	157970	148284	141570	123004	106091	88060	1.34
199244	195673	188302	176854	160516	157970	148284	141570	123004	106091	88060	1.34
197474	192981	186306	175153	158615	155632	147129	139730	122427	105173	87695	1.17
197474	192981	186306	175153	158615	155632	147129	139730	122427	105173	87695	1.11
196773	193192	185648	174767	158578	152147	147015	139590	122117	105030	87836	1.09
191727	188238	181314	171062	155442	148315	144714	136130	119350	103096	86533	0.92
191727	188238	181314	171062	155442	148315	144714	136130	119350	103096	86533	0.88
184452	180895	175595	166761	151787	142563	137603	135338	118571	101737	84952	0.77
184452	180895	175595	166761	151787	142563	137603	135338	118571	101737	84952	0.76
180917	177397	170897	162239	146611	143304	135089	130559	114482	99728	83837	0.52
180975	177409	170858	161997	147119	142721	135045	130452	114214	99742	83847	0.52
171913	167634	161644	153302	137753	132287	126620	123427	108107	94017	79340	0.31
171913	167634	161644	153302	137753	132287	126620	123427	108107	94017	79340	0.33
160513	157524	153137	145282	133159	130143	123800	120800	107174	92702	78602	0.20
160513	157524	152622	145472	133678	130747	122607	120319	106431	92226	78098	0.23
150709	146330	140306	132197	120284	116091	111249	106821	96534	85268	74089	0.17
140289	136740	130961	123831	115057	108067	103822	102048	93032	81717	71164	0.04

Bentonite 6%

Orifice Type:	Short	
Orifice thickness[m]:	0.006	Area[m^2]
Orifice dimension[m]:	0.0322	0.000814332
Pipe Diameter [m]:	0.046	0.001661903
Diameter ratio	0.7	
Aspect ratio	0.19	
g[m/s^2]	9.81	
Material Type:	Bentonite	
Density[kg/m^3]:	1035.9	
Concentration[%]:	6%	
τ_y[Pa]:	2.4	
K [Pa.s]:	0.0241	
n:	1	
PPT used:	110	
Range selected:	0-500	

1/n	n/(n+1)	(n+1)/n	$K^{1/n}$
1	0.5	2	0.0241

	Pod 1	Pod 2	Pod 3	Pod 4	Pod 5	Pod 6	Pod 7	Pod 8	Pod 9	Pod 10	Pod 11
Axial distances	-5.29	-4.68	-3.74	-2.36	-0.06	-0.03	0.03	2.34	4.65	6.97	9.29
N-D distances incl.[L/D]:	-115.05	-101.68	-81.38	-51.27	-1.38	-0.62	0.62	50.83	101.16	151.60	201.92
Distances[m]:	0.00	0.62	1.55	2.93	5.23	5.26	5.32	7.63	9.95	12.27	14.58

Pod 1 [Pa]	Pod 2 [Pa]	Pod 3 [Pa]	Pod 4 [Pa]	Pod 5 [Pa]	Pod 6 [Pa]	Pod 7 [Pa]	Pod 8 [Pa]	Pod 9 [Pa]	Pod 10 [Pa]	Pod 11 [Pa]	Average Q [l/s]
99600	97638	94340	88896	81991	80676	35729	49516	41158	33764	25834	6.05
99748	97544	94023	89213	81714	80940	35077	49482	41635	34026	25841	6.05
89898	87688	84705	80261	73619	72965	33789	45523	38197	31683	24246	5.63
89668	87532	84669	80605	73386	72559	33532	45968	38364	31296	24248	5.63
84921	82682	80033	75964	69523	68725	32650	43548	36525	30155	23332	5.41
84874	82585	79993	75770	69262	67989	32763	43541	36428	30064	23399	5.42
77812	75747	73287	69477	63697	62944	31288	40631	34423	28180	22077	5.14
77645	75977	73138	69544	63423	63707	31072	40445	34342	28040	22116	5.18
72735	70886	68460	65170	59747	58646	29361	37881	32500	26765	21264	4.97
72779	71187	68567	65201	59974	59025	29419	38186	32644	26877	21537	4.98
67239	65822	63626	60412	55183	54898	27663	35757	30319	25338	20125	4.70
67238	65770	63570	60290	55421	54124	27984	35516	30283	25193	19667	4.72
62229	60680	58822	56030	51357	50488	25500	33034	28296	23507	18743	4.54
62081	60686	59083	56200	51554	50825	25228	32873	28425	23248	18721	4.53
57338	55731	53778	51002	47022	46423	24683	30933	26523	22313	17897	4.28

Pod 1	Pod 2	Pod 3	Pod 4	Pod 5	Pod 6	Pod 7	Pod 8	Pod 9	Pod 10	Pod 11	Average Q
[Pa]	[Pa]	[Pa]	[Pa]	[Pa]	[Pa]	[Pa]	[Pa]	[Pa]	[Pa]	[Pa]	[l/s]
57239	55586	53990	51218	46964	46349	24365	31066	26267	22205	17983	4.28
51173	49940	48475	46060	42199	42378	23380	28613	24625	20872	17015	3.94
51160	49973	48329	46109	42367	42473	23670	28814	24728	20967	17138	3.94
47646	46350	44886	42580	39205	39207	23200	27216	23648	20501	17373	3.73
47829	46437	45197	42615	39017	39070	23169	27132	24145	20497	16561	3.73
42503	41739	40541	38379	35468	35150	22295	25451	22308	19901	16853	3.41
42471	41748	40253	38168	35767	35271	21564	25585	22653	20233	17047	3.41
36642	36092	35631	33761	31853	31663	21090	23909	21200	18950	17026	3.09
36642	36092	35669	33761	31853	31422	20833	23385	20965	18983	16537	3.09
36642	36092	35229	33746	31888	31839	25160	26120	23994	21678	19598	2.56
33924	33439	32332	31244	29450	28855	24291	24684	22814	20628	18690	2.13
31795	31519	30929	29963	28177	27676	24912	24612	22742	20860	18933	1.76

Bentonite 9%

Orifice Type:	Short	
Orifice thickness[m]:	0.006	Area[m^2]
Orifice dimension[m]:	0.0322	0.000814332
Pipe Diameter [m]:	0.046	0.001661903
Diameter ratio	0.7	
Aspect ratio	0.19	
g[m/s^2]	9.81	
Material Type:	Bentonite	
Density[kg/m^3]:	1058.2	
Concentration[%]:	9%	
τ_y[Pa]:	7.18	
K [Pa.s]:	0.04	
n:	1.00	
PPT used:	110	
Range selected:	0-500	

1/n	n/(n+1)	(n+1)/n	$K^{1/n}$
1	0.5	2	0.0377361

	Pod 1	Pod 2	Pod 3	Pod 4	Pod 5	Pod 6	Pod 7	Pod 8	Pod 9	Pod 10	Pod 11
Axial distances	-5.29	-4.68	-3.74	-2.36	-0.06	-0.03	0.03	2.34	4.65	6.97	9.29
N-D distances incl.[L/D]:	-115.05	-101.68	-81.38	-51.27	-1.38	-0.62	0.62	50.83	101.16	151.60	201.92
Distances[m]:	0.00	0.62	1.55	2.93	5.23	5.26	5.32	7.63	9.95	12.27	14.58

Pod 1	Pod 2	Pod 3	Pod 4	Pod 5	Pod 6	Pod 7	Pod 8	Pod 9	Pod 10	Pod 11	Average Q
[Pa]	[Pa]	[Pa]	[Pa]	[Pa]	[Pa]	[Pa]	[Pa]	[Pa]	[Pa]	[Pa]	[l/s]
96875	95302	92754	88042	81120	80846	45367	55200	47834	40794	33826	5.61
97058	95366	92741	87625	81246	80372	45749	55009	47502	40659	33826	5.61
87857	85881	83006	79038	72890	69868	42310	49879	43150	37223	31632	5.28
87857	85975	82715	79038	72890	70038	42310	49334	43150	37223	31969	5.27
81398	79820	77289	73649	67704	67430	41918	47387	42152	36215	30154	4.97
81453	79620	77214	73773	67578	68015	41269	47707	41655	36595	30171	4.96
76724	74948	72703	69589	64037	63283	41571	45969	40149	35149	29252	4.51
76540	75053	72808	69267	63900	63186	40659	45902	40204	34931	29312	4.51
73105	71786	69568	66321	60816	59986	43561	46052	40646	35342	29986	3.89
72817	71472	69237	65917	60618	60113	43334	45808	40577	35064	29483	3.89
70931	69444	67439	63941	58810	58153	46294	46690	41643	36812	31353	3.28
69966	69052	66487	63326	58011	57460	45733	45998	41599	37042	31339	3.28
72570	71493	69255	66181	60973	60160	52187	51157	46261	41373	36320	2.77
69092	67831	65841	62780	57796	57156	51753	49642	44938	40412	35063	2.25
67887	66678	64850	61894	56926	56171	53074	50177	45408	40701	35858	1.86
66727	65284	63146	60484	55715	55033	53664	49621	45158	40581	35464	1.50

Water

Orifice Type:	Short	
Orifice thickness[m]:	0.006	Area[m^2]
Orifice dimension[m]:	0.0322	0.000814332
Pipe Diameter [m]:	0.046	0.001661903
Diameter ratio	0.7	
Aspect ratio	0.186	
g[m/s^2]	9.81	
Material Type:	Water	
Density[kg/m^3]:	998.5	
Concentration[%]:	100%	
τ_y[Pa]:	0	
K [Pa.s]:	0.001	
n:	1	
PPT used:	110	
Range selected:	0-500	

1/n	n/(n+1)	(n+1)/n	$K^{1/n}$
1	0.5	2	0.001

	Pod 1	Pod 2	Pod 3	Pod 4	Pod 5	Pod 6	Pod 7	Pod 8	Pod 9	Pod 10	Pod 11
Axial distances	-5.29	-4.68	-3.74	-2.36	-0.06	-0.03	0.03	2.34	4.65	6.97	9.29
N-D distances incl.[L/D]:	-115.05	-101.68	-81.38	-51.27	-1.38	-0.62	0.62	50.83	101.16	151.60	201.92
Distances[m]:	0.00	0.62	1.55	2.93	5.23	5.26	5.32	7.63	9.95	12.27	14.58

Pod 1	Pod 2	Pod 3	Pod 4	Pod 5	Pod 6	Pod 7	Pod 8	Pod 9	Pod 10	Pod 11	Average Q
[Pa]	[Pa]	[Pa]	[Pa]	[Pa]	[Pa]	[Pa]	[Pa]	[Pa]	[Pa]	[Pa]	[l/s]
75155	73692	71144	67797	62733	63331	16558	33736	28769	23424	18117	5.77
74940	73692	71005	67993	62648	63507	16286	33852	28773	23384	18107	5.76
67404	65665	64140	60891	56114	56638	15413	30850	26244	21399	16895	5.42
67187	65665	63706	60690	56313	56683	15526	30699	26053	21464	16888	5.41
59781	58739	57031	54085	50243	50559	14474	27750	23823	19517	15581	5.07
60061	58739	56937	54283	50342	50646	14529	27736	23888	19667	15516	5.07
55521	54295	52564	50092	46484	46711	13963	25973	22410	18451	14671	4.84
55463	54295	52532	49971	46338	46676	13912	25902	22381	18360	14748	4.84
48810	47895	46425	44182	40973	41292	13175	23224	20194	16795	13532	4.49
48932	47895	46342	44222	41009	41349	13106	23262	20153	16798	13505	4.49
43265	42400	41166	39159	36325	36666	12292	21185	18288	15413	12490	4.18
43399	42400	41205	39211	36361	36714	12346	21202	18366	15424	12490	4.17
37702	36937	35810	34249	31736	31962	11582	18869	16486	13950	11445	3.83
37720	36937	35883	34204	31866	32135	11484	18855	16493	13916	11467	3.83
33558	32773	31825	30411	28327	28553	10892	17244	15121	12972	10704	3.56
33461	32773	31840	30515	28418	28562	10789	17295	15200	12877	10743	3.56
29478	28778	28065	26839	25125	25158	10290	15564	13730	11829	9939	3.27
29430	28817	28100	26809	25081	25265	10246	15563	13811	11850	9951	3.27
25169	24747	24057	23039	21450	21573	9578	13760	12282	10720	9152	2.94
25190	24747	23984	23024	21534	21674	9654	13781	12336	10734	9209	2.94
21699	21238	20717	19899	18647	18698	8999	12297	11112	9839	8551	2.64
21589	21238	20697	19918	18630	18677	8948	12331	11140	9828	8529	2.65
15446	15178	14877	14351	13551	13592	7895	9760	9021	8174	7380	2.04
15437	15163	14891	14357	13586	13586	7891	9808	9032	8188	7378	2.04
13069	12827	12629	12195	11642	11649	7447	8770	8167	7569	6958	1.79
13069	12858	12598	12218	11592	11631	7438	8791	8201	7556	6958	1.79